UNIVERSITE BRETAGNE LOIRE

UNIVERSITÉ DE NANTES

Thèse de Doctorat

William DUDEFOI

Mémoire présenté en vue de l'obtention du
grade de Docteur de l'Université de Nantes
sous le sceau de l'Université Bretagne Loire

École doctorale : VENAM

Discipline : Sciences Agronomiques et écologiques

Unité de recherche : INRA UR1268 Biopolymères Interactions Assemblages

Soutenue le 30 Mars 2017

Le dioxyde de titane en alimentation : caractérisation, devenir dans les fluides digestifs et impact sur le microbiote intestinal humain

Titanium dioxide particles in food: characterization, fate in digestive fluids and impact on human gut microbiota

JURY

Président du jury :	**Agnès GRANIER**, Directrice de recherche, Institut des Matériaux Jean Rouxel (IMN), Nantes
Rapporteurs :	**Paul WESTERHOFF**, Professor, Arizona State University, Tempe **Muriel MERCIER-BONIN**, Chargée de Recherche, INRA unité Toxalim, Toulouse
Examinateurs :	**Didier DUPONT**, Directeur de recherche, INRA UMR Science et technologie du lait et de l'oeuf, Rennes **Nicolas FELTIN**, Ingénieur de recherche, Laboratoire national de métrologie et d'essais (LNE), Paris
Invité :	**Christophe PAGNOUT**, Maître de conférences, LIEC, Metz
Directeur de Thèse :	**Marie-Hélène ROPERS**, Chargée de recherche, INRA Unité BIA, Nantes
Co-directeur de Thèse :	**Bernard HUMBERT**, Professeur des universités, Institut des Matériaux Jean Rouxel (IMN), Nantes
Co-encadrant de Thèse :	**Hélène TERRISSE**, Maître de Conférences, Institut des Matériaux Jean Rouxel (IMN), Nantes

Acknowledgements

Je tiens tout d'abord à remercier ma directrice de thèse Mme Marie-Hélène Ropers, mon co-directeur Mr Bernard Humbert ainsi que ma co-encadrante Mme Hélène Terrisse pour m'avoir donné l'opportunité de réaliser ce travail de thèse à leurs côtés. Merci pour tous les conseils que vous m'avez apportés tout au long de ces 3 années, pour tout le temps que vous m'avez consacré et pour toute la confiance que vous m'avez accordée.

Je remercie très sincèrement Mme Muriel Mercier-Bonin, Mr Paul Westerhoff, Mme Agnès Granier, Mr Didier Dupont, Mr Nicolas Feltin ainsi que Mr Christophe Pagnout d'avoir accepté de participer à mon jury de thèse. Je remercie aussi Mme Marie Carrière et Mr Eric Houdeau d'avoir fait partie de mon comité de suivi de thèse durant ces trois années.

Ce travail de thèse a été possible grâce au financement du labex Serenade que je remercie également.

Je tiens à remercier tous les membres du laboratoire Interfaces et Systèmes Dispersés (ISD) et plus globalement de l'unité Biopolymères, Interactions, Assemblages (BIA) de l'INRA de Nantes dans lequel j'ai effectué la majeure partie de mon travail de thèse. Une pensée particulière pour tous les doctorants que j'ai eu la chance de côtoyer et avec qui j'ai partagé de très nombreux moments (Audrey Arnould, Jean-Marc Schwartz, Mathieu Gayral, Mathilde Claude, Glenn Philippe, Thibault Loiseleux, Perrine Gelebart).

Je remercie également tous les membres de l'Institut des Matériaux Jean Rouxel de Nantes (IMN, Université de Nantes) avec qui j'ai eu grand plaisir à collaborer à de nombreuses reprises et sans qui ce travail de thèse n'aurait pas pu être réalisé. Je remercie notamment Mme Mireille Richard-Plouet pour toute son aide sur les analyses XPS, tous ses conseils avisés ainsi que ses relectures de l'article, Mr Eric Gautron pour

toutes les analyses en microscopie électronique à transmission et enfin Mr Florin Popa pour les analyses en diffraction des rayons X.

Ayant eu la chance de réaliser une partie de mon travail de thèse au Canada, je souhaiterais remercier les membres du laboratoire de Virginia K. Walker de la Queen's University. Dear Virginia, it has been a great opportunity for me to be part of your team, I have learned a lot from you and I am very thankful for all the trust you gave me. I would like to address special thanks to Kristy Moniz, who taught me everything I needed to know in order to perform all my experiments, and to all the other ones in the lab for being so nice with me when I was there. Finally, thanks to Ms Emma Allen-Vercoe and Christian Carlucci from Guelph University for providing the MET-1 consortium, essential to this work. Je remercie également l'École internationale de recherche d'Agreenium (EIR-A), la Direction de l'Action Régionale, de l'Enseignement Supérieur et de l'Europe (DARESE), ainsi que l'unité de recherche BIA pour leur contribution dans le financement de cette collaboration à l'étranger.

Je remercie également ma famille et mes amis qui m'ont toujours soutenu tout au long de ce travail de thèse. Merci à mes parents pour m'avoir toujours poussé vers l'avant tout au long de mon parcours, c'est grâce à vous si j'en suis là aujourd'hui, et je ne vous remercierai jamais assez pour tout ce que vous m'avez apporté. Enfin, je remercie tout particulièrement Alicia, mon soutien au quotidien, merci pour tout, tout simplement.

Table of contents

Communications:

Publications:

Dudefoi W., Terrisse H., Richard-Plouet M., Gautron E., Popa F., Humbert B., Ropers M-H. (2017) Criteria to define a more relevant reference sample of titanium dioxide in the context of food: a multiscale approach. *Food Additives and Contaminants Part A.* (accepted: http://dx.doi.org/10.1080/19440049.2017.1284346)

Dudefoi W., Moniz K., Allen-Vercoe E., Ropers M-H., Walker V.K. Impact of food grade and nanoTiO_2 particles on a human intestinal community. *Food and Chemical Toxicology* (in revision)

Dudefoi W., Terrisse H., Gautron E., Popa F., Humbert B., Ropers M-H. Evaluation of the intake of TiO_2 nanoparticles through the consumption of chewing-gums. *Food Additives and Contaminants Part A.* (in preparation)

Dudefoi W., Terrisse H., Humbert B., Ropers M-H. *In vitro* digestion of food grade TiO_2 particles. *Food & Function* (in preparation)

Scientific book chapter:

Ropers M-H., **Dudefoi W.** Controlling the presence of nanoparticles in food products: identification of titanium dioxide and its fate after ingestion. *Special Issue of Innovative Food Science and Emerging Technologies (IFSET)* (submitted)

National and International conferences:

2014

Dudefoi W., Terrisse H., Humbert B., Ropers M-H. Détermination de l'état physico-chimique des nanoparticules alimentaires de TiO_2 dans les fluides digestifs. Application à l'élaboration d'un modèle réaliste de particules de TiO_2 digérées. *Serenade scientific seminar*. June 17th 2014, Technopôle de l'Environnement Aix en Provence, France. (oral).

Dudefoi W., Terrisse H., Humbert B., Ropers M-H. Is p25 a realistic model to study the toxicity of TiO_2 in the gastro-intestinal tract? *International Conference on Safe*

production and use of nanomaterials, Nanosafe 2014, November 18-20th 2014, Grenoble, France. (poster)

2015

Dudefoi W., Terrisse H., Humbert B., Ropers M-H. Is P25 a realistic model to study the toxicity of TiO_2 in the gastro-intestinal tract? Workshop on *Nanoparticules métalliques, biologie, environnement et santé*, 28 janvier 2015, Grenoble, France. (poster)

Dudefoi W., Terrisse H., Humbert B., Ropers M-H. Investigating the fate of food grade titanium dioxide nano- and microparticles in digestive fluids. *6th International Symposium on Delivery of Functionality in Complex Food Systems,* July 14-17, 2015 in Paris, France. (oral)

2016

Dudefoi W., Moniz K., Allen-Vercoe E., Ropers M-H., Walker V.K. Impact of nano-TiO_2 on a defined human intestinal community. *10th INRA-Rowett Joint Symposium on gut microbiology*, June 20th to 23rd 2016, Clermont-Ferrand, France. (poster)

Dudefoi W., Ropers M-H. Suivi des nanoparticules de dioxyde de titane dans les fluides digestifs. *RBPGO7: 7èmes Rencontres Biologie-Physique du Grand Ouest*, June 23rd and 24th 2016 in Nantes, France. (oral)

Dudefoi W., Terrisse H., Richard-Plouet M., Popa F., Gautron E., Humbert B., Ropers M-H. Comparative study of E171 food grade and P25 TiO_2 nanoparticles. *NANO 2016 - XIIIth International Conference on Nanostructured Materials,* August 7th to 12th 2016 in Québec, Canada. (oral)

Dudefoi W., Moniz K., Allen-Vercoe E., Ropers M-H., Walker V.K. Impact of food grade and nano-TiO_2 on human gut microbiota. *NANO 2016 - XIIIth International Conference on Nanostructured Materials,* August 7th to 12th 2016 in Québec, Canada. (oral)

Dudefoi W., Moniz K., Allen-Vercoe E., Ropers M-H., Walker V.K. Testing food grade and nano-TiO_2 on a defined human intestinal community. *11th International Conference on the Environmental Effects of Nanoparticles and Nanomaterials (ICEENN 2016)* August 14th to 18th 2016 in Golden, Colorado, USA. (poster)

Dudefoi W., Terrisse H., Richard-Plouet M., Popa F., Gautron E., Humbert B., Ropers M-H. Characterization of TiO_2 nanoparticles as food additive. *11th International Conference on the Environmental Effects of Nanoparticles and Nanomaterials (ICEENN 2016)* August 14th to 18th 2016 in Golden, Colorado, USA. (poster)

Dudefoi W., Terrisse H., Gautron E., Humbert B., Ropers M-H. TiO_2 nanoparticles release from chewing-gums and candies. *11th International Conference on the Environmental Effects of Nanoparticles and Nanomaterials (ICEENN 2016)* August 14th to 18th 2016 in Golden, Colorado, USA. (poster)

Dudefoi W., Terrisse H., Humbert B., Ropers M-H. Physicochemical behavior of TiO_2 particles in simulated digestive fluids. *11th International Conference on the Environmental Effects of Nanoparticles and Nanomaterials (ICEENN 2016)* August 14th to 18th 2016 in Golden, Colorado, USA. (oral)

Dudefoi W., Ropers M-H. Les nanomatériaux inorganiques dans l'alimentation: de leurs caractérisations à leurs devenirs dans les fluides digestifs. *Colloque R31 « NANO AGRO »* September 16th 2016 in Paris, France. (oral)

French summary

I) Introduction

Le dioxyde de titane (TiO_2) est un oxyde métallique utilisé en tant que pigment blanc dans divers produits tels que les peintures, les plastiques, les encres, les papiers, mais également les produits alimentaires formulés, pharmaceutiques et cosmétiques. Utilisé dans l'agroalimentaire sous l'appellation E171 en Europe et INS171 aux Etats-Unis, on le retrouve principalement dans les produits type confiseries, constituant notamment l'enrobage de bonbons et chewing-gums, à hauteur de 3,88 mg de TiO_2/g de produit (Chen, Cheng, Yang, Cao, & Liu, 2013; Weir, Westerhoff, Fabricius, Hristovski, & Von Goetz, 2012; Yang et al., 2014). Des particules de TiO_2 sont également ajoutées dans certaines préparations fromagères, sauces, et dans des produits à faible teneur en matière grasse tels que le lait écrémé, les crèmes glacées et les pâtisseries (Skocaj, Filipic, Petkovic, & Novak, 2011).

Le TiO_2 a longtemps été considéré comme ne représentant aucun risque pour le consommateur. Cependant, environ 36% des particules sont des nanoparticules (NPs) (Chen et al., 2013; Weir et al., 2012; Yang et al., 2014), c'est-à-dire des particules ayant un diamètre inférieur à 100 nm, et certaines études ont montré que les NPs de TiO_2 peuvent traverser la membrane intestinale (Böckmann, Lahl, Eckert, & Unterhalt, 2000; Gitrowski, Al-Jubory, & Handy, 2014; Koeneman et al., 2010), atteindre le système circulatoire et s'accumuler dans le foie et les reins, (Fabian et al., 2008; Park et al., 2014; Pele et al., 2015; Jiangxue Wang et al., 2007; Xie, Wang, Sun, & Zhong, 2011) tout en induisant des modifications physiologiques et histopathologiques dans les tissus animaux (Bettini et al., 2017). Bien que les NPs de TiO_2 soient classées comme potentiellement cancérogènes pour l'homme via inhalation (Groupe 2B) (IARC 2010), son utilisation en tant qu'additif alimentaire a été récemment prolongée par l'agence européenne de sécurité alimentaire (EFSA) (EFSA, 2016).

Au contraire des particules inhalées, les particules ingérées atteignent les cellules intestinales après un passage dans les différents fluides digestifs, contenant divers ions et protéines présentant des affinités pour le TiO_2 (Domingos, Peyrot, & Wilkinson,

2010). Dans de telles conditions, la charge ainsi que la couverture de surface des particules sont susceptibles d'évoluer, c'est pourquoi les transformations physicochimiques des particules de TiO_2 dans les fluides digestifs doivent être déterminées. De plus, les particules de TiO_2 utilisées en tant que modèle dans un grand nombre d'études de toxicologie sont les particules « P25 », référence de l'OCDE (Organisation de Coopération et de Développement Économiques) qui sont une variété de TiO_2 généralement utilisée dans le domaine de la photo-catalyse, et dont Jovanovic posait la question de leur pertinence (Jovanović, 2015) en tant que modèle de TiO_2 dans le cadre de l'alimentation.

Afin d'apporter de nouveaux éléments de réponse à l'évaluation du risque relatif à l'usage de particules de TiO_2 dans l'alimentation, leur nature physico-chimique ainsi que leur devenir dans les conditions du tractus gastro-intestinal devaient être déterminés. Ce travail de thèse avait pour ambition de répondre à ces questions.

Dans un premier temps, notre objectif a été de déterminer si les particules de P25 et E171 sont similaires ou non, afin de confirmer ou d'infirmer la seule étude existante à ce jour (Yang et al., 2014). Pour cela, nous avons comparé les propriétés de surface et de volume des particules de P25 et E171, suivant les recommandations de l'EFSA (EFSA, 2011). Nous avons également considéré des particules de TiO_2 extraites de l'enrobage de chewing-gums afin de déterminer si les particules restent dans le même état physico-chimique une fois intégrées dans une matrice alimentaire.

L'objectif suivant a été d'analyser l'évolution de l'état physicochimique des particules de TiO_2 tout au long du tractus gastro-intestinal. Un protocole standardisé de digestion *in vitro* a été utilisé et complété afin de mieux mimer le compartiment salivaire, premier fluide en contact avec les particules de TiO_2. Aucune donnée n'existant à ce jour concernant le devenir des particules de TiO_2 dans les fluides digestifs, nous nous sommes intéressés à l'évolution de l'état physicochimique des particules de P25 et E171 après chaque étape de la digestion simulée : étapes salivaire, gastrique puis intestinale. La taille des agglomérats formés et la nature de la couverture de surface enrobant les particules ont notamment été analysées.

Enfin, nous avons étudié la toxicité des particules de TiO_2 sur le microbiote intestinal humain, constituant un véritable écosystème au sein de notre système digestif et d'une grande importance dans de nombreux aspects de notre physiologie (Frank et al., 2007; Ley, Peterson, & Gordon, 2006; Marchesi et al., 2015; Pietroiusti, Magrini, & Campagnolo, 2016). Pour étudier l'impact du dioxyde de titane sur sa viabilité et sa richesse, un modèle de microbiote intestinal humain, produit par l'université de Guelph, a été exposé aux différents types de particules de TiO_2 à des concentrations réalistes, équivalentes à celles atteintes dans l'intestin suite à l'ingestion de une/deux confiseries. L'impact des particules de TiO_2 sur le microbiote a été évalué aux échelles physiologique, biochimique et moléculaire.

II) Etude comparative des particules de TiO_2 de grade alimentaire (E171) et des nanoparticules de P25.

Sept échantillons de TiO_2 de grade alimentaire (E171) issus de trois fabricants et de trois fournisseurs en Europe ainsi que du TiO_2 P25 ont été caractérisés suivant les recommandations de l'agence européenne de sécurité des aliments (EFSA, 2011) à savoir, la distribution de taille, la forme, la cristallinité, la réactivité et les propriétés de surface des particules.

Les analyses en microscopie électronique à transmission (MET) ont montré que le TiO_2 alimentaire et le P25 possèdent tous deux une fraction significative de nanoparticules, mais qu'ils présentent une taille de particules primaires et un pourcentage de nanoparticules différents. En accord avec la littérature (Ohno, Sarukawa, Tokieda, & Matsumura, 2001; Weir et al., 2012; Yang et al., 2014), les particules de P25 ont une taille de particules primaires de 21±8 nm avec 100% de nanoparticules, tandis que les particules de E171 ont une taille moyenne de particules primaires de 131±43nm, avec en moyenne 26% des particules dans la gamme de taille nanométrique (Tableau 1).

Pour les particules de grade alimentaire, le pourcentage en nombre des particules ayant un diamètre inférieur à 100 nm est toujours inférieur à 50%, limite définissant un nanomatériau. En phase aqueuse, les analyses granulométriques réalisées à différents pH ont montré que les particules de TiO_2 de grade alimentaire ont tendance à former des agglomérats de petites tailles à pH 6 et 7, et des plus gros agglomérats aux valeurs de pH inférieures, alors que les particules de P25 ont tendance à former des agglomérats de très grande taille aux valeurs de pH 5 et 6, et des agglomérats de taille moyenne pour les pH 2, 3, 4 et 7. Les points isoélectriques mesurés pour les particules de E171 sont aux alentours de pH 4,2, tandis que le point isoélectrique des particules de P25 est situé à pH 6,4. Ainsi, l'état d'agglomération étant lié à la charge de surface des particules, cette différence de point isoélectrique induit une agglomération des deux types de particules dans des zones de pH différentes. Cette différence peut être liée à la présence de groupements phosphates ou de silice à la surface des particules alimentaire E171, détecté par XPS et ICP-AES. La présence de phosphore pourrait résulter de l'utilisation de surfactants anioniques contenant des

polyphosphates lors de leur préparation, comme proposé dans la littérature (Yang et al., 2014). Les autres analyses ont montré que le dioxyde de titane P25 est un composé très pur constitué d'un mélange de deux phases cristallines, anatase et rutile (85/15%), avec une aire spécifique de 50 m^2/g. Au contraire, le dioxyde de titane E171 est un composé formé d'une seule phase cristalline, l'anatase avec une aire spécifique de 10 m^2/g en moyenne sur les différents échantillons étudiés, parfois composé de silice et d'aluminium, comme démontré par les analyses réalisées en ICP-AES.

Cette étude a permis de démontrer la relative homogénéité des échantillons de E171 entre 6 fabricants et distributeurs en Europe, même si quelques différences ont été détectées entre 2 lots d'un même distributeur. En revanche, les nombreuses différences observées entre les poudres de dioxyde de titane de grade alimentaire E171 et la poudre de P25 démontrent que le P25 ne semble pas être le modèle le plus pertinent pour des études s'intéressant au devenir des particules de TiO_2 après ingestion. C'est pourquoi nous avons considéré dans la suite de ce travail les particules de grade alimentaire et, dans un souci de comparaison avec la littérature, les particules de P25.

Les résultats de cette première partie ont été publiés dans *Food Additives and Contaminants Part A :*

Dudefoi W., Terrisse H., Richard-Plouet M., Gautron E., Popa F., Humbert B., Ropers M-H. (2017) Criteria to define a more relevant reference sample of titanium dioxide in the context of food: a multiscale approach. *Food Additives and Contaminants Part A.* (http://dx.doi.org/10.1080/19440049.2017.1284346)

.

	Propriétés (Techniques)	P25	E171			E171
			E171-1	E171-2	E171-3	Bibliographie
			Moyenne ± SD			
Analyses en bulk	Taille primaire (MET)	**21 nm**	144±43 nm	115±31 nm	122±35 nm	110 nm **Weir 2012** 106±38, 122±48, 132±56, 124±42, 117±41 nm **Yang 2014** 122±48 **Faust 2014**
			131±43 nm			
	Distribution de taille (MET)	**9-48 nm**	51-269 nm	38-203 nm	48-250 nm	30-400 nm **Weir 2012** 51 to 290 nm **Faust 2014** 30 to 600 nm **Peters 2014**
			38-296 nm			
	% de nanoparticules (MET)	**100%**	17%	36%	29%	36 % **Weir 2012** 35, 23, 21, 17, 19% **Yang 2014** 40.0, 43.5, 43.7, 41.4, 42.4, 27.7% **Chen 2013** 10 % **Peters 2014**
			26%			
	Cristallinité (DRX, FT-Raman)	**85 % Anatase 15 % Rutile**	100% Anatase	98% Anatase 2% Rutile	100% Anatase	4 échantillons Anatase / 1 mélange **Yang 2014** 5 échantillons Anatase / 1 Rutile **Chen 2013** Anatase **Faust 2014**
			100% Anatase			
	Chimie de surface (XPS, réflexion diffuse en UV-vis, NIR et MIR, FT-Raman)	**TiO_2**	TiO_2 + P + K	TiO_2 + P + K	TiO_2 + P + K	TiO_2 + P **Yang 2014, Faust 2014**
			TiO_2 + P (+ K + Si)			
	Surface spécifique (Volumétrie d'adsorption des gaz)	**50 m²/g**	8,6 m²/g	10,6 m²/g	8,7 m²/g	8-9 m²/g **Kronos International**
			8,5 m²/g			
	Composition chimique (ICP-AES)	**TiO_2**	TiO_2 + P	TiO_2 + P + Al	TiO_2 + P	Ti, P, Al, Si **Yang 2014** 90–99% TiO_2 **Peters 2014**
			TiO_2 + P (Al + Si)			
Analyses en dispersion	Taille des agglomérats (Granulométrie laser)	**0,060-450 µm**	**0,060-20 µm**			273, 405, 209, 504, 127 nm eau + sonication **Yang 2014** 150 nm in water + BSA + sonication **Weir 2012** 336 nm in serum media + sonication **Faust 2014**
	Point Iso-électrique (Potentiel zêta)	**6,4**	4,1	4,1	4,2	3.2, 3.5, 4.0, et <2,5 **Yang 2014** 3,3 **Faust 2014**
			4,2			

Tableau 1 : Caractérisation physico-chimique des particules de TiO_2 E171 et P25. Les résultats sont présentés pour les échantillons de E171 provenant de trois fabricants, les moyennes sont calculées d'après les 7 échantillons de E171.

III) Caractérisation physicochimique de particules de TiO_2 extraites de chewing-gums et bonbons.

Plusieurs produits alimentaires de type confiseries (4 chewing-gums et 1 bonbon) de couleur blanche et stipulant contenir du E171 ont été étudiés. Dans un premier temps, la présence de TiO_2 a été confirmée par spectrométrie Raman sur les confiseries puis l'enrobage de ces produits a été extrait selon un protocole adapté de la littérature (Chen et al., 2013). Brièvement, les échantillons ont été placés dans de l'eau ultrapure pendant 30 à 60 secondes, temps nécessaire pour disperser l'enrobage sous agitation manuelle. Une fois séchées dans un dessicateur, la nature et la taille des particules constituant les enrobages ont été analysées par FT-Raman, microscopie électronique à transmission (MET), spectrométrie d'émission atomique par plasma induit (ICP-AES) et diffraction des rayons X (DRX) (Figure 1).

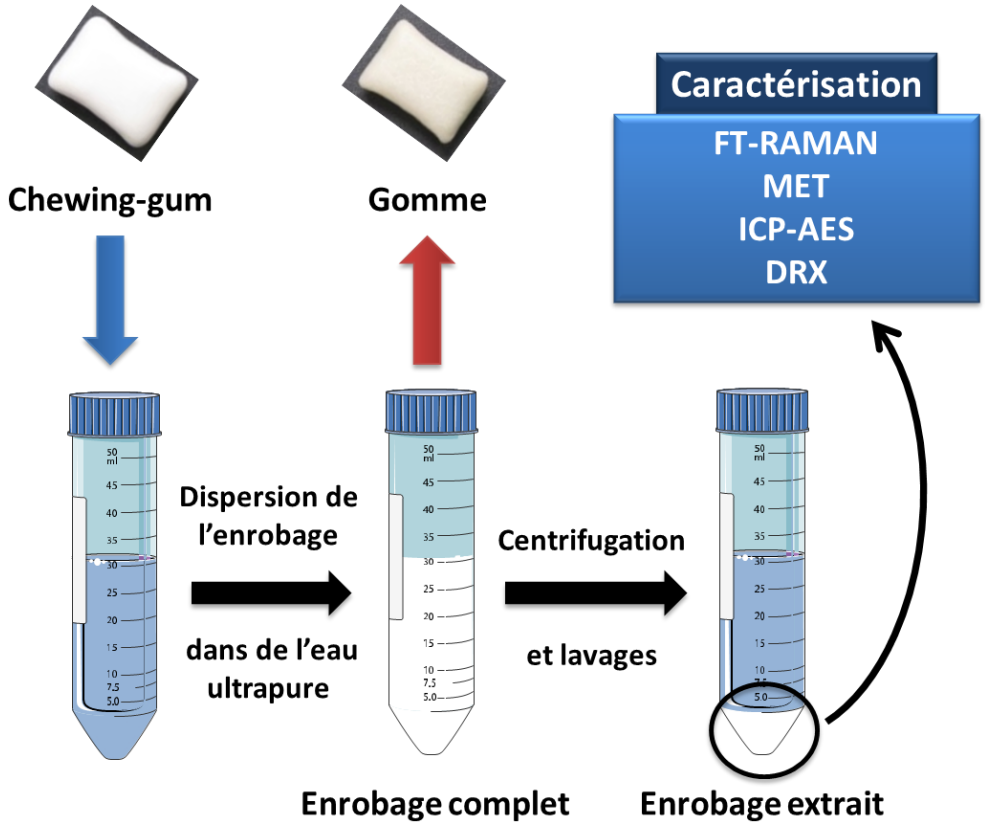

.

Figure 1 : Extraction et caractérisation des particules de TiO_2 extraites d'enrobages de chewing-gums (adapté de (Chen et al., 2013)***)***

D'après les résultats d'ICP-AES, la teneur en TiO_2 varie selon les échantillons de 0,27 à 12,05mg de TiO_2 /g de confiserie. Les mesures en MET ont montré que dans les extraits d'enrobages, entre 16 et 34% des particules de TiO_2 sont de taille nanométrique, en accord avec les données de la littérature sur une large gamme de produits (36% selon (Weir et al., 2012), 27.7 à 43.7% selon (Chen et al., 2013)). En combinant les données d'ICP-AES et de MET, la quantité de nano-TiO_2 a été estimée entre 0,03 et 0,81 mg par chewing-gum, représentant entre $1,7x10^{13}$ et $4,3x10^{14}$ de NPs. Cependant, d'autres particules de tailles supérieures présentes dans les extraits d'enrobages ont également été observées en microscopie électronique (>500 nm, forme de plaquettes). Les analyses EDX, DRX, FT-Raman et ICP-AES ont permis d'identifier ces co-extraits comme étant des traces d'autres additifs alimentaires. Du carbonate de calcium, type calcite ($CaCO_3$) a notamment été retrouvé en grande proportion dans l'un des enrobages analysés, cet additif étant utilisé en tant qu'agent de charge (E170). Des silicates de magnésium ont également été détectés, provenant de l'ajout de talc en tant qu'agent antiagglomérant, agent d'enrobage et agent de texture (E553). Enfin, deux des enrobages analysés étaient constitués d'amas de particules de TiO_2 enrobées dans une matrice organique. Selon les échantillons, les particules de TiO_2 peuvent ainsi être libérées de l'enrobage des chewing-gums soit en tant que particules isolées, soit enrobées et groupées dans une matrice organique, soit en présence d'autres particules plus larges. Les enrobages de chewing-gums les plus riches en TiO_2 ayant une composition complexe et l'enrobage le plus pur en TiO_2 ne permettant de récupérer qu'une très faible quantité de TiO_2 (0,98 mg de TiO_2 par gramme de chewing-gum), considérer les extraits de chewing-gums comme modèle pour déterminer l'agglomération des particules de TiO_2 dans les fluides digestifs était trop complexe. La caractérisation physicochimique des extraits d'enrobages par FT-Raman et DRX a également permis de déterminer que les particules de TiO_2 sont majoritairement sous forme anatase, en accord avec une étude précédente réalisée en Asie (Chen et al., 2013) et correspondent aux particules de E171 caractérisées dans la première partie de nos travaux, démontrant que la nature physicochimique des particules de TiO_2 intégrées dans les enrobages de chewing-gums reste semblable à

celle de l'additif alimentaire E171. Nous avons donc privilégié les particules de E171 comme modèle de particules de TiO_2 pour les études de digestion.

IV) Détermination de l'état physicochimique de particules de TiO_2 au cours d'une digestion simulée.

Les propriétés physico-chimiques des particules de TiO_2 de grade alimentaire (E171) et des NPs photo-catalytiques de P25 (25 nm) ont été déterminées au cours d'un protocole de digestion *in vitro*, en milieux digestifs complets (sels et protéines digestives) puis en milieux digestifs sans protéines. Après chaque étape de la digestion (c'est-à-dire étape salivaire, gastrique puis intestinale), la distribution de taille et la charge de surface des particules ont été caractérisées par granulométrie et par mesures du potentiel zêta. Dans un second temps, la nature des protéines adsorbées à la surface des particules de TiO_2 a été déterminée par électrophorèse en gradient dénaturant. Les particules de TiO_2 de grade alimentaire étant assez similaires entre elles quel que soit le fournisseur, l'une d'elles a été choisie comme référence de E171 (E171-1). Afin de déterminer l'importance de la nature physicochimique de surface des particules, le lot de E171 dont les propriétés de surface sont différentes des autres lots (E171-6a, présence de silicium en surface, point isoélectrique à pH 2) a également été étudié dans ce modèle de digestion. Enfin, les particules de P25 ont également été considérées pour comparer les résultats avec ceux de la litérature.

Les ions présents dans les fluides digestifs ont un impact sur l'agglomération des particules de TiO_2 (P25 et E171). En effet, lorsque les particules sont placées dans les milieux salins de digestion (sans protéines), elles forment de plus gros agglomérats que dans l'eau au même pH (Figure 2, différence de tailles entre le milieu salivaire et la référence pH 7, le milieu gastrique et la référence pH 3, et entre le milieu intestinal et la référence pH 7). Ces différences sont attribuées à des interactions entre les particules de TiO_2 et les carbonates et phosphates présents dans les fluides digestifs (Connor & McQuillan, 1999; Domingos et al., 2010; Gong, 2001). De plus, on observe également une augmentation de la taille des agglomérats formés lorsque l'on passe dans les milieux de digestion complets (avec protéines digestives), traduisant également un impact des protéines sur l'agglomération des particules de TiO_2. On constate aussi que la taille des agglomérats augmente au fur et à mesure du processus

de digestion, de 20 µm dans la phase salivaire jusqu'à 90 µm de diamètre dans la phase intestinale.

Les protéines impliquées dans l'agglomération ont été caractérisées après extraction et séparation des particules. La comparaison des gels d'électrophorèse des extraits de digestats obtenus avec et sans particules montrent que les particules de TiO_2 ont interagi avec l'α-amylase au cours de la digestion simulée (Figure 3, bande à 52 kDa) et que l'échantillon présentant des propriétés de surface particulières (E161-6a) a également interagi avec la pepsine (Figure 3, bande à 35 kDa). Il apparait également que l'adsorption de la pepsine sur les particules de E171-6a induise une diminution de son activité enzymatique, hypothèse récemment vérifiée par Al-Hakeim & Jasem, qui ont montré une inhibition complète de l'activité de la pepsine en présence de particules de TiO_2, notamment en condition de forte force ionique, comme c'est le cas dans le fluide gastrique (SGF) (Al-Hakeim & Jasem, 2016; Zhu, Wang, Sun, Liu, & Wang, 2010).

Les particules de P25 se comportent de manière assez similaire aux particules alimentaires étudiées, avec cependant une distribution plus fine en taille.

Ainsi, les particules de TiO_2 de grade alimentaire (E171) et les NPs de TiO_2 (P25), qui sont déjà initialement agglomérées en phase aqueuse sont encore plus agglomérées dans les milieux digestifs avec formation d'agglomérats d'une taille proche de 100µm. Cependant, il est possible que ces agglomérats de très grande taille formés au cours de la digestion puissent subir des modifications physicochimiques au contact de l'épithélium et éventuellement relarguer des particules de taille nanométrique. De plus, l'étude de digestion *in vitro* ayant été menée avec les particules de TiO_2 E171, il serait à présent intéressant de procéder à ce protocole en utilisant des particules extraites de l'enrobage de chewing-gum afin de se rapprocher le plus possible des conditions réelles d'exposition via ingestion. Enfin l'impact des interactions entre les particules de TiO_2 et les protéines digestives sur leurs activités enzymatiques doit encore être déterminé, car cela pourrait avoir un effet délétère sur le processus de digestion. Ces hypothèses restent à être vérifiées. Par ailleurs, le protocole de

digestion utilisé ne prenant en compte que la physicochimie du système digestif, nous nous sommes intéressés à l'impact des particules de dioxyde de titane sur le microbiote humain.

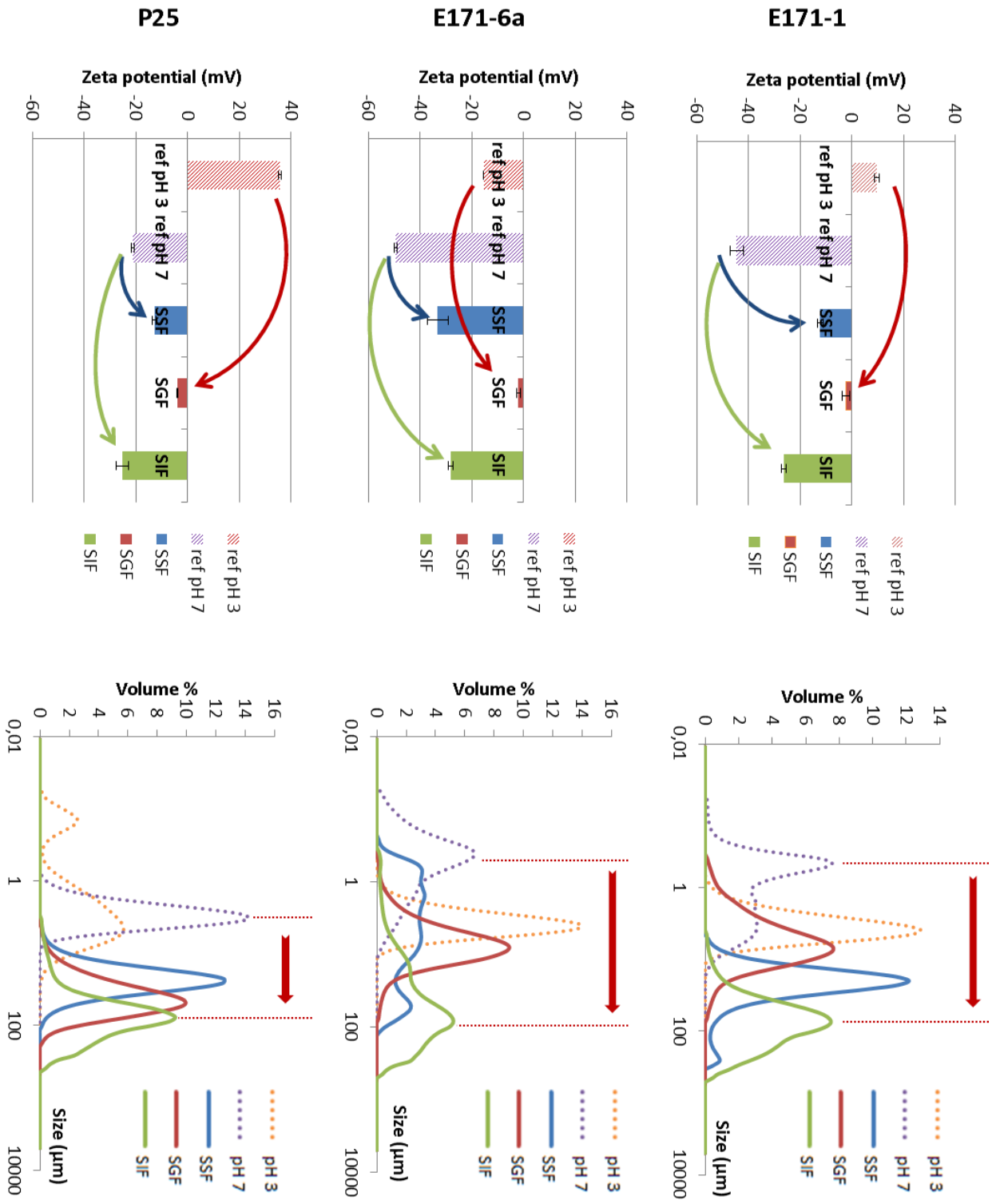

Figure 2: Distribution de taille et mesures du potentiel zêta des particules de E171-1 et E171-6a et P25 au cours du protocole de digestion simulée (SSF pour la phase salivaire, SGF pour la phase gastrique et SIF pour la phase intestinale); comparaison avec les mêmes particules dispersées dans l'eau pure à pH 3 et pH 7. Les flèches soulignent les modifications de charge de surface et de taille des agglomérats formés dans les fluides digestifs en comparaison avec les références correspondantes, à pH 3 et pH 7.

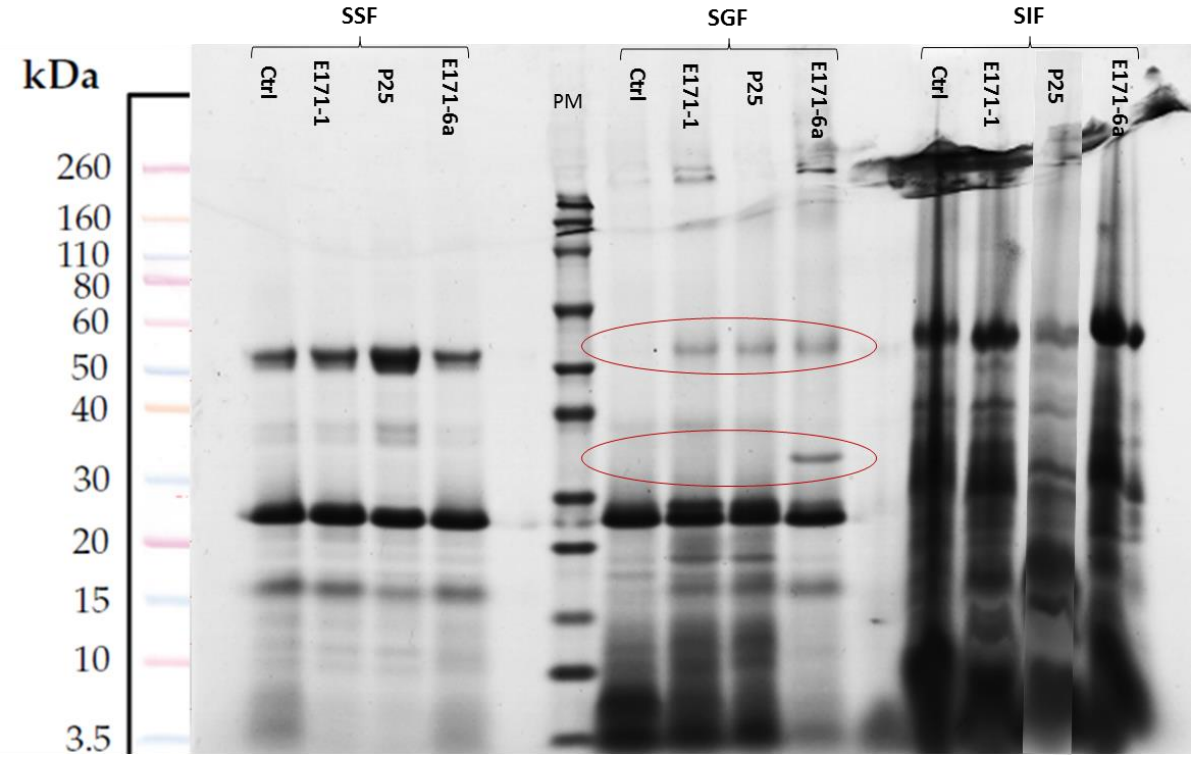

Figure 3: Gel d'électrophorèse des protéines de chaque milieu digestif après interaction avec les particules de TiO_2 E171-1 et E171-6a et P25; comparaison avec une digestion contrôle sans TiO_2. La détection de bandes supplémentaire dans l'un des échantillons en comparaison avec le contrôle traduit l'adsorption de protéines sur les particules de TiO_2 : 52 kDa α-amylase et 35 kDa pepsine.

V) Impact du TiO_2 sur la viabilité et la richesse du microbiote intestinal humain

L'impact des particules alimentaires de TiO_2 (E171) et de NPs de TiO_2 (P25, 25 nm) sur une communauté bactérienne intestinale humaine modèle a été évalué. Le consortium anaérobie, MET-1 (microbial ecosystem therapeutic-1), établi à partir des selles recueillies d'un donneur sain et contenant 33 espèces bactériennes, a été utilisé comme modèle de microbiote intestinal (Petrof et al., 2013). Il a déjà fait l'objet d'autres études, notamment avec des NPs d'argent, qui ont montré la réduction significative de la production de gaz, des modifications dans les profils d'acides gras ainsi que des changements dans l'équilibre des espèces bactériennes composant le microbiote. (P Das, Petrof, & Walker, 2015; Pranab Das, McDonald, Petrol, Allen-Vercoe, & Walker, 2014).

Dans notre cas, les deux formes de dioxyde de titane étudiées en digestion *in vitro* ont été utilisées pour exposer pendant 48h et à 37°C le microbiote intestinal à des concentrations réalistes (100 et 250 ppm, correspondant aux concentrations intestinales en TiO_2 suite à la consommation de deux types de confiseries, C5 et C1, respectivement). Afin de rendre le modèle encore plus réaliste et de déterminer l'effet d'une particule digérée, un mélange de particules alimentaires E171 et d'α-amylase (37,5 U/mL) a également été utilisé : il s'agit en effet d'une enzyme présentant une interaction forte avec TiO_2, selon l'étude de digestion précédemment menée. L'impact des particules de TiO_2 a été évalué en utilisant des tests physiologiques (mesure des gaz produits par chromatographie en phase gazeuse), biochimiques (analyse des acides gras) et moléculaires (analyses ADN : amplification de l'ADN par réaction en chaine par polymérase (PCR), PCR suivie d'une électrophorèse en gradient dénaturant (PCR-DGGE) et séquençage de l'ADN par 454 pyrotag 16S rRNA).

D'après nos résultats (Figure 4), les particules de TiO_2 n'ont pas eu d'impact sur le métabolisme du microbiote. En effet, aux deux concentrations testées, la composition (N_2, CO_2) et le volume de gaz produit par le consortium bactérien furent similaires à

ceux mesurés dans l'échantillon contrôle. De plus, les particules de TiO_2 n'ont pas eu d'impact sur la composition en acides gras des bactéries. Après exposition aux particules de E171-6a, aucune différence n'a été observée parmi les 25 acides gras majoritaires détectés par chromatographie. Seules quelques légères différences ont été observées après exposition aux particules de E171-1 et de P25, ne représentant néanmoins pas plus d'un point de pourcentage (Figure 5). Les profils obtenus en PCR-DGGE et les distributions phylogénétiques obtenues par séquençage 454 pyrotag 16S rRNA ont confirmé le faible impact des particules de TiO_2 sur la communauté bactérienne, qui se traduisait par une diminution significative mais minime du nombre de séquences correspondant à l'espèce bactérienne majeure *Bacteroides ovatus* (-10%) au profit de *Clostridium cocleatum* (+10%; $p<0.05$, Figure 6).

Les variations induites par les NPs de TiO_2 sur le consortium MET-1 peuvent être considérées comme mineures en comparaison de celles engendrées par l'ajout d'α-amylase, qui a induit des modifications majeures aux niveaux biochimiques et moléculaires. En effet, l'addition de l'amylase, qui hydrolyse une partie de l'amidon présent dans le milieu de culture, induit une modification de la composition en acides gras, réduisant la proportion des marqueurs de bactéries Gram négatives et Gram positives, et décalant les profils des acides gras saturés. De plus, les analyses ADN ont également montré une diminution significative des séquences correspondant à *Eubacterium rectale*, bactérie connue pour son utilisation de l'amidon, en faveur de *Bacteroides ovatus*.

Bien que quelques modifications mineures aient été observées suite à l'exposition du microbiote aux particules de TiO_2, nos résultats révèlent l'absence d'effet des particules de TiO_2 alimentaire (E171) ou P25 sur la viabilité et la richesse du microbiote intestinal humain, à des doses réalistes et pendant 48h. Cette étude est une première étape. Les effets cumulatifs de l'ingestion chronique doivent encore être évalués afin de conclure sur la toxicité éventuelle des NPs de TiO_2 par ingestion.

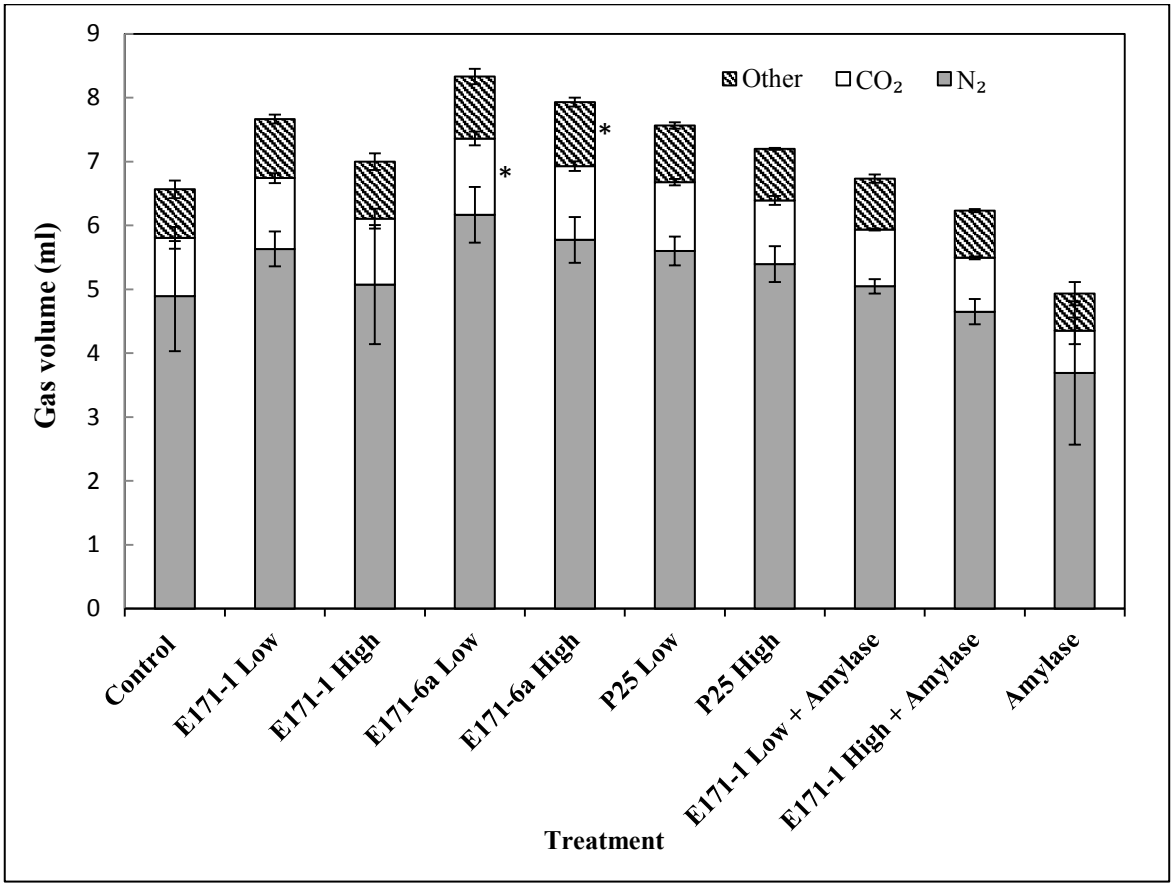

Figure 4: Dioxyde de carbone (CO_2) et diazote (N_2) récupérés à partir du gaz total généré par la communauté MET-1 après 48 h d'exposition au TiO_2 alimentaire (E171-1 et E171-6a) et aux particules de TiO_2 P25, et comparaison avec le contrôle sans particules de TiO_2 (Control). Le symbole * indique les différences significatives avec le contrôle (p <0,05).

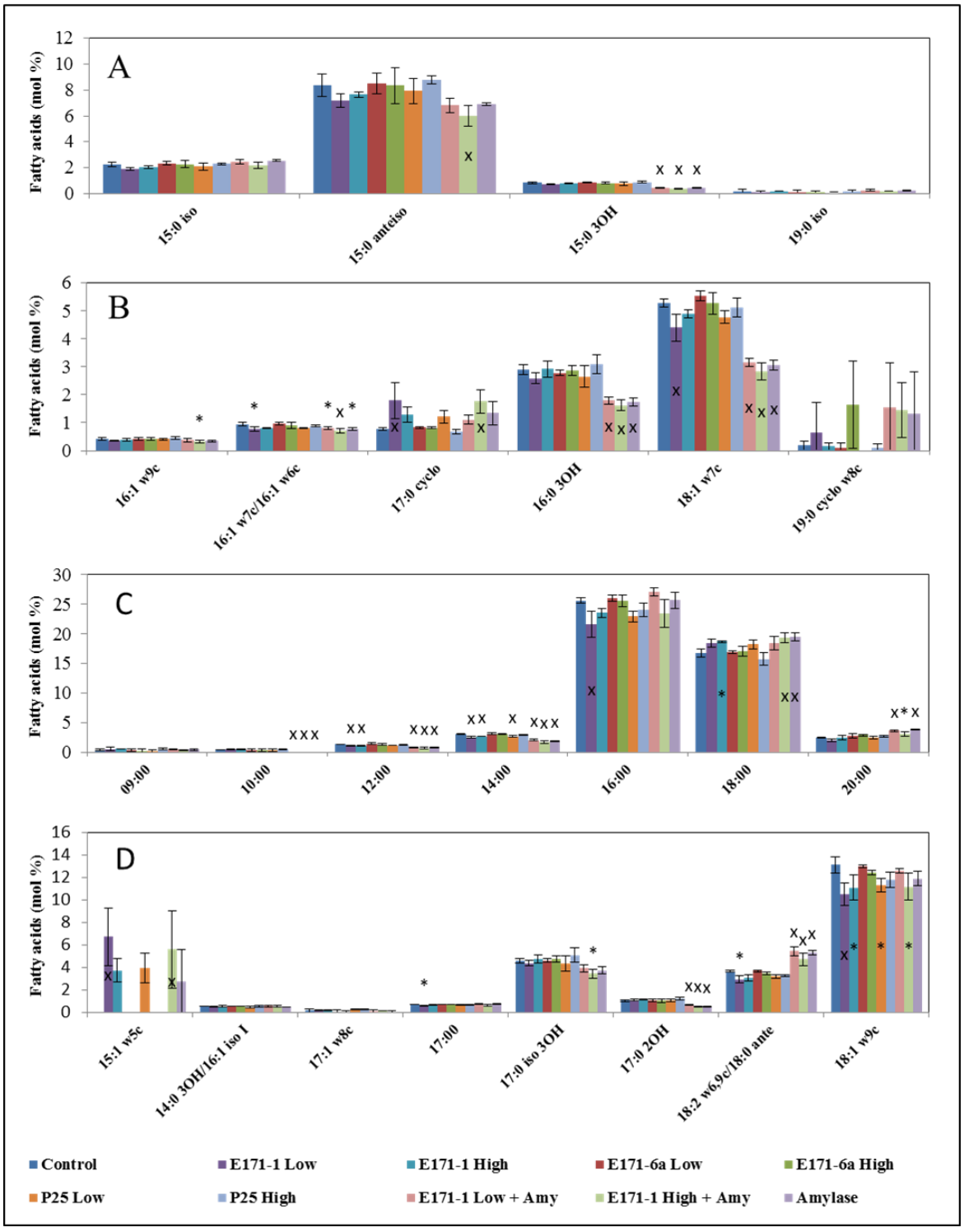

Figure 5: Quantités relatives d'acides gras extraits (mol%) dans les contrôles (sans TiO_2) et après exposition aux particules de TiO_2 à 100 (Low) et 250 (High) mg/L, respectivement. Les barres représentent les moyennes de trois analyses d'acides gras indépendantes et les écarts types. Les acides gras sont classés comme marqueurs des bactéries Gram positives (A), Gram négatives (B), acides gras saturés (C) et acides gras non classifiés (D) selon la convention (Kumar, Palmer, Shah, & Walker, 2014). Les symboles * et x indiquent des différences significatives par rapport au contrôle (p <0,05 et <0,01, respectivement).

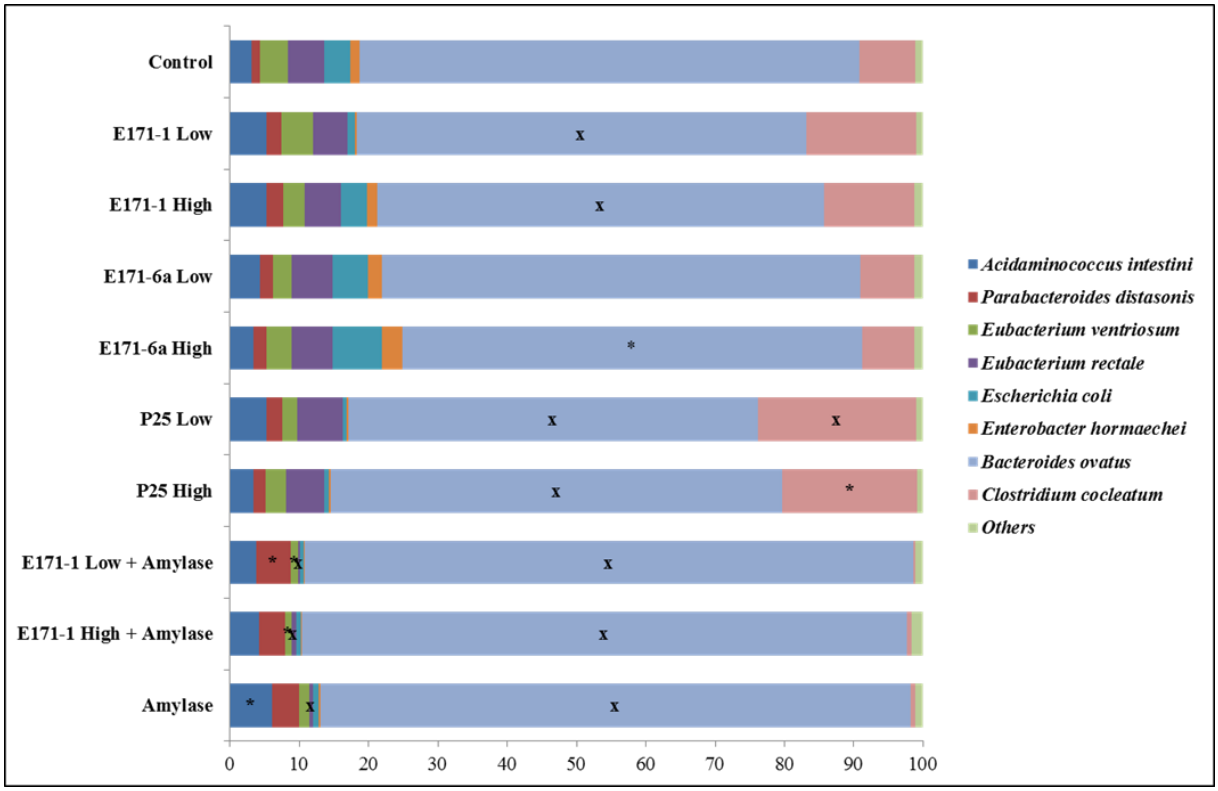

Figure 6: Composition phylogénétique des espèces du consortium MET-1, représentée sous forme de pourcentages après 48 h d'exposition à 100 ppm (Low) et 250 ppm (High) aux particules de E171-1 et E171-6a, ainsi qu'aux particules de TiO_2 P25, en comparaison avec le contrôle. Certains groupes de traitement contenaient également 37,5U / mL d'amylase pancréatique (Amylase). Les pourcentages de distribution sont basés sur les moyennes de trois échantillons (> 1% d'abondance relative, avec les espèces moins abondantes regroupées sous «Others»). Les différences significatives (p <0,05 et p<0,01) par rapport au contrôle sont indiquées par des étoiles * et la lettre x, respectivement, sur les barres de l'histogramme.

VI) Conclusions et perspectives

Ce projet de thèse avait pour objectif d'apporter de nouveaux éléments de réponse concernant l'usage des particules de TiO_2 dans l'alimentation, en déterminant leur nature physico-chimique, leur devenir dans les conditions du tractus gastro-intestinal ainsi que leur toxicité sur le microbiote intestinal humain.

Dans un premier temps, nous avons déterminé les caractéristiques physico-chimiques des particules de l'additif alimentaire E171 en comparaison avec les particules de P25, référence de l'OCDE. Au moyen de plusieurs techniques d'analyse, nos résultats ont montré que tous les échantillons de E171 analysés contiennent des nanoparticules, cependant en proportion inférieure à l'échantillon de P25 (environ 36% contre 100%), et en dessous du seuil définissant l'étiquetage en tant que nanomatériaux. Nous avons aussi comparé les particules de E171 aux particules de P25, qui sont couramment utilisées en tant que référence dans les études de toxicologie, afin d'évaluer leur pertinence en tant que modèle. Nos résultats ayant montré que les particules de E171 et de P25 sont différentes de par leurs compositions chimiques, leurs tailles ainsi que leurs chimies de surface, les particules de P25 semblent ne pas être le modèle le plus pertinent à utiliser pour étudier le devenir et l'impact des particules de TiO_2 via l'ingestion, et ce même pour mimer la fraction nanométrique. Un protocole récemment publié permettrait de séparer la fraction nanométrique du reste des particules composant le E171. (Faust, Doudrick, Yang, Capco, & Westerhoff, 2016)

L'enrobage de plusieurs confiseries (chewing-gums et bonbons) contenant du E171 a également été extrait et analysé afin d'en déterminer la teneur en TiO_2, ainsi que pour déterminer si les particules de E171 restent dans le même état physicochimique une fois intégrées dans une matrice alimentaire. Nos analyses confirment la présence de TiO_2 dans les enrobages de confiseries, entre 0,27 et 12,05 mg de TiO_2 par gramme de chewing-gum, correspondant à 16 et 34% de nanoparticules, représentant entre $1,7x10^{13}$ et $4,3x10^{14}$ nanoparticules de TiO_2 par chewing-gum. De plus, l'étude des extraits d'enrobage a montré que les particules de TiO_2 peuvent être libérées de l'enrobage pures, enrobées dans une matrice organique ou en mélange avec d'autres

particules de taille supérieure, rendant ainsi plus complexe l'étude de l'agglomération des particules de TiO_2 extraites des enrobages au cours de la digestion. Cependant, la caractérisation physico-chimique de ces extraits d'enrobages ayant montré que les particules de TiO_2 ne sont pas modifiées pendant la fabrication des chewing-gums, les particules de E171 ont été utilisées comme modèle pour la suite de l'étude.

Dans un second temps, nous avons étudié le comportement physico-chimique des particules de TiO_2 dans les fluides digestifs. Nous avons pour cela utilisé un protocole de digestion *in vitro* adapté de la littérature. Nos résultats ont montré que les particules de TiO_2 s'agglomèrent fortement au cours de la digestion, formant des agglomérats de plus de 90 µm de diamètre. Cette agglomération est due à des interactions avec les ions et protéines composant les fluides digestifs. En effet, une interaction entre l'α-amylase salivaire et les particules de TiO_2 (E171 et P25) a été détectée, ainsi qu'une interaction entre la pepsine et le E171-6a, ayant une chimie de surface différente des autres échantillons de TiO_2.

Enfin, la dernière étape de ce travail de thèse a été de déterminer l'impact toxicologique des particules de TiO_2 sur le microbiote intestinal humain. Pour cela, un modèle de communauté microbienne a été exposé à des doses réalistes de particules de E171 et de P25 (100 et 250 ppm, correspondant aux concentrations intestinales en TiO_2 suite à la consommation de deux types de confiseries). D'après nos résultats, les particules de TiO_2 n'ont pas d'impact sur la viabilité, le métabolisme et la richesse du microbiote intestinal humain, dans les conditions d'exposition testées.

Ce travail de thèse nous a ainsi permis d'avoir une meilleure connaissance de la nature physico-chimique des particules de TiO_2 alimentaire (Dudefoi et al., 2017), de déterminer leur devenir dans les conditions du tractus gastro-intestinal et de vérifier leur innocuité envers le microbiote intestinal humain.

Il reste cependant certains points à élucider afin de pleinement comprendre ce qui se passe réellement lors de l'ingestion de particules de TiO_2. L'étude de digestion *in vitro* ayant été menée avec les particules de TiO_2 E171, les résultats restent à être validés en

utilisant des particules extraites de l'enrobage de chewing-gum, afin de se rapprocher le plus possible des conditions réelles d'exposition via ingestion. De plus, l'impact des interactions entre les particules de TiO_2 et les protéines digestives sur leurs activités enzymatiques doit encore être déterminé, car cela pourrait avoir un effet délétère sur le processus de digestion. Enfin, les effets d'une exposition chronique aux particules de TiO_2 sur le microbiote intestinal humain restent à déterminer, afin de pouvoir conclure sur les risques associés à l'ingestion de particules de TiO_2.

General introduction

Titanium dioxide (TiO_2) is a white metal oxide employed as a pigment in various products such as paints, plastics, inks, papers, but also in tablets, cosmetic creams and food products. Labelled as E171 in Europe and INS171 in North America, food grade TiO_2 is used in a variety of foods including sugar confectionary, constituting the coating of chewing-gums and candies, and can be found up to 3.88 mg of TiO_2 per g of product (Chen et al., 2013; Weir et al., 2012; Yang et al., 2014). Because of its whiteness and brightness, food grade titanium dioxide is also added in some cheeses and sauces, low-fat products such as skimmed milk, ice-creams and pastries. (Skocaj et al., 2011).

TiO_2 has always been considered safe for consumption its use as a food coloring agent has been permitted in the United States since 1966 (Federal Register, 1966). However, around 36% of particles are nanoparticles (NPs) (Chen et al., 2013; Weir et al., 2012; Yang et al., 2014), i.e., particles having a diameter lower than 100 nm, and some studies showed that TiO_2 NPs can cross the intestinal barrier (Böckmann et al., 2000; Gitrowski et al., 2014; Koeneman et al., 2010), reach the blood circulation then accumulate in the liver, spleen, kidneys, and lung tissues (Fabian et al., 2008; Park et al., 2014; Pele et al., 2015; Jiangxue Wang et al., 2007; Xie et al., 2011), resulting in histopathological and physiological changes in various organs of animals (Bettini et al., 2017). Due to the classification of TiO_2 NPs as potentially carcinogenic for humans via inhalation (Group 2B, IARC), the potential toxicity of TiO_2 NPs via ingestion need to be assessed (Tassinari et al., 2014).

On the contrary of inhaled particles, ingested particles reach the intestinal cells after passing in the various digestive fluids containing many proteins and ions having affinities for titanium dioxide (Domingos et al., 2010). In such conditions, the particle surface coating and thus the NPs size distribution may change. Then, the transformation of TiO_2 particles in the digestive fluids needs to be assessed before putting TiO_2 in direct contact with intestinal cells. Another issue is the use of the OECD (Organization for Economic Co-operation and Development) reference material P25, which is a variety of TiO_2 particles generally used in the field of photo-catalysis and

whose primary size is 25 nm (Ohno et al., 2001). These particles are much smaller than food grade TiO_2 particles (Yang et al., 2014) and are differently charged in media, raising the question of their relevance in the context of food (Jovanović, 2015).

In order to reinforce the safety evaluation of food grade TiO_2 particles, their physicochemical nature and their evolution within the gastrointestinal tract needed to be investigated. This thesis project intended to answer these questions.

First, we determined whether the particles of P25 and E171 are similar or not, to confirm or infirm the solely study available (Yang et al., 2014). Our aim was to analyze their surface and volume physicochemical properties based on the recommendations provided by EFSA. We also considered TiO_2 particles extracted from the coating of chewing-gums to determine if the particles remained in the same physicochemical state once added in food products.

The next step aimed at analyzing the evolution of the physicochemical state of the particles all along the gastrointestinal tract. A standardized static *in vitro* digestion model was considered and completed to better mimic the salivary compartment, which is the first contact of TiO_2 particles with the body fluids. As no data existed regarding the fate of TiO_2 particles in digestive fluids, we studied the evolution of the physicochemical state of P25 and E171 TiO_2 after each stage of a simulated digestion: salivary, gastric and intestinal steps.

Finally, we investigated the toxicity of digested TiO_2 particles on the intestinal microbiota, as this complex ecosystem inhabiting the human gastrointestinal tract is of obvious importance for numerous aspects of human physiology from nutritional status to behavior and stress responses. (Marchesi et al., 2015; Pietroiusti et al., 2016). To study the impact of TiO_2 NPs on microbiota viability and ecological richness, a model of human intestinal microbiota produced by the University of Guelph has been exposed to different kinds of TiO_2 particles at concentrations equivalent to those found in the intestine after the ingestion of 1-2 gum or candy pieces. The impact of TiO_2 was assessed using physiological, biochemical and molecular assays.

The manuscript is organized in 3 chapters. Chapter 1 reviews the literature relevant to NPs in daily life (physicochemical properties, toxicity by ingestion), with a focus on TiO_2 particles. In Chapter 2, the materials and methods used for the characterization, the *in vitro* digestion and the toxicity assessments of TiO_2 particles are described. Chapter 3 displays the results and is divided in four parts: the first part shows the results of the physicochemical characterization of E171 and P25 TiO_2 particles. The second part presents the results related to the extraction and characterization of TiO_2 particles from chewing-gum and candies coatings. The third part focuses on the behavior of TiO_2 particles in digestive fluids. Their impact on the human gut microbiota is discussed in the fourth part. Finally, the main conclusions and outlook from this work are summarized in the last part of this manuscript.

Chapter 1: Background and state-of-the-art

I) Nanoparticles in daily life

1) Definition and interest of nanoparticles

a) Definition of nanomaterials

According to the recommendation on the definition of a nanomaterial 2011/696/EU on 18 October 2011 (EU, 2011), a nanomaterial means a *"natural, incidental or manufactured material containing particles, in an unbound state or as an aggregate or as an agglomerate and where, for 50 % or more of the particles in the number size distribution, one or more external dimensions are in the size range 1 nm - 100 nm"* (Figure 7).

As specified in the definition, NPs can be natural or anthropogenic. For example, particles coming from combustion processes like forest fires and volcanoes are natural NPs. On the opposite, anthropogenic NPs can be unintentionally produced, for example from internal combustion engines, power plants, incinerators or metal fumes, or intentionally manufactured for various applications as engineered NPs. (Oberdörster, Oberdörster, & Oberdörster, 2005) Nanomaterials can have one or more external dimensions in the size range of 1-100 nm, such as nano-films (one-dimension), nanowires and nanotubes (two-dimensions) or nanoparticles (three-dimensions). Moreover, the definition specifies that "i*n specific cases and where warranted by concerns for the environment, health, safety or competitiveness the number size distribution threshold of 50 % may be replaced by a threshold between 1 and 50 %."* This statement highlights the fact that if a material with less than 50% nanoparticles raises concerns, the threshold of 50% may be lowered down to 1% and the material would be considered as a nanomaterial.

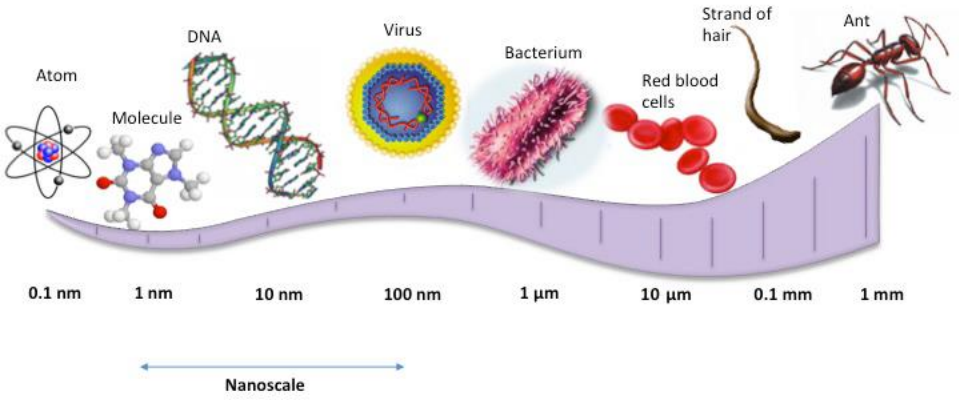

Figure 7: Visual examples of the size and the scale of nanotechnology (Busk, 2011)

b) Impact of the size on particles reactivity

When compared to the bulk material, NPs have a smaller size and so a larger specific surface area, which confer them new physicochemical properties, or enhance existing ones. For example, when the size decreases from 100 nm to 1 nm the number of particles to obtain the same volume is multiplied by 10^6 (Figure 8), and the percentage of surface atoms drastically increases (Figure 9).

The increase of specific surface area induces improvement of the material properties, or even development of new properties such as electric conductivity, elasticity, better solidity or color changing. For example in chemistry, gold is completely inactive at the micrometer scale whereas it becomes an excellent catalyst for chemical reactions at the nanoscale (Haruta, 1997).

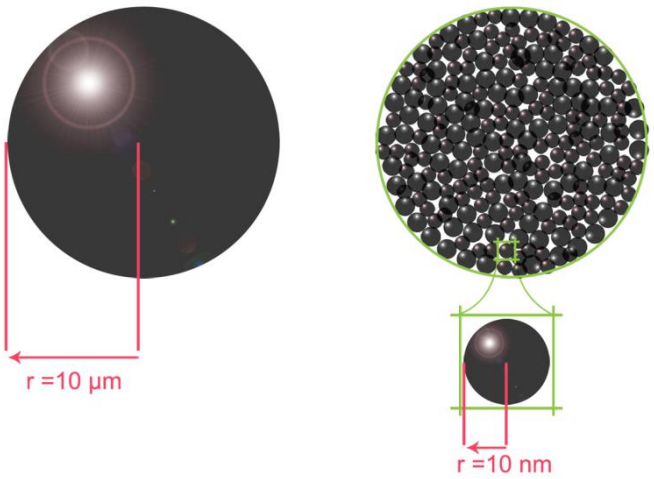

Figure 8 : Schematic representation of the change in the ratio surface/volume between a bulk microsphere and the same microsphere composed by NPs. (Domènech et al., 2012)

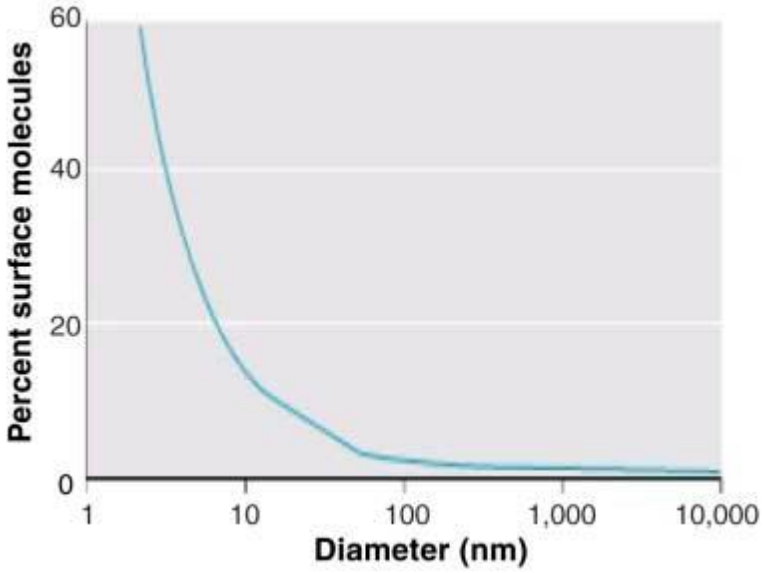

Figure 9: Percentage of surface atoms as a function of particle diameter (Nel, 2007)

2) Nanoparticles production method and estimation

Engineered nanomaterials can be prepared via two routes called bottom-up and top-down routes (Figure 10). The top-down route, mainly used by industries, consists in reducing the macroscopic particles to the nanoscale, step by step from bulk to powder

then NPs. This route is not very suitable to prepare uniform particles but leads to a bigger amount of particles. In contrast, the bottom-up methods, mainly used by laboratories, consist in forming NPs starting from soluble precursors undergoing condensation reactions in solution to form larger particles. This approach is more advantageous because it has a better chance of producing nanostructures with less defects, more homogenous chemical composition, and better short- and long-range ordering (Guduru, Niepel, Vogel, & Groth, 2011).

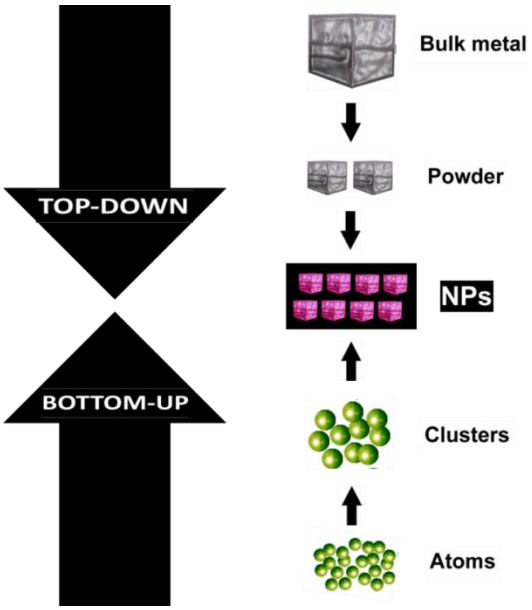

Figure 10: Bottom up and top down processes to get NPs. (Adapted from Domènech et al., 2012)

NPs can be synthetized using several methods, which may be divided into four main groups which are: (Aitken, Creely, & Tran, 2004)

- Gas phase processes (bottom up) including flame spray pyrolysis, high temperature evaporation and plasma synthesis.
- Colloidal or liquid phase methods (bottom up) in which chemical reactions in solvents lead to the formation of colloids by condensation.
- Vapor deposition synthesis (bottom up) including chemical vapor deposition.
- Mechanical processes (top down) including grinding, milling and alloying.

These methods may also be classified in three classes: physical, physicochemical and chemical routes (Figure 11). The chemical ones are generally cheaper and do not require equipment or instruments as specific as the physical methods. (Domènech et al., 2012)

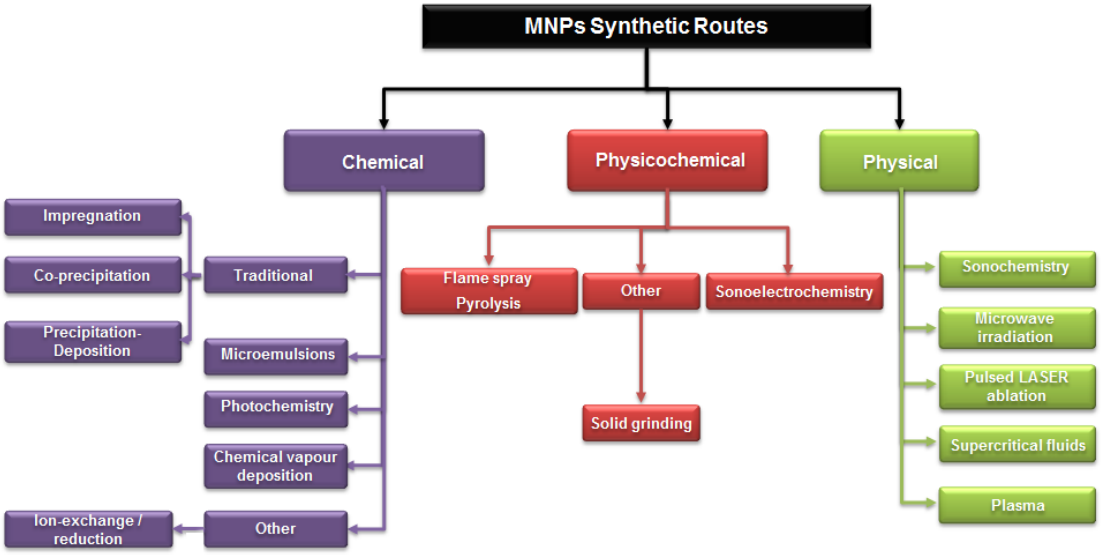

Figure 11: Physical, Physicochemical and Chemical routes for the preparation of nanoparticles (Domènech et al., 2012)

In 2012 the production of metal oxide NPs was estimated at 270,041 tons and is now estimated to increase up to 1,663,168 tons by 2020. (Future Markets Inc, 2013). Based on recent studies, the most produced NPs are TiO_2 NPs (mainly synthetized by sol-gel method and precipitation (Gupta & Tripathi, 2012)), followed by CeO_2, FeO_x, AlO_x, ZnO, and carbon nanotubes (CNT) (Piccinno, Gottschalk, Seeger, & Nowack, 2012).

3) Nanoparticles applications

a) Overview

NPs are spread in a lot of diverse industrial sectors such as the electrical, medical, personal care, agricultural and food sectors. (Chaudhry et al., 2008)

By taking advantage of their unique properties, lots of products from daily life are being improved by the addition of NPs (Table 1). Moreover, each kind of NPs can be used in different kind of applications, such as silver NPs used in paints, textiles and electronics for its antibacterial activity. The sectors of application of the main nanomaterials are listed in Table 2.

SECTORS	CURRENT AND POSSIBLE APPLICATIONS
Automobile, aeronautics and Aerospace engineering	Lighter and stronger materials, exterior paints with color effects, more brilliant, anti-scratch, anti-corrosion and anti-fouling paints; sensors optimizing engine performance; ice detectors on aircraft wings; Diesel additives allowing better combustion; more durable and recyclable tires…
Electronics and communications	High density memories and miniaturized processors; solar cells; handheld electronic libraries; high-performance computers; wireless technologies; flat screens…
Food and agriculture	Active packaging; additives: dyes, anti-caking agents, emulsifiers…
Materials	pigments; charges; ceramic powders; corrosion inhibitors; multifunctional catalysts; textiles and antibacterial and ultra-resistant coatings…
Construction industry	Self-cleaning and anti-pollution cements, self-cleaning and antifouling glass ; paintings; varnishes; glues; mastics …
Health care	Drugs and active agents; anti-allergenic medical adhesive surfaces; custom medicinal products to target specific bodies; biocompatible surfaces for implants; oral vaccines; medical imaging…
Cosmetics	Transparent sunscreens; abrasive toothpaste; makeup with better resistance …
Energy	new generation photovoltaic cells; new types of batteries; smart windows; more efficient insulating materials; hydrogen fuel storage …
Environment	Reduction in carbon dioxide emissions; ultrapure water production from seawater; more effective and less harmful pesticides and fertilizers; specific chemical analyzers …
Security	Detectors of chemical and biological agents; miniaturized surveillance systems; more accurate guidance systems; lightweight and self-repairing textiles …

Table 1: Applications of nanotechnologies and nanomaterials based on industries (Adapted from www.inrs.fr)

Nanomaterial	Product group
Nano-TiO_2	Cosmetics (incl. sunscreens)
	Coatings & cleaning agents
	Plastics
	Paints
	Cement
	Others
Nano-ZnO	Cosmetics (incl. sunscreens)
	Paints
CeO_x	Chemical mechanical planarization
	Fuel catalyst
	UV-coatings, paints
CNTs	Composites & polymer additives
	Materials
	Composites
	Batteries
Fullerenes	R&D
Nano-Ag	Paints, coatings & cleaning agents
	Textiles
	Consumer electronics & conductivity
	Cosmetics
	Medtech
	Anti-microbial coatings
Quantum dots	Light conversion for LED/OLED
	Lab use for imaging

Table 2: Examples for nanomaterials applications, adapted from (Piccinno et al., 2012)

b) Applications of nanomaterials in agronomy

NPs are used in the different parts of the agriculture, feed and food sectors all along the food production chain (RIKILT & JRC, 2014). For example, NPs are used in agriculture in order to increase the delivery of pesticides, in food packaging to detect chemicals of foodborne pathogens and in food products to improve the dispersion, bioavailability and absorption of nutrients, as a flavor enhancer or as a color enhancer. These applications and others of nanomaterials in food products are listed in Table 3 (RIKILT & JRC, 2014).

SECTORS	CURRENT AND POSSIBLE APPLICATIONS
AGRICULTURE	Nanocapsules for more efficient delivery of pesticides, fertilizers and other agrochemicals
	Nanomaterials for detection of animal and plant pathogens
	Nanomaterials for identity preservation and tracking and tracing
FOOD AND FEED	Nanocapsules to improve dispersion, bioavailability and absorption of nutrients
	Nanomaterials as color enhancers
	Nano-encapsulated flavor enhancers
	Nanotubes and nanoparticles as gelation and viscousifying agents
	Nanoparticles for selective binding and removal of chemicals and pathogens from food
FOOD PACKAGING	Nanoparticles to detect chemicals of foodborne pathogens
	Biodegradable nanosensors for temperature and moisture monitoring
	Nanoclays and nanofilms as barrier materials to prevent spoilage and oxygen absorption
	Nanoparticles for antimicrobial and antifungal surface coatings
FOOD SUPPLEMENTS	Nanoparticle suspensions as antimicrobials
	Nano-encapsulation for targeted delivery of nutraceuticals

Table 3: Examples of NPs applications in the agriculture/feed/food sector (Adapted from R Peters, Brandhoff, & Weigel, 2014)

Nanomaterials in food products can be divided into three categories: organic nanomaterials, combined organic/inorganic nanomaterials, and inorganic nanomaterials (Figure 12) (RIKILT & JRC, 2014)

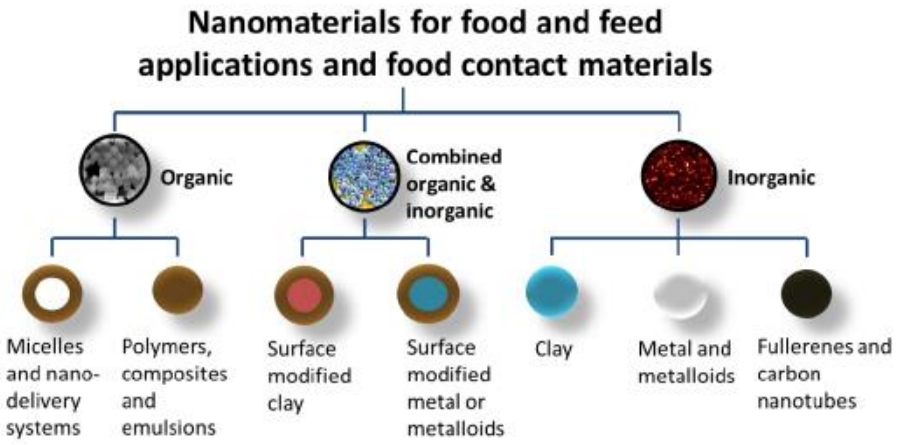

Figure 12: Types of nanomaterials for food and feed applications and food contact materials. (RIKILT & JRC, 2014)

Organic nanomaterials are used as nano-encapsulates for vitamins, antioxidants, colors, flavors and preservatives. Combined organic/inorganic NPs are interesting for making polymer/clay nano-composites with improved physical and mechanical properties. Inorganic NPs as silver, iron, calcium and magnesium, selenium, silicates and titanium dioxide, can be used as such in food and food supplements, or in combination with polymer matrices for food packaging application.

In food packaging, nano-silver and nano-zinc oxides are used for their antimicrobial activity, nano-titanium dioxide for ultraviolet protection and nano-silica for surface coating of packaging materials.

In food products, nano-silver is used in food supplements as an antimicrobial agent (http://www.nanotechproject.org). Silica (E551) has been used in food applications for many years in a form which is called synthetic amorphous silica, or SAS, and is one of the most important anti-caking agents.(R. Peters et al., 2012) Other metallic NPs are used as food or health supplements including nano-selenium (J. Xu, Yang, An, & Hu, 2007), nano-calcium (Hannig & Hannig, 2010), nano-iron (Sekhon, 2010) and colloidal suspensions of metal particles, e.g., copper, gold, platinum, silver, molybdenum, palladium, titanium, and zinc. (Bouwmeester, Brandhoff, Marvin, Weigel, & Peters, 2014)

4) Toxicity concerns

It is likely that the specific useful properties which appear at nanoscale can also lead to adverse effects on both environment and public health (Marano & Guadagnini, 2012). Some of their physico-chemical properties, linked to NPs size, make them more reactive and more toxic at nanoscale than at microscale.

All physicochemical properties are important in determining NPs toxicity (McCracken, Dutta, & Waldman, 2016). For example, the high specific surface area implies an increase of the contact area between NPs and biological surfaces, increasing the possible damaging effect of NPs in comparison to the bulk form (Pietroiusti, 2012). NPs shape, size, and agglomeration state are also very important parameters in mediating NPs toxicity, because they will modify the exposed surface and then the interaction with cells. NPs surface charge is also relevant for toxicity, as charged NPs were found to be more toxic than neutral NPs (Nel et al., 2009). Moreover, the transformation of the NPs themselves into other species plays a role in the toxicity assessment. For example, the dissolution of Ag nanoparticles (Ag(0) to Ag^{+}), is responsible for the antimicrobial nature of Ag NPs (Maurer-Jones, Gunsolus, Murphy, & Haynes, 2013; Xiu, Zhang, Puppala, Colvin, & Alvarez, 2012).

The most studied toxicity mechanism of NPs is the direct or indirect production of reactive oxygen species (ROS), generated as a result of NPs–cell interactions, or by NPs themselves (Fenton reaction). This production of oxidative species induces an imbalance between the generation of ROS and the ability of the cell to deal with them. This imbalance, called oxidative stress, causes damage to cellular components including proteins, lipids and DNA, and to subcellular organelles such as mitochondria, resulting in the activation of cellular stress-dependent signaling pathways and pro-inflammatory signaling cascades, and finally lead to cell apoptosis (blue mechanism in Figure 13) (Nel, 2007; Pietroiusti, 2012; Shang, Nienhaus, & Nienhaus, 2014).

NPs may also directly interact with membrane receptors and induce proliferation, apoptosis, differentiation, or migration (red mechanism in Figure 13)).

The nature of the corona will also mediate the interaction of NPs with the cell and determine further biological responses. By interacting with membrane receptors, the corona will allow the uptake of NPs by the cell, acting as a Trojan horse. All cellular mechanisms of nanoparticles toxicity are represented in Figure 13).

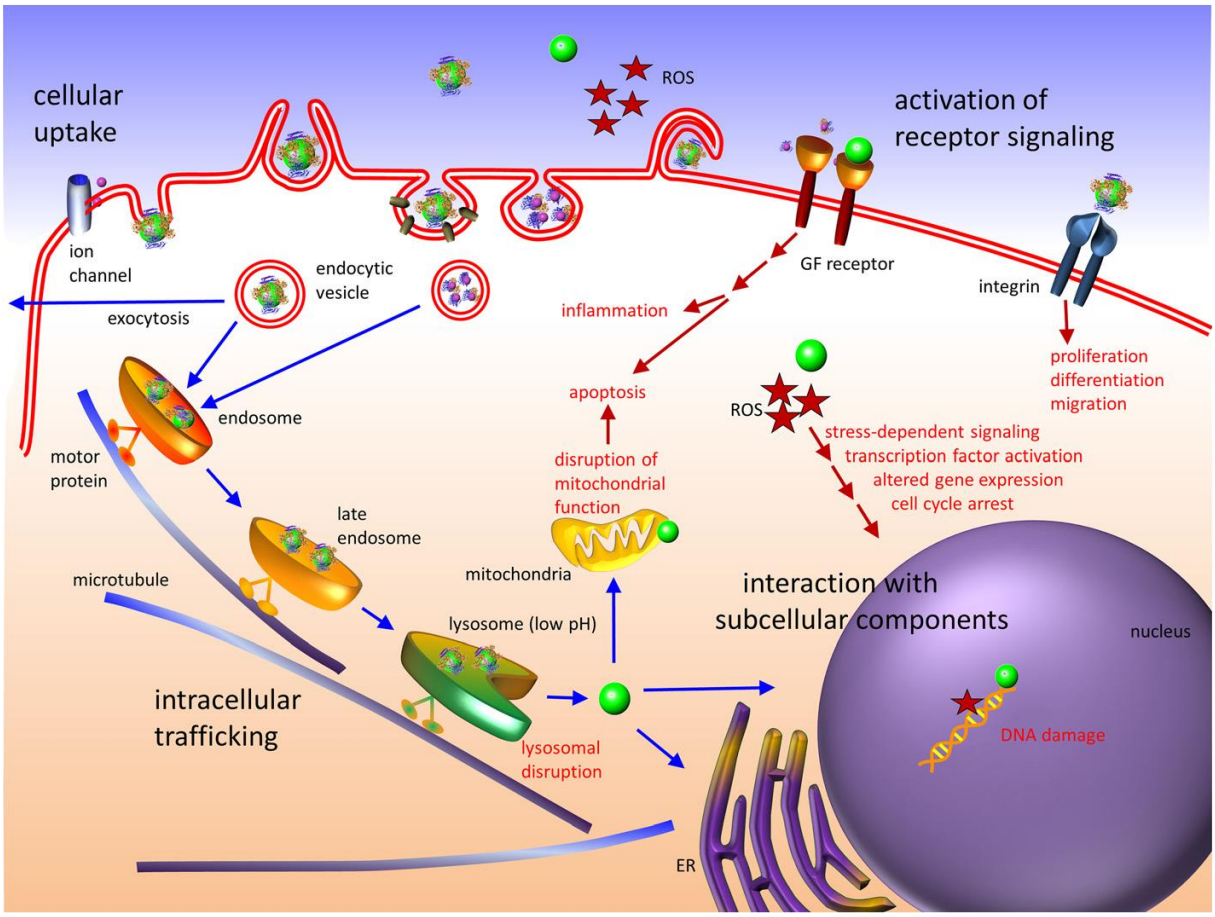

Figure 13 : Cytotoxic effects of NPs: production of ROS leading to (i) activation of cellular stress-dependent signaling pathways, (ii) direct damage of subcellular organelles such as mitochondria and (iii) DNA fragmentation in the nucleus, resulting in cell cycle arrest, apoptosis, and inflammatory response. NPs may interact with membrane-bound cellular receptors, e.g., growth factor (GF) receptors and integrins, inducing cellular phenotypes such as proliferation, apoptosis, differentiation, and migration. (Shang et al., 2014)

II) Digestion of nanoparticles

1) Digestive system overview

Once ingested, NPs will enter the digestive system, also named gastrointestinal system (GIT). The GIT is a group of organs extending from the mouth to the anus and responsible for four major functions which are the ingestion (receiving food), the digestion (breaking it down into nutrients), the absorption (absorbing the nutrients into the bloodstream), and the excretion (eliminating the indigestible parts of food from the body). The digestion process works by moving food through the GIT, beginning in the mouth with chewing and ending in the small intestine (Figure 14). As food passes through the GIT, it mixes with digestive juices, causing large molecules of food to break down into smaller molecules. The body then absorbs these smaller molecules through the walls of the small intestine into the bloodstream, which delivers them to the rest of the body. Waste products of digestion pass through the large intestine and are ejected out of the body as a solid matter called stool.

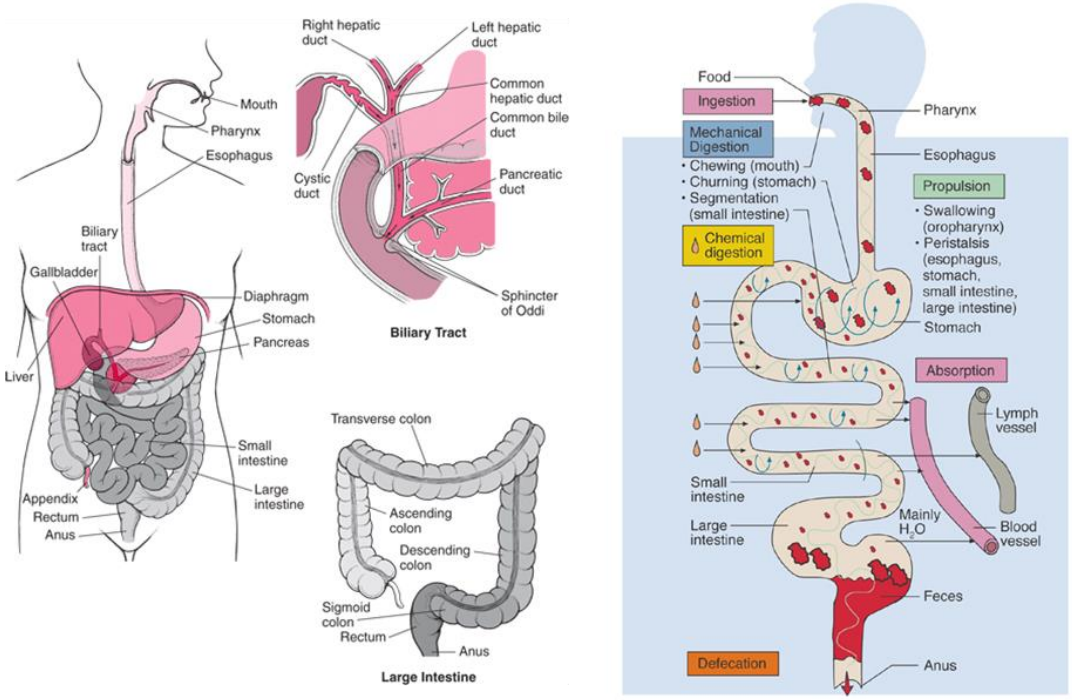

Figure 14: Digestive system overview (www.merckmanuals.com; http://faculty.sdmiramar.edu)

The digestive fluids are composed of different salts and digestive proteins at different pH values which can affect NPs surface chemistry and agglomeration. The luminal pH varies from moderately acidic in the mouth (pH about 5.5 to 6), to very acidic in the stomach (pH about 1.0 to 2.5), to neutral or slightly basic in the distal regions (pH about 6.6 in the proximal small intestine, pH about 7.5 in the terminal ileum, and pH about 6.4 in the caecum) (Alger, Momcilovic, Carlander, & Duncan, 2014). Furthermore, the pH values in each of these regions, and particularly in the mouth and stomach, vary depending on the characteristics of recently consumed foods.

The digestion process also includes bacteria from the GI tract, called gut flora, microbiome or microbiota. The gut microbiota is involved in numerous aspects of normal host physiology, from nutritional status to behavior and stress response. With an estimated surface of 200 m^2, the human gut contains between 10^{13} and 10^{14} bacterial cells (Ley et al., 2006; Mercier-Bonin, Despax, Raynaud, Houdeau, & Thomas, 2016; Sender, Fuchs, & Milo, 2016), representing a bacteria to human cell ratio of 1:1 to 10:1 (Sekirov, Russell, & Antunes, 2010). These bacteria form a complex eco-system composed by up to 36,000 bacterial species inhabiting the length and width of the human gastrointestinal tract (Frank et al., 2007). The majority of the gut microbiota is composed of strict anaerobes, with 2 dominant phyla: the *Bacteroidetes* and the *Firmicutes* (Eckburg et al., 2014).Knowing that changes in microbiota can be associated with important disease states such as obesity, diabetes, rheumatoid arthritis, and inflammatory bowel disease (Marchesi et al., 2015; Pietroiusti et al., 2016), investigations on the impact of NPs including TiO_2 NPs, on human gut microbiota are needed.

2) Uptake of nanoparticles in the GIT

Once ingested, NPs will reach the small and large intestines where the absorption of ingested materials mainly takes place. Since inorganic NPs are not digestible, they may pass through the entire length of the GI tract and be excreted. Alternatively, they may cross the intestinal epithelium with the potential of reaching all other organs of the body. The mechanism of translocation is still under debate since it depends on the particle size. Several specific mechanisms have been identified: the transcellular transport through an epithelial cell (transcytosis), the paracellular transport between adjacent epithelial cells and the transcytosis through microfold (M) cells lining intestinal Peyer's patches, which is the major pathway implicated in the uptake of TiO_2 NPs, due to their agglomeration state (Bellmann et al., 2015; Brun et al., 2014; E. Fröhlich & Roblegg, 2016; Hagens, Oomen, de Jong, Cassee, & Sips, 2007; Higashisaka, Yoshioka, & Tsutsumi, 2015; Lomer, Thompson, & Powell, 2002; Martirosyan, Polet, Bazes, & Sergent, 2012; McCracken et al., 2016; Powell, Faria, Thomas-McKay, & Pele, 2010) (Figure 15). Moreover, in the case of intestinal disease where the integrity of the epithelial barrier is compromised, NPs may freely cross through regions of epithelial damage (Figure 16, D), or by increased paracellular transport as a consequence of dysregulation of intercellular tight junctions (Figure 16, E) (McCracken et al., 2016).

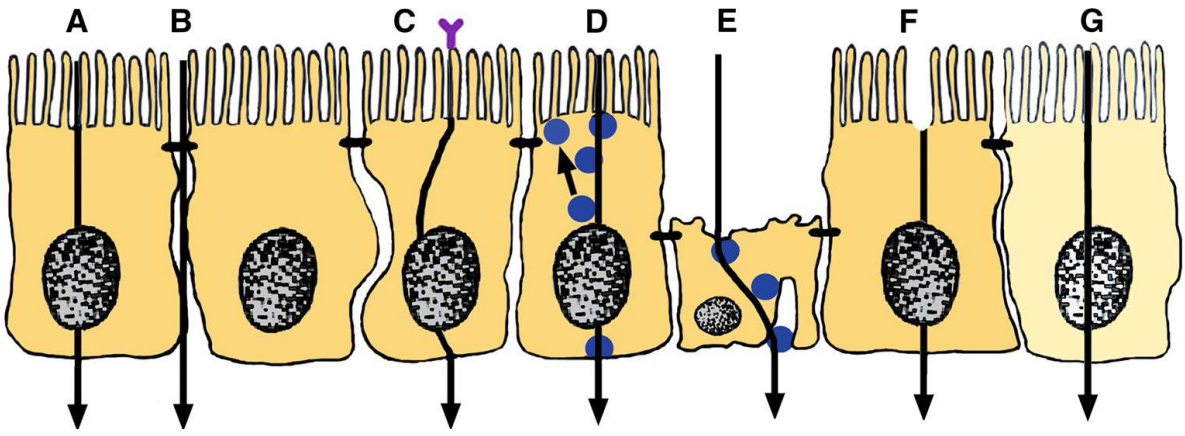

Figure 15: Mechanisms of nanoparticles to cross the intestinal barrier. Diffusion (A), paracellular uptake through intercellular junctions (B), receptor-mediated uptake (C), unspecific absorption by endocytosis with subsequent excretion or transport across the cell/transcytosis (D), M cell-mediated uptake with delivery to intestinal lymph follicles (E), plasma membrane damage (F), persorption via extruded/ dead cells (G) (E. E. Fröhlich & Fröhlich, 2016)

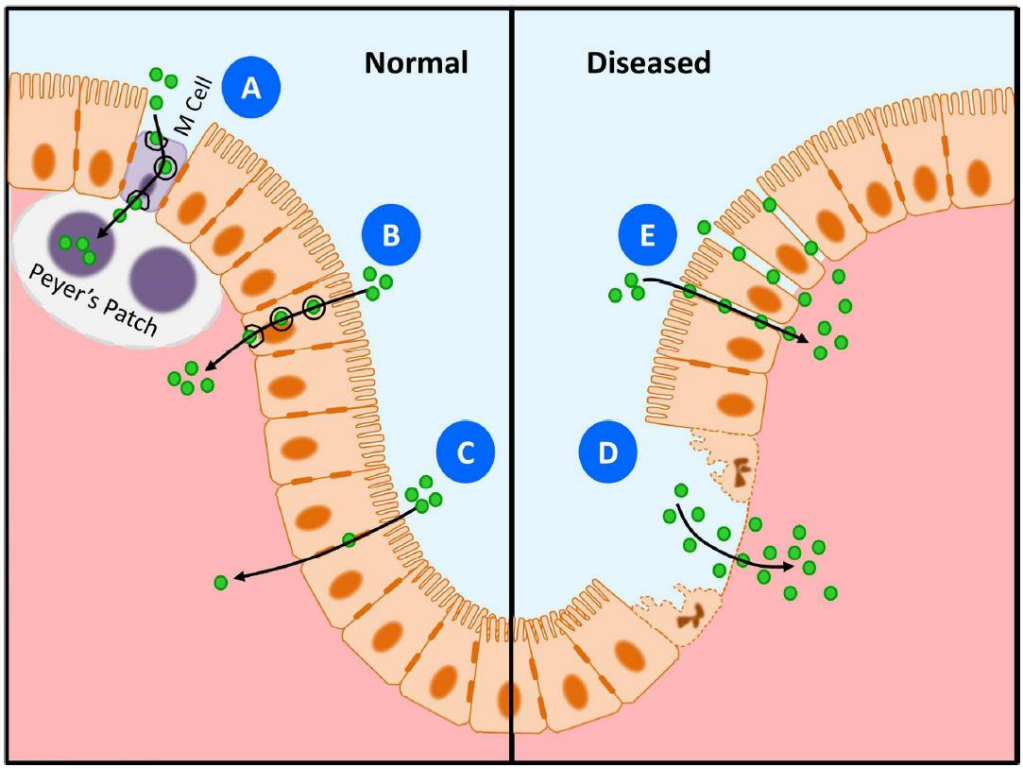

Figure 16 : Mechanisms by which ingested NPs can cross the epithelial barrier in healthy and diseased intestine. (A) Transcytosis to Peyer's patch by M cells; (B) Transcytosis through epithelial cells; (C) paracellular transport through intercellular tight junctions; (D) unrestricted migration through damaged epithelium; (E) paracellular transport through dysregulated intercellular tight junctions.(McCracken et al., 2016)

The uptake of NPs is also determined by their own physicochemical properties such as size, surface charge, hydrophobicity (des Rieux et al., 2005), and dispersion/agglomeration state (Higashisaka et al., 2015). When NPs enter the body, they will not directly interact with cell membranes, but firstly interact with biological molecules such as proteins or lipids, forming a corona which will mediate the fate of NPs (Mercier-Bonin et al., 2016; Shang et al., 2014). The binding of macromolecules forming this corona will also affect the biological action of NPs (Bergin & Witzmann, 2013; Pietroiusti, 2012). By interacting with membrane receptors, the corona will allow the uptake of NPs by the cell, acting as a Trojan horse (Figure 17) (Shang et al., 2014).

After crossing the epithelial barrier, NPs could reach all other organs of the body via the systemic circulation and interact with tissus with potential deleterious effects. For example, NPs may accumulate in the different organs, induce inflammatory responses or toxicity by oxidative stress, resulting in cell death. The different mechanisms of NPs toxicity are described in the next chapter.

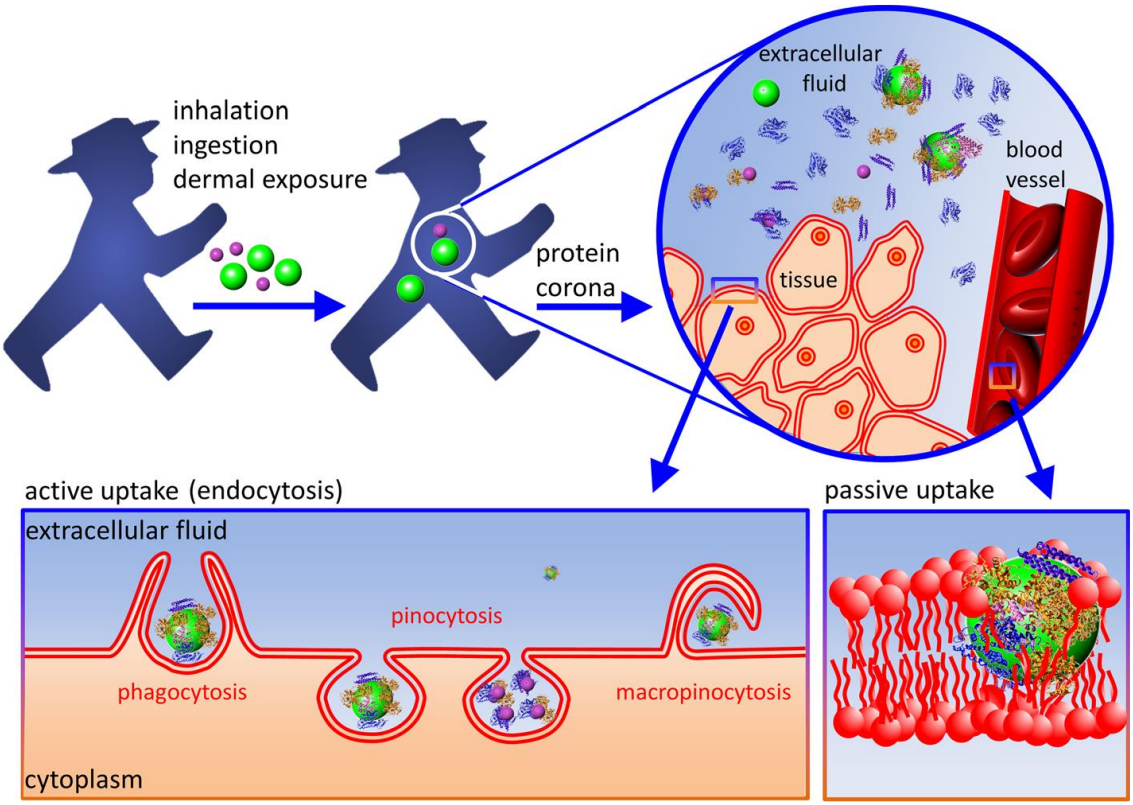

Figure 17 : NPs passive and active uptake, formation of protein corona in the extracellular fluid. (Shang et al., 2014)

3) Models to study NPs fate and toxicity via ingestion

In order to evaluate the toxicity regarding the exposure of workers to NPs, the toxicity of TiO_2 via inhalation was extensively studied, mainly with P25 particles as a reference (NM105). In the recent report of the Organization for Economic Co-operation and Development (OECD) on titanium dioxide, more than 40 toxicological studies were reported, with 37 studies about the toxicity via inhalation. Most of the studies showed an inflammatory response after TiO_2 exposure (OECD, 2015). However, toxicity after oral administration is more rarely studied. Different types of models are currently

being used in order to assess the bioaccessibility, digestion, mucoadhesion, bioavailability and excretion of food-relevant engineered NMs (Figure 18).

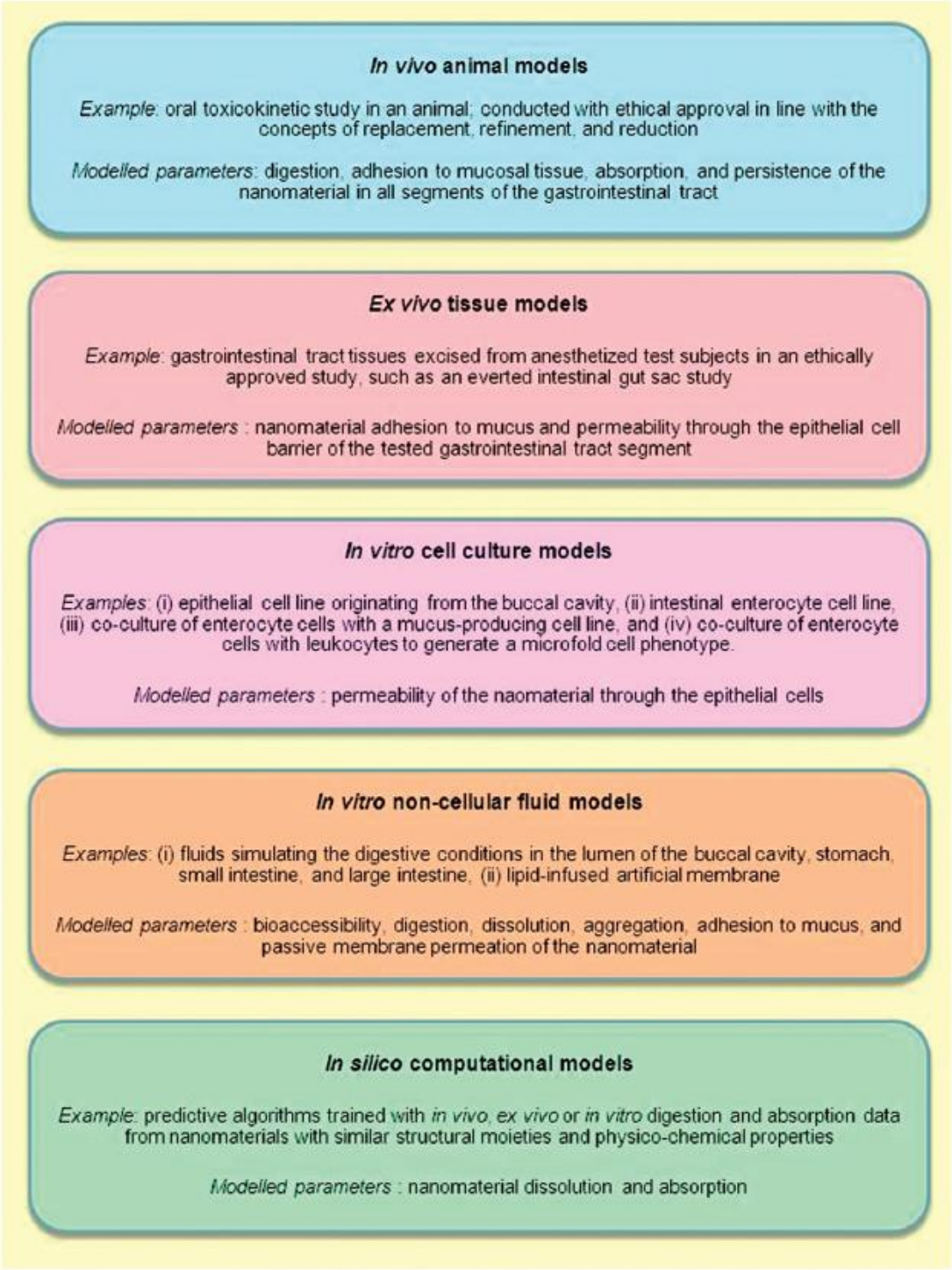

Figure 18: Categories of gastrointestinal tract models for digestion and absorption assessment of NMs released from food (Lefebvre et al., 2015)

Humans and other mammalian species having similar processes of digestion and absorption of nutrients, *in vivo* animal models have historically been used to perform toxico-kinetic studies (Table 4). These models present the advantage of considering the impact of NMs on living animals, and can be considered as the more realistic models. However, ethical consideration and approval are required for the use of animals. Moreover, these models don't have a high throughput and the results are sometimes not accurately transposed to humans (Lefebvre et al., 2015).

Model	Species	Characteristics and applications for conventional chemicals	Limitations	References on conventional uses
Toxicokinetic feeding or gavage studies	Primarily rat, mouse, hamster or guinea pig, unless another species such as pigs or primates is required for regulatory purposes	Assesses systemic absorption, excretion, and persistence of the chemical	Gavage does not represent a realistic exposure scenario; recovery and quantification of administered compounds in animal tissues is a challenge; some species do not accurately predict chemical bioavailability in humans	(OECD, 2010)
In situ intestinal perfusion	Rats or other species	Cannulation of both ends of a segment of the gastro-intestinal tract in a live, anesthetized subject allows infusion of a solution and collection of the perfusate at the distal end; determines permeability through the gastrointestinal tract wall	Requires surgery and anesthesia; can result in abnormal transit times or paralysis of the bowel; digestion is not modeled; not a high throughput model	(J. S. Kim et al., 2006; Lennernas, Lee, Fagerholm, & Amidon, 1997)

Table 4: In-vivo models commonly used for digestion and absorption assessments of NMs, adapted from (Lefebvre et al., 2015)

Ex vivo models are used to assess chemical permeability and consist in the use of tissue samples excised from an anesthetized organism and maintained under conditions supporting certain aspects of normal function. These models allow higher throughputs than *in vivo* models, but suffer the disadvantage of lacking digestive juices (Table 5) (Lefebvre et al., 2015).

Model	Species and tissue of origin	Characteristics and applications for conventional chemicals	Limitations	References on conventional uses
Everted gut sac	Excised intestinal segments from rat or other species	The intestine is everted, ligated at both ends and cultured in an oxygenated nutrient solution; adhesion of an administered compound to the outer mucus layer and permeability through the tissue to the inside of the sac is measured; relatively simple and inexpensive methodology	Careful tissue handling is critical to avoid mechanical damage; appropriate culture conditions must be used to maintain tissue viability; the static fluid in the serosal compartment does not accurately model *in vivo* circulation	(Alam, Al-Jenoobi, & Al-Mohizea, 2012)
Transmucosal perfusion through isolated mucosa	Mucosal layer isolated from biopsies from the buccal cavity or intestine of rat, pig or other species	Perfusion device with a donor and receiver chamber, such as an Ussing chamber or Franz diffusion cell, determines permeability through the mucosal layer; results compare favorably to human data, particularly for passively absorbed substances	Tissue viability declines rapidly	(Roblegg et al., 2012; Rozehnal et al., 2012)

Table 5: Ex-vivo models commonly used for digestion and absorption assessments of NMs, adapted from (Lefebvre et al., 2015)

In vitro cell models are commonly used in chemical risk assessment and consist in the use of various cell lines originating from different segments of the gastro-intestinal tract, in order to screen specific mechanisms of epithelial permeability. These methods can be used in a high-throughput manner to replace in vivo studies (Table 6) (Lefebvre et al., 2015).

Model	Species and tissue of origin	Characteristics and applications for conventional chemicals	Limitations	References on conventional uses
TR146 cells	Human buccal carcinoma	Epithelial origin; forms a multi-layered squamous tissue in culture; a model of chemical permeability through the buccal epithelium	Transport mechanisms require further characterization	(Birgit J. Teubl et al., 2013)
Caco-2 cells	Human colorectal carcinoma	Widely used model of small intestine enterocytes; develop tight junctions, polarization, brush border enzymes and membrane transporters that are responsible for the active uptake of chemicals	Cells vary in phenotype and function according to culture conditions; tight junction permeability is lower than in humans; expression level of some active transporters differs from the human intestine; lacks mucus	(H. J. Kim, Huh, Hamilton, & Ingber, 2012; Prieto et al., 2010; Sambuy et al., 2005)
T84 cells	Human colon carcinoma cells that had metastasized to a pulmonary tumor	Less prone to differentiation than Caco-2 cells; an ideal model of the colon since the cells are capable of regulated chloride secretion and can secrete mucus	Few microvilli on the apical membrane; relatively low monolayer permeability	(Donato et al., 2011)
2/4/A1 cells, IEC-6 cells, or IEC-18 cells	Rat intestinal epithelial cells	Good predictors of paracellular permeability and passive transport in the human duodenum	Lack several active transporters and efflux systems; a poor model of active transport	(Tavelin et al., 2003; Thomas & Oates, 2002; Versantvoort et al., 2002)
Caco-2 with HT29 cells	Human colorectal carcinoma cell lines	Co-culture incorporates a mucus layer on the enterocytes and enhances paracellular permeability	The availability of different cell sub-clones results in interlaboratory variability	(Chen, Elisia, & Kitts, 2010; Walter, Janich, Roessler, Hilfinger, & Amidon, 1996)
Caco-2 with Raji B cells, or Caco-2 with Peyer's patch lymphocytes	Human colorectal carcinoma cells in combination with human Burkitt's lymphoma cells or murine Peyer's patch lymphocytes	Co-culture induces a fraction of the Caco-2 cells to develop the morphology of Peyer's patch epithelial micro-fold cells, including few micro-villi and a soft mucus layer	Variations in primary lymphocyte preparations may influence co-culture characteristics; quantitative correlation to human uptake not fully understood	(des Rieux et al., 2007; Tyrer et al., 2002))
Gut-on-a-chip	Human colorectal carcinoma	Two fluidic channels separated by a Caco-2 monolayer, with microcircuitry to detect absorption of substances	Cells vary in phenotype and function according to culture conditions; tight junction permeability is lower than in humans; expression level of some active trans-porters differs from the human intestine; lacks mucus	(H. J. Kim et al., 2012; Vergères et al., 2012)

Table 6: In-vitro cell culture models commonly used for digestion and absorption assessments of NMs, adapted from (Lefebvre et al., 2015)

In silico programs are complex computational algorithms designed to predict how novel substances will behave in humans by extrapolating available data from *in vivo*, *ex vivo* and *in vitro* models (Table 7) (Lefebvre et al., 2015)(Bellmann et al., 2015).

Model	Capabilities for conventional chemicals	Limitations	References on conventional uses
Compartmental absorption and transit	The dissolution and bioavailability of chemicals in different compartments of the human gastrointestinal tract is modeled based on inputted solubility and permeability data on that chemical from *in vivo*, ex vivo *or in vitro* studies; can incorporate food effects and physiological inter-individual variability	Uses generalized mathematical models; prediction of intrinsic solubility is a challenge	(Bolger, Lukacova, & Woltosz, 2009; Jamei et al., 2009; Sinhaa et al., 2012; Sugano, 2009; L. X. Yu & Amidon, 1999)
Statistical machine learning and Quantitative Structure Property Relationship	Prediction of human intestinal chemical permeability or bioavailability, based on the observed or calculated physicochemical properties of the molecule; trained with existing permeability data from similar molecules in the human intestine or in Caco-2 cells	Molecular descriptor selection is algorithm- and descriptor software package- dependent, leading to variability in prediction results among methods; training data sets limit the applicability domain; relies on correlations with property values only, not on structural features	(Ahmed & Ramakrishnan, 2012; Linnankoski, Ranta, Yliperttula, & Urtti, 2008)
Quantitative Structure- Activity Relationship	Toxicokinetic database that predicts human intestinal absorption based on chemical descriptors or fingerprints in 1-, 2-, and 3-dimensions; computes from patterns of chemical fragments or substructural features; uses multiple algorithmic techniques and decisiontree analysis	Training data sets limit the applicability domain; quality of training sets vary; different validation methods lead to different predictive performance characteristics	(Moda & Andricopulo, 2012; Suenderhauf, Hammann, Maunz, Helma, & Huwyler, 2011; Winkler et al., 2013)

Table 7: In-silico models commonly used for digestion and absorption assessments of NMs, adapted from (Lefebvre et al., 2015)

Finally, *in vitro* fluid models are used to simulate the physicochemical conditions occurring during the digestion process. However, digestive fluids are complex mixtures which are hard to reproduce *in vitro*. From the buccal cavity to the stomach, the small intestine and the large intestine, the physicochemical parameters such as ionic strength, pH, digestives enzymes, bile, and transit time are different. *In vitro* fluid models can be used to assess the bioaccessibility, stability, dissolution and aggregation of digested NMs (Table 8) (Lefebvre et al., 2015). Due to the variability in the currently

used *in vitro* digestion protocols, from a simple pH adjustment (Axson et al., 2015) to a complex mixture of salts and digestive enzymes (Chen et al., 2013; R. Peters et al., 2012; Song et al., 2015), a recent review stated on a standardized *in vitro* digestion protocol (Minekus et al., 2014). This protocol consists in 3 steps which are the salivary, gastric and intestinal steps described in Figure 19. Each step corresponds to a simulated digestive fluid, all with different salt and enzyme compositions. However, this protocol does not include some proteins which we consider of interest, such as lactoferrin, lysozyme and mucin which are known to interact with TiO_2 particles (Kathiravan, Jhonsi, & Renganathan, 2011; Lori & Nok, 2004).

Model	Characteristics and applications for conventional chemicals	Limitations	References on conventional uses
Static digestion models	Synthetic fluids simulate the enzymatic and chemical digestive conditions in the various compartments of the gastrointestinal tract	Lack the mechanical forces that contribute to digestion *in vivo*; metabolites accumulate and can interfere with digestion	(Guhmann et al., 2013; Versantvoort, Oomen, Van De Kamp, Rompelberg, & Sips, 2005)
Dynamic digestion models	Synthetic digestive fluids are mixed and propelled by mechanical forces similar to those encountered *in vivo*; bioaccessibility and digestion are modeled for the various compartments of the gastrointestinal tract	Specialized equipment required to generate the physical forces	(McAllister, 2010; Minekus et al., 1999)
Natural and synthetic mucus	Isolated gastrointestinal mucus incubated *in vitro*; models mucoadhesion and permeation through the mucus	Variations in mucus source and preparation can influence characteristics	(Crater & Carrier, 2010)
Artificial membrane permeability assays	Non-cellular synthesized membrane on a filter support models the cell membrane; lipid composition can be specified; passive transcellular permeability is modeled; both hydrophilic and hydrophobic compounds can be applied	Membrane lacks pores and transporter proteins; does not model active transport or paracellular permeability	(Reis, Sinkó, & Serra, 2010)

Table 8: In-vitro fluid models commonly used for digestion and absorption assessments of NMs, adapted from (Lefebvre et al., 2015)

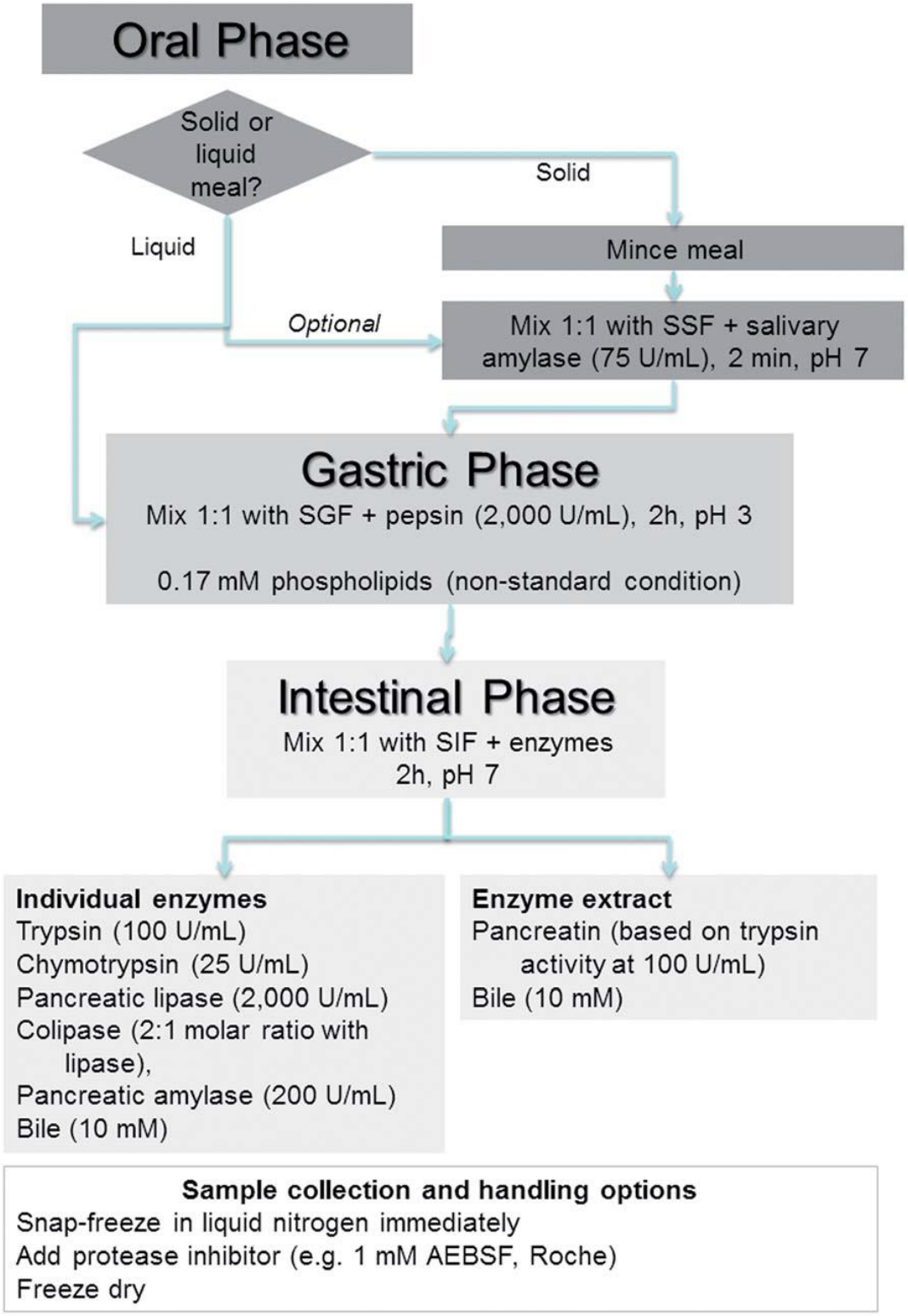

Figure 19: Standardized in vitro digestion protocol (Minekus et al., 2014) with SSF, SGF and SIF for Simulated Salivary Fluid, Simulated Gastric Fluid and Simulated Intestinal Fluid, respectively. Enzyme activities are in units per mL of final digestion mixture at each corresponding digestion phase.

III) Titanium dioxide TiO_2

1) Main applications

Titanium dioxide (TiO_2) is a white metal oxide commonly used in various applications for its whiteness and brightness, UV light resistance and photocatalytic properties (Table 9).

Due to its brightness and very high refractive index (2.4-2.7), TiO_2 is used as a white pigment in various products such as paints and coatings, including glazes and enamels, plastics, paper, inks, fibers, foods (coating of gums and candies), pharmaceuticals and cosmetics (toothpastes and sunscreens) (Mercier-Bonin et al., 2016; Weir et al., 2012; Yang et al., 2014). TiO_2 is also used for its UV light resistance properties, in plastics to prevent the discoloration and in sunscreens to protect the skin, as a blocker of UV. Three photo-induced phenomena can occur at the surface of TiO_2, namely photo-induced super-hydrophilicity, photocatalytic activity, and photovoltaics properties, all with various applications (Carp, 2004). TiO_2 is also used as gas sensor for determination of oxygen and CO concentrations (Dutta et al., 1999; Logothetis & Kaiser, 1983) due to the dependence of the electric conductivity on the ambient gas composition. Finally, TiO_2 is used as a biomaterial (as coating for blood contacting implants) because of its hemocompatibility with the human body. (Maitz, Tsyganov, Pham, & Wieser, 2003; Zhang, Zheng, & Chen, 1998).

In photocatalytic applications such as self-cleaning construction materials (concrete or mineral plasters), or as UV-B absorber for inorganic formulations, the kind of TiO_2 used are P25 particles. These particles are also suitable for the construction of efficient dye-sensitized solar cells, can be added to improve the flammability protection of silicone vulcanizates or as bonding agent, sintering additive, or structural component in ceramics (http://corporate.evonik.com). They serve as reference nanomaterial for the OECD, referred to as NM105, and are widely used as a model of TiO_2 particles in toxicological studies (OECD, 2009; Orts-Gil, Natte, & Österle, 2013; Rasmussen et al., 2014). In terms of physical chemistry, P25 is pure titanium dioxide, composed of 100%

of NPs with a primary size around 25nm and tend to agglomerate into large agglomerates in ultrapure water depending on sonication protocols and durations (up to 210 nm (Yang et al., 2014)). P25 particles are a mixture of 85% anatase and 15% rutile crystal structure, with a specific surface area of 50m²/g and an IEP at pH 6.6 (Guiot & Spalla, 2013; Kosmulski, 2009).

Properties	Products
Brightness and high refractive index	Paints, Plastics, Paper, Inks, Fibers
	Foods (gums and candies)
	Pharmaceuticals
	Cosmetics (toothpastes)
UV-light resistance	Plastics
	Sunscreens
Photocatalytic properties	Medical devices
	Food preparation surfaces
	Air conditioning filters
	Sanitary ware surfaces
Photo-induced super-hydrophilicity	Anti-fogging coatings
	Self-cleaning windows
Photovoltaic properties	Light-emitting diodes
	Liquid crystal displays (LCDs)
	Electrodes for plasma displays
Hemocompatibility	Bone substituent

Table 9 : Examples for TiO_2 NPS application (adapted from (Carp, 2004; Dutta et al., 1999; Logothetis & Kaiser, 1983; Maitz et al., 2003; Weir et al., 2012; Zhang et al., 1998)

TiO_2 food additive is a color additive in food, food supplements and medicinal products and is referred to as E171 in Europe and INS171 in North America. It is mainly used in sugar confectioneries (Figure 20), constituting the coating of sweets and chewing-gums, up to 3.88 mg TiO_2/g food. (Athinarayanan, Alshatwi, Periasamy, & Al-Warthan, 2015; Chen et al., 2013; Faust, Doudrick, Yang, Westerhoff, & Capco, 2014; Lomer, Thompson, Commisso, Keen, & Powell, 2000; Weir et al., 2012) It is also added in some cheeses and sauces, low-fat products such as skimmed milk, ice-creams and pastries. (Skocaj et al., 2011; Weir et al., 2012). In tablets such as medicine and food supplements, TiO_2 is added up to 3.6 mg/g, resulting in a total daily consumption from food and food related products estimated at 1.28 milligrams per kilogram of body weight per day (mg/kg bw/day). (EFSA, 2004) The amount of TiO_2 particles consumed on a daily basis also differs depending on areas and age. For example, the American population consumes around 0.2-0.7 mg TiO_2/kgbw/day while the UK population consumes around 1 mg TiO_2/kgbw/day. Moreover, TiO_2 being particularly present in products such as candy and sweets, children under 10 years old are much more exposed to TiO_2 particles than adults, with an estimation of 1-2 mg TiO_2/kgbw/day for American children and 2-3 mg TiO_2/kgbw /day for children in the UK (Weir et al., 2012).

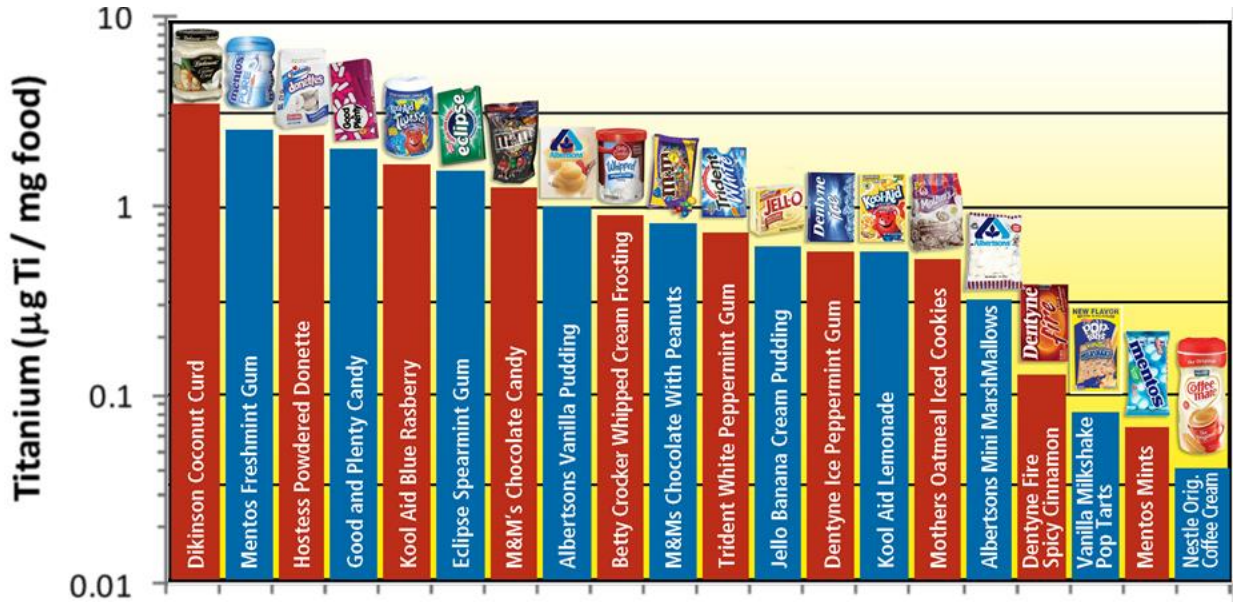

Figure 20: Normalized Ti concentration in food products. (Adapted from Weir et al., 2012)

2) Main physicochemical characteristics

a) Crystalline phases

Titanium dioxide exists in crystalline and amorphous forms. The three most studied crystalline forms of TiO_2 are anatase, rutile and brookite (Figure 21, Figure 22 and Figure 23, (Diebold, 2003; Moellmann, Ehrlich, Tonner, & Grimme, 2012)). The structure of both anatase and rutile is tetragonal whereas the brookite structure is orthorhombic. In all the crystalline forms, each Ti^{4+} is surrounded by 6 oxygen ions forming an irregular octahedron. The difference between anatase and rutile lies in the assembly of these octahedrons and the distortion of each of them. In the rutile structure each octahedron is in contact with 10 neighbors (two sharing edge oxygen pairs and eight sharing corner oxygen atoms) while in the anatase structure each octahedron is in contact with eight neighbors (four sharing an edge and four sharing a corner). The octahedral linkage in brookite is such that three edges are shared per octahedron.

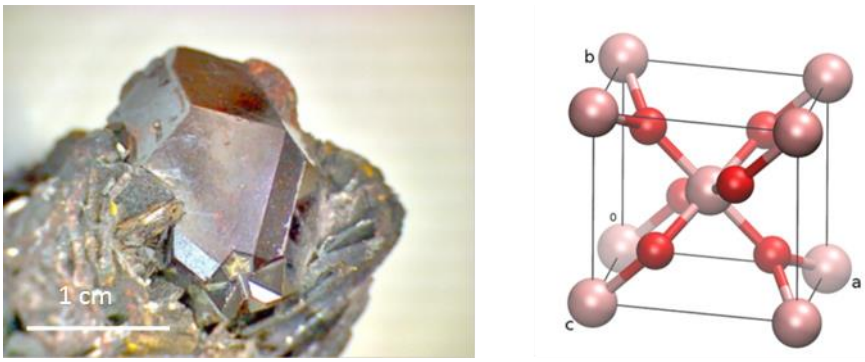

Figure 21: TiO_2 rutile macroscopic picture and crystalline structure (red for O^{2-} and grey for Ti^{4+}) (Moellmann et al., 2012)

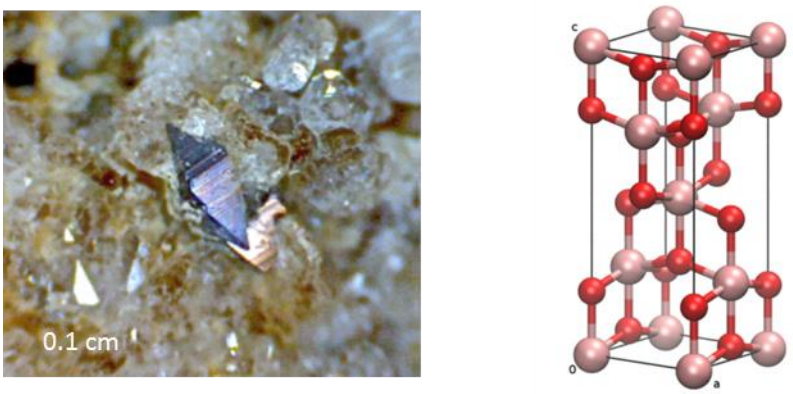

Figure 22: TiO_2 anatase macroscopic picture and crystalline structure (red for O^{2-} and grey for Ti^{4+}) (Moellmann et al., 2012)

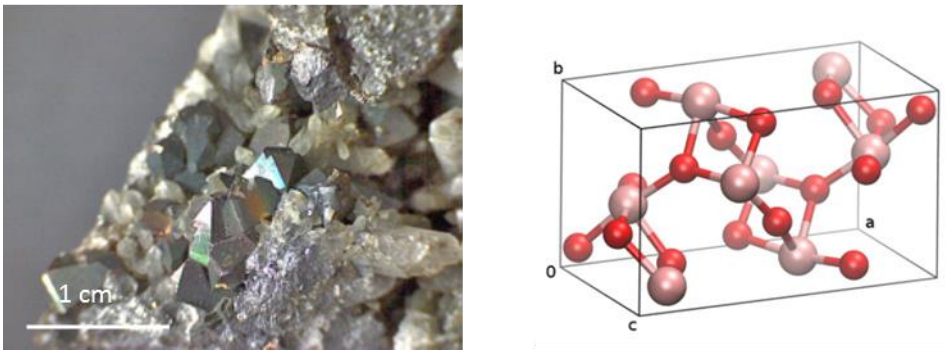

Figure 23: TiO_2 brookite macroscopic picture and crystalline structure (red for O^{2-} and grey for Ti^{4+}) (Moellmann et al., 2012)

Each crystalline structure exhibits specific physical properties, band gap and electronic surface, governing their applications and uses (Koelsch, Cassaignon, Ta Thanh Minh, Guillemoles, & Jolivet, 2004). For example, the estimated band-gap energies for rutile and anatase are 3.0 eV and 3.2 eV respectively, anatase being more reactive and so preferred to rutile for photocatalytic applications. Moreover, the Ti-Ti distances in anatase are longer whereas Ti-O distances are shorter than in rutile. (Burdett, Hughbanks, Miller, Richardson, & Smith, 1987) A comparative study of the 3 different crystalline structures is summarized in Table 10.

Since 2004, E171 can be purchased as rutile or anatase, or as a mixture (EFSA, 2004) and can be coated with less than 2% Al and Si (Joint FAO/ WHO Expert Committee on Food Additives, 2010).

	Anatase	Rutile	Brookite
Formula	TiO_2	TiO_2	TiO_2
Formula Weight	79,890	79,890	79,890
Crystal system	Tetragonal	Tetragonal	Orthorhombic
Space group	$I4_1/amd$	$P4_2/mnm$	Pbca
Point group	4/mmm	4/mmm	mmm
Z (number of formula units per cell)	4	2	8
Unit Cell a(Å)	3,7542	4,5845	9,184
b(Å)	-	-	5,447
c(Å)	9,5146	2,9533	5,145
Unit cell Volume ($Å^3$)	136,25	62,07	257,38
Molar volume (cm3)	20,156	18,693	19,377
Density (mg/m^3)	3,895	4,2743	4,123

Table 10: Comparative study of different phases of titanium dioxide (Adapted from Smyth & Mccormick, 1995)

b) Behavior of TiO_2 particles in solution

The stability and aggregation/agglomeration of TiO_2 NPs depend on the chemical conditions in the solution such as pH, ionic strength and cation valence of inorganic ions (W. Liu, Sun, Borthwick, & Ni, 2013). Indeed, TiO_2 particles in solution are known to interact with ions such as phosphates (Connor & McQuillan, 1999; Gong, 2001) and calcium (Domingos et al., 2010; French et al., 2009) but also with proteins such as BSA (Ji et al., 2010; Kathiravan & Renganathan, 2008) and phospholipids (Le, Ropers, Terrisse, & Humbert, 2014).

In order to obtain conclusive and reproducible results from toxicity and fate assessments of nano-TiO_2, a standardized dispersion protocol was developed and validated by the National Institute of Standards and Technology (NIST), jointly with the

Center for the Environmental Implications of Nanotechnology (CEINT) (Taurozzi, Hackley, & Wiesner, 2013) to get weakly agglomerated and stable dispersions of TiO_2. This protocol includes sonication in order to enhance the percentage of NPs by reducing the agglomeration (Figure 24) and has been developed using the NIST Standard Reference Material (SRM) 1898a, corresponding to Aeroxide TiO_2 P25 powder (Evonik Industries, Germany, (NIST, 2012)).

Using the NIST protocol, the obtained P25 aqueous dispersion is monomodal, with a volume-based mean particle diameter of 108-116 nm at a pH varying between 3.7 and 4.9. Although this sonicated suspension is very well dispersed and stable, it still needs to be adjusted to pH 7 to be suitable for application in biological media.

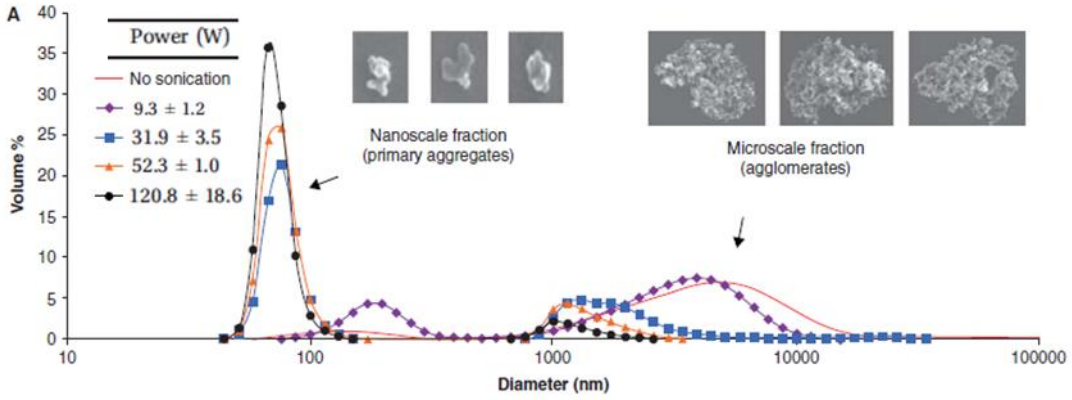

Figure 24: Particle size distribution profiles of P25 suspensions subjected to different levels of sonication power for 1 min in continuous mode. Inset micrographs show FE-SEM images of primary aggregates and agglomerates. (Adapted from Taurozzi et al., 2013)

In order to prepare a suspension of NPs with sufficient stability in pH-neutral and significant ionic strength media, a pH adjusted-BSA protocol was developed. The basic idea of the protocol is to adsorb BSA onto TiO_2 NPs in a pH range where the BSA and TiO_2 NPs are of identical sign (i.e at acidic pH, Figure 26), and form a stable and well dispersed suspension. Then, the pH is rapidly increased up to the target value of 7 by addition of NaOH solutions. (Figure 26) (Guiot & Spalla, 2013)

More specifically, stable NPs and BSA suspensions are prepared by ultrasonication in pH 2. BSA in then added to NPs in a ratio BSA/NPs 1:1 allowing a full covering of the NPs. BSA will then adsorb onto TiO_2 (Giacomelli, Avena, & De Pauli, 1997; Rezwan, Studart, Voros, & Gauckler, 2005; Tantra, Tompkins, & Quincey, 2010) which stays positively charged at this pH (such as BSA, see Figure 26). In the last step, the fast increase of pH to the target value of 7 induces a charge reversal (BSA IEP is around pH 5 particles (Giacomelli et al., 1997; Salis et al., 2011)) but adsorbed BSA protects TiO_2 particles from flocculation. This protocol results in a stable suspension of TiO_2 particles at pH 7, suitable for application in biological media (Guiot & Spalla, 2013).

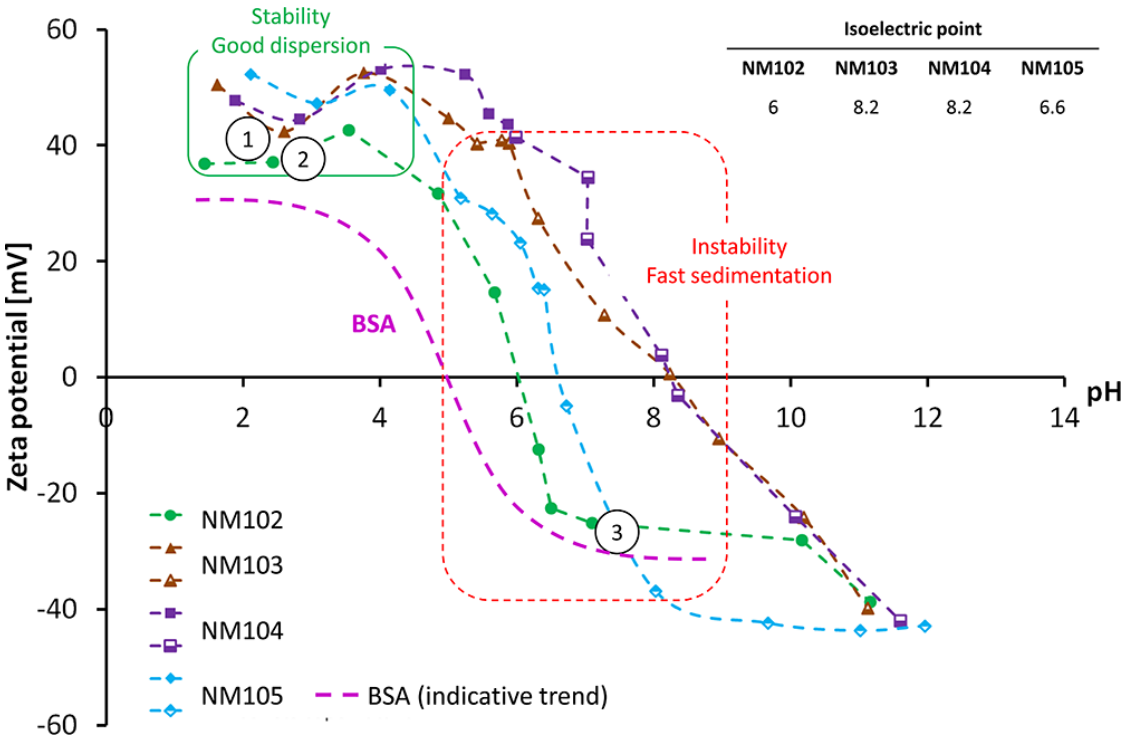

Figure 25: ζ-Potential–pH for TiO_2 NPs suspensions and BSA (IEP pH 5), highlighting domains of stability for acidic pH and instability around isoelectric points (values in insert) (Guiot & Spalla, 2013)

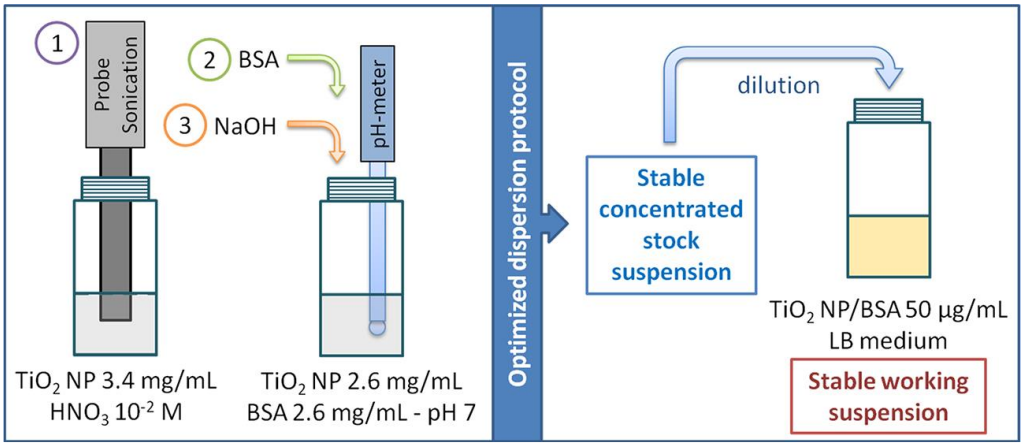

Figure 26: Dispersion protocol for TiO_2 particles for application in biological media (LB for Lysogeny broth, culture media) (Guiot & Spalla, 2013)

As recommended by the OECD, toxicological studies are widely performed using P25 particles, prepared with this standardized dispersion protocol associating sonication and sometimes BSA (Othman, Abdul Rashid, Mohd Ghazi, & Abdullah, 2012; Taurozzi et al., 2013).

However, even if particle agglomeration upon introduction to biological media may complicate both the determination of the delivered NPs dose and the discrimination of size-specific particle effects (Taurozzi et al., 2013), the sonication and the addition of BSA induce changes in agglomeration and surface chemistry which can, in some cases, have a significant effect on particle toxicity (Murdock, Braydich-Stolle, Schrand, Schlager, & Hussain, 2008).

3) Food grade TiO_2 physicochemical characteristics

Only a few studies investigated the physicochemical nature of food grade TiO_2 particles (Athinarayanan et al., 2015; Chen et al., 2013; Faust et al., 2014; R. J. B. Peters et al., 2014; Weir et al., 2012) and only one of these study resulted in a full characterization of these particles (Yang et al., 2014). Briefly, the E171 samples are mainly anatase TiO_2 particles, with 17 to 44% of nanoparticles, a mean diameter of around 120 nm, a size distribution in the range of 30 to 600 nm, an isoelectric point around pH 3.5 and a surface coated with phosphorus (Figure 27, Table 11).

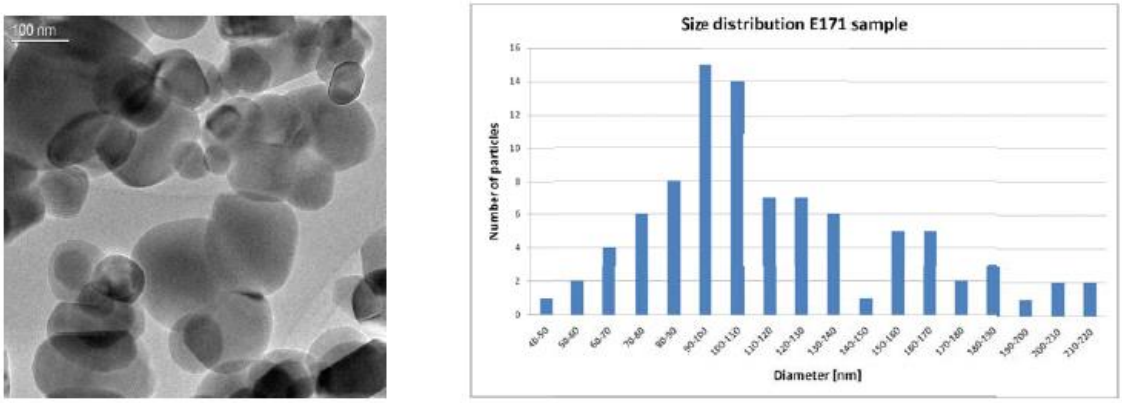

Figure 27: TEM analysis of E171 and analysis of the size distribution (based on TEM images) (Weir et al., 2012)

	Properties	E171 Literature data
Bulk properties	Primary size	110 nm **Weir 2012** 106±38, 122±48, 132±56, 124±42, 117±41 nm **Yang 2014** 122±48 **Faust 2014**
	Size distribution	30-400 nm **Weir 2012** 51 to 290 nm **Faust 2014** 30 to 600 nm **Peters 2014** 30 to 250 nm **Athinarayanan 2015**
	% of nanoparticles	36 % **Weir 2012** 35, 23, 21, 17, 19% **Yang 2014** 40.0, 43.5, 43.7, 41.4, 42.4, 27.7% **Chen 2013** 10 % **Peters 2014**
	Crystalline structure	4 samples Anatase / 1 mixture **Yang 2014** 5 samples Anatase / 1 Rutile **Chen 2013** Anatase **Faust 2014**
	Surface chemistry	TiO_2 + P **Yang 2014, Faust 2014**
	Specific surface area	8-9 m^2/g **Kronos International**
	Chemical composition	Ti, P, Al, Si **Yang 2014** 90–99% TiO_2 **Peters 2014**
In solution properties	Agglomeration	273, 405, 209, 504, 127 nm eau + sonication **Yang 2014** 150 nm in water + BSA + sonication **Weir 2012** 336 nm in serum media + sonication **Faust 2014**
	Isoelectric point	3.2, 3.5, 4.0, and <2,5 **Yang 2014** 3,3 **Faust 2014**

Table 11: Physicochemical properties of food grade TiO_2 (E171), data from (Athinarayanan et al., 2015; Chen et al., 2013; Faust et al., 2014; R. J. B. Peters et al., 2014; Weir et al., 2012; Yang et al., 2014)

4) Case of TiO_2 NPs after ingestion

Based on the literature, some proteins of the different digestive fluid can interact with TiO_2 particles, such as mucins (Lori & Nok, 2004) and lysozyme (Bentaleb, Ball, Haikel, Voegel, & Schaaf, 1997; Kathiravan et al., 2011; Z. Xu, Liu, Ma, & Gao, 2010) secreted in the saliva. In the oral cavity, TiO_2 particles were found to highly agglomerate (Birgit J Teubl et al., 2015). Yet, a small fraction of particles remained as NPs (10%) and were found to penetrate the upper and lower buccal epithelium, independently of the hydrophilicity (Tay et al., 2014; Birgit J Teubl et al., 2015; Birgit Johanna Teubl et al., 2014).

When introduced directly in the gastric fluid, TiO_2 NPs agglomerated as well (Jones et al., 2015), still with a fraction remaining as primary entities, yet in a lower proportion (Chen et al., 2013). This was attributed to the presence of proteins and electrolytes (Chen et al., 2013; Jones et al., 2015). An interaction between TiO_2 NPs and the pepsin, secreted in the gastric fluid, was also detected and was found to induce an inhibition of its enzymatic activity (Al-Hakeim & Jasem, 2016; Zhu et al., 2010).

In the intestine, TiO_2 particles accumulated in macrophages of human gut-associated lymphoid tissue, where the earliest signs of lesions in Crohn's disease are observed (Lomer et al., 2002). Some *in vivo* studies showed that TiO_2 NPs have an extremely low absorption rate and are then mostly excreted in feces (Cho et al., 2013; Xie et al., 2011). These results were confirmed by several *in vitro* studies which showed that TiO_2 NPs cannot cross the epithelial barrier, and that a high percentage of the ingested particles are finally excreted (Janer, Mas del Molino, Fernández-Rosas, Fernández, & Vázquez-Campos, 2014; Jones et al., 2015; MacNicoll et al., 2015; Song et al., 2015).

However, some studies showed contradictory results. Other i*n vitro* studies probed that TiO_2 NPs are able to reach the systemic circulation (Gitrowski et al., 2014; Koeneman et al., 2010) and accumulate in the intestinal cells (Veronesi, Brun, Fayard, Cotte, & Carrière, 2012). This contradiction may come from the different culture conditions used in these *in vitro* studies, and from the use of different kinds of TiO_2 NPs with various physicochemical properties, which are known to mediate the uptake

of TiO_2 NPs (Higashisaka et al., 2015; Song et al., 2015). In the same way, some *in vivo* studies also evidenced that TiO_2 particles could reach the blood circulation and be transported to other tissues and organs after uptake by gastrointestinal tract, then bioconcentrate, bioaccumulate, and biomagnify in the liver, spleen, kidneys, and lung tissues (Fabian et al., 2008; Park et al., 2014; Pele et al., 2015; Jiangxue Wang et al., 2007; Xie et al., 2011), resulting in histopathological and physiological changes in various organs of animals.

All available *in vivo* studies investigating TiO_2 toxicity after oral administration were collected in a review published (Jovanović, 2015) and evaluated according to several characteristics including the relevance of the administered dose (0.2 to 2mg/kg body weight per day, (Weir et al., 2012)) and the specification of the particles basic characteristics, *i.e.* crystal structure, primary particle size, and hydrodynamic diameter. Based on this criteria, only 16 studies were considered as plausible and are presented in Table 12, completed with two recently performed studies. Of those, 16 reported toxic effects or bioaccumulation of TiO_2, whereas only two studies detected no negative effects and a low absorption (Cho et al., 2013; Jones et al., 2015). However, the results of this review showed that most of these studies were performed using very small NPs (between 5 and 30 nm), a lot smaller than food grade TiO_2 particles used in only one study (Bettini et al., 2017). Moreover, this review highlighted the lack of information on the physical chemistry of used TiO_2, such as the hydrodynamic diameter, the primary size, and the crystal structure, and we know that all physicochemical properties are important in determining NPs toxicity (McCracken et al., 2016). The most common missing points are the lack of hydrodynamic diameter and lack of crystal phase specification. Furthermore, the assessments were often performed at very high doses of TiO_2, exceeding the potential dose that a human could consume, resulting in studies which are not relevant to daily human uptake.

At last, only few studies investigated the impact of TiO_2 particles on the gut microbiota. Taylor et al., reported that TiO_2 NPs (P25) can cause minimal phenotypic changes in a model colon gut microbiota including increases in cellular hydrophobicity

and of the sugar content of the extracellular polymeric substance (EPS), and a small decrease in cell radius. However, their demonstrated no significant impact of TiO_2 NPs on cell concentration, protein content of the EPS, conductivity, and short-chain fatty acids production (Taylor, Marcus, Guysi, & Walker, 2015). On the other hand, Liu et al., reported that TiO_2 NPs (10, 50 and 100 nm in size) can inhibit the growth of Drosophila intestinal commensal bacteria *in vitro*, yet do not induce similar effects *in vivo*, where they demonstrated no impact of TiO_2 NPs on the amount of intestinal commensal bacteria (L. Y. Liu, Sun, Zhong, Zhu, & Song, 2016). However, these studies were performed using nonfood grade TiO_2 and only one was performed on a model of human microbiota. The toxicity on food grade TiO_2 particles on the human gut microbiota still remains unknown.

Study	Dose (mg/kg b.w.)	Crystal Structure	Primary particle diameter (nm)	Hydrodynamic diameter (nm)	Duration of study (d)	Model species used	Main effect observed
(Cho et al., 2013)	260–1041 daily	A/R (80:20)	30	38	91	Rat, 11/group	Low absorption and no toxic effect observed
(Cui et al., 2010)	5–50 every 2nd day	Anatase	7	Not reported	60	Mouse, 20/group	Liver damage, hepatocyte apoptosis, ROS accumulation in liver
(Cui et al., 2011)	5–50 daily	Anatase	5	Not reported	60	Mouse, 20/group	Liver toxicity (induction of hepatitis molecular pathway) and bioaccumulation
(Duan et al., 2010)	62.5–250 every 2nd day	Anatase	5	Not reported	30	Mouse, 20/group	Liver histopathology, immune suppression, body weight reduction
(Gui et al., 2013)	2.5–10 daily	Anatase	5	294	90	Mouse, 30/group	Nephrotoxicity, inflammatory response, oxidative stress
(Hu et al., 2010)	5–50 every 2nd day	Anatase	5	Not reported	60	Mouse, 20/group	Impairment of spatial recognition memory, brain pathology
(Jani, Halbert, Langridge, & Florence, 1989)	12.5 daily	Rutile	475	Not reported	10	Rat, 10/group	Accumulation in the intestines and translocation of liver and spleen
(Nogueira et al., 2012)	100 daily	Anatase	66 and 260	Hard to interpret	10	Mouse, 12/group	Mucosal epithelium hypertrophy and hyperplasia in small intestine
(Bu et al., 2010)	160–1000 daily	A/R	50	Not reported	14	Rat, 16/group	Energy and amino acid metabolism disturbance
(Sang et al., 2012)	2.5–10 daily	Anatase	5	294	90	Mouse, 20/group	Spleen histopathology, splenocyte apoptosis, immunosuppression
(Sang et al.,	10 daily	Anatase	5	294	90	Mouse,	Spleen bioaccumulation,

2013)						20/group	oxidative stress, splenic inflammation and necrosis, reduction in body weight
(Sang et al., 2014)	2.5–10 daily	Anatase	5	294	90	Mouse, 30/group	Spleen and thymus bioaccumulation, spleen histopathology and splenocyte apoptosis, increase in levels of inflammatory proteins
(Tassinari et al., 2014)	1–2 daily	Anatase	25	284	5	Rat, 14/group	Spleen and ovaries bioaccumulation, alteration in thyroid function and testosterone levels
(Jue Wang et al., 2011)	5–150 daily	Anatase	7.5	Not reported	30	Mouse, 20/group	Oxidative stress via p38-Nrf-2 signaling pathway, congestion in spleen
(Y. Wang et al., 2013)	10–200 daily	Anatase	75	473	30	Rat, 7/group	Liver edema, heart injuries, mast cells activation
(Jones et al., 2015)	5, single dose	Anatase Rutile Rutile	15 <100 nm <5 µm	Up to 1µm 1 µm sized Few µm	3	Humans 9 volun-teers	No evidence of significant absorption of titanium dioxide in humans after an oral dose, regardless of particle size.
(Bettini et al., 2017)	10 daily	Anatase (E171)	118	373	100	Rats 10/group	Cross the gut barrier, reach liver without altering intestinal permeability or causing DNA damage in Peyer's patches. Affect dendritic cell frequencies and T cell populations in the Peyer's patches and cause imbalances in intestinal and systemic immune responses. Initiate and promote preneo-plastic lesion formation in the colon and induce mucosal low-grade inflammation.

Table 12: In vivo toxicity studies of TiO_2 after oral administration on mammalian species, adapted from (Jovanović, 2015)

IV) Bibliographic summary

NPs are really interesting because of their new properties related to their size and their higher specific area. They are spread in a lot of diverse industrial sectors such as the electrical, medical, personal care, agricultural and food sectors for various applications. However, it is likely that the specific useful properties which appear at nanoscale can also lead to adverse effects on both environment and public health, especially for NPs in food.

The use of inorganic particles like TiO_2 in food applications raised some concerns as TiO_2 NPs were found to be able to cross the human intestinal barrier (Lomer et al., 2002) reach the systemic circulation (Gitrowski et al., 2014; Koeneman et al., 2010) and bioaccumulate, bioconcentrate and biomagnify in the liver, spleen, kidneys, and lung tissues (Fabian et al., 2008; Park et al., 2014; Pele et al., 2015; Jiangxue Wang et al., 2007; Xie et al., 2011), inducing histopathological and physiological changes in various organs of animals (Jovanović, 2015). Determining the impact of food grade TiO_2 via ingestion is thus of high interest, however, some improvements of the currently used models are needed.

Food grade TiO_2 has only recently been investigated and the data on this material are still quite sparse. A full characterization of food grade TiO_2 (E171) is then needed, in order to confirm the solely available study published during the completion of ours (Yang et al., 2014). Moreover, a comparison between E171 and P25 particles must be undertaken in order to evaluate the relevance of P25 particles as a model, and to determine the validity of the previous toxicological studies.

When NPs enter the body they will firstly interact with biological molecules such as proteins or lipids, which may result in the formation a corona around the inorganic particles. This corona will mediate the interaction of NPs with cells and determine further biological responses (Bergin & Witzmann, 2013; Pietroiusti, 2012; Shang et al., 2014). Moreover, the physicochemical characteristics of this corona will be modified when NPs move from one biological compartment to another. However, there is a lack of data concerning the fate of food grade TiO_2 particles during digestion, *i.e.* their

physicochemical transformations, agglomeration behavior and their interactions with proteins all along the gastro-intestinal tract.

Finally, toxicity assessments, performed on epithelial cells in addition to whole animals, did not examine the potential impact of TiO_2 NPs on the human gut microbiota. This complex ecosystem in the gastrointestinal tract is involved in numerous aspects of human physiology, from nutritional status to behavior and stress responses that we are just starting to appreciate. Knowing that microbiota changes can be associated with important disease states such as obesity, diabetes, rheumatoid arthritis, and inflammatory bowel disease (Marchesi et al., 2015; Pietroiusti et al., 2016), analyzing the impact of TiO_2 on the human intestinal microbiota will inform us on potential risks associated to the ingestion of these particles.

These questions are important from a public health perspective as we are daily exposed through foods or drugs, and as children under 10 years old are much more exposed than adults to this food additive (Weir et al., 2012).

V) Scientific approach

The first objective of this work was to finely characterize the physicochemical state of food grade TiO_2 sold in Europe and to determine whether they are similar to the toxicological reference P25. For this purpose, several food grade TiO_2 samples and P25 particles were investigated for their physicochemical characteristics (size distribution, shape, crystallinity, reactivity, surface properties). Several methods relevant from physical chemistry were applied: transmission electron microscopy (TEM), X-ray diffraction (XRD), laser scattering particle size distribution analyzer, X-ray photoelectron spectrometry (XPS), zeta potential measurements, Raman and IR spectroscopies, Inductively coupled plasma atomic emission spectroscopy (ICP-AES), diffuse reflectance infrared Fourier transform spectroscopy (DRIFTS) and specific surface area analysis. In order to determine if E171 remains in the same physicochemical state once integrated in the final food products, we also extracted the coating of several chewing-gums and candies and compared them to the properties of E171 powders.

The second objective of this work was to determine the fate of TiO_2 particles in digestive fluids. To that end, the behavior of food grade TiO_2 and P25 particles was determined through a standardized static *in vitro* digestion protocol and compared to control digestions (digestion without NPs, and digestion of NPs without digestive proteins). After each step of the digestion (*i.e.* saliva, gastric and intestinal step), the size of the particles and the surface charge changes were characterized using laser particle size distribution analysis and zeta potential measurements. Finally, the nature of the adsorbed proteins was determined by denaturing gradient gel electrophoresis (DGGE) after separation from the TiO_2 particles.

Finally, the last objective of this work was to assess the toxicological impact of TiO_2 to the human gut microbiota by following physiological, biochemical and molecular assays. These included measurements of gas production using gas chromatography to determine if the bacterial metabolism was impacted, fatty acid methyl ester (FAME) analysis using the MIDI Sherlock Microbial Identification System protocol to detect any impact on bacterial membranes. DNA analysis were performed to get to the

phylogenetic composition of the microbiota, including polymerase chain reaction, denaturing gradient gel electrophoresis (PCR-DGGE) and 16S ribosomal RNA gene fragment 454-pyrosequencing.

Chapter 2: Materials and methods

I) Physicochemical characterization of food grade TiO_2 and P25 particles

1) TiO_2 Samples

a) E171 TiO_2 from manufacturers and suppliers

Seven samples of food grade TiO_2 (E171) particles were purchased from different sources: three from different manufacturers in Europe coded as E171-1, E171-2 and E171-3 and four batches from three suppliers in France were also studied, coded as E171-4, E171-5, E171-6a and E171-6b. Nonfood grade P25 particles were purchased from Evonik Industries (Degussa, Essen, Germany). All samples were received in powder form and stored in dark condition.

Figure 28: TiO_2 E171-1 powder form.

b) TiO_2 extracted from chewing gums and candies

Products selection

Several commercial products mentioning TiO_2 as an ingredient were purchased in a local store (September 2013, Nantes, France). Four menthol flavored chewing-gums, coded as S1, S2, S3 and S4 and one candy (S5) were selected for their very white color and the indication of TiO_2 content (E171) in the ingredients list (Table 13 and Table 14).

S1	Sweeteners (sorbitol, maltitol, maltitol syrup, aspartame, acesulfame K), gum base, bulking agent (E170), flavors, licorice extract, thickener (E414), **coloring (E171)**, emulsifier (sunflower lecithin), coating agent (E903), antioxidant (E321).
S2	Sweeteners: Sorbitol, maltitol, maltitol syrup, mannitol, aspartame, aspartame-acesulfame, acesulfame-K, gum base (contains soy lecithin), emulsifier: glycerol, flavoring, thickener: gum arabic (E414), coating agent calcium carbonate, **coloring: E171**, glazing agent: carnauba wax (E903), antioxidant BHA (E320)
S3	Sweeteners (xylitol (32%, 16% in the center), erythritol, maltitol, mannitol, sorbitol, maltitol syrup, acesulfame-K, aspartame, sucralose), gum base, flavoring, thickening agent (gum arabic), gelatine, stabilizer (glycerol), **coloring (titanium dioxide**, brilliant blue FCF), emulsifier (soy lecithin), natural green tea extract, glazing agent (carnauba wax, E903), antioxidant (BHA,E320)
S4	Sweeteners (maltitol, sorbitol, maltitol syrup, Aspartame, Acesulfame K), gum base, Flavoring, emulsifier (E422) Gelatine, Emulsifier (Sunflower Lecithin), **Coloring (E171**, E133), glazing agent (E903) Thickener (E466).
S5	Sugar, molassed sugar syrup (contains sulphites), Wheat Flour, Glucose syrup, Vegetable fat, Whole milk powder, salt, gelatin, licorice extract, ammonium chloride, flavoring, vegetable oil, coating agent: Gum Arabic (E414), Carnauba wax (E903), **coloring agent: E171**.

Table 13: List of ingredients composing the selected chewing-gums and candies

Sorbitol	**E420**
Maltitol	**E965**
Maltitol syrup	**E956**
Aspartame	**E951**
Acesulfame K	**E950**
Aaspartame-acesulfame	**E962**
Xylitol	**E967**
Erythritol	**E968**
Sucralose	**E955**
Glycerol	**E422**
Calcium carbonate, Chalk	**E170**
Gum arabic	**E414**
Gelatine	**E441**
Titanium dioxide	**E171**
Brilliant blue FCF	**E133**
Carnauba wax	**E903**
Butylated hydroxyanisole BHA	**E320**
Butylated hydroxytoluene (BHT)	**E321**
Carboxymethyl cellulose	**E466**

Table 14 : List of food additives used in chewing-gums and candies, and corresponding E-numbers.

Protocol setup to extract TiO_2 particles from gum coating

To extract the white coating from the gum base, we adapted a protocol from the literature (Chen et al., 2013). Briefly, the commercial product was placed in ultrapure water (10 pieces in 30 mL) and manually agitated for 30-60 seconds, time required to separate the coating from the gum base. After picking out the gum base, the solution was centrifuged at 3500 *g* for 15 min at 20°C. The supernatant was discarded, and the pellet was washed twice with milliQ water then dried in a desiccator with silica gel as dehydrating material.

c) Samples preparation

Preparation of aqueous dispersions of TiO_2

Dispersions were prepared in ultrapure water (Simplicity 185, Merck Millipore, Darmstadt, Germany) and adjusted to the desired pH by adding HCl/NaOH. Dispersions were stored in dark under stirring (150 rpm) at 4°C for 7 days to reach equilibrium. Then, pH values were checked at the end of this 7 days period. Unless otherwise specified in the text, the concentration was 50 µg/mL.

Drying of TiO_2 dispersions

Samples were characterized either as received or after drying from dispersion. Dispersions of TiO_2 were centrifuged at 4°C, 3500 *g* for 20 minutes. The supernatants were discarded whereas the pellets were spread on the centrifugation tubes then left in a desiccator under vacuum with freshly dried silica gel for at least 3 days. Once dried, the powders were grinded in an agate mortar then stored in the desiccator until use.

2) Physicochemical methods for TiO_2 characterization

a) Recommendations on the characterization of nanomaterials

E171 and P25 samples of TiO_2 were characterized according to the EFSA and EOCD recommendations (EFSA, 2011; OECD, 2014) including the primary size and size distribution, the state of dispersion and agglomeration, the crystallographic structure, the surface area, and the surface reactivity. For this purpose, several methods relevant from physical chemistry were applied (Table 15): transmission electron microscopy (TEM), X-ray diffraction (XRD), laser scattering particle size distribution analysis, X-ray photoelectron spectrometry (XPS), zeta potential measurements, Raman scattering spectroscopy and IR absorption spectroscopy, inductively coupled plasma atomic emission spectroscopy (ICP-AES), diffuse reflectance infrared Fourier transform spectroscopy (DRIFTS) and specific surface area analysis by physical volumetric gas adsorption.

	Properties	Techniques	Samples
Bulk properties	Primary size Morphology Size distribution	TEM	Powder under high vacuum after dispersion in ethanol
	Crystalline structure	XRD, FT-Raman	Bulk powder
	Surface chemistry	XPS	Powder under high vacuum
		DRIFTS UV-diffuse reflectance FT-Raman	Bulk powder
	Specific surface area	Physical volumetric gas adsorption	Bulk powder under primary vacuum
	Chemical composition	ICP-AES	Powder digested in HNO_3/HCl/HF
In-solution properties	Agglomeration	Laser scattering	Powder in solution at pH 2-9
	Surface charge	Zeta potential measurements	Powder in solution at pH 2-9

Table 15: Summary of studied physicochemical properties and used techniques

b) Transmission Electron Microscopy (TEM)

Principle

The transmission electron microscope is the most suitable technique to determine the particle size and morphology of materials. TEM operates on the same basic principles as the light microscope but uses electrons instead of light. Because the wavelength of electrons is much smaller than the wavelength of light, the optimal resolution for TEM is way better and allows a closer visualization of samples structure. A high energy beam of electrons is sent through the sample, parts of it are transmitted then focused into an image on a phosphor screen or a charge coupled device (CCD) camera allowing the user to visualize the sample. The produced three-dimensional images are composed by darker and lighter areas, representing the relative extent of penetration of electrons. TEM can be coupled with energy dispersive X-ray (EDX) analysis to get information about the chemical composition of the sample (Williams & Carter, 1996)

.

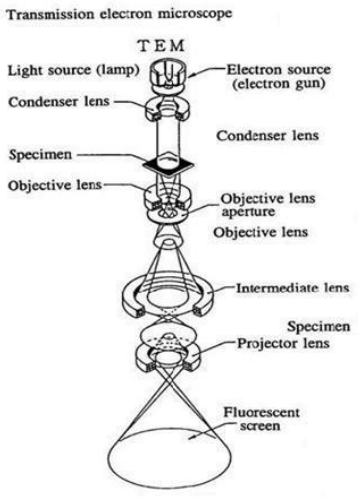

Figure 29: General layout of a TEM (https://www2.warwick.ac.uk)

Measurements & Sample preparation

The primary size distributions and the projected shape of particles were determined by transmission electron microscopy (TEM) using a Hitachi H-9000 NAR (300 kV, Scherzer resolution 0.18 nm). TEM was coupled to an energy dispersive X-ray spectrometer (EDX, Kevex) to determine the chemical composition. A tiny amount of powder was dispersed in ethanol. The suspensions were sonicated for 10 minutes, and one drop was deposited on the surface of a copper grid covered with a thin holey carbon film. Once dried, the grid was inserted in the TEM. To obtain a representative size distribution, at least 300 particles of each sample identified on at least 7 different locations on the grid were analyzed using ImageJ software (version 1.48v). The equivalent circle diameter (ECD) corresponding to the diameter of a circle with an equivalent area was deduced.

c) X-Ray diffraction (XRD)

Principle

X-ray diffraction (XRD) is used for phase identification of a crystalline material and provides information on unit cell dimensions. When an X-ray beam hits a crystalline sample, part of it is diffracted differently depending on the nature of the mineral. Diffracted X-rays are then detected, processed and counted (Figure 30). By scanning the sample through a range of 2θ angles, all possible diffraction directions of the lattice should be attained due to the random orientation of the powdered material. By applying Bragg's Law: $n\lambda = 2d \sin\theta$ (Figure 31), the distances between the planes of the atoms constituting the sample can be determined. Each mineral having a unique set of d-spacings, the mineral can be identified by comparison with standard references. The setup is presented in Figure 31. (http://serc.carleton.edu)

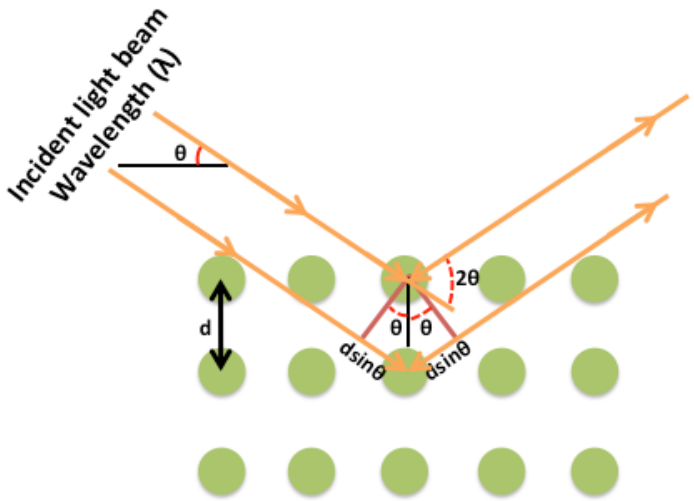

Figure 30: Schematic description of Bragg's Diffraction Law. n is the order of the diffracted beam, λ is the wavelength of the incident X-ray beam, d is the distance between adjacent planes of atoms (the d-spacing), and ϑ is the angle of incidence of the X-ray beam (Agrawal & Barron, 2013)

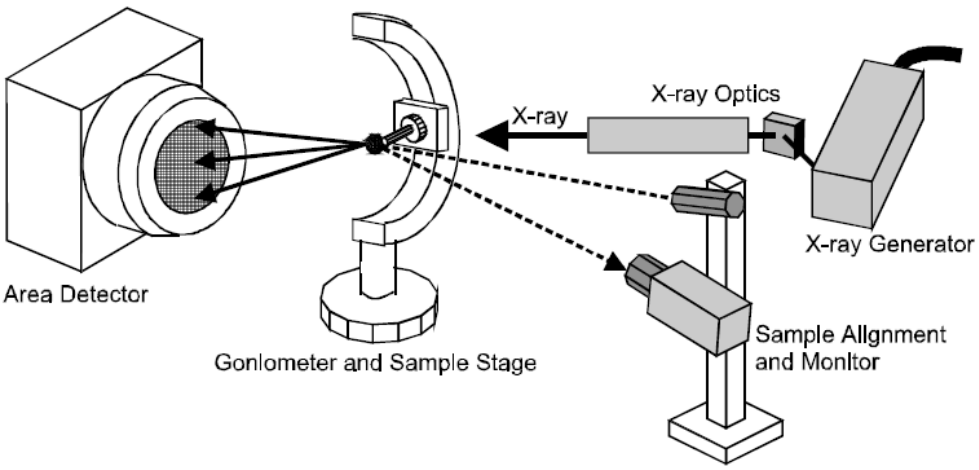

Figure 31: Schematic illustration of basic 2D XRD setup (He, Preckwinkel, & Smith, 1999)

Measurements & Sample preparation

Crystalline structures of raw powder samples were characterized by X-ray diffraction (XRD) (Bruker AXS D8 Advance, Bruker, Germany) working at the Cu Kα1 radiation wavelength. Each sample was scanned from 20° to 80°. Diffractograms were analysed with the software Diffrac plus Eva to assign the diffraction peaks to the known crystalline structures integrated in the software.

d) FT-Raman spectroscopy

Principle

Raman spectroscopy is an inelastic light scattering technique based on Raman Effect and probing the molecular vibrations. In Raman spectroscopy, the sample is illuminated with a monochromatic laser beam which interacts with the molecules resulting in a scattered light. Much of this scattered radiation has a frequency which is equal to the frequency of the incident radiation and constitutes the Rayleigh scattering. Only a small fraction of the scattered radiation ($1/10^{+6}$) has a different frequency and constitutes Raman scattering (Figure 32). A Raman spectrum is presented as an intensity-versus-wavenumber shift and can be recorded over a range of 4000–10 cm^{-1} (Bumbrah & Sharma, 2016; Raman & Krishnan, 1928).

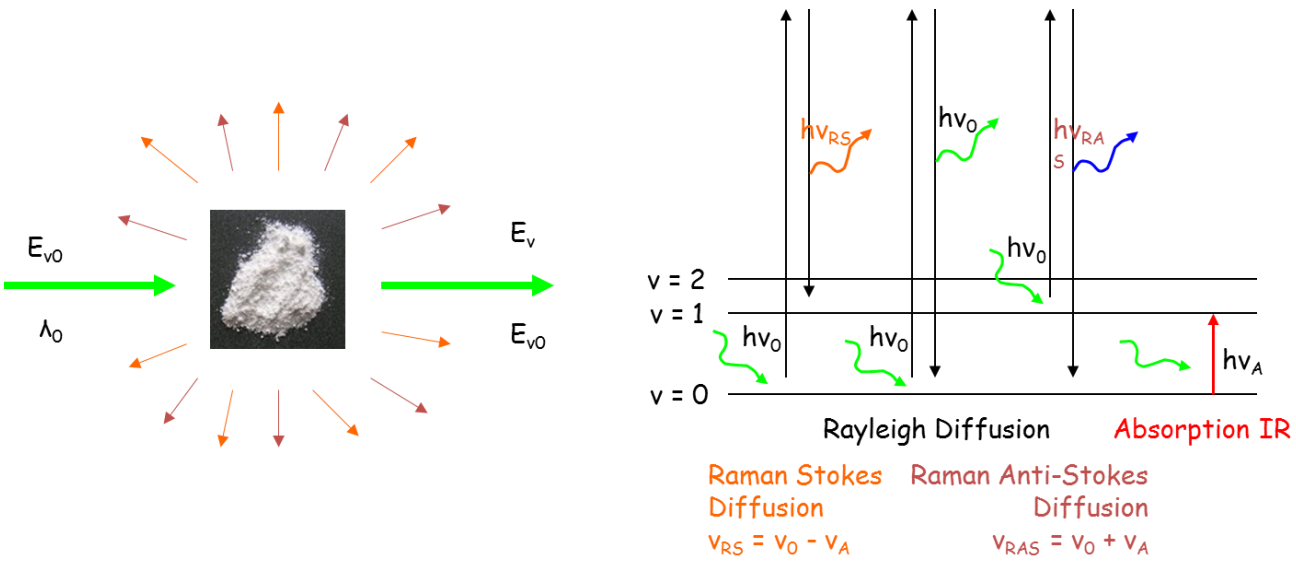

Figure 32: Raman spectroscopy principle

Measurements & Sample preparation

The inelastic Raman vibrational spectra of TiO_2 samples were recorded with a Fourier-transform spectrometer (MultiRam Raman Spectrometer, Bruker, Germany) combined to the software OPUS. The Raman signals were excited by focusing a near infrared beam (Nd:YAG laser) at 1064 nm on an area of around 100x100 µm² with a power of 150 mW. The system was equipped with a 143K cooled InGaAs detector. The cell was filled with TiO_2 powder and covered by a glass slide then positioned in the focal plan. The backscattered spectra were recorded with 100 scans and a spectral resolution of 4 cm^{-1} at room conditions. Spectra (in the FT configuration here) are given with a high precision in wavenumber (in vacuum) better than 0.1 cm^{-1}.

e) Ultraviolet–Visible Light Diffuse Reflectance (UV–vis DR)

Principle

Light can interact with samples in different ways, it can be absorbed, reflected or scattered. When incident light is reflected symmetrically with respect to the normal line, the phenomenon is called "specular reflection," while when incident light is scattered in different directions it is called "diffuse reflection" (Figure 33).

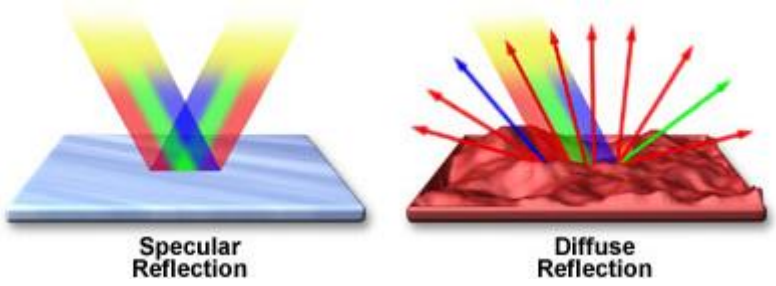

Figure 33: Interactions of light with samples, specular and diffuse reflection *http://micro.magnet.fsu.edu/*

Ultraviolet-visible diffuse reflection spectroscopy measures the percentage of radiation reflected by the sample at each wavelength during a scan of a wavelength range between 200 and 800 nm.

Measures & Sample preparation

UV-visible reflectance spectra of TiO_2 powders were recorded using a Perkin Elmer UV-visible-NIR spectrometer (Lambda 1050) equipped with a 150 mm integrating sphere designed to measure the diffuse reflectance of solid samples. Raw reflectance spectra were corrected for the reflectance of a reference material (Spectralon®, Labsphere, North Sutton, USA) as well as the dark level of the sphere in order to get the absolute reflectance in percentage.

f) X-ray Photoelectron Spectroscopy (XPS)

Principle

X-ray photoelectron spectroscopy (XPS) is a spectroscopic technique used to identify the atomic composition and the chemical nature (such as atomic oxidation state) of a sample surface. In XPS, the sample is irradiated with a beam of soft X-ray radiations (monochromatic, 200-1500 eV) in an ultrahigh vacuum to induce the production of a photoelectrons by photoionization of the top 10 nm of the sample surface (Figure 34).

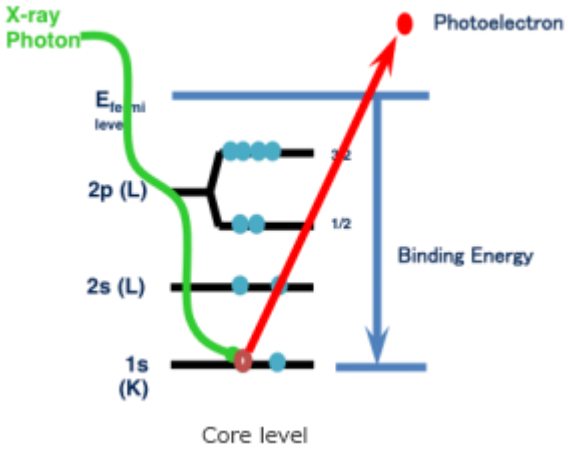

Figure 34: X-rays photoelectron spectroscopy principle (www.ulvac-phi.com)

The kinetic energies and the amount of emitted photoelectrons (Ek) are then measured. Knowing the X-rays energy hv, the binding energies of the photoelectrons (Eb) can be plotted on a spectrum using the Einstein equation (Equation 1). By comparing the measured binding energies with known references, the atomic composition of the sample surface can be determined. Moreover, by measuring the relative areas of the photoelectron peaks the composition can be quantitatively determined.

$$E_B = h\nu - E_K + \Phi$$

Where:

E_B = binding energy
$h\nu$ = photon energy
E_K = kinetic energy
Φ = work function

Equation 1: Einstein equation, with E_K the kinetic energy of emitted photoelectrons, hν the X-rays energy, E_B the binding energy of the photoelectrons and Φ the work function

Measures & Sample preparation

Surface chemistry composition of TiO_2 samples was analysed by X-ray photoelectron spectroscopy (XPS) using an AXIS Nova model from Kratos Analytical Company with a monochromatic Al Kα source at hν=1486 eV, a pressure below 6.7×10^{-7} Pa, and a spot analysis size of 400X700 μm^2. TiO_2 samples were prepared by pressing 100 mg of the powder into a pellet then deposited on the sample holder. The samples were electrically isolated from the holder to limit possible uncompensated charge effects. Charge compensation was achieved using a low-energy electron flow gun. Survey spectra (Pass Energy 160 eV) and scans of region of interest (Pass Energy 20 eV) focused on the detected elements were recorded. The data were treated by Casa XPS software (Neal Fairley, Copyright© 2005 Casa Software Ltd, 2005.), using Shirley backgrounds and Gaussian-Lorentzian (70-30 ratio) function to account for the different components. The estimated depth of analysis is approximately 6.6 nm as determined from the inelastic mean free path of electron scattering for TiO_2 (Tanuma, Powell, & Penn, 1994). The adventitious carbon peak was used for calibration (285 eV).

g) Diffuse reflectance Infrared Fourier transform Spectroscopy (DRIFTS)

Principle

Diffuse Reflectance Infrared Fourier Transform Spectroscopy (DRIFTS) is an infrared analysis used to determine the infrared absorption spectra of powders. Due to the optical processes during interaction light-matter, by comparison with the usual absorption spectroscopy recorded in transmission. Such as the UV-vis reflection spectroscopy, the DRIFTS technique is based on the diffuse reflectance phenomenon (Dalibart & Servant, 2000). DRIFTS analysis of powders is conducted by focusing infrared light onto the powder and the scattered and diffused light is collected and relayed to the IR detector. Thus the functional groups at the surface of particles were probed.

Measures & Sample preparation

The spectra were recorded in the diffuse reflectance mode with a Harrick HVC accessory (Harrick Scientific Products Inc, NY) and a Vertex 70 spectrometer (Bruker, Ettlingen, Germany) in the medium (MIR) and near infrared (NIR) ranges. A DTGS detector and a KBr beam splitter in the Michelson interferometer were used for both spectral ranges NIR (8000 – 4000 cm^{-1}) and MIR (4000 - 400 cm^{-1}). Powder samples were poured in the sample cell and the average plan of the powder was leveled by removing the excess with a glass plate. Once the sample support was introduced in the praying mantis, spectra were recorded with a spectral resolution of 4 cm^{-1} every 5 minutes for 2h, time required to dehydrate the sample under flushed dried air. The final humidity around the sample was measured to be lower than 1% at 298K. The last 800 scans were averaged and presented in this work. The sample spectra are presented as a pseudo absorbance, plotted as log (R_{sample}/R_{ref}) where R_{sample} and R_{ref} are respectively the diffuse single-beam reflectance of the sample and the reference.

h) Gas volumetry for determining specific surface area

Principle

The main method to determine the specific surface area of particles is the physical gas adsorption coupled to the Brunauer, Emmett and Teller (BET) analysis.

The BET theory is based on several assumptions which are

(i) Gas molecules multilayer physically adsorb on the surface of solids

(ii) There are no interaction between each adsorption layer

(iii) The first layer corresponds to Langmuir adsorption

(iv) The adsorption enthalpy of the second and higher layers is equal to the heat of condensation

(v) At saturation pressure, the number of layer is infinite

(vi) The Langmuir theory can be applied to each layer

The first step is to outgas the powder sample by heating it under vacuum or with flowing gas in order to remove adsorbed contaminants acquired from atmosphere exposure (e.g. CO_2 and H_2O). After the out-gassing step, the sample is cooled down to cryogenic temperature (77 K, boiling point of liquid N_2) under vacuum, and then adsorptive gas (like N_2 or Ar) is injected and dosed on the surface of samples with controlled increments. At each dose, the pressure of the system is allowed to equilibrate and subsequently the amount of adsorbed gas is calculated. The relationship between the amount of adsorbed gas and the gas pressure at constant temperature is established (adsorption isotherm). This relationship, after linearization in the relative pressure range 0.05-0.30 (P/P_0, P_0 being the saturated vapor pressure), determines the specific surface area of samples (Equation 2).

(1) $$\frac{1}{W\left(\left(P_0/P\right)-1\right)} = \frac{1}{W_m C} + \frac{C-1}{W_m C}\left(\frac{P}{P_0}\right)$$

(2) $$S_t = \frac{W_m \; N \; A_{cs}}{M}$$

(3) $$S = S_t / w$$

Equation 2:

(1) BET equation, with W the weight of gas adsorbed, P/P_0 the relative pressure, W_m the weight of adsorbate as monolayer and C the BET constant

(2) Total surface area (S_t) equation, with N the Avogadro's number, M the molecular weight of adsorbate and A_{cs} the adsorbate cross sectional area

(3) Specific surface area (S) equation, with S_t the total surface area and w the sample weight

Measures & Sample preparation

The specific surface areas of TiO_2 samples were determined by multipoint Brunauer–Emmett–Teller treatment (BET method) from the volumetric adsorption isotherms at 77 K of nitrogen gas using a Micromeritics TriStar II 3020 Physisorption Analyzer (Norcross, Georgia, U.S.A.). Samples were degassed under primary vacuum for one hour at ambient temperature before experiment, except P25 which was moreover heated at 70°C in order to eliminate potentially adsorbed species.

i) Inductively coupled plasma atomic emission spectrometry Principle (ICP-AES)

Principle

Inductively coupled plasma atomic emission spectrometry (ICP-AES) or inductively coupled plasma optical emission spectrometry (ICP-OES) is a sensitive technique for identification and quantification of elements in a sample.

Liquid sample is exposed to the extremely high temperature of an argon plasma (up to 10 000 K) that breaks the sample into atoms, ionizes part of these atoms, and electronically excites both atoms and their resulting ions. As they return to ground states, excited electrons in these ions or atoms emit light at a characteristic wavelength. This emitted light is specific of each element and serves as a fingerprint. Because the sample contains a mixture of elements, a spectrum of light wavelengths is emitted. The light is then focused through a lens and passed through an entrance window to the monochromator (diffraction grating and prism) where it is separated into individual wavelengths. Finally, the light is directed to a charge-coupled device (CDD) detector where thousands of individual picture elements (pixels) capture the light and turn it into a digital signal. A computer converts the electronic signal into concentrations. Thus, by measuring the wavelengths and intensity of the emitted light, elements are identified and quantified (Figure 35).

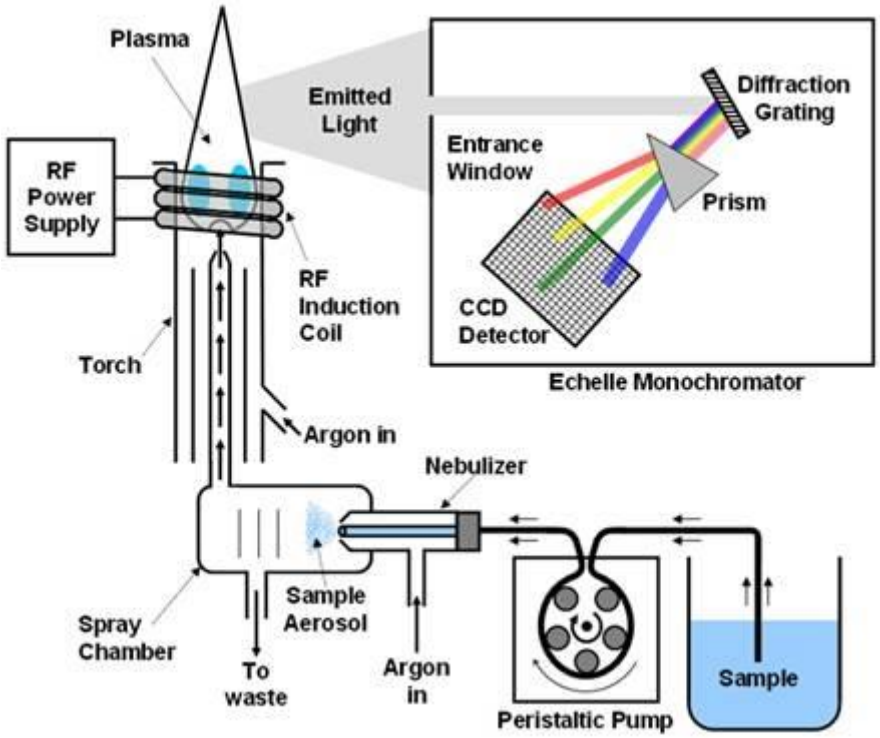

Figure 35: design of an ICP-AES instrument (http://sites.cord.edu/chem-330-lab-manual)

Measures & Sample preparation

Ti, Si, Al, Ca, Mg and P elemental concentrations in E171 food grade and P25 particles were determined using Inductively Coupled Plasma–Atomic Emission Spectroscopy (ICP–AES) (Thermo Scientific iCAP 6300 radial, MA, USA). Seventy five mg of TiO_2 powder were placed in PTFE digestion vials with 2.5 mL of inverted aqua regia (66% of concentrated HNO_3 and 33% of concentrated HCl) and 25 drops of concentrated HF for digestion at 110°C for 12 hours. After cooling, 30 g of boric acid was added to neutralise HF, and then ultrapure milliQ water was introduced to reach a total solution volume of 100 mL. A few days later, solutions were analysed by ICP-AES with 3 ICP single element standards at 1000 µg/mL from Chem Lab (Zedelgem, Belgium).

j) Laser diffraction

Principle

Laser diffraction is used to measure particles size distribution of particles between 0.01 and 5000 µm. Powder sample can be dispersed in a liquid medium, but it is also possible to analyze directly the powder through dispersion in pressurized air. A laser beam composed by two light sources with different wavelengths (He-Ne) passes through the dispersion medium and is diffracted by the particles (Figure 36). The blue laser is used for measuring the small particles, while the red one detects the larger particles. The diffraction pattern is then recorded by detectors, and the signal is transformed to a particle size distribution based on an optical model.

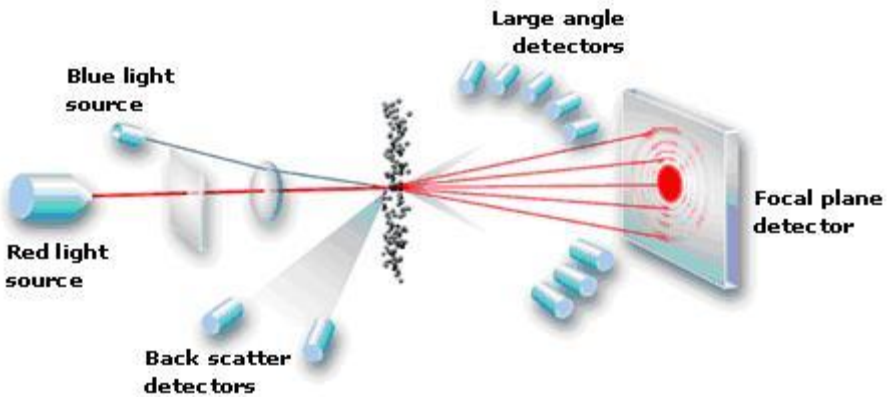

Figure 36: Laser diffraction principle (http://particle.dk)

Mie theory is used to convert the measured data to a particle size distribution. Mie theory provides the greatest accuracy for small particles for which refraction is the main mechanism of light diffusion. However, the use of Fraunhofer approximation is suitable for large particles, since refraction can then be neglected.

Measures & Sample preparation

A laser diffraction particle size analyser (Partica LA-960, Horiba, Japan) was used to determine the size distribution of TiO_2 particles dispersed in aqueous solutions with various pH values at room temperature. The instrument consists of two light sources (655 nm laser diode and 405 nm light emitting diode), a sample handling system and an array of high quality photodiodes to detect the scattered light over a wide range of angles. The scattered light collected on the detectors is used to calculate the particle size distribution of the sample using single scattering Mie Theory. Experiments were performed using the intern cell (volume 15 mL) filled with the dispersion medium (deionised water adjusted with HCl/NaOH at the desired pH). Depending on pH, 1 to 5 mL of the TiO_2 dispersions prepared as written above were introduced in the cell to reach an obscuration percentage ranging between 3 and 5 % (*i.e.* a transmittance value around 95-97% for both the blue LED beam and the red laser beam). The alignment was performed before each measurement and data acquisition times were set as default (25 seconds). TiO_2 refractive index was fixed at 2.40 (655 nm) and 2.70 (405 nm) for food grade samples, and 2.45 (655 nm) and 2.76 (405 nm) for P25 sample, based on the anatase/rutile ratio and the refractive indices of pure crystalline phases. (Jellison, Boatner, Budai, Jeong, & Norton, 2003) The imaginary part of refractive index was fixed at 0 for both wavelengths. The particle size is reported as a volume equivalent sphere diameter.

k) Laser Doppler Electrophoresis

Principle

Zeta potential measurements are used to determine the surface charge of particles. Also known as laser Doppler electrophoresis or laser Doppler velocimetry techniques, zeta potential measurements give indirect information on the agglomeration state of particles, then on their stability in solution. Indeed, the more the particles are

charged, the more they will repulse themselves and get dispersed, and the more the solution will be stable.

The surface charge of a particle affects the ionic distribution in the interfacial zone between the particle and the liquid. This is the electrical double layer model composed by the compact internal layer (Stern) and the diffuse external layer (Gouy) (Figure 37). The zeta potential (ζ) is the electric potential in the interfacial double layer (DL) at the location of the shear plane relative to a point in the bulk fluid away from the interface.

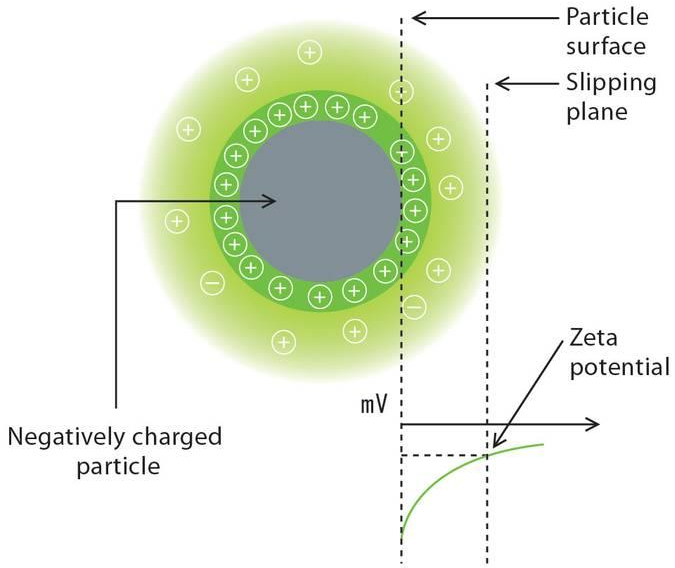

Figure 37: Surface charge of a particle, electrical double layer model (http://www.horiba.com)

The principle of zeta potential measurements is based on electrophoresis phenomenon, while electro-osmosis constitutes a parasite one, which has to be overcome during the measurement. Due to the application of an electrical field, charged particles are attracted towards the opposite charge electrode (Figure 38). When equilibrium is reached, the particle migrates with a constant velocity, depending on its charge (zeta potential), the electrical field, the dielectric constant and the viscosity of the dispersant. A laser beam is then sent through the sample and get scattered by the particles in movement. These movements induce a frequency

shift of the scattered light which is directly proportional to the electrophoretic velocity. By applying Henry equation, which can be simplified in most cases through Smoluchowski approximation, the zeta potential of particles can be calculated (Equation 3).

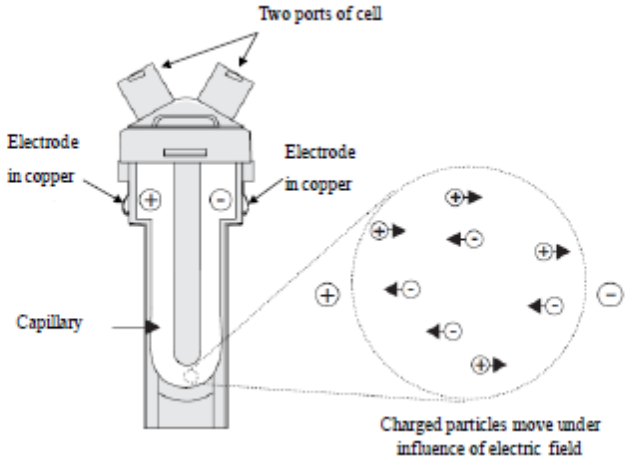

Figure 38: Capillary cell used for zeta potential measurements (Le, 2014)

Henry relation:

$$\mu_E = \frac{2\varepsilon\varepsilon_0\zeta}{3\eta} f(\kappa a)$$

Smoluchowski limit:

$$\mu_E = (\varepsilon\varepsilon_0 / \eta) \times \zeta$$

Equation 3: Henry relation and Smoluchowski limit, with ζ the zeta potential, μ_E the electrophoretic mobility, $\varepsilon\varepsilon_0$ the dielectric constant of the liquid, and η the viscosity

Measures & Sample preparation

Zeta potentials were determined with a Zetasizer Nano ZS instrument equipped with a 633 nm He-Ne laser (Malvern Instruments Ltd., Malvern, Worcestershire, UK), measuring the scattered light at an angle of 173°. Experiments were performed at 37°C with and without NaCl (4.10^{-2}M) added to the previously prepared dispersions.

For each sample, after an equilibration time of 2 minutes to reach 37°C, three electrophoretic mobility measurements (each one including 5 runs of 18 seconds) were performed to ensure repeatability. For easier comparison with other published data, our measurements were converted into zeta potential values, using Henry's equation and applying Smoluchowski approximation.

II) *In vitro* digestion of food grade TiO_2 particles

1) *In vitro* digestion protocol

The behavior of food grade TiO_2 and TiO_2 P25 in simulated digestive fluids was determined through a standardized static *in vitro* digestion protocol. The applied protocol, adapted from an *in vitro* digestion model (Minekus et al., 2014) consists in 3 steps which are the salivary, gastric and intestinal steps. Each step corresponds to a simulated digestive fluid (coded as SSF, SGF and SIF, respectively), all with different salts and enzymes compositions, which are described in the Table 16 and Figure 39. In the original protocol, the SSF medium was only containing α-amylase. As some proteins from saliva are known to interact with TiO_2 particles such as lactoferrin, lysozyme and mucin we completed the salivary step (Kathiravan et al., 2011; Lori & Nok, 2004). The saliva enzyme concentrations were set by averaging the literature values. (Aydin, 2007; Brandon et al., 2014; Dodds, Johnson, & Yeh, 2005; Dziemiańczyk, Grabowska, & Balicki, 2005; Mass, Gadoth, Harell, & Wolff, 2002; Nater et al., 2005; Payment, Liu, Offner, Oppenheim, & Troxler, 2000; Rantonen, 2003; Rudney & Smith, 1985; Sarkar, Goh, & Singh, 2009; Versantvoort et al., 2005; Yeh, Dodds, Zuo, & Johnson, 1997) The values are given in Table 17 for each digestive fluid. For simplicity, the porcine pancreatic α-amylase was used instead of human salivary amylase. The human pancreatic and salivary α-amylases are very similar with 97% homology (Brayer, Luo, & Withers, 1995), and porcine and human pancreatic amylase have a homology of 87% in their amino acid sequence (Gnoth, Kunz, Kinne-Saffran, & Rudloff, 2000).

Components	SSF	SGF	SIF
	mmol/L	mmol/L	mmol/L
K^+	18.8	7.8	7.6
Na^+	13.6	72.2	123.4
Cl^-	19.5	70.2	55.5
$H_2PO_4^-$	3.7	0.9	0.8
$HCO3^-$, CO_3^{2-}	13.7	25.5	85
Mg^{2+}	0.15	0.1	0.33
NH_4^+	0.12	1	x
Ca^{2+}	1.5	0.15	0.6

Table 16: Salts concentrations in simulated digestive fluids (SSF for Simulated Salivary Fluid, SGF for Simulated Gastric Fluid and SIF for Simulated Intestinal Fluid) (Minekus et al., 2014)

DIGESTIVE STEP	pH and duration	ENZYMES		
		NAME	CONCENTRATION	REFERENCE
ORAL PHASE SSF	pH 7 2 min 37°C	α-Amylase from porcine pancreas	10 mg/ml	A317
		Lysozyme human	4 µg/ml	L1667
		Lactoferrin human	5 µg/ml	L1294
		Mucin type II from porcine stomach	300 µg/ml	M2378
GASTRIC PHASE SGF	pH 3 2 hours 37°C	Pepsin from porcine gastric mucosa	1 mg/ml	P7012
INTESTINAL PHASE SIF	pH 7 2 hours 37°C	Pancreatin from porcine pancreas	25 mg/ml	P7545
		Bile extract porcine	17 mg/ml	B8631

Table 17: Enzyme composition of the simulated digestive fluids (SSF for Simulated Salivary Fluid, SGF for Simulated Gastric Fluid and SIF for Simulated Intestinal Fluid)

The simulated digestion protocol (Figure 39) was performed at 37°C, under magnetic stirring and in dark conditions: TiO_2 particles were suspended in the salivary fluid at pH 7 for 2 minutes, then this fluid was mixed with gastric fluid at pH 3 for 2 hours and finally this mixture was mixed with intestinal fluid at pH 7 for 2 hours. Experiments were also performed without proteins to determine the impact of salts separately from the impact of proteins, and without TiO_2 particles as a control.

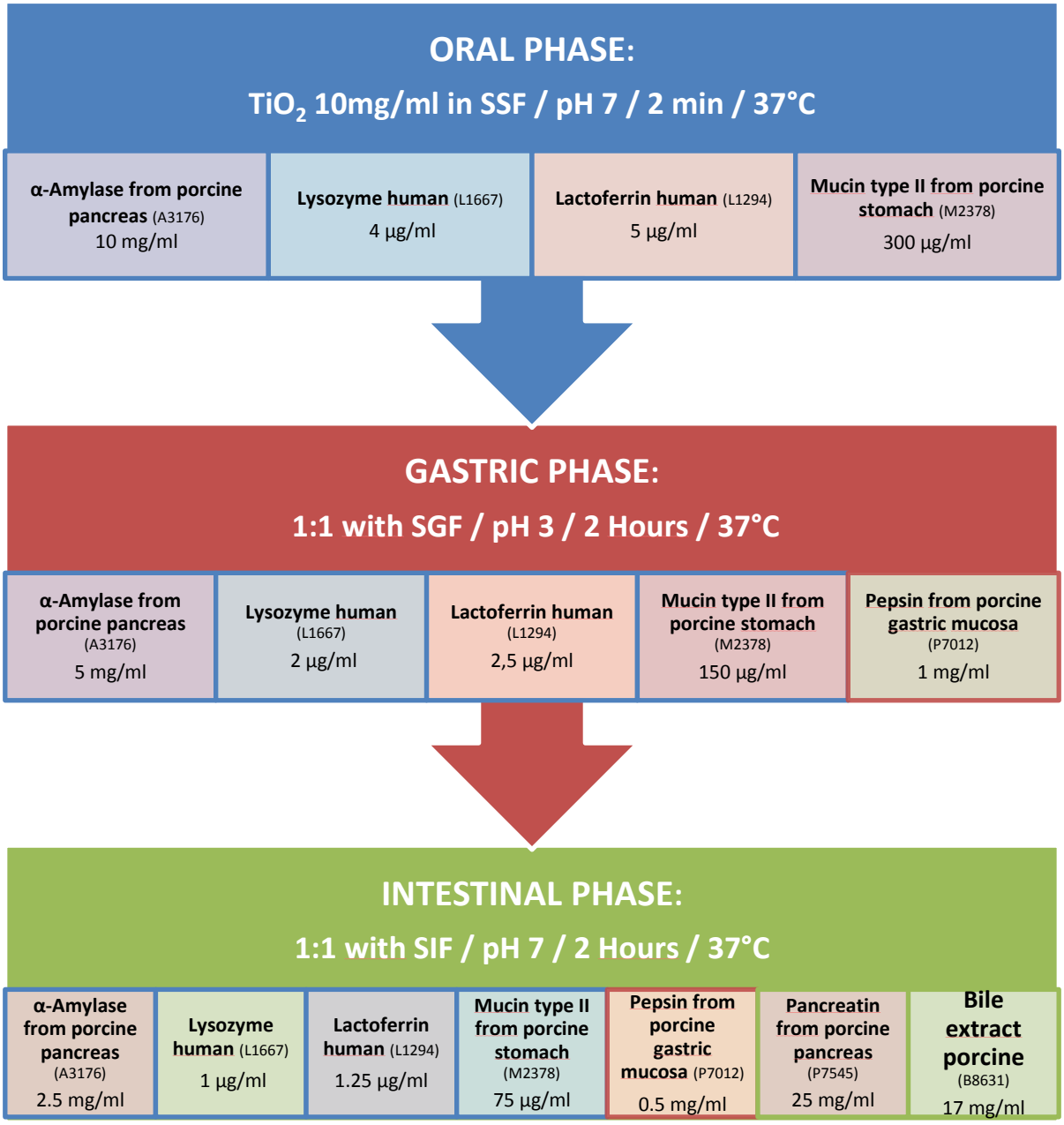

Figure 39: Simulated digestion protocol, adapted from (Minekus et al., 2014)

2) Characterization of TiO_2 particles in simulated digestive fluids

After each step of the simulated digestion (*i.e.* saliva, gastric and intestinal step), aliquots were taken and analyzed within one day. The size of the particles and the surface charge changes were characterized by laser diffraction and laser Doppler electrophoresis. The nature of the adsorbed proteins was determined by SDS-page after separation from the TiO_2 particles (Figure 40).

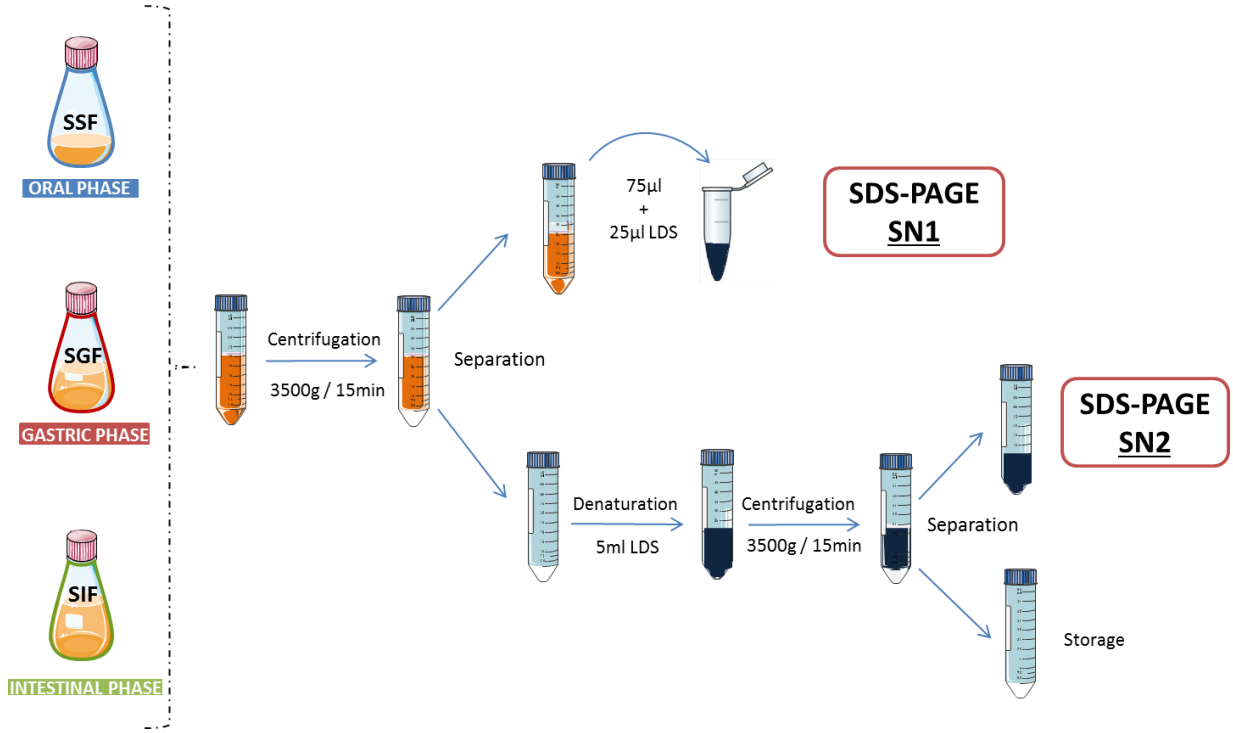

Figure 40: Protocol for the characterization of TiO_2 particles during simulated digestion

a) Size distribution and zeta potential measurements

Sample preparation

When the digestion was performed with proteins, a preliminary centrifugation at 3500 *g* for 15 minutes was necessary to separate the TiO_2 in the pellet from the proteins in the supernatant. Particles were then re-suspended in the corresponding saline fluid, without proteins to get a suitable concentration for the analysis (50µg/ml). Size distribution analyses were performed in the intern cell of the Horiba laser scattering particle size distribution analyzer (LA-960) filled with the corresponding digestive fluid (without proteins). Zeta potential measurements were performed as described previously (in Chapter 2-2-k).

b) SDS-page electrophoresis

Principle

Gel electrophoresis are used to separate macromolecules differing in their molecular size, charge or conformation. This method is based on the migration of equally charged molecules through a matrix under the application of an electric field. Then, the smaller is the molecule, the greater is the distance it will travel through the gel, allowing the separation of all the different molecules (Figure 41).

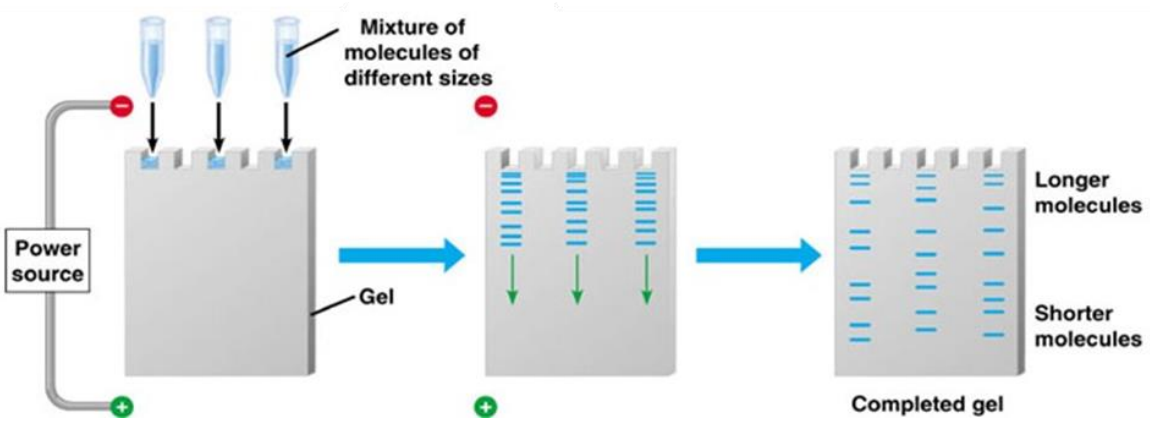

Figure 41: Gel electrophoresis principle (Copyright © 2005 Pearson Education, Inc. Publishing as Benjamin Cummings)

To separate proteins according to their size, detergents as sodium dodecyl sulfate (SDS) or lithium dodecyl sulfate (LDS) are added to the sample in order to unfold and negatively charge the proteins, allowing the migration. Moreover, the gel has to be immersed in an adapted buffer solution, needed to provide ions to create electrical current and to maintain pH at a relatively constant value. Finally, a loading dye is added to the sample, containing glycerol to help the loading of the sample and a dye to monitor the migration. Following electrophoresis, the gel may be stained using Coomassie Brilliant Blue G-250, allowing visualization of the separated proteins as distinct bands within the gel. The corresponding molecular mass of each band can be deduced by comparing with a molecular weight size marker.

Sample preparation

Each aliquot removed from the digestive medium was centrifuged at 3500 *g* for 15 minutes to separate TiO_2 with adsorbed proteins in the pellet from the non-interactive proteins in the supernatant (SN1). This supernatant was analyzed to identify any change in intensity which could be a sign of adsorption. 75 µL of SN1 samples were mixed with 25 µL of NuPAGE® LDS (4X, Thermo Fisher Scientific, MA, USA) for further electrophoresis analyses.

In a second time, the pellet was re-suspended in 500µl of LDS denaturing solution and stirred for 1 hour using a Heidolf Multi Reax shaker (Heidolf, Germany), to denature and desorb the previously adsorbed proteins. Once again, samples were centrifuged to separate TiO_2 particles from the desorbed proteins obtained in the supernatant (SN2). These supernatants were then analyzed by denaturing gradient gel electrophoresis.

Sample Analysis

Denaturing gradient gel electrophoreses were performed with a NuPAGE® electrophoresis system using NuPAGE® Bis-Tris Precast Gels (4-12% polyacrylamide, 15 wells) with MES SDS Running Buffer. 20 µL of previously denatured SN1 and SN2 were loaded into the gel. The electrophoreses were run with 2 gels in the same time, at 200 mA for 10 minutes then 140 mA for 1 hour. Following migration, gels were stained using Coomassie Brilliant Blue G-250.

Briefly, gels were immersed in 2% phosphoric acid and 50% ethanol for 30 minutes. Then, gels were immersed in 2% phosphoric acid for another period of 30 minutes, then in 17% ethanol, 15% ammonium sulfate and 2% phosphoric acid for 20 minutes. Finally, 0.03% coomassie G-250 was added and the coloration was allowed to stand overnight. The next day, gels were immersed 3 times for 10 minutes in milliQ water, then 10 minutes in 20% ethanol and finally stored in milliQ water. Visualization of the separated proteins was performed using an ImageScanner III LabScan 6.0 (GE Healthcare, Little Chalfont, UK). Samples molecular masses were determined by comparing the migration with the Novex® Sharp Pre-Stained Protein Standard (Thermo Fisher Scientific, MA, USA).

III) Impact of food grade TiO_2 particles on gut microbiota

1) Samples and cellular culture for the assessment of the impact of TiO_2 on gut microbiota

a) TiO_2 samples preparation

Food grade TiO_2 from two suppliers (E171-1 and E171-6a, characterized in the first part of our work, (Dudefoi et al., 2017)) as well as control P25 Degussa particles were assessed for their toxicology using a model gut bacterial community. Particle sterility was interrogated by inoculation of the food additives and the TiO_2 NPs (5 mg each) into sterile 10% tryptic soy culture medium, incubation at 37 °C for 2 days and subsequent plating (100 µL) on 10% TSA (tryptic soy agar) at 37°C. Stock solutions of TiO_2 particles (5 mg/mL) and α-amylase (50 mg/mL) were prepared in sterilized milliQ water in sterile serum bottles fitted with sterile rubber stoppers and crimped with a metal band. The bottles were agitated for 1 h before the bacterial community was added to the vials.

b) Human gut ecosystem culture

The defined MET-1 bacterial community has been previously described (Petrof et al., 2013). Prior to use, each of the component 33 bacterial strains (see Table 18) was individually cultured on fastidious anaerobe agar (Acumedia) containing 5% defibrinated sheep's blood (Hemostat Laboratories) under anaerobic conditions, and the biomass was used to inoculate a chemostat bioreactor, which was run for 1 day in batch followed by 10 days under flow conditions using a medium approximating the content of the human colon (400 ml/day). Control of both pH and temperature was maintained throughout (pH 6.8, 37ºC), as well as gentle agitation and constant sparging of sterile N_2 gas through the culture to maintain anaerobic conditions. Full details of chemostat set-up and culture, including media components are described by

McDonald et al. (McDonald et al., 2013). After 10 days of growth under these conditions, MET-1 attains steady-state equilibrium. The MET-1 suspension was harvested from the chemostat vessel and 450 µL was aliquoted into 4050 µL of sterile growth medium (1:10) in individual autoclaved glass serum bottles that were then placed in an anaerobic chamber (90% N_2, 5% CO_2, 5% H_2, Figure 42).

Strain designation	*Closest species match	#% Homology
14 LG	*Acidaminococcus intestini*	99
3FMU	*Akkermansia muciniphila*	100
5 MM	*Bacteroides ovatus*	99
11 FAA	*Bifidobacterium adolescentis*	99
20 MRS	*Bifidobacterium adolescentis*	99
2 FAA	*Bifidobacterium longum*	99
4 FM	*Bifidobacterium longum*	99
27 FM	*Blautia stercoris*	99
21 FAA	*Clostridium cocleatum*	92
3 FM	*Collinsella aerofaciens*	99
10 FAA	*Dorea longicatena*	99
42 FAA	*Dorea longicatena*	99
3 FM 4i	*Escherichia coli*	100
48 FAA	*Butyricicoccus pullicaecorum*	95
F1 FAA	*Eubacterium eligens*	99
13 LG	*Eubacterium limosum*	97
6 FM	*Eubacterium rectale*	99
29 FAA	*Eubacterium rectale*	99
1 FAA	*Eubacterium rectale*	99
18 FAA	*Eubacterium rectale*	99
47 FAA	*Eubacterium ventriosum*	99
40 FAA	*Faecalibacterium prausnitzii*	99
34 FAA	*Lachnospira pectinoschiza*	95
6 MRS	*Lactobacillus casei*	99
25 MRS	*Lactobacillus paracasei*	99
5 FM	*Parabacteroides distasonis*	99
BF 7	*Enterobacter aerogenes*	100
39 FAA	*Roseburia faecis*	99
31 FAA	*Roseburia intestinalis*	99
11 FM	*Ruminococcus obeum*	99
2 MRS	*Blautia luti*	95
30 FAA	*Ruminococcus torques*	99
9 FAA	*Ruminococcus torques*	99
50 FAA	*Streptococcus mitis*	99

Table 18: Strains present in MET-1, and their closest species matches. * As inferred by 16S rRNA gene sequence homology across the full-length gene to the RDP database (Cole et al., 2014); # % Match of full-length 16S rRNA gene sequence to closest species.

c) *Batch cultures*

Experimental serum bottles had been amended with one of two realistic concentrations of TiO_2 particles (100-250 ppm), which were based on a single unit of gum and defined from previous experiments (the *in vitro* digestion process from (Minekus et al., 2014) recommends to use 1g of food in 1mL of saliva, 2 mL of gastric fluid and then 4 mL of intestinal fluid; considering that 1 g of chewing-gum leads to the intake of around 0.4 and 1 mg of TiO_2 for C5 and C1, this leads to a final concentration of 100 and 250 ppm of TiO_2 in the intestinal fluid). Experiments involved three kinds of TiO_2 particles, including the toxicological reference P25 Degussa particles, and two kinds of food grade TiO_2, E171-1 and E171-6a (batch n°1) for their different surface chemistry. Finally, a mixture of food grade TiO_2 (E171-1, 100-250 ppm) and α-amylase (37.5 U/mL, α-Amylase from porcine pancreas, A317, Sigma Aldrich) was included to model the addition of human digestive enzyme to the gut bacterial community along with TiO_2. Control experiments were also conducted: control culture bottles contained MET-1 only, as well as MET-1 and α-amylase. The final volume of each serum bottle was brought to 5 mL with the addition of sterile, milliQ water. Samples were sealed with sterile rubber stoppers and aluminum caps crimped to the neck of the bottles. Grouped by 6, the culture bottles were placed in an air-tight double-sealed bag containing anaerobic gas packs (Beckton Dickinson) and allowed to incubate in batch culture for 48 h at 37 °C in the dark, with agitation. All sample compositions are detailed in Table 19.

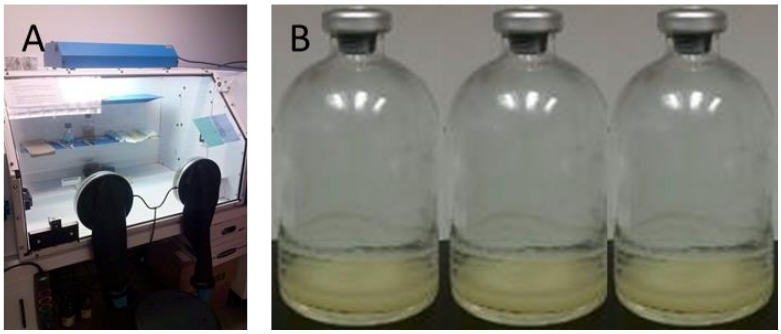

Figure 42: A) Anaerobic chamber and B) Glass serum bottles, stoppered and crimped and containing 5mL of MET-1

Sl.	Treatment Name	Treatment Code	TiO_2 NPs (µL)	α-Amylase (µL)	MilliQ H2O (µL)
1	Control without nano	Ctrl 1	0	0	500
2	Control without nano	Ctrl 2	0	0	500
3	Control without nano	Ctrl 3	0	0	500
4	E171-6a 100mg/L	E171-6a L 1	100	0	400
5	E171-6a 100mg/L	E171-6a L 2	100	0	400
6	E171-6a 100mg/L	E171-6a L 3	100	0	400
7	E171-6a 250 mg/L	E171-6a H 1	250	0	250
8	E171-6a 250 mg/L	E171-6a H 2	250	0	250
9	E171-6a 250 mg/L	E171-6a H 3	250	0	250
10	E171-1 100mg/L	E171-1 L 1	100	0	400
11	E171-1 100mg/L	E171-1 L 2	100	0	400
12	E171-1 100mg/L	E171-1 L 3	100	0	400
13	E171-1 250 mg/L	E171-1 H 1	250	0	250
14	E171-1 250 mg/L	E171-1 H 2	250	0	250
15	E171-1 250 mg/L	E171-1 H 3	250	0	250
16	P25 100mg/L	P25 L 1	100	0	400
17	P25 100mg/L	P25 L 2	100	0	400
18	P25 100mg/L	P25 L 3	100	0	400
19	P25 250 mg/L	P25 H 1	250	0	250
20	P25 250 mg/L	P25 H 2	250	0	250
21	P25 250 mg/L	P25 H 3	250	0	250
22	E171-1 100 mg/L + α-Amylase	E171-1 LA 1	100	250	150
23	E171-1 100 mg/L + α-Amylase	E171-1 LA 2	100	250	150
24	E171-1 100 mg/L + α-Amylase	E171-1 LA 3	100	250	150
25	E171-1 250 mg/L + α-Amylase	E171-1 HA 1	250	250	0
26	E171-1 250 mg/L + α-Amylase	E171-1 HA 2	250	250	0
27	E171-1 250 mg/L + α-Amylase	E171-1 HA 3	250	250	0
28	α-Amylase control	Amy 1	0	250	250
29	α-Amylase control	Amy 2	0	250	250
30	α-Amylase control	Amy 3	0	250	250
31	Control without nano for GC	0GC1	0	0	500
32	Control without nano for GC	0GC2	0	0	500

Table 19: Experimental design for the assessment of TiO_2 toxicity on MET-1 consortium

2) Culture analyses

a) Physiological assay: Gas generation analysis

Gas production was monitored in the serum bottles after 48 h of incubation, following the protocol described by Das et al (Das, et al., 2014). Briefly, gas was sampled *in situ* using 10 mL syringes (Figure 43, Luer-LokTM Tip BD with 22G1 Precision GlideR needles, Becton Dickinson & Co, NJ) then immediately injected using a split-less mode into an Agilent Technologies 7890B Gas Chromatograph (GC; Palo Alto, California, USA), equipped with a stainless steel column (50 m×0.53 mm internal diameter, 10 µm film thickness) and packed with Agilent J&W PoraBOND Q (Palo Alto, California, USA). Total gas production was measured in the syringe, and the amount of produced CO_2 and N_2 was determined using Agilent Technologies Chem Station Integration Software (Palo Alto, California, USA).

Figure 43: In situ sampling of produced gas after 48 h using a syringe fitted with a needle

b) *Biochemical assay: Fatty acid analysis*

Immediately after recording gas production after the 48 h incubation, a sample (1 mL) from each serum bottle was centrifuged at 2000x g for 10 min and the pellets were placed into 2 mL cryo-tubes. They were stored at -80 °C until shipped for fatty acid methyl ester (FAME) analyses (Figure 44, Keystone Labs; Edmonton, Canada). The commercial laboratory extracted phospholipid fatty acids from the pellets using the MIDI Sherlock Microbial Identification System (Microbial ID Inc., Newark, DE, USA) as described in the literature (P Das et al., 2015). Briefly, each pellet was saponified, methylated, extracted, washed and finally analyzed through a gas chromatograph equipped with an Ultra 2 column followed by a flame ionization detector (Agilent). For each sample, the resulting chromatographic peak areas were converted into the percentage of total fatty acids (mol %).

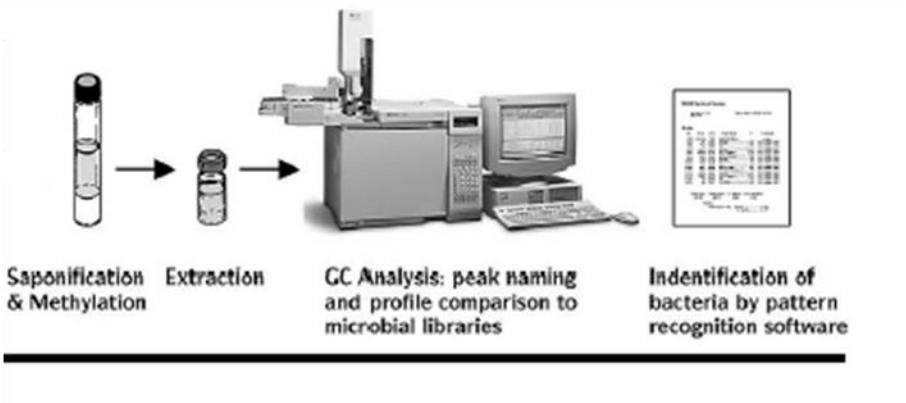

Figure 44: MIDI's Fatty Acid-based Microbial Identification System workflow (Kunitsky, 2006)

c) Molecular assay: DNA analysis

DNA extraction

The impact of TiO_2 particles on the microbial ecosystem was also assessed with molecular assays, namely two types of DNA analysis. After gas analysis and sampling for fatty acids, samples (3 x 200 µL) were removed from each serum bottle and placed into 2 mL cryotubes. These were then flash frozen in liquid nitrogen and then stored at -80 °C. DNA was subsequently extracted using a QIAamp DNA stool mini kit (Qiagen Sciences, LLC, MD, USA, Cat° 51504) following the "Isolation of DNA from Stool for Human DNA Analysis" protocol. Briefly, the procedure comprises 3 main steps including a lysis of the sample in Buffer ASL (a proprietary buffer), an adsorption of impurities to an InhibitEX matrix, and a purification of DNA on QIAamp Mini spin columns. (Figure 45)

The last step of the extraction was modified from the manufacturer's recommended protocol. Rather than using 200 µL of Buffer AE (a proprietary buffer), 50 µL of sterile milliQ water were added in order to avoid any potential undesirable effects of the undescribed buffer for the next step of the experiments. The extracted DNA was stored at -20 °C.

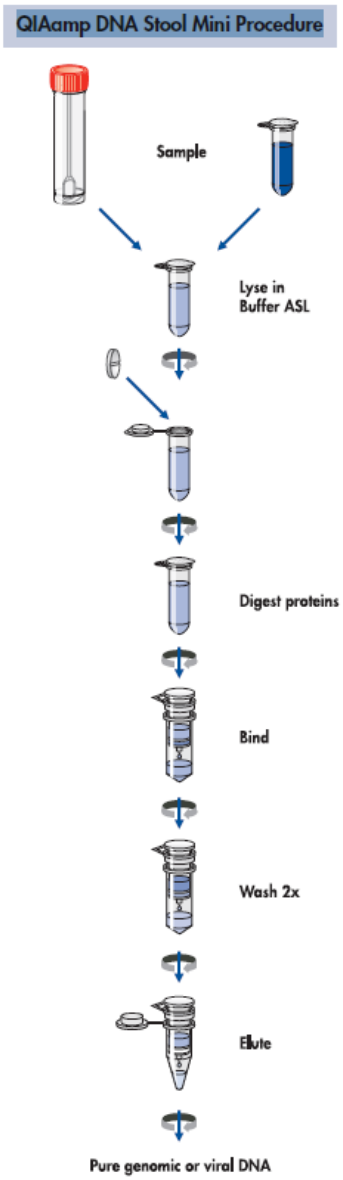

Figure 45: An overview of the QIAamp DNA Stool Mini Kit principle (www.qiagen.com)

DNA amplification by polymerase chain reaction (PCR)

PCR principle

The purpose of a PCR (Polymerase Chain Reaction) is to increase the quantity of a portion of DNA in a sample. PCR is a three-step cycling process repeated 30 to 40

times, including thermal denaturation of the double-stranded DNA, annealing of primers and primer extension (Figure 46).

The first step consists in the thermal denaturation of DNA resulting in the separation of double-stranded DNA. The second step is the annealing reaction where primers base pair with either the proximal or the distal side of the dissociated DNA strands. Finally, the third step is the extension reaction where the added DNA polymerase catalyzes the synthesis of new strands of DNA by adding nucleotides complementary to those in the unpaired DNA strand onto the annealed primer. The quantity of DNA is then multiplied by 2 after each cycle. After 30 cycles, a single copy of DNA can be increased up to 1 million copies (Figure 47).

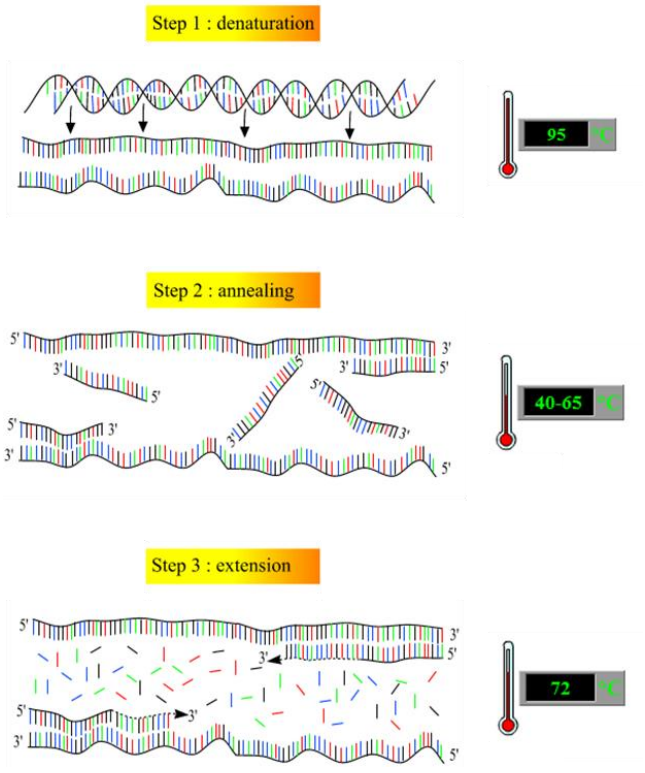

Figure 46: Polymerase chain reaction principle (Adapted from http://users.ugent.be/~avierstr/principles/pcr.html)

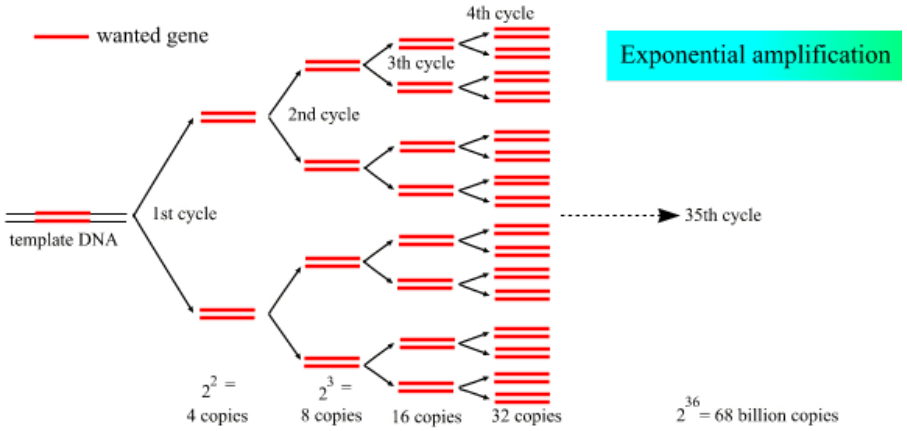

Figure 47: Exponential amplification of DNA by PCR (Adapted from http://users.ugent.be/~avierstr/principles/pcr.html)

Applied PCR protocol

Genomic DNA was PCR amplified in triplicates in a Veriti® 96 Well Thermal Cycler (Applied Biosystems, Burlington, Canada) using the primer pairs: 28F (5'-GAGTTTGATCNTGGCTCAG -3) and 519R (5'-GTNTTACNGCGGCKGCTG -3') as described by Fan, McElroy, & Thomas, 2012. PCR reaction mixtures were prepared with 4 µL of DNA template, 2.5 µL of each primer (10 µM), 5 µL of 10X Buffer (Vivantis VSPL1202 containing $MgCl_2$), 0.4 µL of dNTP mix (12.5 mM; Thermo Scientific), 1 µL of bovine serum albumin (5 mg/mL), 0.5 µL of recombinant Taq DNA polymerase (5u/µL; Vivantis, Malaysia, (Lee et al., 2009) and 34.1 µL of sterile water, to a total volume of 50µL. The PCR conditions included a first step of denaturation for 5 min at 95 °C, followed by 30 cycles of 1 min at 95 °C (denaturation), 1:30 min at 50 °C (annealing), 1:45 min at 72 °C (extension) with a final extension for 7 min at 72 °C. Controls with and without DNA were always included as positive and negative controls.

Agar gel electrophoresis

The concentration and integrity of the amplified DNA was assessed by electrophoresis on 1% agarose gels stained with ethidium bromide and viewed on a UV transilluminator. A solution of 1% agarose was prepared by mixing 500 mg of agarose with 50mL of TAE (Tris-Acetate-EDTA, 1X) and was melted in the microwave for 2 min so that it completely dissolved. After 5 min cooling, 4 µL of ethidium bromide (10mg/ml) were added (to a total of 0.8 µg/mL) and the 1% agarose solution was poured into the gel former. A comb was placed into the solution. After 10 min, 5 µL of each of the amplified DNA samples were mixed with 2 µL of 6 X loading dye and loaded into a single well for electrophoresis at 95V for 15 min. (White, 1993) The migrated PCR products were observed through protective eye wear on a UV transilluminator (Alpha Innotech, Santa Clara, USA) and images recorded.

Polymerase chain reaction (PCR) product purification

To remove primers, dNTPs, unincorporated labeled nucleotides, enzymes, and salts from the PCR amplified products, they were purified using the GeneJET PCR Purification Kit (Thermo-Scientific, K0702) and following the "DNA purification using centrifuge" protocol. (www.thermofisher.com)

Polymerase chain reaction (PCR) product quantification

The concentration and purity of the amplified DNA was assessed by spectrophotometric analysis using a NanoDrop 1000 (NanoDrop-1000 Ver.3.7.1; Thermo Scientific, Wilmington, USA) (Passalacqua et al., 2009). DNA samples (1 µL) in triplicate were placed in the NanoDrop device in order to obtain the DNA concentration in ng/µL based on the absorbance at 260 nm. Sample purity was assessed based on the ratio of absorbance at 260 nm and 280 nm.

Sequencing of 16S ribosomal RNA gene fragments

After amplification by PCR and purification, DNA samples were sequenced in triplicate using 454 pyrosequencing technology to identify the different species of bacteria. Each sequencing was performed by the Research and Testing Laboratory (MR DNA; Shallowater, TX, USA) using a Genome Sequencer Roche 454 FLX Titanium platform (Roche, Nutley, NJ) and following the manufacturer's recommendations. Raw sequence information was clustered into operation taxonomic units (OTus) based on 97% identity. They were then taxonomically classified using the BLAST.n algorithm by comparing the OTUs to a curated database derived from GreenGenes, RDPII and the 16S sequences of the National Center for Biotechnology Information (NCBI) (www.ncbi.nlm.nih.gov, (DeSantis et al., 2006), http://rdp.cme.msu.edu). OTUs were then compiled into each taxonomic level into both "counts" and "percentage" files, representing the actual number and the relative percentage of sequences within each sample that map to the designated taxonomic classification. Routinely, sequences representing less than 0.1% of the reads were discarded since it is likely that these represent sequence errors.

Amplification using nested PCR

Nested PCR reactions were performed on the purified DNA initially amplified using the 28F and 519R primer pairs in order to generate amplified products of a suitable size for PCR- denaturing gradient gel electrophoresis (PCR-DGGE) analyses. This second PCR was performed using the primer pair: 338F (5'-ACTCCTACGGGAGGCAGCAG GC-3') with an additional 40-nucleotide GC-rich sequence on the 5'-end (GC clamp) (5'-CGCCCGCCGCGCGCGGCGGGCGGGGCGGGGGCACGGGGGG-3') and the reverse primer 519R (5'-GTNTTACNGCGGCKGCTG -3') as described by Bakke, De Schryver, Boon, & Vadstein, 2011. Taking the PCR products from the first PCR as DNA template for the second one, the applied protocol included a denaturation for 5 min at 95 °C, followed

by 18 cycles of 1 min at 95 °C (denaturation), 1:15 min at 67 °C (annealing), 1:30 min at 72 °C (extension) with a final extension for 7 min at 72 °C. The presence and integrity of the amplified products were confirmed by electrophoresis in 1% (w/v) agarose gels stained with ethidium bromide and viewed on a UV transilluminator (Alpha Innotech, Santa Clara, USA) as previously detailed.

PCR-DGGE

The nested-PCR products were subjected to denaturing gradient electrophoresis (DGGE) using a DGGEK-2401 System (CBC Scientific, Del Mar, USA) (Tok, Szabolcs, & Silvers, 1998). Briefly, samples were mixed (1:1) with 2X loading dye and 15 µL were loaded onto 8% (w/v) polyacrylamide gels with a denaturing gradient ranging from 30% to 70% of urea (Sonthiphand & Neufeld, 2013). Gels were prepared using a stock denaturing solution of 40% formamide and 7M Urea as described by Myers & Fischer, 1985. Once loaded, gels were electrophoresed at 120V for 3 min then 70V for 18 h in 1X TAE buffer at 60°C. Following electrophoresis, gels were stained in TAE 1X containing ethidium bromide (0.5 mg/L) then rinsed in TAE 1X buffer for 5 min. Gels were visualized using an Alpha Innotech UV transilluminator and photographed using AlphaEase® FC software (Version 6.0, Alpha Innotech, Santa Clara, CA, USA). Finally, intensities of the DGGE-generated images were analyzed using Syngene Genetools software (version 4.03.03, Synoptics Ltd.).

3) Statistical analysis

The assessment of the impact of TiO2 on the model gut microbiota culture through gas production measurements, FAME analysis, PCR-DGGE and DNA sequencing was analyzed statistically. A one-way ANOVA (ANalysis Of VAriance) with post-hoc Tukey HSD (Honestly Significant Difference) test calculator was used to compare multiple treatments and to evaluate significant differences in comparison to the control

(bilateral Dunnet test) using Xlstat (v 2014.1.08, Addinsoft. 2016. XLSTAT 2016: Data Analysis and Statistical Solution for Microsoft Excel. Paris, France, 2016). Differences were considered not significant for p values >0.05.

Chapter 3: Results

I) Physicochemical characterization of E171 and P25 particles

To determine whether P25 and E171 particles are similar or not, several food grade TiO_2 samples and P25 particles were investigated for their physicochemical characteristics (size distribution, shape, crystallinity, reactivity, surface properties). Several methods relevant from physical chemistry were applied: transmission electron microscopy (TEM), X-ray diffraction (XRD), laser scattering particle size distribution analysis, X-ray photoelectron spectrometry (XPS), zeta potential measurements, usual vibrational Raman and IR spectroscopies, inductively coupled plasma atomic emission spectroscopy (ICP-AES), diffuse reflectance infrared Fourier transform spectroscopy (DRIFTS) and specific surface area analysis.

1) Elemental analysis of TiO_2 powders

Concentrations of elements Ti, Si, Al, Ca, and P in P25 and E171 food grade particles were determined by ICP–AES. Results are given in Table 20 for the three manufacturers' batches and for the distributors' batches. TiO_2 represents in weight 98.1%, 99.1%, 97.5%, 98.6%, 97.6% and 95.7% of the powder in P25, E171-1, E171-2, E171-3, E171-4, and E171-6a, respectively. Whereas TiO_2-P25 powder only contains elements Ti and O, all food grade TiO_2 samples also contain elements Al, Si and/or P. Phosphorus is present in all of them (between 0.6 and 1.6 mg/g). In addition to phosphorus, E171 samples may contain either aluminium (E171-2) or silicon (E171-1, E171-6a) or none of them (E171-3, E171-4). The equivalent amount of silica (SiO_2) and Alumina (Al_2O_3) is in any case lower than 0.5 wt% in accordance with the maximal limit of 1 or 2% specified by the U.S. Food and Drug Administration and the Joint FAO/WHO Expert Committee on Food Additives (Joint FAO/ WHO Expert Committee on Food Additives, 2010)

Samples	Al (mg/g)	Ca (mg/g)	Si (mg/g)	P (mg/g)	Ti (mg/g)	TiO_2 %
E171-1	0.00 ± 0.00	0.00 ± 0.00	0.11 ± 0.188	1.12 ± 0.002	594.09 ± 1.984	99.12 ± 0.33
E171-2	0.43 ± 0.006	0.00 ± 0.00	0.00 ± 0.00	1.24 ± 0.004	584.21 ± 1.168	97.47 ± 0.195
E171-3	0.00 ± 0.00	0.00 ± 0.00	0.00 ± 0.00	1.19 ± 0.007	590.87 ± 1.253	98.58 ± 0.21
E171-4	0.00 ± 0.00	0.08 ± 0.005	0.00 ± 0.00	0.61 ± 0.002	585.07 ± 7.323	97.62 ± 1.22
E171-6a	0.00 ± 0.00	0.00 ± 0.00	0.39 ± 0.046	1.66 ± 0.013	573.45 ± 4.766	95.68 ± 0.795
P25	0.00 ± 0.00	0.00 ± 0.00	0.00 ± 0.00	0.00 ± 0.00	587.72 ± 2.778	98.06 ± 0.46

Table 20: Elemental compositions of Ti, Al, Si and P in the reference sample TiO_2-P25 and three manufacturers' batches of E171 as determined by ICP-AES. Data are given in weight percent of TiO_2, SiO_2 and Al_2O_3 for Ti, Si and Al respectively in accordance with regulations.

2) Determination of the primary size distribution of TiO_2 particles

The number-based particle size distributions determined by TEM (Figure 48) for manufacturers' samples and Figure 49 for distributors' samples) are clearly different between the reference material and the food grade samples. P25 particles have a mean diameter of 23±9 nm (average ± one standard deviation), with 100% of NPs in accordance with previous works (Le et al., 2014; Motzkus, Macé, Vaslin-Reimann, Ausset, & Maillé, 2013; Ohno et al., 2001; Ohtani, Prieto-Mahaney, Li, & Abe, 2010; Yang et al., 2014). TEM analyses confirmed the presence of nanosized particles in E171 food grade samples, but the fraction of NPs (*i.e.* having an equivalent area diameter below 100 nm) was clearly below 50% in number (17, 36, 29, 27, 34, 21 and 18% from E171-1 to E171-6b, equivalent to 3.1, 12.5, 8.7, 5.9, 6.5, 3.4 and 4.7% in mass, respectively). The mean diameters of these samples are 144±43, 115±31, 122±35, 131±43, 129±52, 145±52 and 131±36nm, respectively (average ± standard deviation calculated on the 300 measured particles). Additionally, some large objects (Figure 50a) were also observed at several places in sample E171-2. Electron diffraction performed on such large objects (Figure 50b) revealed a rutile TiO_2 structure.

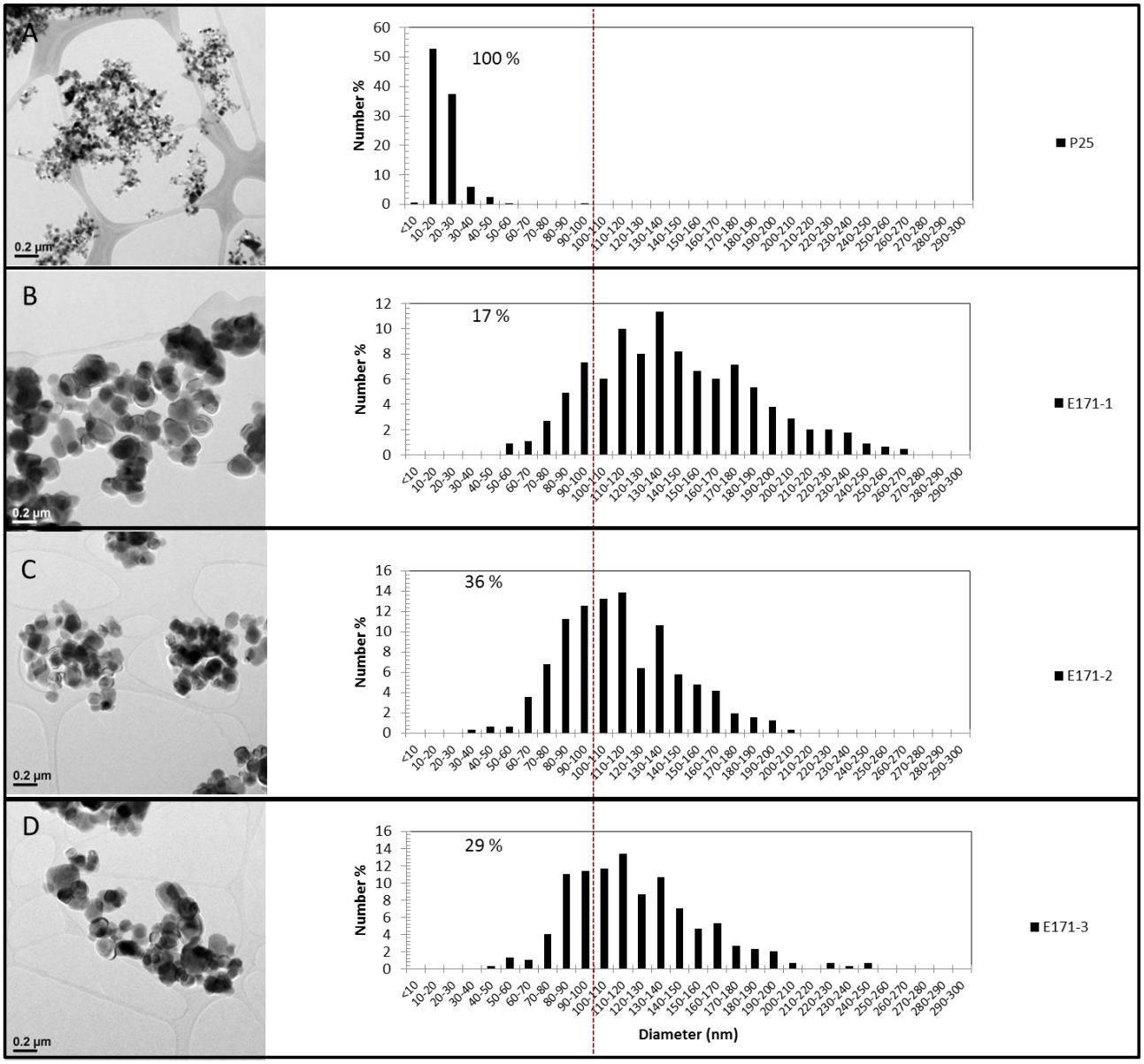

Figure 48: Left side: TEM micrographs at the same magnification of P25 and E171 food-grade titanium dioxide from different manufacturers (E171-1 to E171-3). Right side: particle size distributions derived from TEM images using ImageJ. For P25 particles, the size analysis was estimated from images obtained at higher magnification. The percentages indicate the fraction (in number) of particles having an equivalent area diameter below 100 nm.

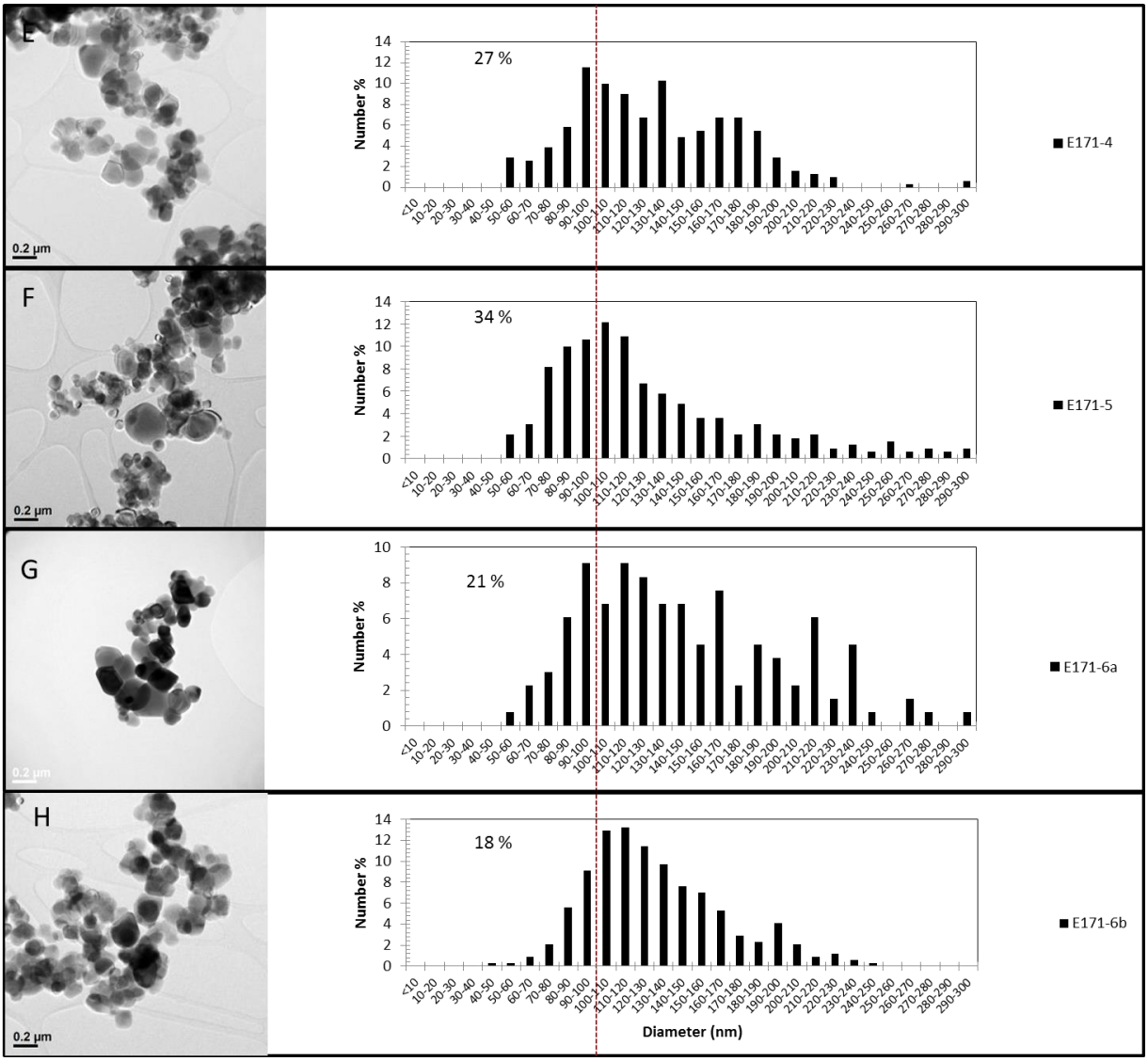

Figure 49: Left side: TEM micrographs at the same magnification of E171 food-grade titanium dioxide from different manufacturers (E171-4 to E171-6b). Right side: particle size distributions derived from TEM images using ImageJ. The percentages indicate the fraction (in number) of particles having an equivalent area diameter below 100 nm.

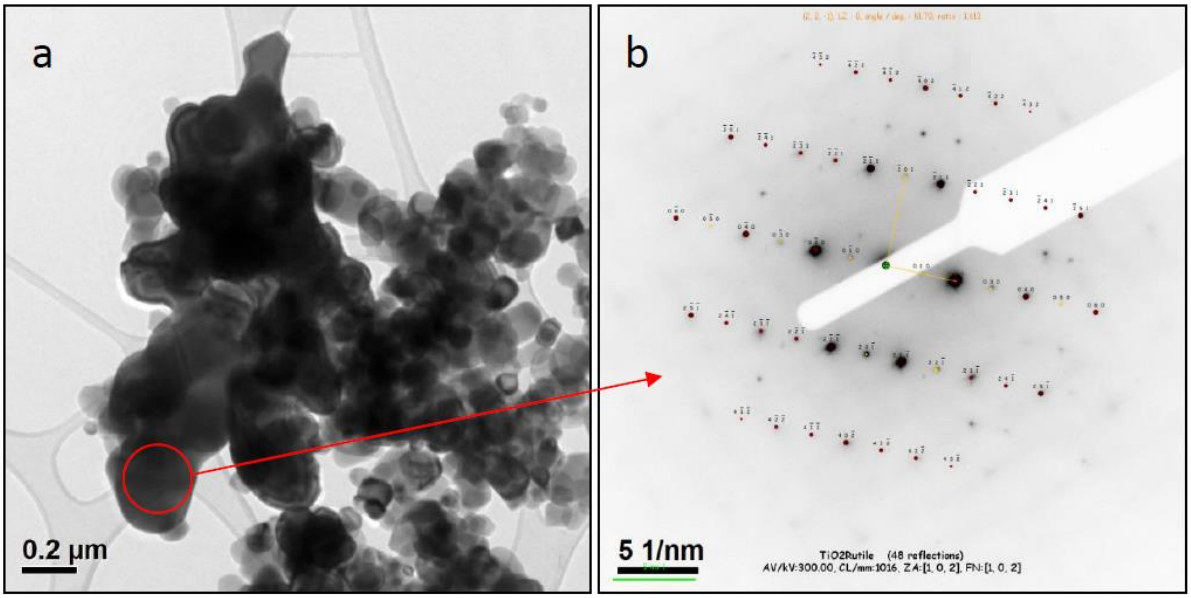

Figure 50: (a) TEM image of sample E171-2 where larger objects were observed. (b) Their crystalline structure was identified as rutile by selected area electron diffraction.

3) Determination of the crystal structure by XRD and FT-Raman Spectroscopy

X-ray powder diffractograms of the whole set of E171 samples (Figure 51 and Figure 52) reveal that anatase is the main phase. In the diffractogram of E171-2, which was previously shown to exhibit some large objects of rutile structure, the main rutile reflection being the (110) reflection at 2θ = 27.41° could be detected, confirming the presence of a tiny amount of rutile in the sample (however in a too low amount to be accurately estimated). As expected, P25 sample is a mixture of anatase and rutile, with a composition of 15 % rutile and 85% anatase, as determined by previous analyses. (Le et al., 2014) P25 diffraction peaks are broader than E171 peaks in good agreement with the smaller particle size of P25 in comparison to E171 samples. Raman spectroscopy also allows discrimination between anatase and rutile crystalline phases since their respective characteristic modes possess different eigenvalues frequencies. The peaks observed at 144, 198, 397, 516 and 640 cm^{-1} are unambiguously assigned to anatase phase whereas the peaks at 235, 449, 603 cm^{-1} are associated to rutile (Balachandran, Eror, & Mammone, 1982; Mazza et al., 2007; Ohsaka, Izumi, & Fujiki,

1978). The rutile phase having a lower scattering cross section and being in lower proportions than anatase, the most intense Raman active modes of rutile at 435 cm^{-1} and 611 cm^{-1} are hardly detected in the spectrum of TiO_2-P25 (Figure 53). For the whole set of food grade TiO_2 (manufacturers and distributors), the anatase crystalline phase is confirmed as well (Figure 53).

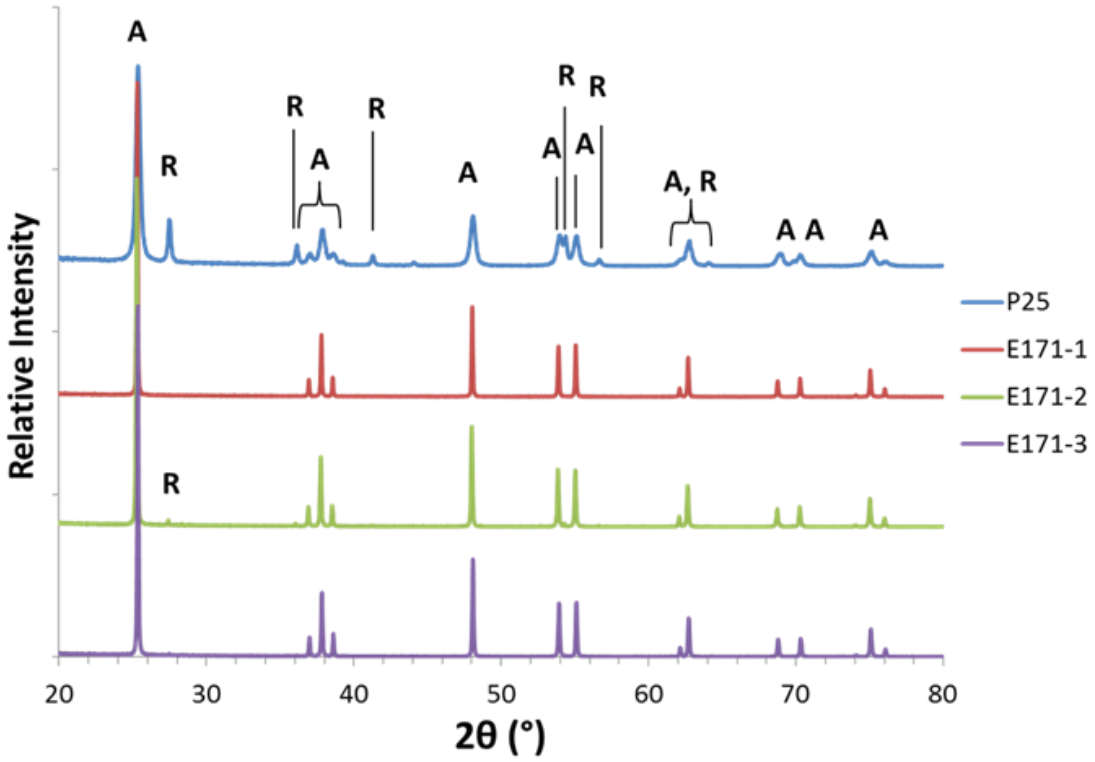

Figure 51: X-ray diffraction patterns of food-grade TiO_2 from manufacturers (E171-1, -2 and -3) and P25 particles. The assignment was made according to the reference patterns of anatase TiO_2 (JCPDS 89-4921) and rutile TiO_2 (JCPDS 89-4202).

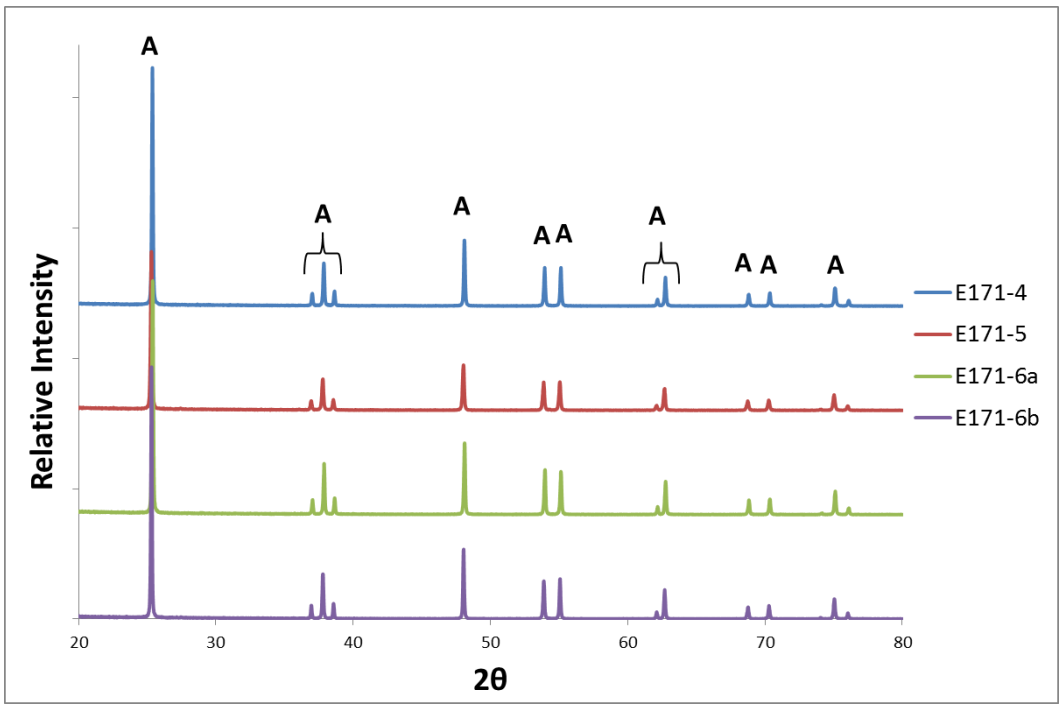

Figure 52: X-ray diffraction patterns of TiO_2 powders from distributors.

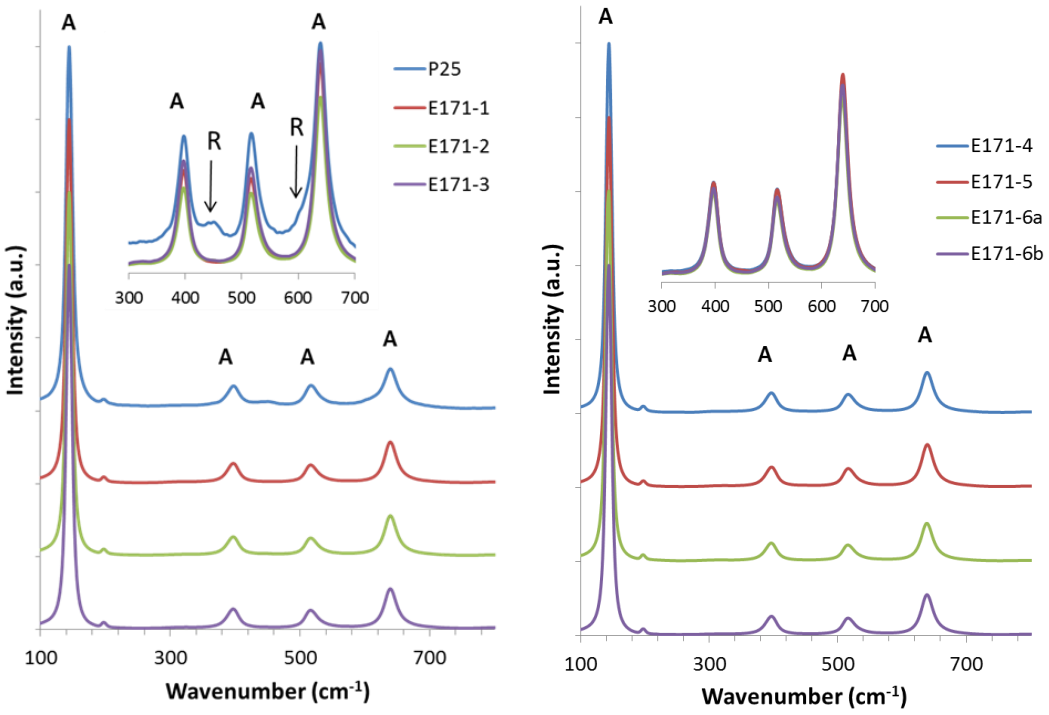

Figure 53: Raman spectra of TiO_2 powders (E171 and P25) from manufacturers, presented with an offset. (spectra were normalized on the intensity of the peak at 144 cm^{-1}). Symbols A and R refer to anatase and rutile. In the insert, the same spectra are given in the reduced wavenumber range from 300 to 700 cm^{-1} to highlight the peak relative to the rutile phase.

4) Specific surface area

The specific surface area value of P25 particles is in accordance with the value given by the provider (35-65 m^2/g) and those found in the literature data. (Le et al., 2014; Motzkus et al., 2013; Ohno et al., 2001) It is roughly five times larger than that of food grade samples (Table 21) which have specific surface areas comprised between 5.4 and 10.6 m^2/g. Here again, the values obtained are in accordance with suppliers' information. Moreover, the lower specific surface area of food additives is in accordance with their larger particle size as measured by TEM.

Samples	Specific surface area (m^2/g)
P25	50.0 ± 0.3
E171-1	8.63 ± 0.02
E171-2	10.67 ± 0.02
E171-3	8.77 ± 0.03
E171-4	9.08 ± 0.03
E171-6a	5.40 ± 0.08

Table 21: Specific surface area values of TiO_2 powders from manufacturers (food grade and P25), as determined by N_2 gas volumetry and interpreted by BET analysis.

5) Ultraviolet–Visible Light Diffuse Reflectance

TiO_2 is a semiconductor which strongly absorbs light at energies close to the band gap, *i.e.* equivalent to a wavelength below 365 nm (Diebold, 2003) This phenomenon is identified by an absorption edge in the UV-Visible absorbance spectrum. All TiO_2 samples fully absorb light below 340 nm and scatter very well light above 400 nm (Figure 54 and Figure 55). In-between, the slope of the curve differs according to the nature of particles. It is monotonous for E171 samples and composed of two slopes for P25 particles so that P25 particles better absorb light in the range 370-400 nm than E171 and reversely in the range 330-370 nm. These differences arise from the presence of rutile in a significant amount in P25. Indeed, this variety possesses a higher reflectance and a smaller electronic gap (3.0 eV for rutile and 3.2 eV for anatase, *i.e.* an absorption edge at 367 nm for rutile and at 387 nm for anatase). (Diebold, 2003) Beyond 400 nm, P25 sample exhibits a greater reflected visible light ability than food grade samples (98% against 88-94% of reflectance, respectively), certainly due to the smaller particle size of P25 in comparison to E171 (Figure 48).

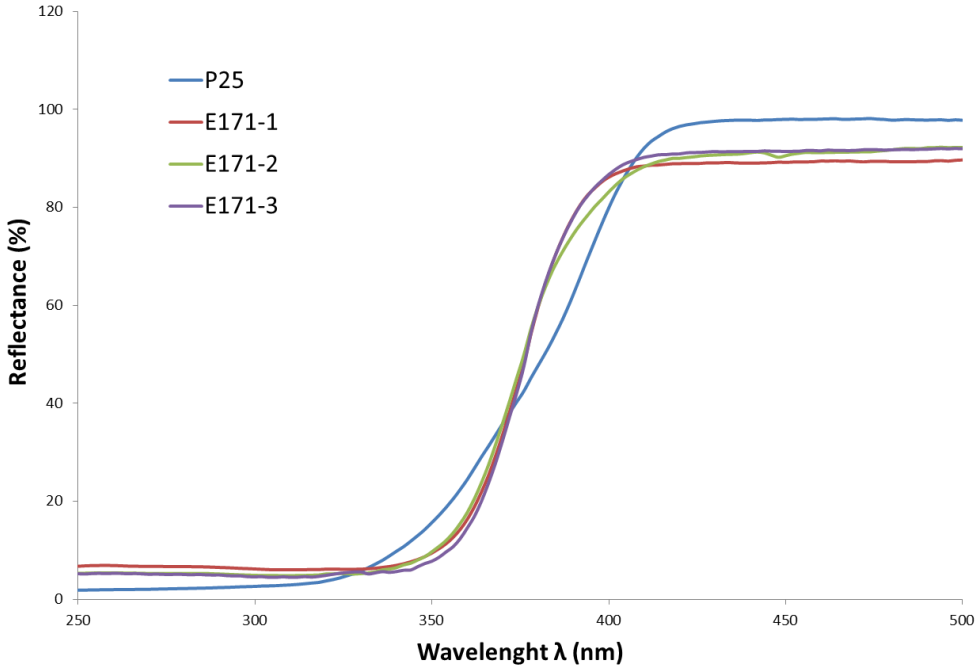

Figure 54: Ultraviolet-visible light diffuse reflectance (UV-vis DR) spectra of TiO_2 samples (P25 and food-grade) obtained from manufacturers.

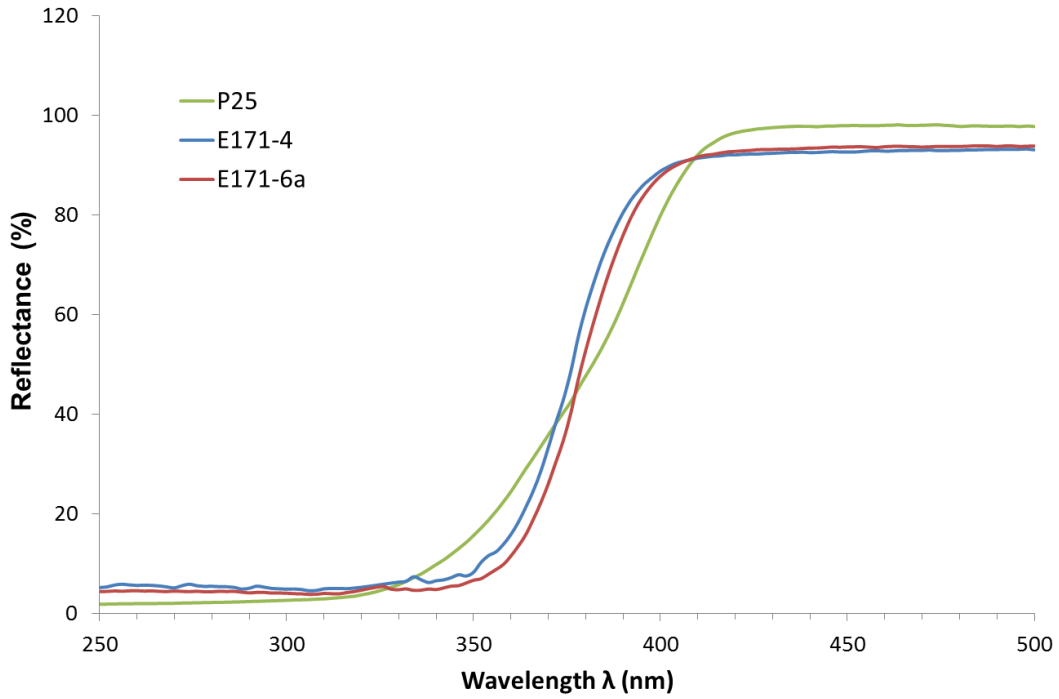

Figure 55: Ultraviolet–visible light diffuse reflectance (UV–vis DR) spectra of TiO_2 samples (P25 and food-grade from distributors).

6) Surface analysis

The O 1s peak of XPS spectra could be decomposed into only two components: one at 530 eV, which is characteristic of oxygen atoms belonging to the Ti-O framework (Moulder, Stickle, Sobol, & Bomben, 1992) and one broad band close to 532 eV which encompasses O belonging to O-H (Gao, Masuda, & Koumoto, 2004; J. C. Yu, Zhang, Zheng, & Zhao, 2003), O-C (Alexander, Beamson, Blomfield, Leggett, & Duc, 2001; L. Q. Wang, Ferris, Shultz, Baer, & Engelhard, 1997) and O=C (Brown, Hewitt, & Meenan, 1992). The component C 1s is relatively high but constant over all measurements; it mainly corresponds to adventitious carbon. The analysis of TiO_2 powders by XPS (Table 22) shows that P25 sample has a highly pure surface with the main oxygen peaks (O 1s) corresponding to the oxygen atoms involved in TiO_2 (Ti-O-Ti at 530 eV) and to the oxygen elements involved in O-H bonds (O 1s OH at around 532 eV). The stoichiometry O/Ti in P25 samples was close to 2.3 with a ratio OH/Ti close to 0.55. In the case of food grade samples from E171-1 to E171-6b, the elements Ti and O

relative to O belonging to O-H, O-C and O=C are found as well but the stoichiometry is different: O/Ti varies from 1.68 to 1.80 and the ratio of OH/Ti (including all forms O-C and O=C) is higher (from 0.63 to 1.04). Additionally, some other elements mainly K (293 eV), P (133 eV) were detected in small proportions relative to Ti element (around 0.07). The stoichiometry between these elements and Ti observed by XPS is higher than those determined by ICP-AES. This means that these elements are found at the outermost surface of TiO_2. In one case (E171-6a), chlorine and silicon were detected as well but were no longer detected in the second batch (E171-6b). The presence of phosphorus was tentatively explained by the use of polyphosphates-containing surfactants in the synthesis of titanium dioxide. (Yang et al., 2014)

Overall, food grade samples seem to be more hydroxylated at the surface than the photocatalytic sample. The relative number of hydroxyl groups and their nature were investigated by infrared spectroscopy in both the near- and mid-infrared ranges. To avoid any misinterpretation due to a surface acidity, which modifies the infrared band profiles (Le, 2014), samples were dispersed in solutions at different pH values and dried before analysis by DRIFT. (Yang et al., 2014) Spectra were recorded with both infrared sources but only data obtained with the NIR source in the spectral range 7500-2500 cm^{-1} are reported here at pH 2 (Figure 56). The full set of spectra, which were recorded in the mid- and near-infrared range at any pH, are provided in Figure 57. It appears clearly that the spectra of food grade samples resemble each other and differ from the spectra of P25 particles although they all are constituted of a large fraction of anatase (from 85 to 100%). The differences mainly lie in the intensity and shape of bands which are related to the adsorbed water and the number of hydroxyl groups according to the works of several groups (Burneau, Humbert, Barrès, Gallas, & Lavalley, 1994; Delpuech et al., 2014; Humbert, Carteret, Burneau, & Gallas, 2006; Martra, 2000; Rinnert et al., 2005).

In the range 2500-3800 cm^{-1} (mid-infrared range), absorption bands are associated to the fundamental OH stretching modes. The spectrum of P25 sample resembles those previously described in the literature (Burneau et al., 1994; Delpuech et al., 2014;

Martra, 2000; Rinnert et al., 2005; Takeuchi, Martra, Coluccia, & Anpo, 2005). It is composed of two main absorption bands. The first one is a complex band extending between 3600 and 3800 cm^{-1} with two narrow peaks at 3632 cm^{-1} and 3679 cm^{-1} and a series of shoulders overlapping in-between. It was assigned to the stretching mode of different types of H-bond free hydroxyl groups (Martra, 2000). Interestingly, the spectrum of TiO_2 from Merck which was described in the same paper (Martra, 2000) is very similar to the spectra of our food grade samples E171-1, -2 and -3. The intensity of the OH vibration modes of pure anatase from Merck between 3600 and 2600 cm^{-1} is less intense than in the spectra of P25, similarly as our observations. This feature was interpreted by the author as a lower amount of H_2O dissociated on the surface of TiO_2 from Merck and a higher dissociation of water molecules on the surface of P25 samples. The second absorption band is broad, from around 3600 to 2600 cm^{-1}, and its non-Gaussian shape suggests the presence of overlapped absorption bands. The latter have been assigned to the overlap of the vOH modes of bonded hydroxyl groups, symmetric and antisymmetric vOH modes of molecular water coordinated to Ti^{4+} ions and physically adsorbed water molecules. The shape is in fact governed by the H-bond strengths. Indeed, the transition infrared moment is higher when the H-bond is stronger, *i.e.*, the absorption is dramatically enhanced when the wavenumber of the stretching mode is weaker (Humbert et al., 2006). In this spectra range, the sample E171-2 also exhibits absorption bands between 2800 and 3000 cm^{-1} which correspond to CH_2 stretching vibration modes. These bands have been identified in the raw powder as well (data not shown) and could be partially removed by washing the powder.

In the range 4000-7500 cm^{-1} (near-infrared range), the overtones of the OH stretching are found. Here again, the absorption bands of food grade TiO_2 (E171-1, -2 and -3) resemble between each other with bands at 7300-7050, 4400-4100 and 3670-3500 cm^{-1}. Those bands were assigned to vibration modes of free hydroxyl groups (Martra, 2000). The broad band centred at 5200 cm^{-1} is assigned to the overtone of water molecular forms (stretching combined with bending modes) sorbed at the surface (Burneau et al., 1994; Humbert et al., 2006; Rinnert et al., 2005). The integrated intensity of this band can be used here to compare the quantity of sorbed water

similarly as on silica (Burneau et al., 1994; Humbert et al., 2006), clays (Rinnert et al., 2005) or nanoporous silicon samples (Delpuech et al., 2014), instead of the bending mode of water molecules at around 1620 cm^{-1} since overtones and combination modes of bulk Ti-O-Ti phonon appear in the same spectral range as the bending mode of water molecules. The amount of superficial sorbed water is significantly lower for E171 samples than for the P25 sample. Additionally, the combinations of Ti-OH and Ti-O(H)-Ti groups which are localized between 4500 and 4000 cm^{-1}, are used to give a relative comparison of the amount of superficial hydroxyl groups. The TiOH hydroxyl group content is 5 to 6 times higher for P25 than for other samples in correlation with the higher specific area of P25 (Table 21). At last, the E171 samples are all characterized by a small well defined band at 4650 cm^{-1}, assigned in a previous work to hydroxyl groups of phosphate anions adsorbed on TiO_2 (Le, 2014). It is corroborated with the presence of phosphorus atoms detected on XPS spectra.

These observations apply at higher pH values as well (Figure 57). Finally, the surface of food grade samples is characterized by a more homogeneous surface with the presence of superficial phosphate groups, a lower amount of undissociated and adsorbed water at the surface, resulting in a lower content in hydroxyl groups TiOH than for the P25 sample.

Sample	Attribution	Position (eV)	FWHM (eV)	% Concentration	Stoichiometry /Ti
P25	O 1s Ti	530.2	1.23	45.82	2.37
P1-1	O 1s OH	531.7	1.85	10.98	0.57
	Ti 2p 4+	459.0	1.06	12.89	1.00
	Ti 2p 4+	464.7	2.02	6.45	
	C 1s p	285.0	1.42	16.56	0.86
	C 1s C-O	286.5	1.89	4.11	0.21
	C 1s C=O	288.8	1.65	3.20	0.17
P25	O 1s Ti	530.3	1.16	45.72	2.23
P1-2	O 1s OH	531.8	1.84	10.59	0.52
	Ti 2p 4+	459.1	0.97	13.64	1.00
	Ti 2p 4+	464.8	2.01	6.82	
	C 1s p	285.1	1.37	15.42	0.75
	C 1s C-O	286.3	2.19	4.93	0.24
	C 1s C=O	289.0	1.57	2.89	0.14
E171-1	O 1s Ti	529.8	1.03	37.18	1.70
P1-1	O 1s OH	530.7	2.03	18.49	0.84
	O 1s O=C	532.9	1.6	1.93	0.09
	Ti 2p 4+	458.7	0.89	14.60	1.00
	Ti 2p 4+	464.4	2.02	7.30	
	C 1s p	285.0	1.75	10.60	0.48
	C 1s C-O	286.9	2.68	4.38	0.20
	C 1s C=O	289.5	1.18	0.89	0.04
	K 2p +	293.0	1.42	1.66	0.11
	K 2p +	295.8	1.41	0.83	
	N 1s 1	399.8	1.74	0.31	0.01
	P 2p phos	133.2	1.29	1.22	0.08
	P 2p phos	134.0	1.25	0.61	
E171-1	O 1s Ti	529.9	1.01	37.79	1.68
P1-2	O 1s OH	530.7	2.01	19.38	0.86
	O 1s O=C	533.0	1.66	1.37	0.06
	Ti 2p 4+	458.7	0.88	14.99	1.00
	Ti 2p 4+	464.4	2.02	7.50	
	C 1s p	285.0	1.7	10.33	0.46
	C 1s C-O	286.9	2.12	2.86	0.13
	C 1s C=O	289.2	1.55	1.06	0.05
	K 2p +	293.1	1.45	1.71	0.11
	K 2p +	295.9	1.43	0.85	
	N 1s 1	399.9	1.82	0.31	0.01
	P 2p phos	133.2	1.3	1.24	0.08
	P 2p phos	134.1	1.27	0.62	
E171-2	O 1s Ti	530.0	1.079	36.86	1.75
	O 1s OH	530.8	2.456	21.43	1.01

	Ti 2p 4+	458.8	0.987	14.08	0.67
	Ti 2p 4+	464.4	1.91	7.04	0.33
	C 1s p	285.0	1.613	11.77	0.56
	C 1s C-O	286.5	2.108	3.20	0.15
	C 1s C=O	288.8	1.71	1.69	0.08
	K 2p +	293.3	1.518	1.22	0.09
	K 2p +	296.1	1.512	0.61	
	P 2p a	133.4	1.418	0.98	0.07
	P 2p a	134.3	1.392	0.49	
	N 1s NH4+	400.1	1.967	0.64	0.03
E171-3	O 1s Ti	530.0	1.124	37.78	1.78
	O 1s OH	531.0	2.445	18.47	0.87
	Ti 2p 4+	458.8	1.043	14.11	0.67
	Ti 2p 4+	464.5	1.943	7.06	0.33
	C 1s p	285.0	1.421	12.10	0.57
	C 1s C-O	286.4	2.185	5.74	0.27
	C 1s C=O	288.8	1.484	1.51	0.07
	K 2p +	293.2	1.444	0.77	0.05
	K 2p +	296.0	1.478	0.39	
	P 2p a	133.5	1.357	0.82	0.06
	P 2p a	134.4	1.372	0.41	
	N 1s NH4+	400.2	1.876	0.84	0.04
E171-4	O 1s Ti	529.9	1.099	43.05	1.80
	O 1s OH	530.8	2.337	15.04	0.63
	Ti 2p 4+	458.7	1.005	15.94	0.67
	Ti 2p 4+	464.4	1.927	7.97	0.33
	C 1s p	285.0	1.459	10.49	0.44
	C 1s C-O	286.6	1.776	2.97	0.12
	C 1s C=O	288.8	1.581	1.47	0.06
	K 2p +	293.2	1.446	0.88	0.06
	K 2p +	295.9	1.432	0.44	
	P 2p a	133.4	1.41	0.57	0.04
	P 2p a	134.3	1.367	0.29	
	N 1s NH4+	400.1	1.847	0.89	0.04
E171-5	O 1s Ti	529.9	1.03	38.42	1.63
	O 1s OH	530.7	2.304	19.67	0.84
	Ti 2p 4+	458.8	0.94	15.68	1.00
	Ti 2p 4+	464.4	1.866	7.84	
	C 1s p	285.0	1.875	10.89	0.46
	C 1s C-O	286.9	1.235	1.10	0.05
	C 1s C=O	288.6	2.106	1.75	0.07
	K 2p +	293.3	1.564	1.47	0.09

	K 2p +	296.0	1.525	0.74	
	P 2p a	133.4	1.359	1.16	0.07
	P 2p a	134.3	1.337	0.58	
	N 1s NH4+	400.0	1.918	0.70	0.03
E171-6a	O 1s Ti	529.3	1.06	26.34	1.80
	O 1s OH	530.5	1.72	15.18	1.04
	O 1s O=C	532.4	1.54	4.75	0.33
	O 1s O-Na	535.1	2.43	1.44	0.10
	Na KLL Na+	496.2	2.28	4.81	0.33
	Ti 2p Ti4+	458.1	0.93	9.74	1.00
	Ti 2p Ti4+	463.8	2.05	4.87	
	C 1s p	285.0	1.29	19.2	1.31
	C 1s C-O	286.3	1.38	5.08	0.35
	C 1s C=O	288.1	1.78	2.59	0.18
	K 2p K+	292.7	1.4	0.97	0.10
	K 2p K+	295.5	1.39	0.48	
	Cl 2p Cl-	198.1	1.23	0.33	0.03
	Cl 2p Cl-	199.8	1.19	0.17	
	P 2s Phosph	190.3	2.39	1.67	0.11
	P 2p phosph	132.7	1.23	1.10	0.11
	P 2p phosph	133.6	1.23	0.55	
	Si 2p Si4+	102.2	1.44	0.49	0.05
	Si 2p Si4+	103.1	1.43	0.24	
E171-6b	O 1s Ti	530.0	1.097	39.47	1.74
P1-1	O 1s OH	530.9	2.286	18.84	0.83
	Ti 2p 4+	458.8	1.015	15.13	0.67
	Ti 2p 4+	464.5	1.937	7.57	0.33
	C 1s p	285.0	1.443	10.37	0.46
	C 1s C-O	286.4	2.124	3.57	0.16
	C 1s C=O	288.8	1.637	1.39	0.06
	K 2p +	293.3	1.487	0.91	0.06
	K 2p +	296.1	1.495	0.45	
	P 2p a	133.5	1.341	1.00	0.07
	P 2p a	134.4	1.305	0.5	
	N 1s NH4+	400.2	1.93	0.8	0.04
E171-6b	O 1s Ti	530.0	1.08	38.43	1.73
P2-1	O 1s OH	531.0	2.3	18.84	0.85
	Ti 2p 4+	458.8	0.96	14.78	1.00
	Ti 2p 4+	464.5	2.08	7.39	
	C 1s p	285.0	1.46	10.9	0.49
	C 1s C-O	286.6	2.33	4.56	0.21
	C 1s C=O	289.2	1.59	1.31	0.06
	K 2p +	293.1	1.39	1.02	0.07
	K 2p +	295.9	1.36	0.51	

	N 1s 1	400.1	1.73	0.53	0.02
	N 1s 2	401.9	1.22	0.04	0.00
	P 2p phos	133.4	1.38	1.12	0.08
	P 2p phos	134.3	1.39	0.56	
E171-6b	O 1s Ti	530.0	1.04	39.58	1.75
P2-2	O 1s OH	531.0	2.16	18.1	0.80
	Ti 2p 4+	458.8	0.91	15.07	1.00
	Ti 2p 4+	464.5	2.02	7.54	
	C 1s p	285.0	1.43	11.00	0.49
	C 1s C-O	286.6	2.04	3.55	0.16
	C 1s C=O	289.1	1.57	1.28	0.06
	K 2p +	293.2	1.43	1.06	0.07
	K 2p +	296.0	1.4	0.53	
	N 1s 1	400.1	1.73	0.56	0.02
	N 1s 2	401.6	1.58	0.04	0.00
	P 2p phos	133.4	1.37	1.13	0.07
	P 2p phos	134.3	1.37	0.56	

Table 22: Attribution of XPS peaks for food grade and P25 samples of titanium dioxide. The label Px-y indicates the number x of the pellet P followed by the number of the position

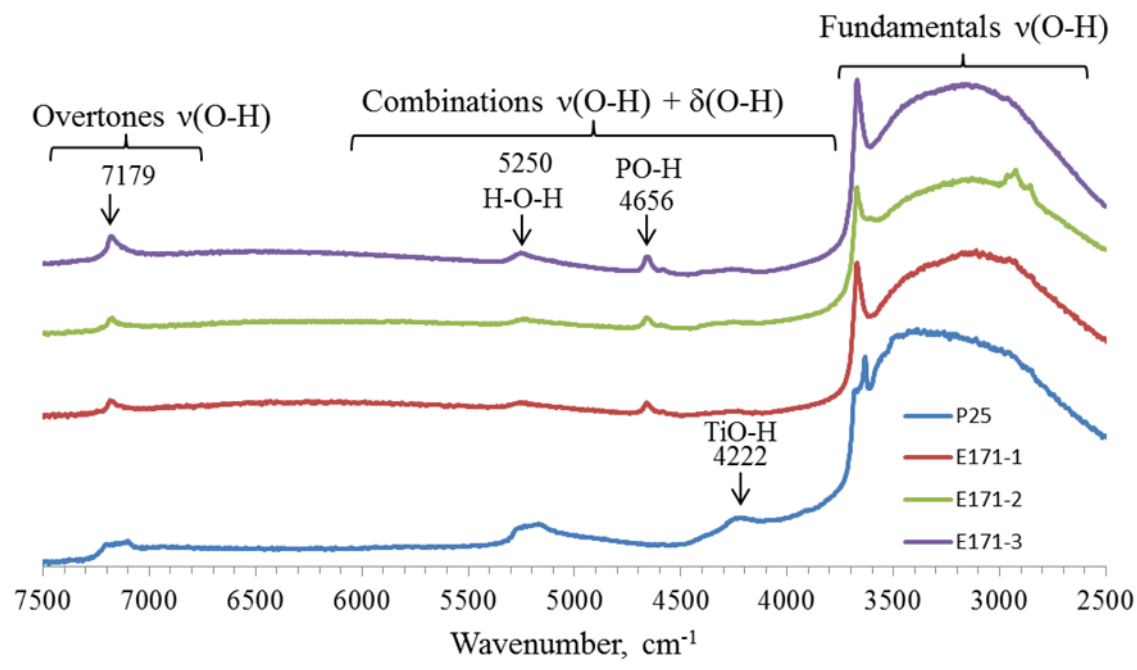

Figure 56 Infrared spectra in diffuse-reflectance mode of E171 and P25 samples of TiO_2 powders after dehydration of their dispersions prepared at pH 2 (relative humidity < 2% at 298 K). For clarity, spectra have been presented with an offset.

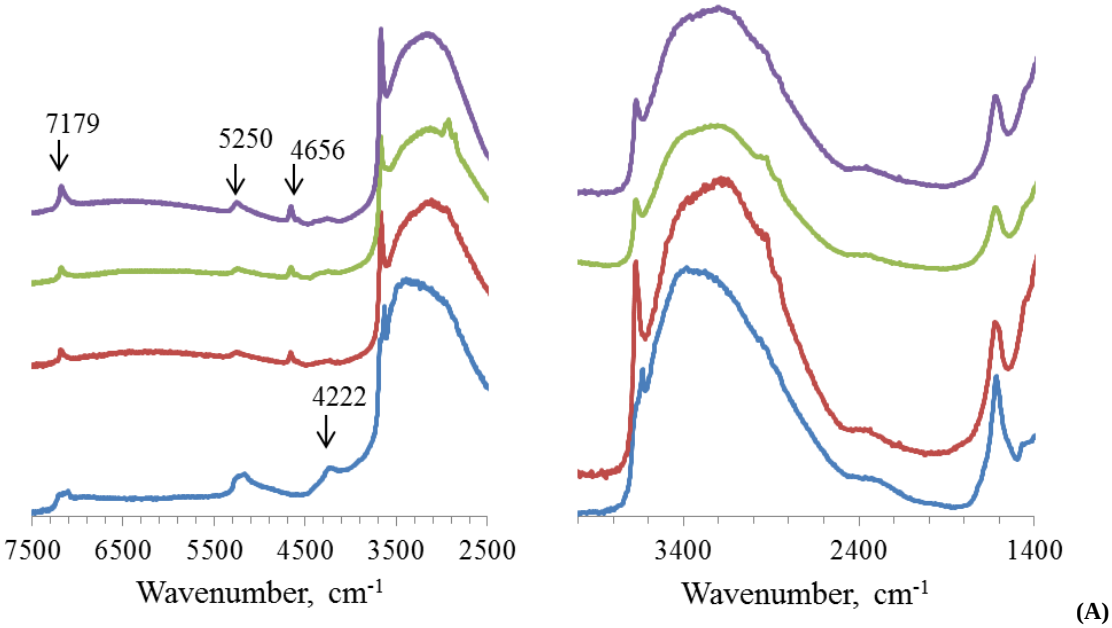
7179
5250
4656
4222
7500 6500 5500 4500 3500 2500
Wavenumber, cm-1
3400 2400 1400
Wavenumber, cm-1

(A)

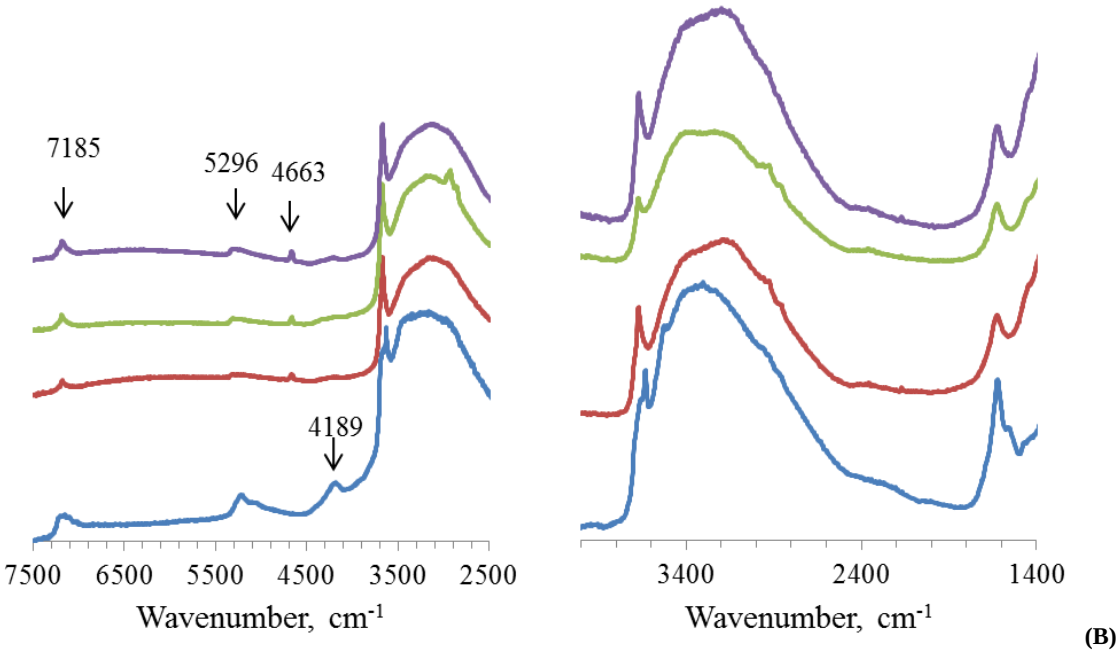
7185
5296
4663
4189
7500 6500 5500 4500 3500 2500
Wavenumber, cm-1
3400 2400 1400
Wavenumber, cm-1

(B)

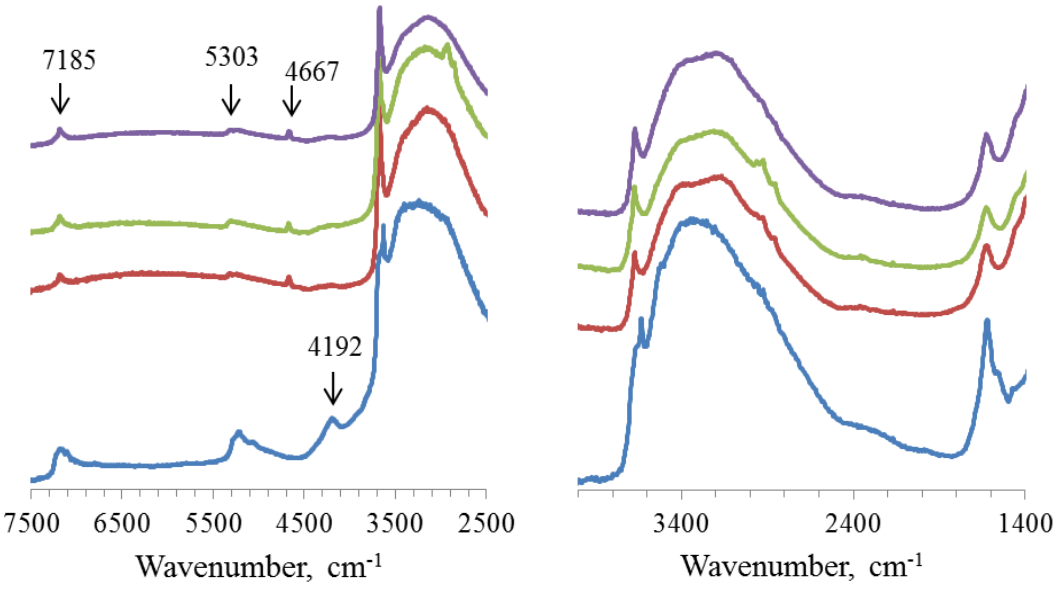

(C)

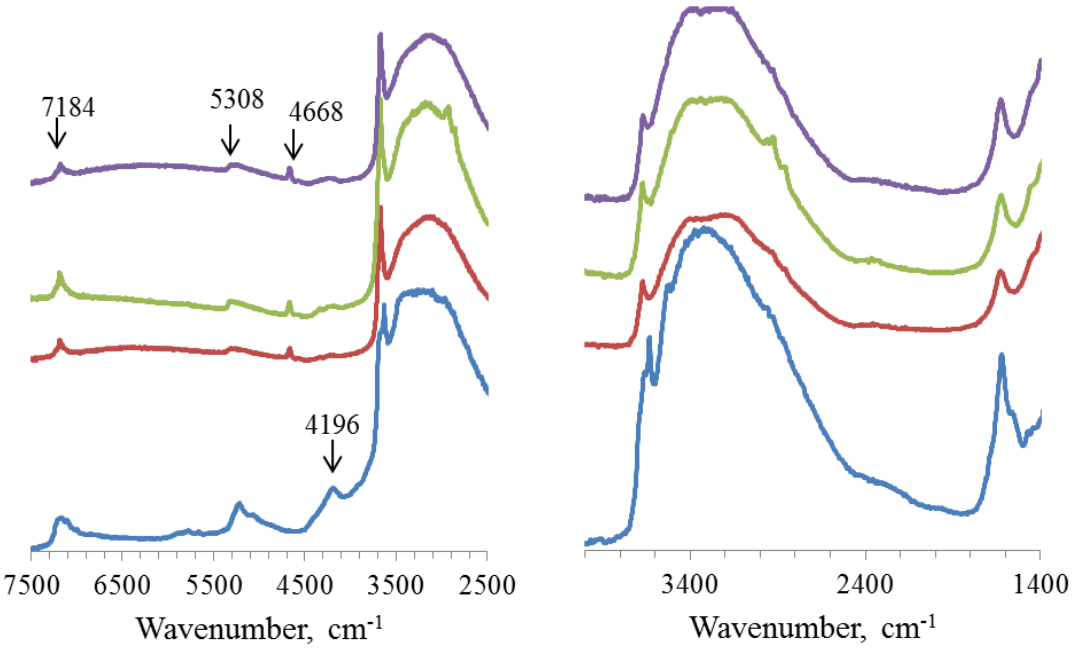

D)

Figure 57: Infrared spectra in diffuse-reflectance mode of E171 and P25 particles of titanium dioxide obtained as powders after dehydration of their dispersions at pH (A) 2, (B) 4, (C) 6 and (D) 8. The spectra were recorded with a near-infrared source (left hand side) and with a middle-infrared source (right hand side). Lines' color refer to (—) P25, (—) E171-1, (—) E171-2 and (—) E171-3.

7) Zeta potential and agglomeration in aqueous phases

The zeta potential values recorded in pure water (no NaCl salt) at discrete pH values ranging between 1 and 9 are given for both P25 and E171 producers in Figure 58 and for TiO_2 suppliers in Figure 59. The isoelectric points (IEP) of E171-1, E171-2, E171-3, E171-4, E171-5 and E171-6b samples range between 4.0 and 4.2 in accordance with a previous work, (Yang et al., 2014) whereas E171-6a sample has an isoelectric point of 2.4. The IEP values of E171-1 and E171-6a were confirmed through measurements in salty solutions (4.0 10^{-2} mol.L^{-1}), showing maximum differences of only 0.2 units compared to pure water. These results are presented in Figure 60. IEP of P25 sample was 6.4 (6.6 in salty solutions), in accordance with previous works (Le et al., 2014; Yang et al., 2014).

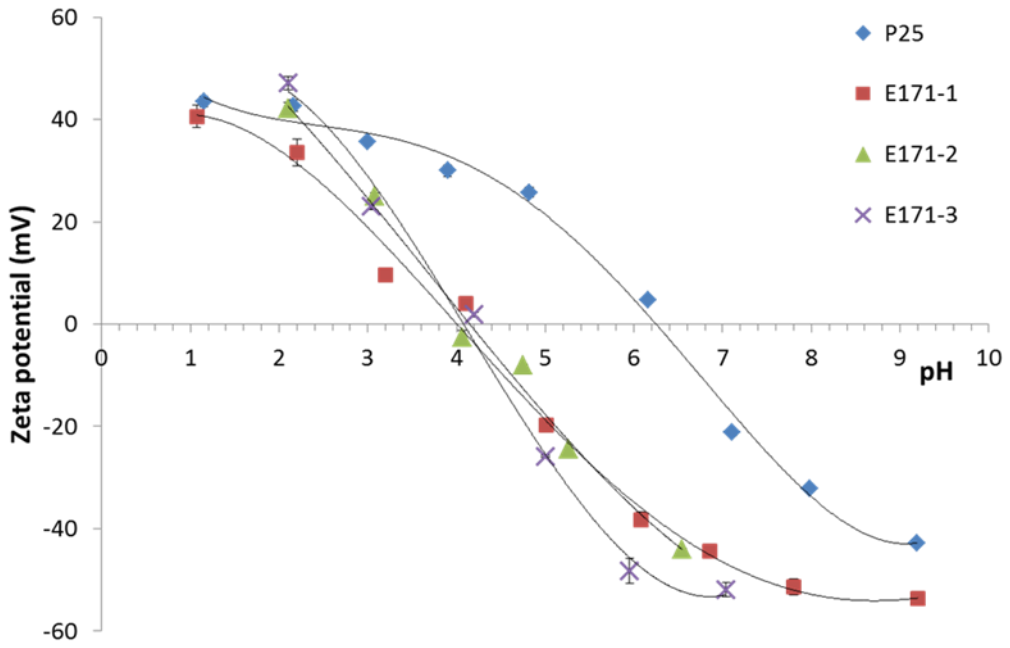

Figure 58: ζ potential values of food-grade E171 and P25 samples of titanium dioxide particles dispersed in aqueous solution between pH 1 and 9. Lines are guides for the eyes.

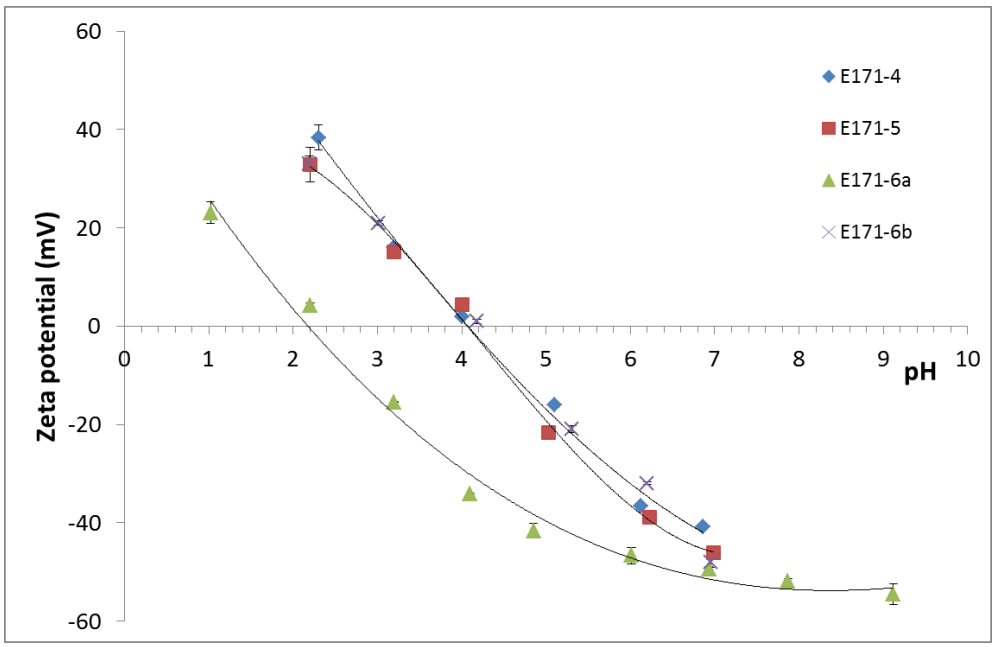

Figure 59: ζ potential values of food-grade E171 particles of TiO_2 dispersed in aqueous solution adjusted at pH varying between 1 and 9 (salt concentration 0M).

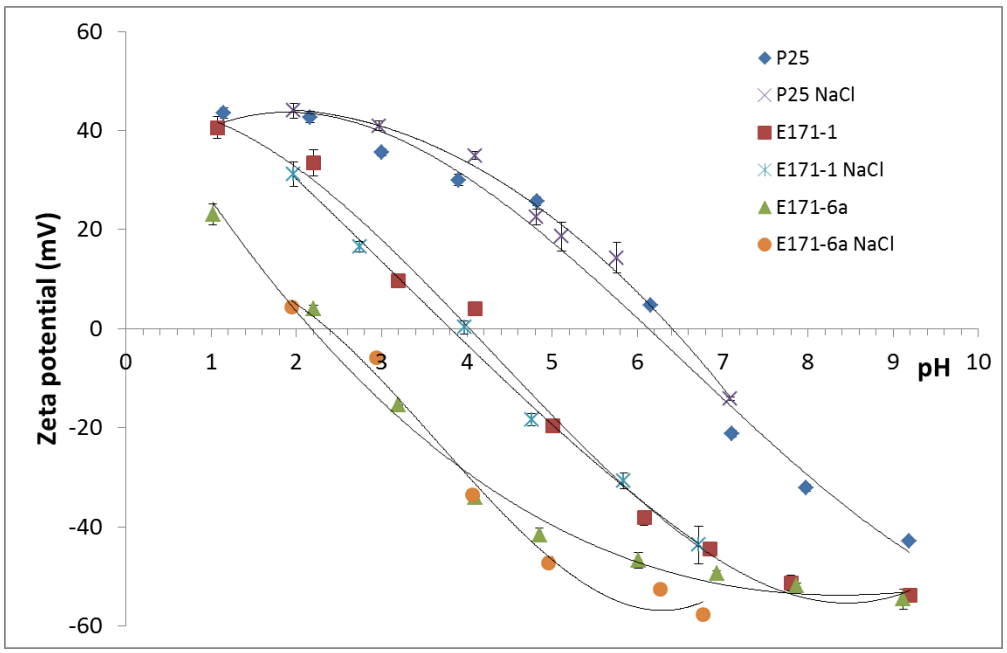

Figure 60: ζ potential values of food-grade E171 and P25 particles of TiO_2 dispersed in aqueous solutions adjusted at pH varying between 1 and 9 (salt concentration 0 or 4.10^{-2} M).

The IEP values are expected to impact the agglomeration state and then the size distributions as shown in Figure 61 and Figure 62. The results are summarised in Table 23 where the three kinds of populations observed in Figure 61 and Figure 62 are reported for every sample at each pH value. Food grade samples present a similar behaviour in aqueous phase with one to two main populations depending on pH. They form small agglomerates at pH 9 (less than 1 µm) and bigger agglomerates (medium-sized agglomerates from 1 to 30 µm) at pH 2 and 3. In-between, the volume proportion of medium sized agglomerates tends to decrease by increasing pH. The peculiar sample E171-6a forms small agglomerates for pH larger than 4, whereas samples E171-2, -3 and -6b form small agglomerates at pH higher than 6 and samples E171-1, -4 and -5 over pH 7. P25 sample presents a more complex behaviour than E171 samples, with a multimodal distribution showing two to three populations, spanning from small agglomerates to large agglomerates. More precisely, at pH 2, 3 and 4, P25 particles agglomerate in small and medium sized objects. Then at pH 5, P25 particles tend to form larger agglomerates in addition to the previous ones. Finally, from pH 6 to higher values, P25 particles form mainly medium-sized agglomerates, which are up to 200 times larger than that of food grade agglomerates at the same pH. The isoelectric point values explain the difference in size distributions between P25 (IEP = 6.4) and E171-6a (IEP = 2.4) When pH value is near their IEP, particles are less charged, and tend to form large agglomerates. For the other samples, agglomerates' size is smaller at pH ≥ 6, since their IEP values are close to 4. As a conclusion, the agglomerates of E171 particles are more homogeneous in size than those of P25 on a large pH range. Moreover, the particle distribution does not span as much as that of P25: they are neither higher than 20 µm nor smaller than 100 nm, in contrast to P25 particles.

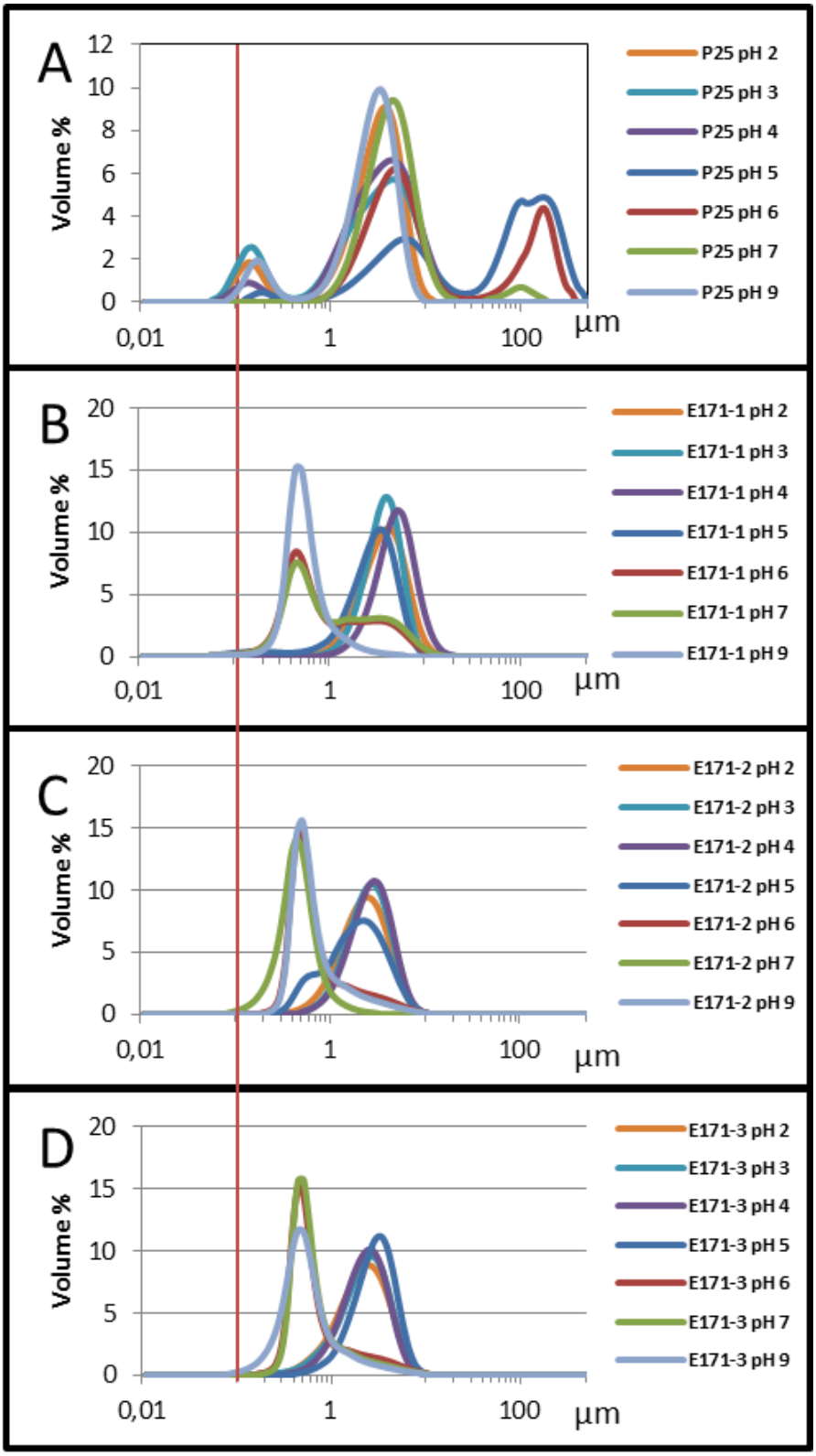

Figure 61: Volume-based distributions of the diameter of P25 and E171 particles dispersed at pH ranging between 2 and 7, determined by laser scattering. Graphs refer to (A) P25, (B) E171-1, (C) E171-2, (D) E171-3.

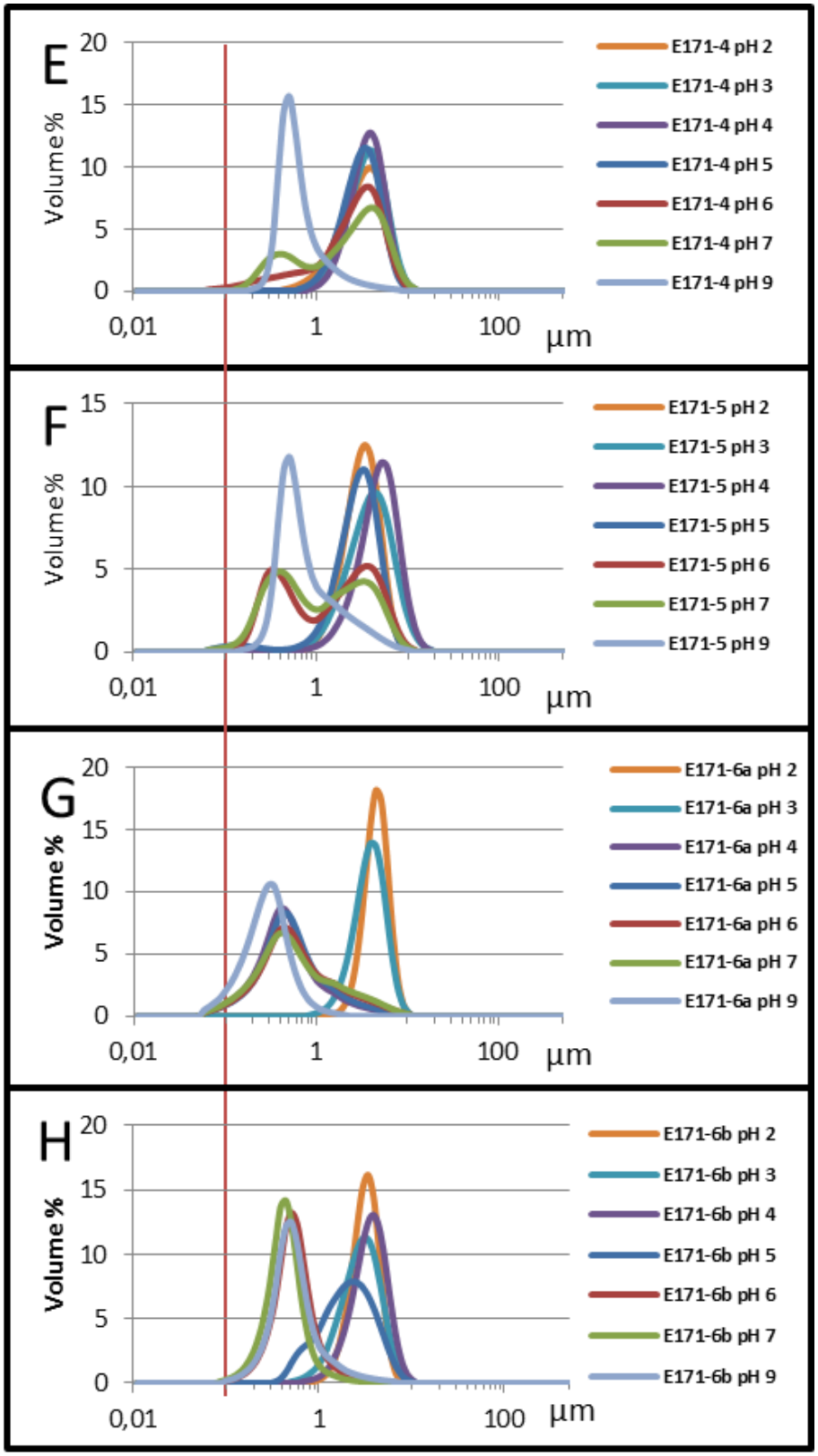

Figure 62: Volume-based distributions of the diameter of E171 particles dispersed at pH ranging between 2 and 7, determined by laser scattering. Graphs refer to (E) E171-4, (F) E171-5, (G) E171-6a, (H) E171-6b.

Sample	pH / IEP	2	3	4	5	6	7	9
P25	6.2	M+S	M+S	M+S	L+M+S	M+L	M+L	M+S
E171-1	4.0	M	M	M	M	S+M	S+M	S
E171-2	4.2	M	M	M	M+S	S	S	S
E171-3	4.1	M	M	M	M	S	S	S
E171-4	4.1	M	M	M	M	M	M+S	S
E171-5	4.1	M	M	M	M	M+S	S+M	S
E171-6a	2.0	M	M	S	S	S	S	S
E171-6b	4.1	M	M	M	M+S	S	S	S

Table 23: Population of agglomerates (in volume) in TiO_2 dispersions as a function of pH. Letters S, M and L stand for respectively small agglomerates having a diameter (D) lower than 1 µm, agglomerates with a medium size (1<D<30 µm) and large agglomerates (D>50 µm). Shoulders at the foot of peaks were not taken into account. In the case of more than one population, the letters are given in the decreasing order of importance in the volume distribution.

8) Discussion

The physicochemical characterization of E171 samples relatively to the P25 reference material showed that E171 samples present a fraction of NPs with a distribution in number being less than 50%, in accordance with a previous independent study (Yang et al., 2014). According to the European definition, it may thus not be considered as a nanomaterial. The fraction in NPs is only one parameter among the numerous parameters which differ between E171 and P25 particles. For example, the rutile to anatase ratio is 0 for E171 samples and 0.17 for P25 particles. The differences in size and crystalline structure impact the reflectance threshold which is shifted at higher wavelengths for E171 samples. The chemical composition is also different due to the surface composition: whereas P25 powder only contains Ti and O, all food grade TiO_2 samples contain phosphorus and some of them also contain aluminium and silicon. The comparison between XPS and ICP-AES data showed that these elements are found at the surface of TiO_2 and IR spectroscopy evidenced that phosphorus is present under the form of phosphate species. XPS also showed that the O/Ti and OH/Ti ratios (in

ultra-vacuum) in E171 samples are different from those of the P25 sample, in accordance with the specific surface area which is 5 times higher for P25 than for E171 samples. The presence of superficial phosphate groups explains the lower isoelectric point of E171 particles than that of P25 particles, as anionic adsorption induces an IEP shift towards lower pH. In the same manner, the presence of silicon on the sample E171-6a explains its lower IEP in comparison to other E171 samples. Indeed, IEP of silica particles is around pH 2 (Iler, 1979; Júnior & Baldo, 2014). These different surface compositions thus led to different agglomeration behaviours: the size distribution of agglomerates for E171 particles is less spread and more homogeneous than that observed for P25 agglomerates.

The differences between the food grade particles and the particles of reference material P25 were analysed from a statistical point of view. The physicochemical characteristics of each sample were considered for a principal component analysis (PCA), namely nanoparticle content (NP), percentage of anatase (A), specific surface area (SSA), reflectance gap (G in wavelength), surface elemental analysis (stoichiometric ratios of oxygen at ≈ 531 eV, phosphorus and potassium versus titanium), agglomerate size (diameter from the peak position in granulometry at pH 2 and pH 9 denoted D2 and D9 respectively) and isoelectric point (IEP). The diameters of agglomerates were taken at extreme pH to compare monomodal distributions as much as possible. The results of PCA are given in Figure 63.

The two first dimensions (dim 1 78.18% and dim 2 11.19%) express the majority of the variance of the system (more than 90%) and the plan 1-2 is thus sufficient to describe the system. The individuals factor map (Figure 7, top) clearly confirms the previous qualitative conclusion that the particles of reference material P25 and the food grade particles E171 are not similar. The variables factor map (Figure 63, bottom) indicates that all variables are described along one axis and most variables are strongly correlated with the axis 1. The parameters D9, SSA, IEP and NP are negatively correlated with axis 1 whereas the elemental surface analysis (K, O and P), the reflectance gap (G) and the anatase amount (A) are positively correlated with axis 1. These parameters discriminate E171 samples from the reference P25 sample.

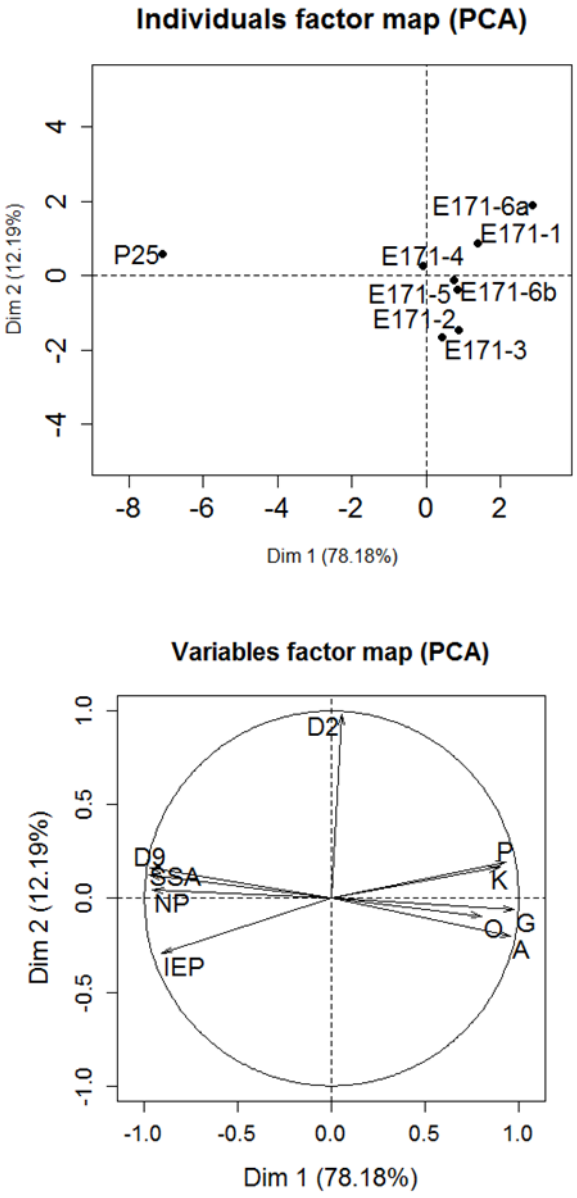

Figure 63: (Top) Individuals factor map and (bottom) variables factor map of the principal component analysis performed on data of Table S4 (reduced variables).

Since the TiO_2 form P25 from Evonik presents significantly different properties than the food grade materials (investigated in this study and in Yang et al. (Yang et al., 2014)), the choice of a food grade material may be preferred to cover the scenario of human exposure by ingestion. Except sample E171-6a, the set of E171 samples is quite homogeneous. They have in common to possess the same surface chemistry:

presence of phosphate on the surface, an isoelectric point of 4.1, a low specific area (around 10 m^2/g) and a crystalline phase anatase. Any sample with these properties can be thus used as model of TiO_2 food additive. As regards the batch E171-6a, it is different from the others, recalling us to properly characterise the batches before use.

9) Conclusions

The physicochemical characterisation of food grade (E171) TiO_2 confirmed the presence of NPs in E171 samples with a significant difference in the primary size and the percentage of nano-sized particles compared to P25 sample: 23 nm with 100% of NPs in P25 and 131 nm with 26% of NPs in average in all food grade samples. Considering our study and a previous one performed independently (Yang et al., 2014), the food additive E171 may not be regarded as a nanomaterial as its NPs size distribution in number is lower than 50%. The physicochemical characterization of food grade TiO_2 NPs (E171) also shows that they differ from P25 particles by many aspects, in particular surface properties, related to the presence of phosphate. Therefore, P25 particles may not be the most relevant model when studying the fate of TiO_2 particles via ingestion. This difference should be taken into account in the future when considering any sample of TiO_2 for toxicological studies. The results of this first part of our work has been published in *Food Additives and Contaminants Part A:*

Dudefoi W., Terrisse H., Richard-Plouet M., Gautron E., Popa F., Humbert B., Ropers M-H. (2017) Criteria to define a more relevant reference sample of titanium dioxide in the context of food: a multiscale approach. *Food Additives and Contaminants Part A.* (http://dx.doi.org/10.1080/19440049.2017.1284346).

II) Extraction and physicochemical characterization of TiO_2 from food products

In order to determine if E171 remains in the same physicochemical state once integrated in the final food products as chewing-gums and candies, the white coatings of 5 food products were extracted then characterized for their size distribution, shape, crystallinity, and chemical composition using transmission electron microscopy (TEM), coupled to an energy dispersive X-ray spectrometer (EDX), Raman scattering spectroscopy, and inductively coupled plasma atomic emission spectrometry (ICP-AES).

1) Extraction of coatings from gums and candies

The coatings from four chewing-gums (S1 to S4) and one candy (S5) were extracted from the outer shell of the product using an adapted protocol from the literature (Chen et al., 2013). For all tested products, the coatings were easily dispersed in deionized water after one minute of manual agitation, and the resulting pieces of gum-bases were almost completely destitute of their white coating (Figure 64). The extraction protocol was performed with 100 pieces of each sample, and the total masses of extracted coating after washing and drying are reported in Table 24 (coded as C1 to C5). The amount of extracted coating varies from 0.99 mg to 24 mg of coating per gram of chewing-gum (C1 and C2), and is even lower for the candy (0.39 mg, C5).

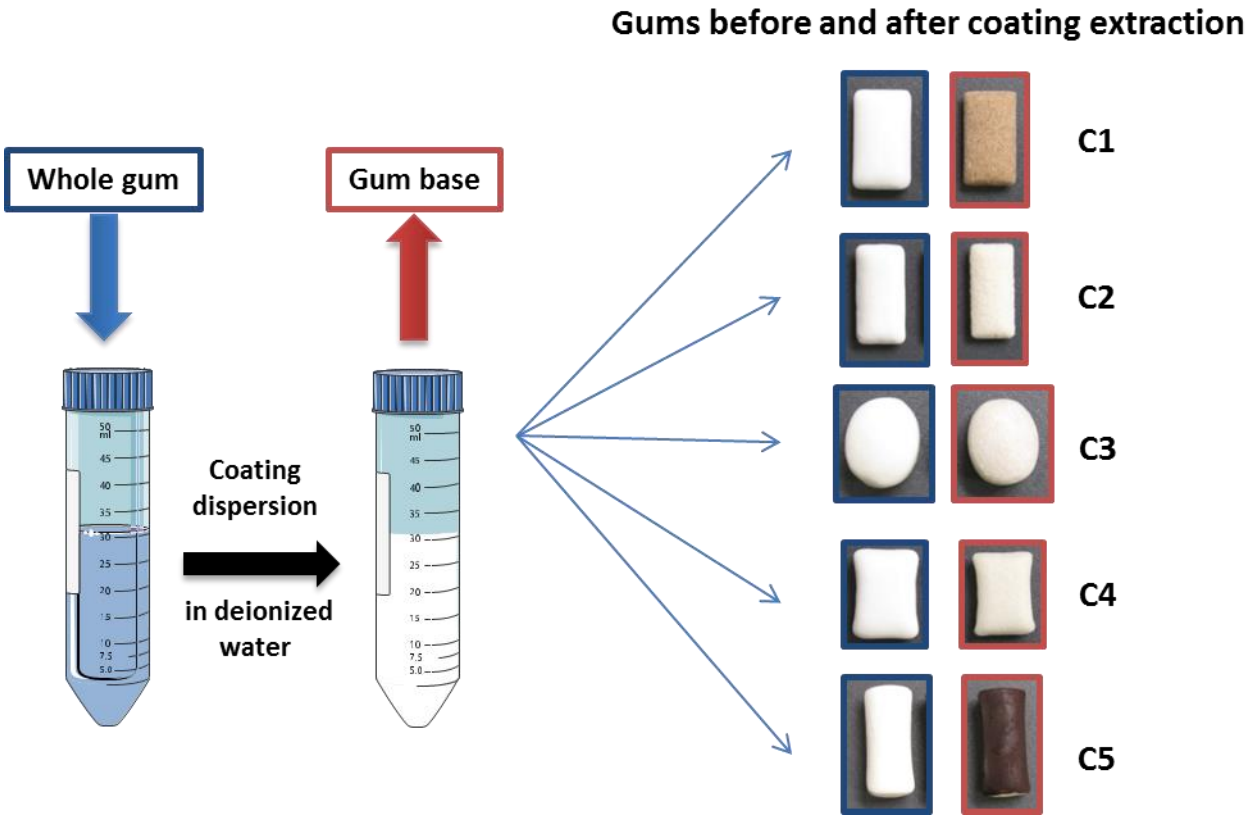

Figure 64: Extraction of TiO_2 coating from commercial products adapted from (Chen et al., 2013).

	S1	S2	S3	S4	S5
mass of a piece of sample (g)	1.415±0.027	1.440±0.030	2.048±0.044	2.240±0.086	3.319±0.307
mass of extracted coating/gum (mg)	1.4±0.2	34.9±2.3	14.3±1.5	22.5±2.1	1.3±0.3
mg of extracted coating / g of gum	0.99±0.02	24.2±0.50	6.98±0.15	10.04±0.38	0.39±0.04

Table 24: Amount of extracted coating from gums and candies.

2) Chemical analysis of extracted coatings (FT-Raman spectroscopy)

FT-Raman spectra of the whole coatings wrapping the base gums (S, dotted lines) and of the coating extracted from the chewing-gum then washed (C, solid lines) are given in full in Figure 65 and enlarged in Figure 66 to see the less intense peaks.

Every whole coatings (S, dotted lines) presented an intense band between 3000-2800 cm^{-1}, a sharp and intense peak at 144 cm^{-1}, a more or less thin and intense peak at 1468 cm^{-1} and lots of peaks between 50-1500 cm^{-1} corresponding respectively to the stretching of CH_2 ($\nu_{(C-H)}$), a lattice vibration mode of Ti-Ti atoms, specific to the structure anatase of TiO_2 (Ohsaka et al., 1978), the bending modes $\delta(CH_2)$ and vibrations of skeletons of organic molecules present on the coating.

Once extracted and washed (C, solid lines), the other TiO_2 anatase peaks were detected in all coatings, with the characteristic peaks at 197 (weak intensity), 399, 513, 519 and 639 cm^{-1} (Ohsaka et al., 1978). Only TiO_2 signals were detected in C1 and C5 coatings. In addition, C3 and C4 spectra show a peak around 2900 cm^{-1}, related to the stretching vibration mode of C-H groups and indicating the remaining of organic matter which was not removed by the washing process (Figure 65). Finally, spectrum of C2 also shows some thin peaks at 287, 712 and 1087 cm^{-1} (Figure 66), revealing the presence of calcite $CaCO_3$ (De La Pierre et al., 2014).

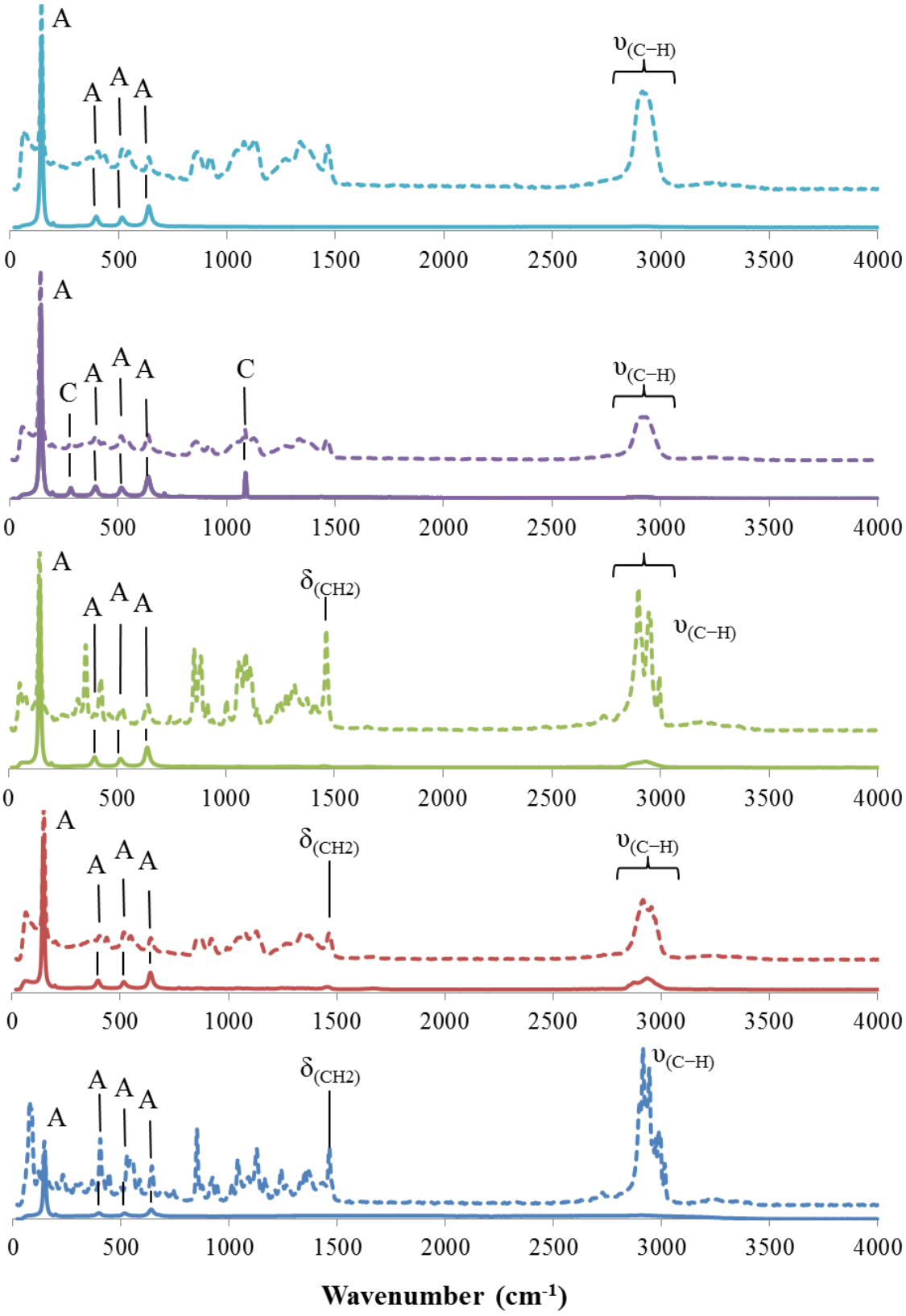

Figure 65: FT-Raman spectra of coatings before (dotted lines) and after (solid lines) washing. Spectra are reported from the top to the bottom in the order S1 and C1 (—), S2 and C2 (—), S3 and C3 (—), S4 and C4 (—), and S5 and C5 (—). They were normalized on the intensity of the strongest peak at 144 cm^{-1}. Letter "A" notes the peak position of TiO_2 anatase, and letter C note the peak of calcite.

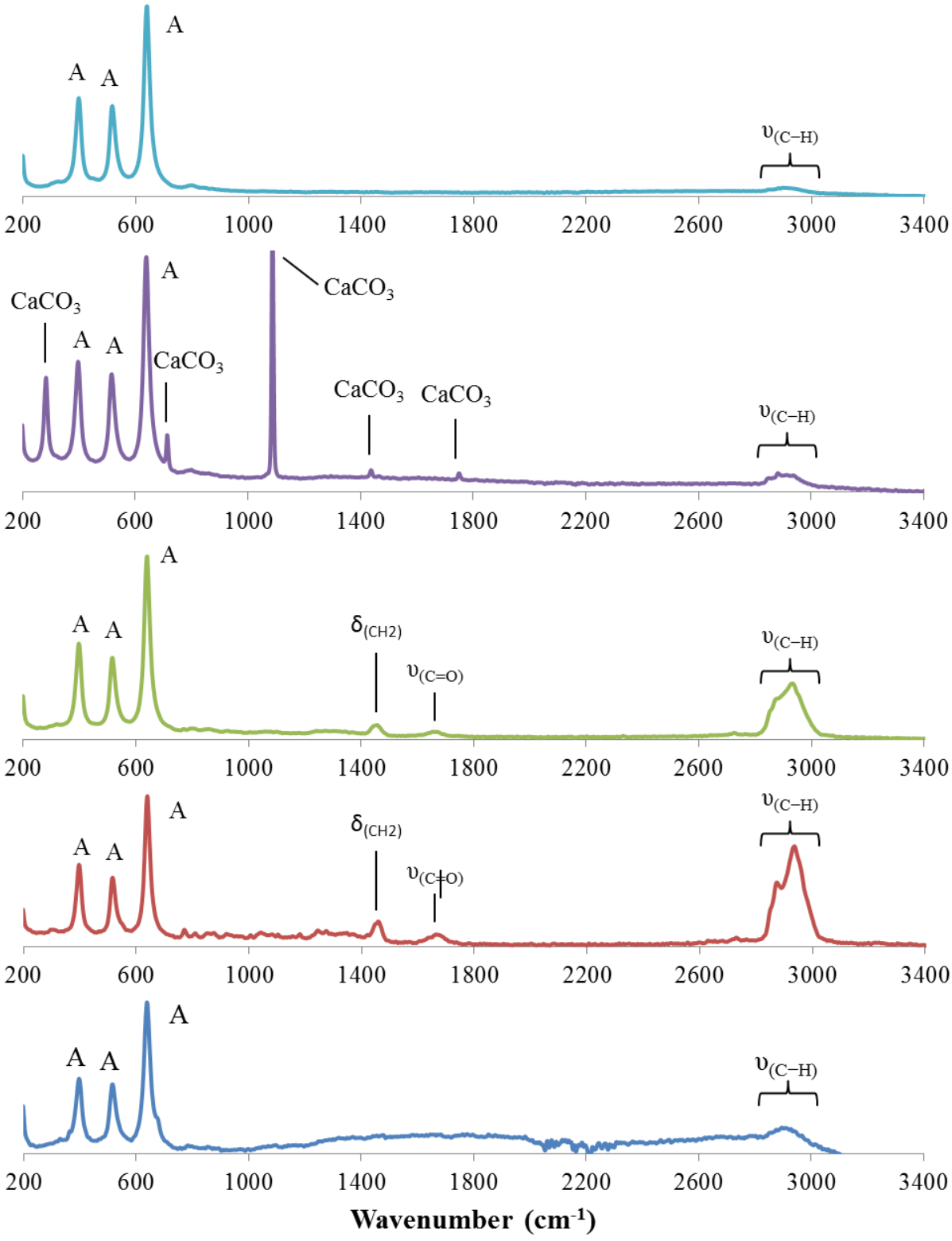

Figure 66: Enlarged FT-Raman spectra of coatings before (dotted lines) and after (solid lines) washing. Spectra are reported from the top to the bottom in the order C1 (—), C2 (—), C3 (—), C4 (—) and C5 (—). They were normalized on the intensity of the strongest peak at 144 cm^{-1}. Letter "A" notes the peak position of TiO_2 anatase, and $CaCO_3$ note the peak of calcite.

3) Elemental analysis of gums and candies coatings (ICP-AES)

The extracted coatings were analyzed by ICP-AES to determine the elemental compositions in Ti, Ca, Si, Al, Mg and P. According to the list of ingredients and the nature of food grade TiO_2, no other element than those investigated was expected in the coating. In addition, the element P was quantified due to its presence in the bulk powder of E171 TiO_2. (Dudefoi et al., 2017; Yang et al., 2014) Moreover, Si and Al were considered since they can be used to coat the surface of TiO_2 (FAO 2012).

Knowing the amount of Ti in the samples in mg/g of coating, we calculated the concentration of TiO_2 in percent in the gum coating. Table 25 summarises the results expressed in mg/g of coating.The concentrations in Ti are very different in the five extracts; they vary from 28.39 to 593.73 mg/g (i.e., a ratio of 21). The equivalent amount of TiO_2 represents 4.7 wt% to 99.1 wt% and increase in inverse proportion to the intensity signal of ν(CH2). The coating C1 can be ranked as pure TiO_2 (99% TiO_2) in contrast to the four other ones which have only 4.7 to 67.7 wt% TiO_2. This low percentage of TiO_2 in these coatings is due to the presence of other compounds composing the outer shell of the products, such as aluminium, calcium, magnesium and silicon, in the coating C2 (significant amount of calcium), C3 and C5. The very low concentration in minerals in the coating C4, both in Al, Ca, Si, Mg and Ti, and the intense signal ν(CH2) in Raman spectra hint that this coating was more organic than inorganic.

Knowing the weight of a piece of gum, we also expressed the amount of each component in mg per g of chewing-gum and in mg per piece of chewing-gum (Table 26 and Table 27, respectively). From this calculation, C2 and C3 coatings, which were composed by only 49.7 and 33.04 wt% of TiO_2, were actually the more concentrated gums when normalized to the whole chewing-gum, with 17.34 and 4.73 mg of TiO_2/piece of gum. On the opposite, C1 coating, which was the more concentrated coating (99.06 wt% of TiO_2), was 12 times less concentrated than C2, with 1.39 mg of TiO_2/piece of gum.

Finally, we also estimated the amount of nano-TiO_2 in mg/gum (Table 28) by using TEM measurements (presented in 5)) and attributing a mass to each class of size (from % in number to % in mass, considering TiO_2 particles as spheres and using TiO_2 density 3.895 g/cm^3). We then used the percent of each class of size composing the samples, the mass of each class of size and the total mass of nanoTiO_2 in the gum in order to estimate the number of nano-TiO_2 particles per piece of gum (Table 28). The amount of nano-TiO_2 was estimated between 0.04 and 0.81 mg per piece of gum, representing about $1.8x10^{13}$ to $4.6x10^{14}$ NPs (for C4 and C2, respectively), meaning that the ingestion of one piece of C2 would result in an intake of nano-TiO_2 more than 20 times greater that the intake from the ingestion of one piece of C4. These results highlight the importance of considering both the concentration within the coating but also the concentration normalized to the whole piece of chewing-gum, as C1 coating was 99 wt% TiO_2, but was not the most concentrated sample when normalized to the whole food product.

	mg Element / g of coating						
Element / Samples	Al (mg/g)	Ca (mg/g)	Si (mg/g)	P (mg/g)	Mg (mg/g)	Ti (mg/g)	TiO2 %
C1	0.06 ± 0.05	0.56 ± 0.004	0.25 ± 0.01	0.82 ± 0.011	0.00 ± 0.00	593.73 ± 8.49	99.06 ± 1.42
C2	5.34 ± 0.59	67.45 ± 5.45	52.8 ± 4.58	0.54 ± 0.011	32.02 ± 4.68	297.87 ± 15.97	49.7 ± 2.66
C3	0.79 ± 0.08	0.65 ± 0.06	37.02 ± 1.58	0.34 ± 0.032	19.2 ± 2.51	198.05 ± 22.66	33.04 ± 3.78
C4	0.00 ± 0.00	0.00 ± 0.00	0.00 ± 0.00	0.08 ± 0.009	0.00 ± 0.00	28.39 ± 7.78	4.74 ± 1.30
C5	9.15 ± nd	1.2 ± nd	72.78 ± nd	0.74 ± nd	46.82 ± nd	406.11 ± nd	67.76 ± nd

Table 25: ICP-AES results expressed in mg of element per gram of coating (mg element / g of coating) for the characterization of coatings extracted from gums and candy. "nd" standard deviation was not determined due to troubles in the chemical digestion of two of the triplicates.

	mg Element / g of chewing-gum						
Element / Samples	Al (mg/g)	Ca (mg/g)	Si (mg/g)	P (mg/g)	Mg (mg/g)	Ti (mg/g)	TiO_2 (mg/g)
C1	0.00 ± 0.00	0.00 ± 0.00	0.00 ± 0.00	0.00 ± 0.00	0.00 ± 0.00	0.59 ± 0.01	0.98 ± 0.01
C2	0.13 ± 0.01	1.64 ± 0.13	1.28 ± 0.11	0.01 ± 0.00	0,78 ± 0,11	7.22 ± 0.39	12.05 ± 0.65
C3	0.01 ± 0.00	0.00 ± 0.00	0.26 ± 0.01	0.00 ± 0.00	0.13 ± 0,02	1.38 ± 0.16	2.31 ±0.26
C4	0.00 ± 0.00	0.00 ± 0.00	0.00 ± 0.00	0.00 ± 0.00	0.00 ± 0.00	0.29 ± 0.08	0.48 ± 0.13
C5	0.00 ± nd	0.00 ± nd	0.03 ± nd	0.00 ± nd	0.02 ± nd	0.16 ± nd	0.27 ± nd

Table 26: ICP-AES results expressed in mg of element per gram of chewing-gum (mg element / g of CG) for the characterization of coatings extracted from gums and candy. "nd" standard deviation was not determined due to troubles in the chemical digestion of two of the triplicates.

	mg Element / chewing-gum						
Element / Samples	Al (mg/gum)	Ca (mg/gum)	Si (mg/gum)	P (mg/gum)	Mg (mg/gum)	Ti (mg/gum)	TiO_2 (mg/gum)
C1	0.00 ± 0.00	0.00 ± 0.00	0.00 ± 0.00	0.00 ± 0.00	0.00 ± 0.00	0.83 ± 0.01	1.39 ± 0.02
C2	0.19 ± 0.02	2.35 ± 0.19	1.84 ± 0.16	0.02 ± 0.00	1.12 ± 0.16	10.40 ± 0.56	17.34 ± 0.93
C3	0.01 ± 0.00	0.01 ± 0.00	0.53 ± 0.02	0.00 ± 0.00	0.27 ± 0.04	2.83 ± 0.32	4.73 ± 0.54
C4	0.00 ± 0.00	0.00 ± 0.00	0.00 ± 0.00	0.00 ± 0.00	0.00 ± 0.00	0.64 ± 0.18	1.07 ± 0.29
C5	0.01 ± nd	0.00 ± nd	0.09 ± nd	0.00 ± nd	0.06 ± nd	0.53 ± nd	0.88 ± nd

Table 27: ICP-AES results expressed in mg of element per piece of chewing-gum (mg element / piece of CG) for the characterization of coatings extracted from gums and candy. "nd" standard deviation was not determined due to troubles in the chemical digestion of two of the triplicates.

Recap chart for TiO_2							
Element / Samples	Ti (mg/g of coating)	TiO_2 % in coating	TiO_2 (mg/g of gum)	TiO_2 (mg/gum)	TiO_2 % in gum	Nano-TiO_2 (mg/gum)	Nano-TiO_2 (Number/gum)
C1	593.73 ± 8.49	99.06 ± 1.42	0.98 ± 0.01	1.39 ± 0.02	0.10 ± 0.00	0.06± 0.00	$3.9 \pm 0.055 \times 10^{13}$
C2	297.87 ± 15.97	49.7 ± 2.66	12.05 ± 0.65	17.34 ± 0.93	1.2 ± 0.06	0.81± 0.04	$4.6 \pm 0.25 \times 10^{14}$
C3	198.05 ± 22.66	33.04 ± 3.78	2.31 ±0.26	4.73 ± 0.54	0.23 ± 0.03	0.25± 0.00	$1.7 \pm 0.009 \times 10^{14}$
C4	28.39 ± 7.78	4.74 ± 1.30	0.48 ± 0.13	1.07 ± 0.29	0.05 ± 0.01	0.04± 0.00	$2.4 \pm 0.013 \times 10^{13}$
C5	406.11 ± nd	67.76 ± nd	0.27 ± nd	0.88 ± nd	0.03 ± nd	0.05± nd	3.8×10^{13} ± nd

Table 28: ICP-AES recap chart for TiO_2 in chewing-gum coatings. "nd" standard deviation was not determined due to troubles in the chemical digestion of two of the triplicates.

4) Determination of the crystal structure by X-ray Diffraction (XRD)

X-ray powder diffractograms of the extracted coatings (Figure 67) showed the presence of the anatase phase of TiO_2 in all samples (main peak at 2θ = 25.30°) with also some traces of rutile in C1 and C5 coatings ((110) reflection at 2θ = 27.41°), in accordance with previous studies (Chen et al., 2013). In C2 sample, the observed diffraction peaks were attributed to the anatase phase of TiO_2 and to calcite ($CaCO_3$, 2θ = 29.40°), previously identified by FT-Raman spectroscopy and listed in the ingredient list of this gum (E170, calcium carbonate). In the coating C3 and C5, most of peaks were associated to TiO_2 anatase and the additional one was attributed to magnesium silicate ($MgSiO_3$) at 2θ = 28.96°, as indicated on the ingredient list (E553), also known as talc and usually used to avoid the sticking between pieces of chewing gums during elaboration. Although the concentration in Si was higher in C2 than in C3, the presence of talc could not be identified in C2. Finally, C4 diffractogram was a bit noisier than the other samples, this could be explained by the lower content in inorganic compounds measured by ICP-AES (only 4.7%, Table 25) but the main peaks of anatase could still be clearly identified.

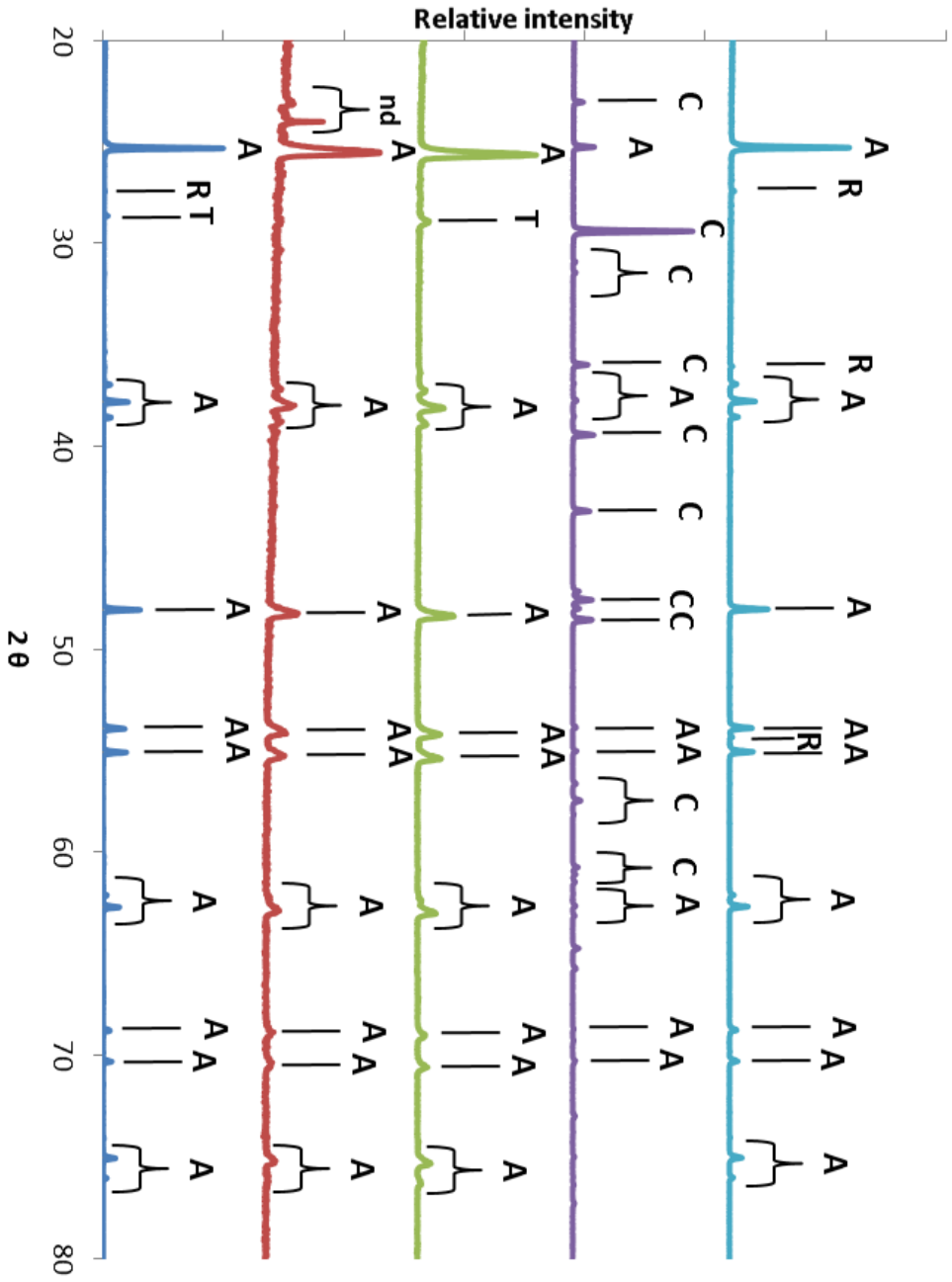

Figure 67: X-ray diffraction patterns of coatings C1 (—), C2 (—), C3 (—), C4 (—) and C5 (—), from the top to the bottom. The assignment was made according to the reference patterns of anatase TiO_2 (JCPDS 89-4921) and rutile TiO_2 (JCPDS 89-4202). Symbols A and R refer to anatase and rutile respectively, C refers to calcite ($CaCO_3$) and T refers to talc ($MgSiO_3$). The two peaks below 25° in C4 diffractogram were not attributed (n.a.) and could result from molecules remaining adsorbed onto particles after water washing.

5) Morphology and primary size of TiO_2 particles extracted from chewing-gums

TEM coupled to Energy Dispersive X-ray spectroscopy analysis (EDX) confirmed the presence of TiO_2 particles in all extracted coatings, with highly contrasted and spherical shaped particles composed of Ti and O (Figure 68). Size distribution analysis showed that all extracted coatings contained TiO_2 NPs, between 16 and 34% depending on the sample. The mean size of TiO_2 particles was 131±34, 137±40, 133±39, 137±40 and 130±55 nm for C1 to C5, respectively, *i.e.* 134±42 nm in average. These values are in accordance with the size distribution of E171 raw powders, determined in the first part of our work. (Dudefoi et al., 2017)

In addition, the nature of the extracted coatings was found to be different depending on the sample, with the presence of other objects with different shapes and chemical composition (Figure 69).

In C1 coating, which was mainly composed of TiO_2 NPs as seen in ICP-AES, was also detected a few poorly contrasted objects with sharp edges and composed of silicon and magnesium. These elements were previously detected in low amounts by ICP-AES and were associated to the crystalline structure of talc ($MgSiO_3$) by XRD analysis. The presence of aluminium was also detected by EDX but it could not be deduced whether it was associated to a coating of TiO_2 particles or to the talc, since both objects were detected together under the incident beam.

Two kinds of larger objects were also detected in C2 coating, along with TiO_2 particles. Some dense and long objects (>500 nm) were identified by EDX as being composed of Ca and C, corresponding to $CaCO_3$ (E170) as previously detected by FT-Raman spectroscopy and X-Ray diffraction. Some poorly contrasted objects composed of Si and Mg were also detected in this coating, in accordance with ICP-AES measurements. In addition, some aluminum was detected on the surface of TiO_2 particles.

Interestingly, TEM analysis showed that in C3 and C4, TiO_2 particles were found to be trapped in an organic matrix, explaining the strong signal of organic compounds detected in FT-Raman spectroscopy and the low content in inorganic elements

measured by ICP-AES. Moreover, C3 coating was also composed of Si and Mg detected by EDX, here again in accordance with X-ray diffraction and ICP-AES measurements, and corresponding to magnesium silicate ($MgSiO_3$).

Finally, C5 coating was also composed of larger objects (>500 nm) containing Mg, Si and Al detected by EDX, confirming ICP-AES and XRD analyses, which could be attributed to magnesium and aluminum silicates ($MgSiO_3$, E553 and E559) widely used in chewing-gums.

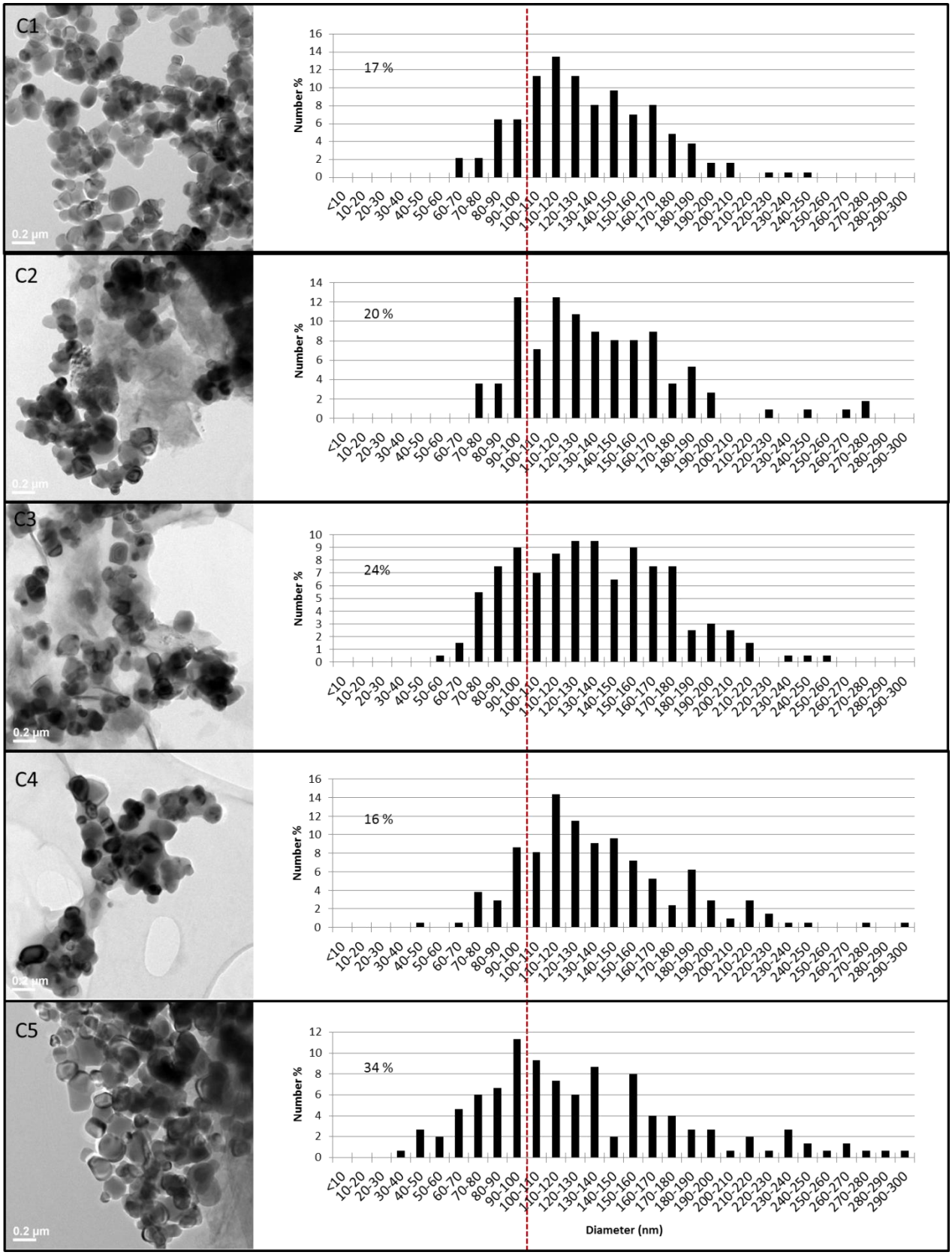

Figure 68: TEM observation and size distribution analyses of TiO_2 coatings extracted from gums and candy.

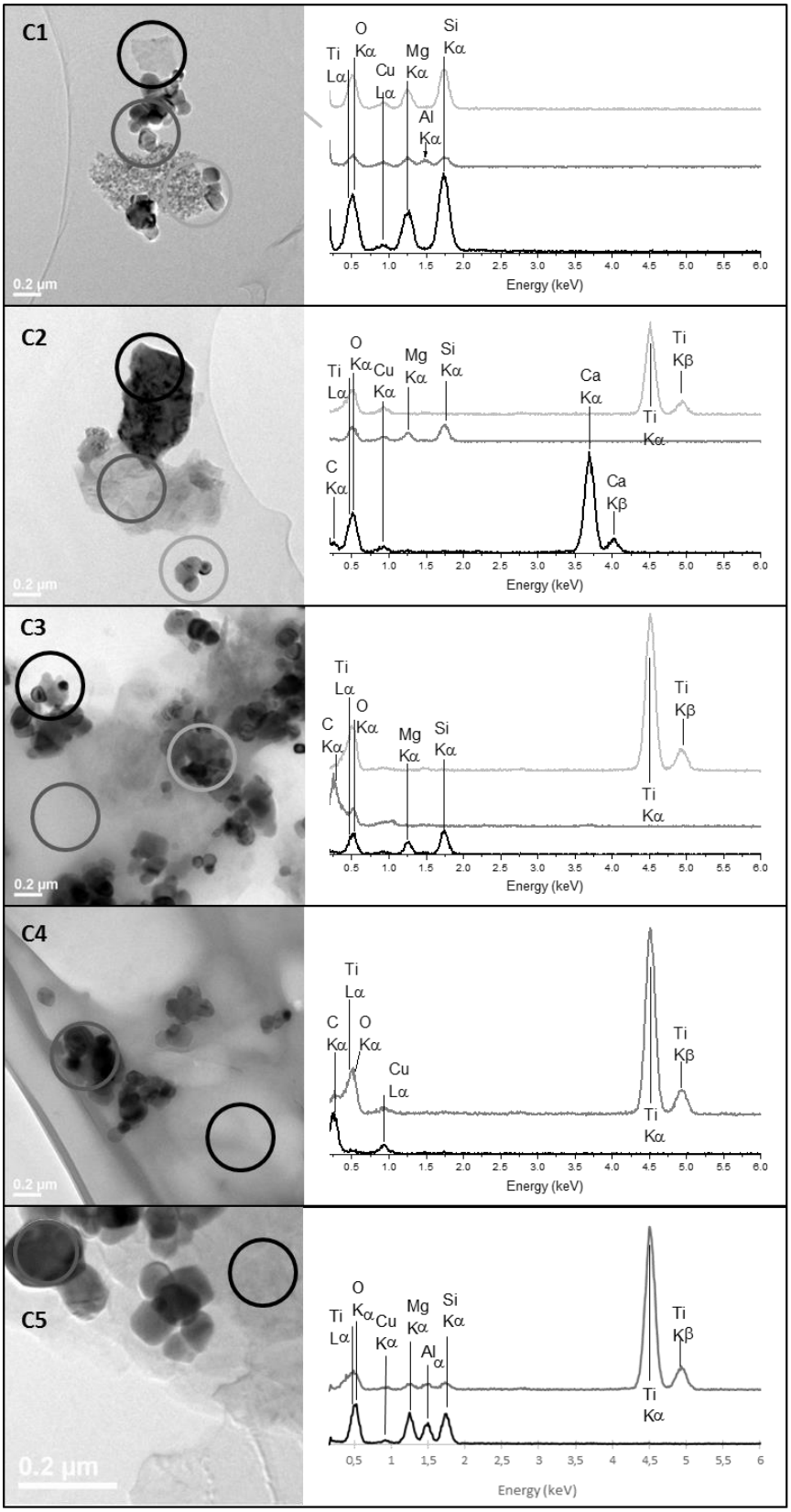

Figure 69: (left) TEM images of co-extracted objects composing the coating of chewing gums. (right) EDX spectra corresponding to the spot highlighted in the left images for the coatings.

6) Conclusions

TiO_2 was detected in the coating of chewing-gums and candies, in the range of 0.27 to 12.05 mg/g of gum, in accordance with previous data (0.12 to 2.64 mg/g of gum (Weir et al., 2012), 1.51 to 3.88 mg/g (Chen et al., 2013)). Within the extracted coatings, 16 to 34% of TiO_2 were found to be NPs, which is slightly different from the previous work of (Chen et al., 2013) who found a greater percentage of NPs in gums coatings (40.0, 43.5, 43.7, 41.4, 42.4, and 27.7%) while using the same extraction protocol. This difference could be sample-related (different chewing-gums with different compositions) or due to the way particles were measured from TEM images. Using TEM and ICP-AES results, we estimated the amount of nano-TiO_2 between 0.04 to 0.81 mg per piece of gum, representing about $2.4x10^{13}$ to $4.3x10^{14}$ NPs (for C2 and C4, respectively), meaning that the ingestion of one piece of C2 would result in an intake of nano-TiO_2 more than 20 times greater that the intake from the ingestion of one piece of C4. These results highlight the importance of considering both the concentration within the coating but also the concentration normalized to the whole piece of chewing-gum, as C1 coating was 99 wt% TiO_2, but was actually not the most concentrated sample when normalized to the whole food product.

Moreover, other larger particles (>500 nm, thick and flat objects) were also detected by TEM in the extracted coatings, and identified by XRD and EDX as $CaCO_3$ in C2, magnesium silicate ($MgSiO_3$) in C1, C2, C3, and aluminum silicates in C5, corresponding to food additives E170, E553 and E559, respectively. The presence of an organic matrix in C3 and C4 coatings which was not removed by the washing led to the formation of large objects which embedded TiO_2 particles, and resulted in a low content of TiO_2 per gram of coating (33 and 3%, in C3 and C4, respectively). TiO_2 particles are then released from chewing-gum coatings either as isolated particles, as embedded in an organic matrix forming large objects, or in the presence of other large particles depending on the samples, which can make more complicated the determination of TiO_2 particles fate during the digestion process if taken from confectionaries.

However, the physicochemical characterization of these extracted coatings by EDX and XRD showed that TiO_2 particles are mainly anatase, in accordance with (Chen et

al., 2013; Yang et al., 2014) and correspond to the food grade TiO_2 (E171), characterized in the first part of our work. These results tend to show that TiO_2 particles from chewing-gum coatings are not modified during the preparation of the products and remain as E171. Moreover, the amount of TiO_2 per chewing-gum being very small (0.88 to 17.34 mg/piece of chewing-gum), we decided to use TiO_2 food grade additive E171 as a model for digestion experiments performed during our work.

The results of this work will be submitted in *Food Additives and Contaminants Part A.*

III) *In vitro* digestion of food grade TiO_2 particles

To determine the physicochemical behavior of TiO_2 during digestion, the agglomeration state of two kinds of E171 (E171-1 and E171-6a, with different surface chemistry, 17 and 21% NPs) and P25 TiO_2 (toxicological reference, 100% NPs) was determined through a standardized static *in vitro* digestion protocol and compared to the control digestion (with and without the digestion enzymes). After each step of the digestion (*i.e.* saliva, gastric and intestinal step), the size of the particles and the surface charge changes were characterized using laser particle size distribution analysis and zeta potential measurements. Finally, the nature of the adsorbed proteins was determined by denaturing gradient gel electrophoresis (DGGE) after separation from the TiO_2 particles.

1) Size distribution and zeta potential of TiO_2 particles during simulated digestion

Size distribution analyses and zeta potential values of TiO_2 particles after each step of the simulated digestion protocol are shown in Figure 70. The size distribution of TiO_2 particles is progressively shifted towards larger sizes during the simulated digestion, suggesting an agglomeration during the digestion. Moreover, the size of the objects was, in each compartment, larger than the size measured in the control solutions (pH 7 and pH 3 without any salt or protein). For all samples, the largest sizes were obtained at the intestinal phase, with the formation of agglomerates whose size distributions were centered at around 80 µm of diameter, for all tested TiO_2 particles (Figure 70). The formation of such large agglomerates during digestion may explain the very low absorption rate of TiO_2 particles after ingestion described in the literature (Cho et al., 2013; Xie et al., 2011). The difference with controls suggests that proteins and/or ions from the digestive fluids have induce a larger agglomeration of TiO_2 particles.

Zeta potential measurements showed an increase to higher values when passing from the SSF to the SGF followed by a decrease from the SGF to the SIF ($p < 0.05$). In the

simulated digestive fluids, the zeta potential values of P25 and E171-1 samples were similar. Initially at around -12mV in the SSF, the zeta potential increased close to -2mV in the SGF and decreased to -23mV in the SIF. For E171-6a, the difference in zeta potential was larger when passing from the SSF to the SGF due to a lower initial value in the SSF (-33mV against -12mV). The values in the SGF and SIF were however similar for all TiO_2 samples. When comparing these values with those obtained in the control solutions (pH 3 and pH 7), the zeta potential values measured in the digestive fluids were significantly different from the reference values ($p<0.05$), suggesting that all TiO_2 samples interacted with some proteins and/or ions during the simulated digestion. This explains the formation of larger agglomerates, compared to controls. In the following, the roles of ions and proteins were investigated independently.

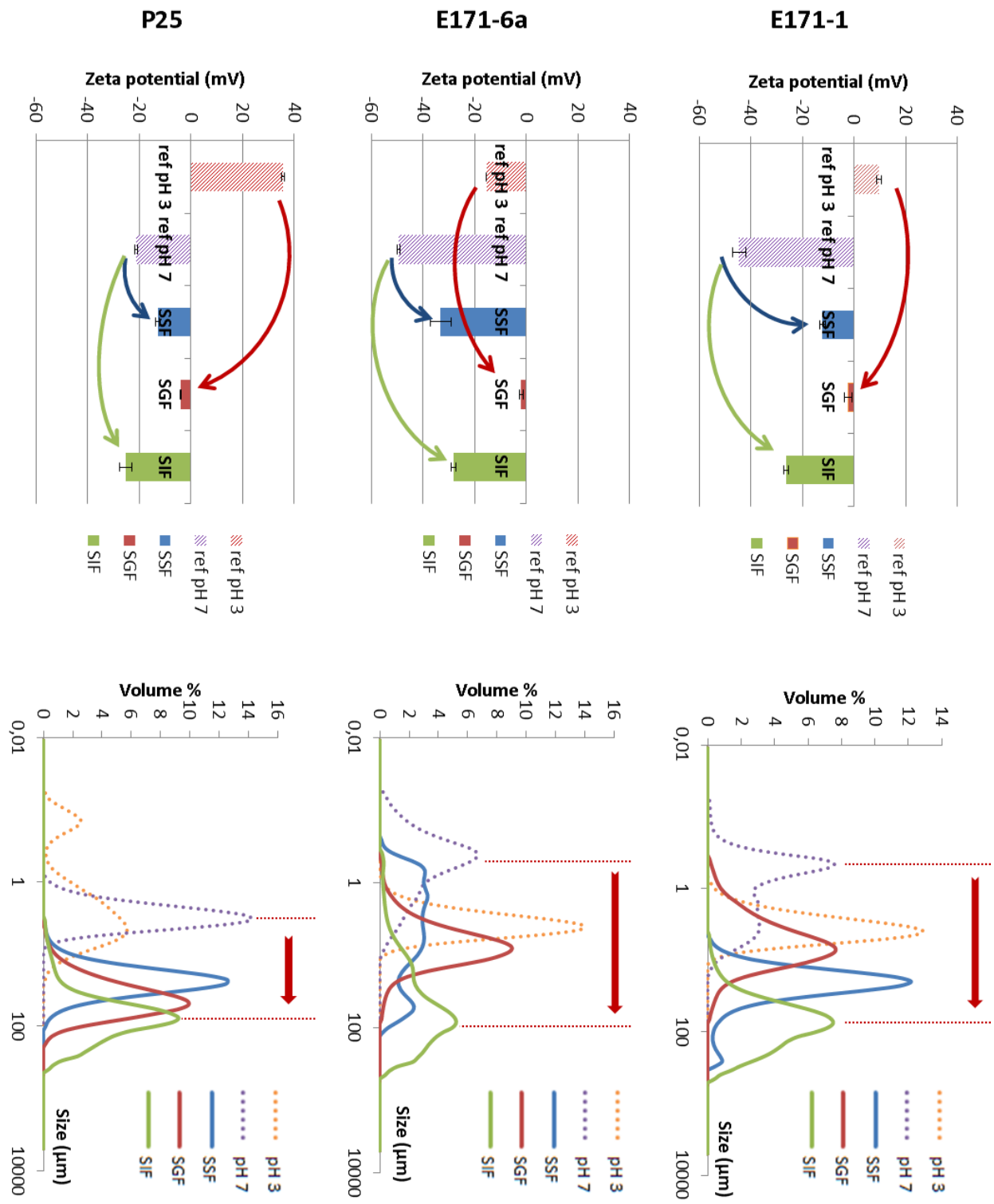

Figure 70: Size distribution and zeta potential measurements of E171 (E171-1 and E171-6a) and P25 particles during simulated digestion in full digestive fluids (SSF for simulated salivary fluid, SGF for simulated gastric fluid and SIF for simulated intestinal fluid); comparison with pH 3 and pH 7. Arrows highlight surface charge and agglomeration changes in comparison with corresponding control, at pH 3 and pH 7.

2) Identification of proteins adsorbed on TiO_2

The nature of the adsorbed proteins was determined by SDS-page electrophoresis after separation from the TiO_2 particles. Each sample was compared with a digestion blank control performed without TiO_2 particles to identify the adsorbed proteins and to check the effect of the centrifugation on the digestive proteins. The first samples to be analyzed were supernatants number 1 (SN1), considered as the non-interacting proteins, subsampled after separation from TiO_2 particles by centrifugation. The objective here was to try to detect the disappearance of one or several bands of proteins that would have interacted with TiO_2 and would have been brought to the pellet during centrifugation, whereas they would have remained in the supernatant in the control. However, no clear differences were observable between samples and the controls on the electrophoresis gel of supernatant number 1 (SN1), at all steps of the simulated digestion (Figure 71). This observation may mean that either TiO_2 particles did not interact with proteins during the simulated digestion protocol, or that the amount of protein that interacted with TiO_2 particles was not large enough for the difference to be detected on this gel.

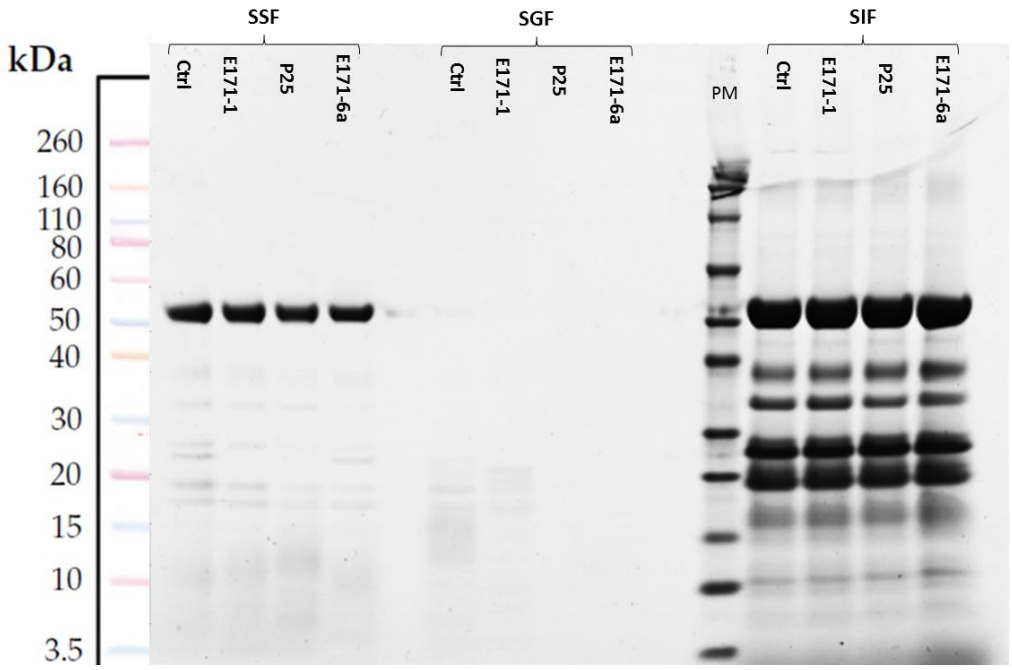

Figure 71: Electrophoresis gel of supernatant number 1, SN1

After the addition of a denaturing solution to desorb the originally adsorbed proteins from TiO_2 particles and their separation by centrifugation, supernatants number 2 (SN2) were analyzed by electrophoresis (Figure 72). The presence of bands in the control is the sign of the precipitation of enzymes during centrifugation. No main differences between the control and the samples were observed at the salivary step of the simulated digestion (SSF). The presence of a band at 52kDa in TiO_2 samples may result either from the precipitation of α-amylase, or from both precipitation and a possible adsorption on TiO_2 particles.

However, for all tested TiO_2 samples, some differences from the blank control were observed at the gastric step (SGF). First, we observed the appearance of the α-amylase spot for all TiO_2 treatments, while it did not appear in the control. Secondly, a spot at 35kDa was also detected for E171-6a, corresponding to the main gastric protein: pepsin. This is the sign of the adsorption of α-amylase onto TiO_2 particles when entering the gastric phase, and of the specific adsorption of pepsin on the silica-covered TiO_2 E171-6a.

Moreover, the E171-6a SN2 presents fewer bands of low molecular weight proteins than the blank and the two other TiO_2 samples, which could reveal an inhibition of the pepsin lysing activity due to its adsorption on TiO_2 particles. These hypothesis was recently confirmed by Al-Hakeim & Jasem (Al-Hakeim & Jasem, 2016), who showed that in a high ionic strength media, which is the case in the gastric fluid, TiO_2 NPs can cause a complete inhibition of pepsin activity. The loss of activity may be explained by changes on the secondary structure of pepsin being unfolded after treatment with TiO_2 NPs (Zhu et al., 2010), leading to the loss of fit between the active site of pepsin the substrate and resulting in the reduction of the enzyme activity.

Interestingly, this interaction with pepsin was only observed for E171-6a, and not for the other TiO_2 samples. This difference of interaction could be related to the different surface chemistry of E171-6a sample, which was found to be coated with silica by XPS analysis, and to have a different IEP than the other batches of E171, as determined in the first part of our work. In order to get further in the interpretation of this difference, it would have been interesting to compare our samples with the samples

used in these two studies, but unfortunately, the surface chemistry of the tested TiO_2 samples was not described enough.

Finally, a lot of bands appeared in the simulated intestinal fluid, due to the large number of enzymes composing the pancreatin (trypsin, amylase and lipase, ribonuclease, and protease). No clear differences were observable between the control and the food grade TiO_2 samples (E171-1 and E171-6a). However, a decrease of the intensity was detected for several bands in the P25 treatment, including the α-amylase, and attributed to the enhanced photocatalytic activity of these particles, which may have degraded some on the proteins composing the intestinal fluid.

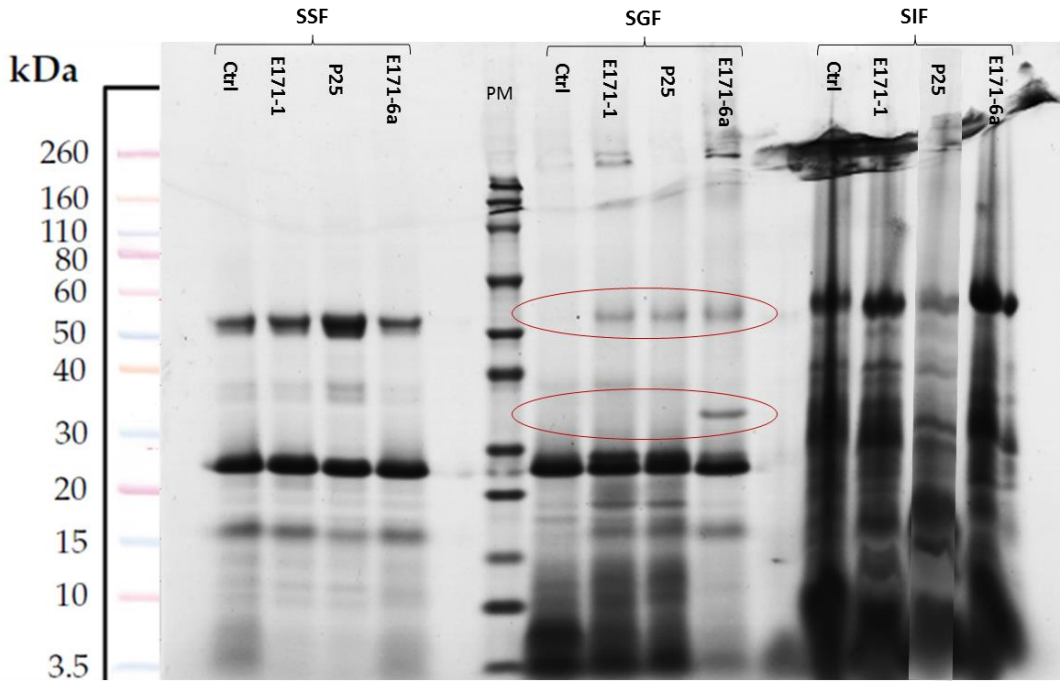

Figure 72: Electrophoresis gel of supernatant number 2, SN2

3) Impact of salts on TiO_2 agglomeration during simulated digestion

In order to determine the role of the salts in the agglomeration behavior of TiO_2 particles, the simulated digestion protocol was applied without proteins. For all samples, laser diffraction analyses showed a size distribution of TiO_2 agglomerates in saline solutions hardly modified along the digestion and close to a few µm, even in the saline fluid of the intestinal compartment. The maximum of the distribution at the end of digestion is centered at 7.70, 8.8 and 7.70 µm for E171-1, E171-6a and P25, respectively. The agglomeration of P25 particles is weakly affected by ions and pH along the digestion process, compared to controls. Only the size distributions of E171 particles are significantly shifted to higher values at pH 7 (Figure 73) but are similar to the size distributions found at pH in the presence of enzymes (SSF). The agglomeration of TiO_2 particles in the full media results from the adsorption of enzymes in the SGF and in the SIF. As regards to zeta potential, the values shifted in saline solutions when compared to controls. P25 particles showed the main shift in the simulated gastric fluid (SGF), with a decrease from +36 mV (pH 3) to -14 mV. In the same way, E171-1 particles also showed an inversion of their surface charge between the pH 3 control and the simulated gastric fluid (SGF), with a decrease from +10 to -22 mV. These inversions of surface charge may be attributed to strong adsorptions of carbonates and phosphates on the surface of TiO_2 particles. (Connor & McQuillan, 1999; Domingos et al., 2010; Gong, 2001).

All TiO_2 samples interacted with some ions during the simulated digestion, increasing the agglomerates sizes when compared to water, with the largest agglomerates still obtained in the simulated intestinal fluid (SIF), but yet forming smaller agglomerates than in the full digestion fluids (with proteins) meaning that both salts and proteins in the digestive fluids had an impact on TiO_2 agglomeration.

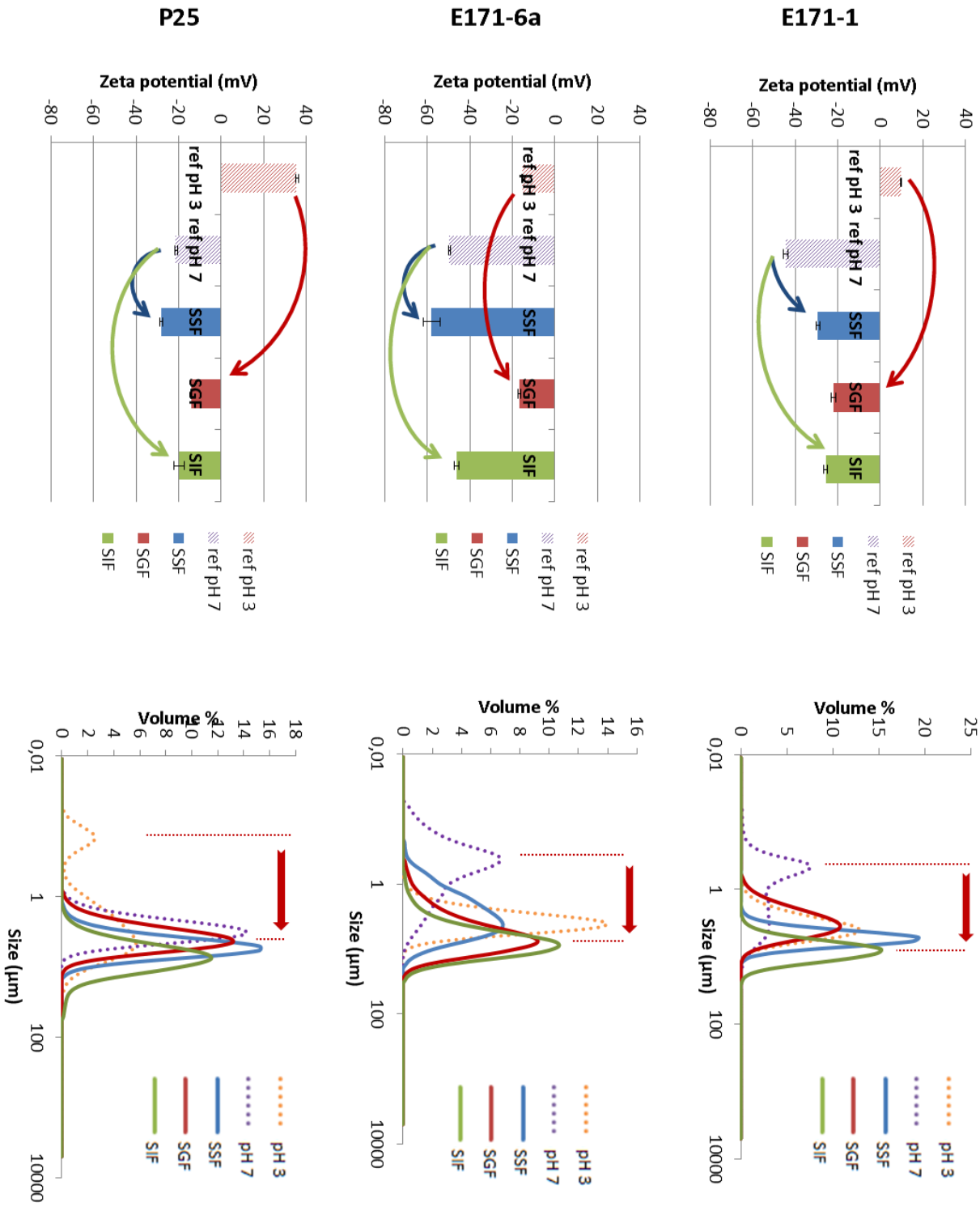

Figure 73: Size distribution and zeta potential measurements of E171-1, E171-6a and P25 particles during simulated digestion without digestive proteins; comparison with pH 3 and pH 7.

4) Conclusions

TiO_2 NPs agglomerated during digestion and formed large agglomerates up to 90 µm in the intestinal fluid, which may explain the low absorption rate of TiO_2 particles after ingestion reported in the literature (Cho et al., 2013; Xie et al., 2011). This agglomeration was due to interactions of TiO_2 with both ions (probably calcium and phosphates (Connor & McQuillan, 1999; Domingos et al., 2010; Gong, 2001)) and proteins in the digestive fluids. Indeed, an interaction with the salivary enzyme α-amylase was detected for all TiO_2 samples, and with pepsin for one of the food grade sample having a different surface chemistry. Moreover, the adsorption of the digestive proteins on TiO_2 particles could induce an inhibition of their enzymatic activity, as described in the literature for the pepsin after TiO_2 treatment. (Al-Hakeim & Jasem, 2016; Zhu et al., 2010).

Considering that the interactions occurring between TiO_2 particles and the digestive proteins may modify their enzymatic activity, and *in fine* have deleterious consequences on the overall digestion process, the impact of these interactions will have to be more deeply investigated. Moreover, in order to confirm our results and get more realistic data, the simulated digestion protocol will have to be applied to full chewing-gums extracts.

Finally, as the *in vitro* digestion protocol used here was only considering the physical chemistry of the gastrointestinal tract, we wanted to consider the biological aspect of the human gastrointestinal tract, in studying the impact of TiO_2 particles on the human gut microbiota in the last part of our work.

The results of this work will be submitted in *Food & Function.*

IV) Impact of food grade TiO_2 particles on gut microbiota

The impact of food-grade TiO_2 was assessed on a defined gut bacterial community, MET-1 (microbial ecosystem therapeutic-1), as a model human intestinal community. The anaerobic consortium containing 33 bacterial species was batch cultured for 48 h at 37°C in a starch-based medium. Food-grade TiO_2 from several suppliers (E171-1 and E171-6a, 17 and 21% NPs, with different surface chemistry) and Degussa P25 (toxicological reference, 100% NPs) were used to amend the cultures at two realistic concentrations (100-250 ppm, based on a single unit of gum and defined from previous experiments). As we observed a potential interaction between TiO_2 particles and the α-Amylase during the *in vitro* digestion protocol, the impact of a mixture of E171-1 and α-Amylase was also assessed, as a model of digested TiO_2 particles. The impact of TiO_2 was assessed using physiological, biochemical and molecular assays.

1) Physiological assay: Gas generation analyses

For the most part, after 48 h of incubation, all serum bottles, irrespective of the treatment groups, showed levels of CO_2 and N_2 as well as total gas volumes that were similar to control, non-amended cultures (Figure 74). This suggests that the addition of food additives and the TiO_2 NPs had no significant influence on bacterial metabolism. In the E171-6a-amended sample there was a small variation in gas volume at both concentrations ($p<0.05$). However, these p-values were only just within the limit of significance ($p= 0.041$ and 0.046) and only one gas per treatment was involved. Therefore we suggest that the amendments had no overall impact on bacterial respiration.

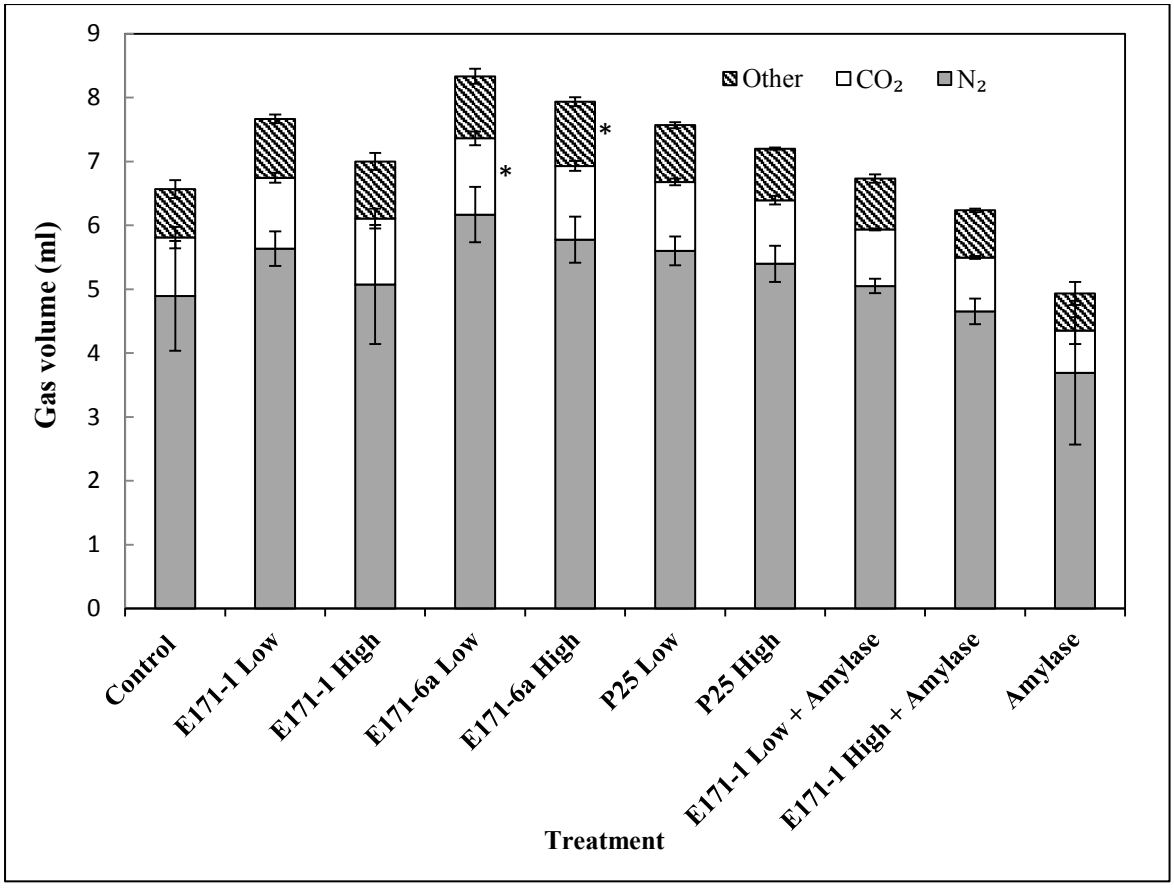

Figure 74: Carbon dioxide (CO_2), nitrogen (N_2) and other gases recovered from the total gas generated by the MET-1 communities after 48 h exposure to food grade (E171-1 and E171-6b) and P25 TiO_2 particles at 100 (Low) and 250 (High) mg/L, and control (with no TiO_2 particles). The star symbol indicates significance differences ($p<0.05$) in gas composition (volume) compared to the unamended controls.

2) Biochemical assay: Fatty acid analyses

A total of 54 different phospholipid fatty acid peaks were seen in chromatographs obtained from the treated MET-1 cultures. For each sample, the chromatographic peak areas were converted to percentage of total fatty acids (mol %), and of these, 25 dominant fatty acids were selected for comparative analysis and characterized into Gram negative, Gram positive, saturated and unclassified groups (Figure 75) according to conventional classification (e.g. (Bartelt-Ryser, Joshi, Schmid, Brandl, & Balser, 2005); but see (Suutari & Laakso, 1994) for cautionary interpretive advice). Overall, the food additives and TiO_2 NPs had little to no impact on the overall fatty acid compositions. There were some modest changes that were significant for E171-1

(Figure 75), with small variations in the saturated fatty acids composition for C12:00, C14:00, C16:00 and C18:00, respectively, at both additive concentrations, Gram negative fatty acids markers (16:1 w7c/16:1 w6c, 17:0 cyclo and 18:1) and four of the unclassified fatty acids (15:1 w5c, 17:00, 18:2 w6, 9c/18:0 ante and 18:1 w9c). However, most of these represented less than a 1 percentage point change. Only two fatty acids appeared to decrease slightly (14:00 and 18:1 w9c) after incubation with the P25 particles and there were no changes in any fatty acids with the E171-6a additive.

In contrast with these very limited effects, the addition of pancreatic amylase, and the mixture of amylase and E171-1, to MET-1 induced significant shifts in all classes of fatty acids when compared to controls ($p<0.05$; Figure 2). Amylase addition reduced some Gram positive (15:0 3OH) and Gram negative signatures (16:1 w7c/16:1 w6c, 16:0 3OH and 18:1 w7c) and shifted saturated fatty acids profiles (10:00, 12:00, 14:00, 18:00 and 20:00) and unclassified fatty acids proportions (17:0 2OH and 18:2 w6,9/18:0 ante) indicating that the batch MET-1 cultures were physiologically responsive.

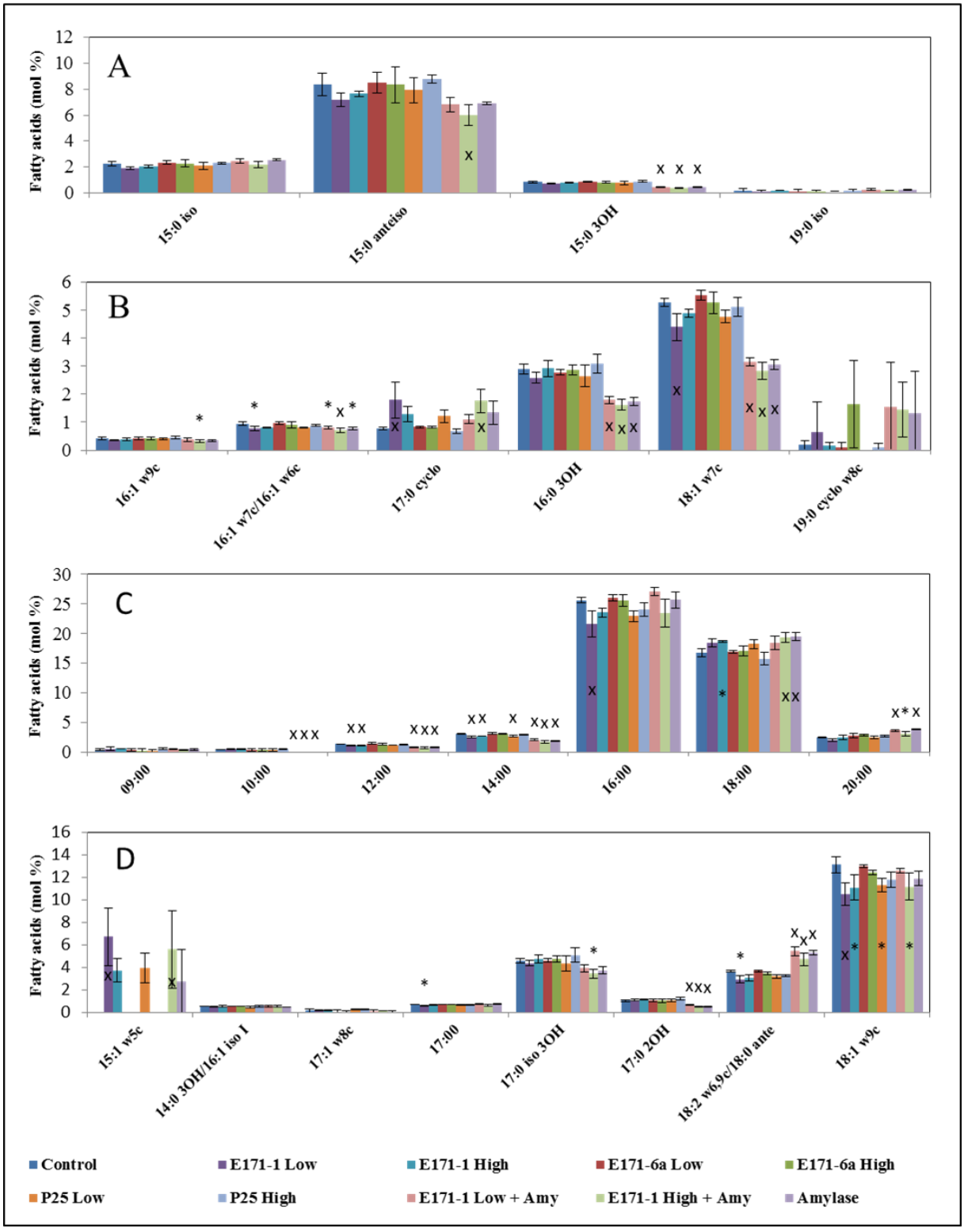

Figure 75: Relative amounts (mol %) of extracted fatty acids in control (no nano-TiO2) and nano-TiO_2 treatments at 100 mg/L (Low) and 250 mg/L (High) concentrations. The bars represent the means of three independent fatty acid assessments and standard errors. The fatty acids were classified as (A) Gram positive, (B) Gram negative, (C) saturated, and (D) unclassified fatty acids for ease of analysis, however, note that assignments to specific groupings may be problematic (see Results). Stars and letter x symbols indicate significant differences at $p<0.05$ and $p<0.01$, respectively, compared to the controls.

3) DNA analyses

a) PCR-DGGE

After TiO_2 amendment, PCR-DGGE banding patterns appeared identical to the controls, with the consistent appearance of 6 major bands (Figure 76), suggesting that TiO_2 NPs at the concentrations used had no impact on the MET-1 ecosystem. In contrast, consistent differences in banding patterns and intensities were seen in treatment groups containing amylase compared to controls. In particular, one band (numbered '4'; Figure 76) disappeared in three treatment groups containing pancreatic amylase additions (amylase controls and the E171 food additive containing the enzyme).

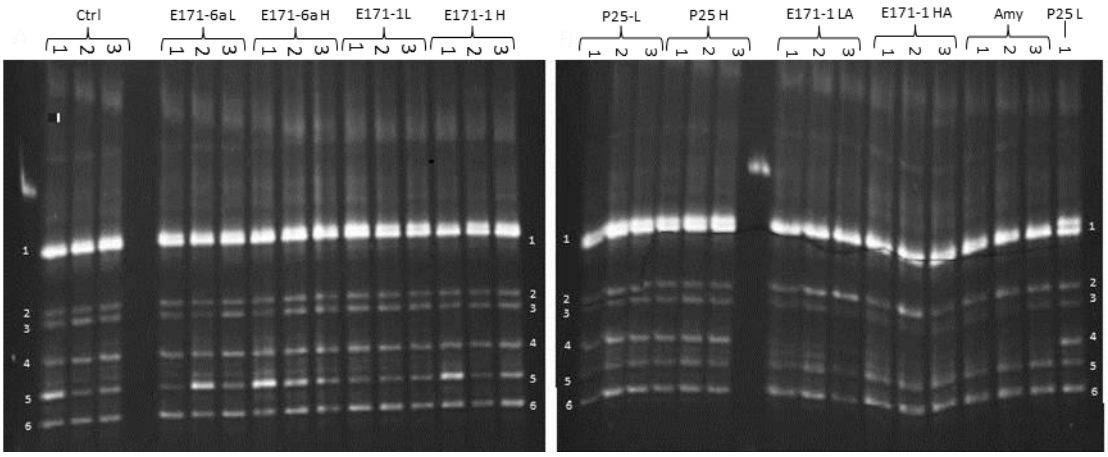

Figure 76: PCR-DGGE band patterns in controls (Ctrl) and after exposure to E171 food grade TiO_2 particles (E171-1 and E171-6a) and to TiO_2 NPs (P25) at 100 ppm (low; L) and 250 ppm (high; H) concentrations, without and in the presence of amylase (Amy). Porcine pancreatic amylase (37.5 U/ml) was added alone or as a mixture with E171-1 at both concentrations (E171-1 LA and E171-1 HA). Numbers at the end of the descriptors (1, 2, 3) indicate replicate samples. Numbers next to the bands mark those that were analyzed for intensity variations. Unmarked lanes contained marker DNA.

b) Phylogenetic distribution as indicated by sequence analysis

After incubation, the cultured consortium was dominated by 8 strains, and thus although results were obtained for the entire MET-1 community, only the most abundant bacteria were examined in detail since any modest perturbations of very minor species contributors would be of no interest to consumers or regulators. Consistent with the PCR-DGGE analysis, phylogenetic distributions obtained from 454 pyrotag 16S rRNA gene sequencing showed that there were no substantial differences between the E171-6a treatment groups and controls. In the E171-1 (250 ppm) food additive group there was an 8 percentage point decrease in the OTUs attributed to *Bacteroides ovatus* (strain 5 MM; Figure 77), but there were no other significant changes. The 7 and 13 percentage point decrease in *B. ovatus* in the P25 treatment groups, at 100 and 250 ppm, respectively, was correlated with a 11 and 14 percentage point increase in the abundance of strain 21FAA (closest database relative *Clostridium cocleatum;* $p<0.05$; Figure 77). When the taxonomic distribution was normalized to total fatty acids (Figure 78), there appeared to be no negative impact on consortium viability after TiO_2 treatments. P25 and E171-6a treatments induced no significant differences when compared to controls, with some small increases in the relative proportions of *Acidaminococcus intestini*, *Eubacterium ventriosum* and *Eubacterium rectale* strains (4.4, 0.5 and 2.6 percentage points, respectively) in the E171-1 amendment groups (Figure 77).

In contrast to the results for the titania amendments alone, treatment groups containing pancreatic amylase, in the presence or absence of E171-1, resulted in a consistent and significant 4.8 percentage point reduction of *Eubacterium rectale* (represented by four strains), a species known for its starch-utilization pathways, in favor of the predominant bacteria in the consortium, *B. ovatus*, which increased by 13 percentage points ($p<0.01$; Figure 77; Figure 78).

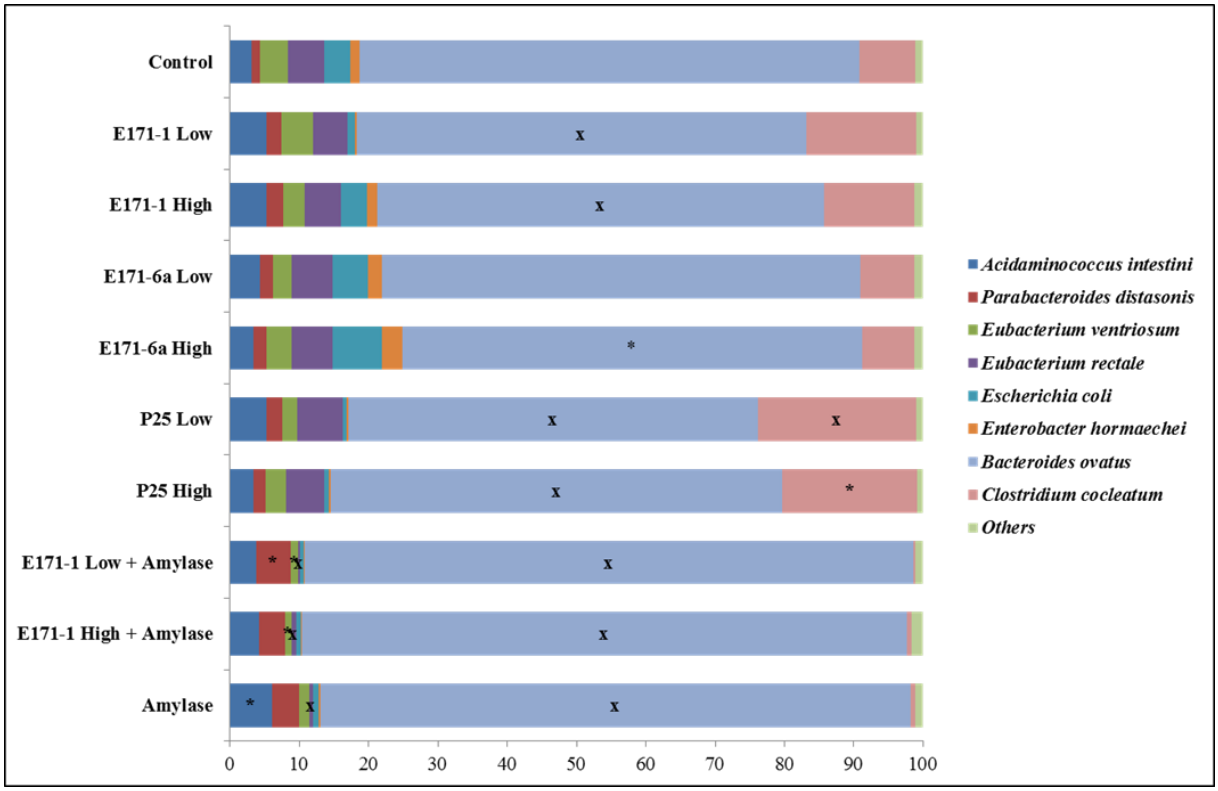

Figure 77: Phylogenetic composition to species in the MET-1 consortium represented as distribution percentages after 48 h exposure to 100 ppm (Low) and 250 ppm (High) concentrations of food grade E171-1 and E171-6a, as well as to P25 TiO_2 NPs (P25), compared to control (Control). Treatment groups containing pancreatic amylase (37.5U/ml; Amylase) are indicated. Distribution percentage of each species (indicated on the color key) is based on the means of triplicate samples of those contributing >1% relative abundance (for figure clarity less abundant species are indicated as 'Others'). Significant differences ($p<0.05$ and $p<0.01$, respectively) compared to the control cultures are indicated by stars and the letter x, respectively, on the bars.

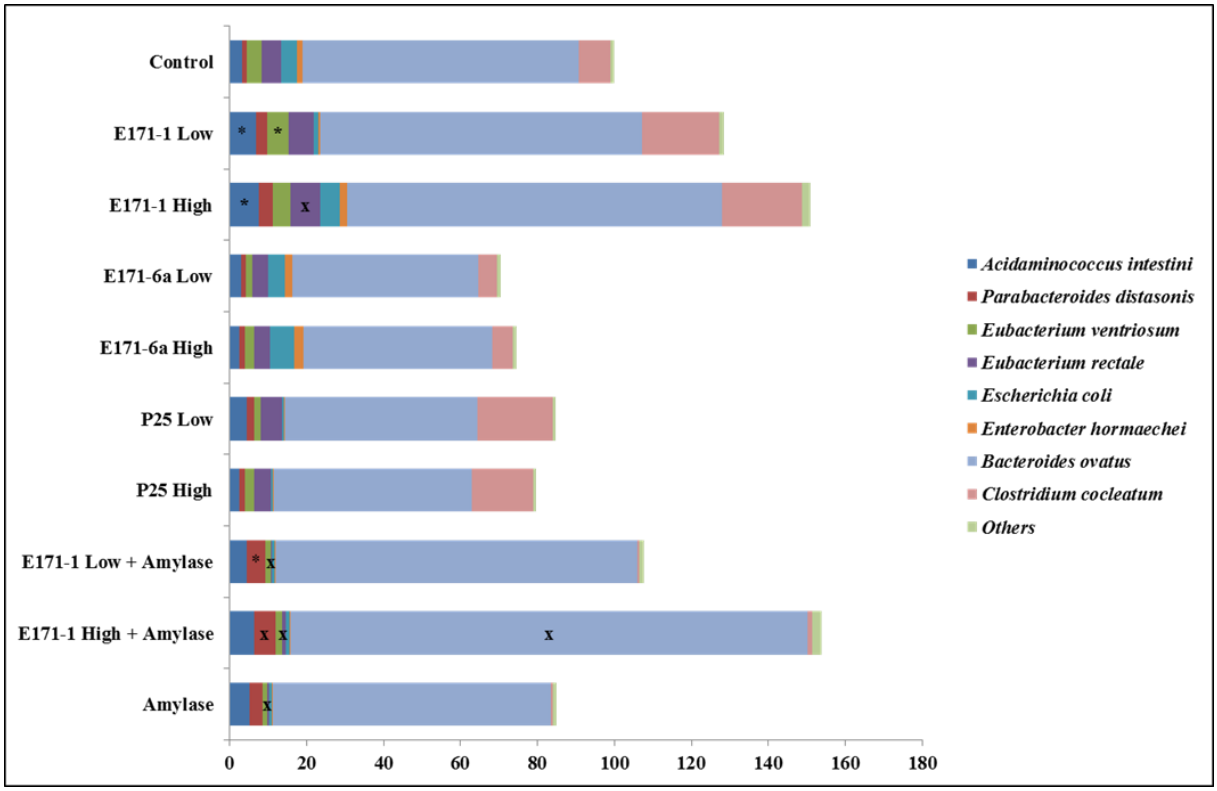

Figure 78: MET-1 phylogenetic composition to species normalized to total fatty acid abundance in each treatment group, after 48 h exposure to 100 ppm (Low) and 250 ppm (High) food grade E171-1 and E171-2, as well as to TiO_2 NPs (P25), compared to controls (Control). Treatment groups containing 37.5 U/ml of pancreatic amylase are noted (Amylase). Estimated species numbers are based on means of triplicate samples (>1% relative abundance with less abundant species shown as 'Others'). Significant differences ($p<0.05$ and $p<0.01$, respectively) compared to the control are indicated by stars and the letter x, respectively, on the bars.

4) Discussion

The gastrointestinal microbiota is frequently exposed to NPs after the deliberate or accidental ingestion of various foods, water, and personal care products (E. E. Fröhlich & Fröhlich, 2016). Nonetheless, experimental work on the impact of NPs on the gut microbiota remains meager. Knowing that changes in microbiota can be associated with important disease states such as obesity, diabetes, rheumatoid arthritis, and inflammatory bowel disease (Marchesi et al., 2015; Pietroiusti et al., 2016) gives impetus to such investigations. Here we show that food-grade whitening and brightening additives containing ~20% TiO_2 NPs do not have a major impact on the human gut microbiota when used at concentrations that mimic the concentration in the adult intestine after chewing a single piece of gum. Although these results should be greeted as good news for consumers, a minor impact was seen with the TiO_2 NPs (P25) amendment, as evidenced by a modest decrease in the proportion of *B. ovatus* and an increase in *C. cocleatum* strains, suggesting that a cautious approach be taken to the ingestion of larger amounts of these food additives within a single meal.

The modest impact of TiO_2 NPs on the MET-1 consortium contrasts with results obtained after amending this community with silver NPs, which induced major changes in the ecosystem as indicated by a significant reduction in gas production, changes in fatty acid methyl ester profiles and shifts in the community structure (Pranab Das et al., 2014). Thus titania particles clearly have little impact on the microbiome in comparison to these NPs. To ensure that the MET-1 community remained sensitive to amendment, pancreatic amylase was added to the consortium, as well as to the E171-1 treatment groups. The results clearly showed that the addition of the enzyme alone or in combination with nano-titania had a significant impact on the consortium. Pancreatic amylase would have hydrolyzed a portion of the starch substrate, which in turn would have modified the nutrient availability in the culture media. The result was a shift in some fatty acids when compared to controls ($p<0.05$), the reduction of some identified Gram negative and Gram positive signatures, and changes in the saturated and unclassified fatty acids profiles. Correspondingly, DNA analysis demonstrated the

disappearance of a band in PCR-DGGE, and the significant reduction of sequences corresponding to the four strains of *E. rectale*, a species known for its starch-utilization pathways, in favor of the abundant Bacteroidetes member of the model gut consortium, *B. ovatus* ($p<0.01$). This perturbation of the microbial consortium in response to the addition of the amylase clearly demonstrates the ability of the MET-1 cultures to respond to modification and thus helps establish this as an appropriate model system to assess food additives, including TiO_2 NPs.

The small differences in the impact of the two additives, E171-1 and E171-6a, may not only be due to their variance in total TiO_2 NPs but also their different chemistries, with E171-6a's silica coat possibly maximizing water molecule contacts and thus having the potential to reduce the formation of adhesive interactions between the particles and the bacteria. As well, the impact on the MET-1 community depends on the properties of the individual participants. For example, the toxicity of TiO_2 NPs on bacteria has been reported to be less effective against Gram negative species (Bonnet, Massard, Veisseire, & Camares, 2015; Rincón & Pulgarin, 2005). In accordance with this prediction, *B. ovatus*, which showed a decreased abundance in the nano-titania-treatment groups, is Gram negative, and the *C. cocleatum* strain, which showed an increased abundance in the P25-treatment group, is Gram positive. Although the nano-toxicity mechanism is unknown, it has been suggested that NPs interact with bacteria to produce reactive oxygen species (ROS), which in turn can damage DNA, RNA and proteins (Cabiscol, Tamarit, & Ros, 2000). Thus Gram positive bacteria, with their thick peptidoglycan and lipoteichoic cell walls may be better protected against ROS damage. Further, nano-titania absorbs ultraviolet light and is in consequence an important photocatalyst, generating ROS which then can oxidize organic compounds (Barnes, Molina, Xu, Dobson, & Thompson, 2013). Indeed, TiO_2 NPs appear to be significantly less toxic in the dark (Bonnet et al., 2015; Tsuang et al., 2008). Notably, the experiments with MET-1 were conducted in the absence of oxygen and also in the dark, possibly explaining the very low toxicity observed here. These results further suggest that TiO_2-containing food additives could be of lesser concern for consumers since these two conditions are also found in the human gut.

5) Conclusions

Titanium dioxide is a white metal oxide commonly employed as a pigment in food products that have been found to contain up to and including up to ~40% NPs. Based on our investigations using the defined anaerobic gut bacterial community MET-1, the addition of relevant concentrations of commercial food additives (100 - 250 mg/L) had little impact as assessed through bacterial respiration, fatty acid profiles and phylogenetic composition. Taken together, our results should reassure consumers that food grade TiO_2 particles do not significantly alter the human gut microbiota. However, we caution that the cumulative effects of chronic ingestion and the impact of higher concentrations of nano-titania are still to be assessed before there can be assurance that there is no significant toxicity to our microbiome by these ubiquitous food additives.

The results of this last part of our work has been accepted with revisions in *Food and Chemical Toxicology*.

General conclusions and outlook

This thesis project intended to reinforce the safety evaluation of food grade TiO_2 particles by investigating their physicochemical nature, their evolution within the gastrointestinal tract and their toxicity on the human gut microbiota.

As a first step, we investigated the physicochemical properties of food grade TiO_2 material (E171) and compared them to the reference material P25 in order to evaluate its relevance. Ours results showed that all the investigated E171 samples contained a fraction of NPs but smaller than the reference material P25 (up to 36% against 100%), and below the threshold defining the labelling of nanomaterial. Since our results showed that E171 and P25 particles are different by many aspects (composition, size and surface chemistry), P25 may not be the most realistic model to study the fate and impact of TiO_2 via ingestion, even to mimic the nano-sized fraction.

In order to determine if TiO_2 particles remained in the same state once added in food products, we also characterized TiO_2 particles extracted from the coating of chewing-gums. TiO_2 was detected in the range of 0.27 to 12.05 mg/g of gum with 16 to 34% of TiO_2 as NPs, representing about $1.7x10^{13}$ to $4.3x10^{14}$ NPs per piece of gum. Moreover, we found that TiO_2 particles can be released from the coating as pure particles, as embedded in an organic matrix, or also released with other larger particles, which make more complex the study of the agglomeration of TiO_2 particles from gums coatings during the digestion process. However, the physicochemical characterization of these extracted coatings showed that TiO_2 in chewing-gums remained similar to the E171 particles characterized in the first part of our work, with the same crystallinity, morphology and a percentage of NPs in the same range as the food additive powder. E171 particles could then be used as model for the digestion study.

The second step was to determine the physicochemical behavior of TiO_2 particles in digestive fluids. Using a standardized static *in vitro* digestion protocol, we found that TiO_2 particles agglomerated all along digestion and formed large agglomerates up to 90 µm in the intestinal fluid, which may explain the low absorption rate of TiO_2 particles after ingestion reported in the literature. This agglomeration was due to interactions of TiO_2 with both ions and proteins in the digestive fluids. An interaction

with the salivary enzyme α-amylase was detected for all TiO_2 samples, and with pepsin only for the food grade sample of having a different surface chemistry.

The last objective of this work was to assess the toxicity of TiO_2 to the human gut microbiota. The impact of E171 and P25 particles on a model human intestinal community was assessed with physiological, biochemical and molecular assays. Based on our investigations, TiO_2 treatments (100 - 250 mg/L, concentrations equivalent to those found in the intestine after the ingestion of one to two pieces of confectionary) had little to no impact on the human gut microbiota (bacterial abundance, phylogenetic distribution and metabolic activity).

Finally, this thesis project resulted in a better knowledge of the physical chemistry of food grade TiO_2 particles and allowed us to define the criteria for a relevant sample of food grade TiO_2 (Dudefoi et al., 2017), that will be useful for the next risk assessment studies by ingestion. It also led to the demonstration of their agglomeration in digestive fluids in taking into account the whole digestive tract and of their innocuousness on the human gut microbiota, based on a realistic single exposure.

There are still some points to investigate to fully understand what really happens after the ingestion of TiO_2 particles. Our work applies for all chewing-gums where TiO_2 is freely released from the coating. For those where TiO_2 was embedded in an organic matrix or mixed with calcium carbonate, a further study using full chewing-gums extracts has to be undertaken to get more realistic data. Moreover, the impact of the interactions occurring between TiO_2 particles and the digestive proteins on their enzymatic activity has to be determined, as it could have deleterious consequences on the overall digestion process. Furthermore, the effects of TiO_2 particles on the human gut microbiota through a chronic exposure are still to be investigated.

At last, if we consider the global life cycle of these food grade TiO_2 particles, we were interested in their physical chemistry after their production as food additive, after their addition within the food product and after their uses by the consumers. To complete the risk assessment of these particles, their fate at the end-of-life is also important to determine, *i.e.* first in wastewater treatment plants and then in the environment.

Literature references

Agrawal, A., & Barron, A. R. (2013). Wide Angle X-ray Diffraction Studies of Liquid Crystals. Retrieved April 26, 2016, from http://core.ac.uk/download/pdf/10587419.pdf

Ahmed, S. S. S. J., & Ramakrishnan, V. (2012). Systems biological approach of molecular descriptors connectivity: Optimal descriptors for oral bioavailability prediction. *PLoS ONE*, *7*(7). https://doi.org/10.1371/journal.pone.0040654

Aitken, R., Creely, K., & Tran, C. (2004). Nanoparticles: An Occupational Hygiene Review. *Health & Safety Executive*, 113.

Al-Hakeim, H. K., & Jasem, K. M. (2016). High Ionic Strength Enhances the Anti-Pepsin Activity of Titanium Dioxide Nanoparticles. *Nano Biomedicine and Engineering*, *8*(3). https://doi.org/10.5101/nbe.v8i3.p136-143

Alam, M. A., Al-Jenoobi, F. I., & Al-Mohizea, A. M. (2012). Everted gut sac model as a tool in pharmaceutical research: Limitations and applications. *Journal of Pharmacy and Pharmacology*, *64*(3), 326–336. https://doi.org/10.1111/j.2042-7158.2011.01391.x

Alexander, M. R., Beamson, G., Blomfield, C. J., Leggett, G., & Duc, T. M. (2001). Interaction of carboxylic acids with the oxyhydroxide surface of aluminium: poly(acrylic acid), acetic acid and propionic acid on pseudoboehmite. *Journal of Electron Spectroscopy and Related Phenomena*, *121*(1–3), 19–32. https://doi.org/http://dx.doi.org/10.1016/S0368-2048(01)00324-3

Alger, H., Momcilovic, D., Carlander, D., & Duncan, T. V. (2014, July 21). Methods to evaluate uptake of engineered nanomaterials by the alimentary tract. *Comprehensive Reviews in Food Science and Food Safety*. https://doi.org/10.1111/1541-4337.12077

Athinarayanan, J., Alshatwi, A. a, Periasamy, V. S., & Al-Warthan, A. a. (2015). Identification of Nanoscale Ingredients in Commercial Food Products and their Induction of Mitochondrially Mediated Cytotoxic Effects on Human Mesenchymal Stem Cells. *Journal of Food Science*, *80*(2), N459–N464. https://doi.org/10.1111/1750-3841.12760

Axson, J. L., Stark, D. I., Bondy, A. L., Capracotta, S. S., Maynard, A. D., Philbert, M. a., … Ault, A. P. (2015). Rapid Kinetics of Size and pH-Dependent Dissolution and Aggregation of Silver Nanoparticles in Simulated Gastric Fluid. *The Journal of Physical Chemistry C*, *119*(35), 20632–20641. https://doi.org/10.1021/acs.jpcc.5b03634

Aydin, S. (2007). A comparison of ghrelin, glucose, alpha-amylase and protein levels in saliva from diabetics. *BMB Reports*, *40*(1), 29–35.

Bakke, I., De Schryver, P., Boon, N., & Vadstein, O. (2011). PCR-based community structure studies of bacteria associated with eukaryotic organisms: a simple PCR strategy to avoid co-amplification of eukaryotic DNA. *Journal of Microbiological Methods*, *84*(2), 349–51. https://doi.org/10.1016/j.mimet.2010.12.015

Balachandran, U., Eror, N. G., & Mammone, R. (1982). Raman Spectra of Titanium

Dioxide. *Ournal of Solid State Chemistry*, *42*(3), 276–282.

Barnes, R. J., Molina, R., Xu, J., Dobson, P. J., & Thompson, I. P. (2013). Comparison of TiO2 and ZnO nanoparticles for photocatalytic degradation of methylene blue and the correlated inactivation of gram-positive and gram-negative bacteria. *Journal of Nanoparticle Research*, *15*(2). https://doi.org/10.1007/s11051-013-1432-9

Bartelt-Ryser, J., Joshi, J., Schmid, B., Brandl, H., & Balser, T. (2005). Feedbacks of plant diversity on soil microbial communities and subsequent plant growth. *Perspectives in Plant Ecology, Evolution, and Systematics*, *7*(1), 27–49. https://doi.org/http://dx.doi.org/10.1016/j.ppees.2004.11.002

Bellmann, S., Carlander, D., Fasano, A., Momcilovic, D., Scimeca, J. a, Waldman, W. J., … Lefebvre, D. E. (2015). Mammalian gastrointestinal tract parameters modulating the integrity, surface properties, and absorption of food-relevant nanomaterials. *Wiley Interdisciplinary Reviews: Nanomedicine and Nanobiotechnology*, *7*(5), 609–622. https://doi.org/10.1002/wnan.1333

Bentaleb, A., Ball, V., Haikel, Y., Voegel, J., & Schaaf, P. (1997). Kinetics of the homogeneous exchange of lysozyme adsorbed on a titanium oxide surface. *Langmuir*, *7463*(15), 729–735. https://doi.org/10.1021/la9605192

Bergin, I. L., & Witzmann, F. a. (2013). Nanoparticle toxicity by the gastrointestinal route: evidence and knowledge gaps. *International Journal of Biomedical Nanoscience and Nanotechnology*, *3*(1–2), 163–210. https://doi.org/10.1504/IJBNN.2013.054515

Bettini, S., Boutet-Robinet, E., Cartier, C., Coméra, C., Gaultier, E., Dupuy, J., … Bird, R. P. (2017). Food-grade TiO2 impairs intestinal and systemic immune homeostasis, initiates preneoplastic lesions and promotes aberrant crypt development in the rat colon. *Scientific Reports*, *7*(June 2016), 40373. https://doi.org/10.1038/srep40373

Böckmann, J., Lahl, H., Eckert, T., & Unterhalt, B. (2000). Titan-blutspiegel vor und nach belastungsversuchen mit titandioxid. *Pharmazie*, *55*(2), 140–143.

Bolger, M. B., Lukacova, V., & Woltosz, W. S. (2009). Simulations of the nonlinear dose dependence for substrates of influx and efflux transporters in the human intestine. *The AAPS Journal*. https://doi.org/10.1208/s12248-009-9111-6

Bonnet, M., Massard, C., Veisseire, P., & Camares, O. (2015). Environmental Toxicity and Antimicrobial Efficiency of Titanium Dioxide Nanoparticles in Suspension. *Journal of Biomaterials and Nanobiotechnology*, *6*(July), 213–224. https://doi.org/http://dx.doi.org/10.4236/jbnb.2015.63020

Bouwmeester, H., Brandhoff, P., Marvin, H. J. P., Weigel, S., & Peters, R. J. B. (2014). State of the safety assessment and current use of nanomaterials in food and food production. *Trends in Food Science & Technology*, *40*(2), 200–210. https://doi.org/10.1016/j.tifs.2014.08.009

Brandon, E. F. a, Bakker, M. I., Kramer, E., Bouwmeester, H., Zuidema, T., & Alewijn, M. (2014). Bioaccessibility of vitamin A, vitamin C and folic acid from dietary supplements, fortified food and infant formula. *International Journal of Food Sciences and Nutrition*, *65*(4), 426–35. https://doi.org/10.3109/09637486.2013.869795

Brayer, G. D., Luo, Y., & Withers, S. G. (1995). The structure of human pancreatic a-amylase at 1.8 A resolution and comparisons with related enzymes. *Protein Science*, *4*, 1730–1742. https://doi.org/10.1002/pro.5560040908

Brown, N. M. D., Hewitt, J. A., & Meenan, B. J. (1992). X-ray-induced beam damage observed during x-ray photoelectron spectroscopy (XPS) studies of palladium electrode ink materials. *Surface and Interface Analysis*, *18*(3), 187–198. https://doi.org/10.1002/sia.740180304

Brun, E., Barreau, F., Veronesi, G., Fayard, B., Sorieul, S., Chanéac, C., … Carrière, M. (2014). Titanium dioxide nanoparticle impact and translocation through ex vivo, in vivo and in vitro gut epithelia. *Particle and Fibre Toxicology*, *11*, 13. https://doi.org/10.1186/1743-8977-11-13

Bu, Q., Yan, G., Deng, P., Peng, F., Lin, H., Xu, Y., … Zhao, Y.-L. (2010). NMR-based metabonomic study of the sub-acute toxicity of titanium dioxide nanoparticles in rats after oral administration. *Nanotechnology*, *21*(12), 125105. https://doi.org/10.1088/0957-4484/21/12/125105

Bumbrah, G. S., & Sharma, R. M. (2016, June). Raman spectroscopy ??? Basic principle, instrumentation and selected applications for the characterization of drugs of abuse. *Egyptian Journal of Forensic Sciences*. Forensic Medicine Authority. https://doi.org/10.1016/j.ejfs.2015.06.001

Burdett, J. K., Hughbanks, T., Miller, G. J., Richardson, J. W., & Smith, J. V. (1987). Structural-electronic relationships in inorganic solids: powder neutron diffraction studies of the rutile and anatase polymorphs of titanium dioxide at 15 and 295 K. *Journal of the American Chemical Society*, *109*(12), 3639–3646. https://doi.org/10.1021/ja00246a021

Burneau, A., Humbert, B., Barrès, O., Gallas, J. P., & Lavalley, J. C. (1994). Fourier Transform Infrared and Raman Spectroscopic Study of Silica Surfaces. In *The Colloid Chemistry of Silica* (Vol. 234, pp. 200–222). American Chemical Society. https://doi.org/doi:10.1021/ba-1994-0234.ch01010.1021/ba-1994-0234.ch010

Busk, S. (2011). Nanostructured titanium dioxide: fate in the aquatic environment and effects on the marine mussel mytilus edulis.

Cabiscol, E., Tamarit, J., & Ros, J. (2000). Oxidative stress in bacteria and protein damage by reactive oxygen species. *International Microbiology*, *3*(1), 3–8. https://doi.org/10.2436/im.v3i1.9235

Carp, O. (2004). Photoinduced reactivity of titanium dioxide. *Progress in Solid State Chemistry*, *32*(1–2), 33–177. https://doi.org/10.1016/j.progsolidstchem.2004.08.001

Chaudhry, Q., Scotter, M., Blackburn, J., Ross, B., Boxall, A., Castle, L., … Watkins, R. (2008). Applications and implications of nanotechnologies for the food sector. *Food Additives & Contaminants. Part A, Chemistry, Analysis, Control, Exposure & Risk Assessment*, *25*(3), 241–58. https://doi.org/10.1080/02652030701744538

Chen, X. M., Elisia, I., & Kitts, D. D. (2010). Defining conditions for the co-culture of

Caco-2 and HT29-MTX cells using Taguchi design. *Journal of Pharmacological and Toxicological Methods*, *61*(3), 334–342. https://doi.org/10.1016/j.vascn.2010.02.004

Chen, Cheng, B., Yang, Y., Cao, A., & Liu, J. (2013). Characterization and preliminary toxicity assay of nano-titanium dioxide additive in sugar-coated chewing gum. *Small*, *9*(9–10), 1765–1774. https://doi.org/10.1002/smll.201201506

Cho, W.-S., Kang, B.-C., Lee, J. K., Jeong, J., Che, J.-H., & Seok, S. H. (2013). Comparative absorption, distribution, and excretion of titanium dioxide and zinc oxide nanoparticles after repeated oral administration. *Particle and Fibre Toxicology*, *10*(1), 9. https://doi.org/10.1186/1743-8977-10-9

Cole, J. R., Wang, Q., Fish, J. A., Chai, B., McGarrell, D. M., Sun, Y., … Tiedje, J. M. (2014). Ribosomal Database Project: Data and tools for high throughput rRNA analysis. *Nucleic Acids Research*, *42*(D1), 633–642. https://doi.org/10.1093/nar/gkt1244

Connor, P. A., & McQuillan, A. J. (1999). Phosphate adsorption onto TiO2 from aqueous solutions: an in situ internal reflection infrared spectroscopic study. *Langmuir*, *15*(8), 2916–2921. https://doi.org/10.1021/la980894p

Crater, J. S., & Carrier, R. L. (2010). Barrier Properties of Gastrointestinal Mucus to Nanoparticle Transport. *Macromolecular Bioscience*, *10*(12), 1473–1483. https://doi.org/10.1002/mabi.201000137

Cui, Y., Gong, X., Duan, Y., Li, N., Hu, R., Liu, H., … Hong, F. (2010). Hepatocyte apoptosis and its molecular mechanisms in mice caused by titanium dioxide nanoparticles. *Journal of Hazardous Materials*, *183*(1–3), 874–880. https://doi.org/10.1016/j.jhazmat.2010.07.109

Cui, Y., Liu, H., Zhou, M., Duan, Y., Li, N., Gong, X., … Hong, F. (2011). Signaling pathway of inflammatory responses in the mouse liver caused by TiO2 nanoparticles. *Journal of Biomedical Materials Research - Part A*, *96 A*(1), 221–229. https://doi.org/10.1002/jbm.a.32976

Dalibart, M., & Servant, L. (2000). Spectroscopie dans l'infrarouge. *Techniques de L'ingénieur*, *33*, 26.

Das, P., McDonald, J. A., Petrol, E. O., Allen-Vercoe, E., & Walker, V. K. (2014). Nanosilver-Mediated Change in Human Intestinal Microbiota. *Journal of Nanomedicine & Nanotechnology*, *5*(5), 1000235. https://doi.org/10.4172/2157-7439.1000235

Das, P., Petrof, E., & Walker, V. (2015). Perturbation of a Human Gut Ecosystem by Silver Chloride Colloids. *Journal of Environmental & …*, *5*(4). https://doi.org/10.4172/2161-0525.1000294

De La Pierre, M., Carteret, C., Maschio, L., André, E., Orlando, R., & Dovesi, R. (2014). The Raman spectrum of CaCO3 polymorphs calcite and aragonite: a combined experimental and computational study. *The Journal of Chemical Physics*, *140*(16), 164509. https://doi.org/10.1063/1.4871900

Delpuech, N., Mazouzi, D., Dupré, N., Moreau, P., Cerbelaud, M., Bridel, J. S., … Humbert, B. (2014). Critical Role of Silicon Nanoparticles Surface on Lithium Cell

Electrochemical Performance Analyzed by FTIR, Raman, EELS, XPS, NMR, and BDS Spectroscopies. *The Journal of Physical Chemistry C*, *118*(31), 17318–17331. https://doi.org/10.1021/jp503949y

DeSantis, T. Z., Hugenholtz, P., Larsen, N., Rojas, M., Brodie, E. L., Keller, K., … Andersen, G. L. (2006). Greengenes, a chimera-checked 16S rRNA gene database and workbench compatible with ARB. *Applied and Environmental Microbiology*, *72*(7), 5069–72. https://doi.org/10.1128/AEM.03006-05

des Rieux, A., Fievez, V., Théate, I., Mast, J., Préat, V., & Schneider, Y. J. (2007). An improved in vitro model of human intestinal follicle-associated epithelium to study nanoparticle transport by M cells. *European Journal of Pharmaceutical Sciences*, *30*(5), 380–391. https://doi.org/10.1016/j.ejps.2006.12.006

des Rieux, A., Ragnarsson, E. G. E., Gullberg, E., Préat, V., Schneider, Y.-J., & Artursson, P. (2005). Transport of nanoparticles across an in vitro model of the human intestinal follicle associated epithelium. *European Journal of Pharmaceutical Sciences : Official Journal of the European Federation for Pharmaceutical Sciences*, *25*(4–5), 455–65. https://doi.org/10.1016/j.ejps.2005.04.015

Diebold, U. (2003). The surface science of titanium dioxide. *Surface Science Reports*, *48*(5), 53–229. https://doi.org/10.1016/S0167-5729(02)00100-0

Dodds, M. W. J., Johnson, D. a, & Yeh, C.-K. (2005). Health benefits of saliva: a review. *Journal of Dentistry*, *33*(3), 223–33. https://doi.org/10.1016/j.jdent.2004.10.009

Domènech, B., Bastos-Arrieta, J., Alonso, A., Macanás, J., Muñoz, M., & Muraviev, D. N. (2012). Bifunctional Polymer-Metal Nanocomposite Ion Exchange Materials. *Ion Exchange Technologies*, 35–72. https://doi.org/http://dx.doi.org/10.5772/51579

Domingos, R., Peyrot, C., & Wilkinson, K. (2010). Aggregation of titanium dioxide nanoparticles: role of calcium and phosphate. *Environmental Chemistry*, *7*(1), 61. https://doi.org/10.1071/EN09110

Donato, R. P., El-Merhibi, A., Gundsambuu, B., Mak, K. Y., Formosa, E. R., Wang, X., … Powell, B. C. (2011). Studying permeability in a commonly used epithelial cell line: T84 intestinal epithelial cells. *Methods in Molecular Biology*, *763*, 115–137. https://doi.org/10.1007/978-1-61779-191-8_8

Duan, Y., Liu, J., Ma, L., Li, N., Liu, H., Wang, J., … Hong, F. (2010). Toxicological characteristics of nanoparticulate anatase titanium dioxide in mice. *Biomaterials*, *31*(5), 894–899. https://doi.org/10.1016/j.biomaterials.2009.10.003

Dudefoi, W., Terrisse, H., Richard-Plouet, M., Gautron, E., Popa, F., Humbert, B., & Ropers, M.-H. (2017). Criteria to define a more relevant reference sample of titanium dioxide in the context of food: a multiscale approach. *Food Additives & Contaminants: Part A*, *0*(ja), null. https://doi.org/10.1080/19440049.2017.1284346

Dutta, P. K., Ginwalla, A., Hogg, B., Patton, B. R., Chwieroth, B., Liang, Z., … Akbar, S. (1999). Interaction of Carbon Monoxide with Anatase Surfaces at High Temperatures: Optimization of a Carbon Monoxide Sensor. *The Journal of Physical*

Chemistry B, *103*(21), 4412–4422. https://doi.org/10.1021/jp9844718

Dziemiańczyk, D., Grabowska, S., & Balicki, R. (2005). Evaluation of secretory mucin concentration of patients with squamous cell carcinoma oral cavity. *Rocz Akad Med Bialymst*, *50*, 334–338.

Eckburg, P. B., Bik, E. M., Bernstein, C. N., Purdom, E., Dethlefsen, L., Sargent, M., … Relman, D. A. (2014). Diversity of the Human Intestinal Microbial Flora. *Science*, *1635*(2005), 1635–1638. https://doi.org/10.1126/science.1110591

EFSA. (2004). *Opinion of the Scientific Panel on Food Additives, Flavourings, Processing Aids and materials in Contact with Food on a request from the Commission related to the safety in use of rutile titanium dioxide as an alternative to the presently permitted anatas*. *The EFSA Journal* (Vol. 163).

EFSA. (2011). Guidance on the risk assessment of the application of nanoscience and nanotechnologies in the food and feed chain. *EFSA Journal*, *9*(February), 1–36. https://doi.org/10.2903/j.efsa.2011.2140.

EFSA. (2016). Re-evaluation of titanium dioxide (E 171) as a food additive. *EFSA Journal*, *14*(9), e04545. https://doi.org/10.2903/j.efsa.2016.4545

EU. (2011). *Commission Recommendation of 18 October 2011 On The Definition of Nanomaterial (2011/696/EU)*. *Official Journal of the European Union*.

Fabian, E., Landsiedel, R., Ma-Hock, L., Wiench, K., Wohlleben, W., & van Ravenzwaay, B. (2008). Tissue distribution and toxicity of intravenously administered titanium dioxide nanoparticles in rats. *Archives of Toxicology*, *82*(3), 151–7. https://doi.org/10.1007/s00204-007-0253-y

Fan, L., McElroy, K., & Thomas, T. (2012). Reconstruction of ribosomal RNA genes from metagenomic data. *PloS One*, *7*(6), e39948. https://doi.org/10.1371/journal.pone.0039948

Faust, J. J., Doudrick, K., Yang, Y., Capco, D. G., & Westerhoff, P. (2016). A Facile Method for Separating and Enriching Nano and Submicron Particles from Titanium Dioxide Found in Food and Pharmaceutical Products. *PLOS ONE*, *11*(10), e0164712. https://doi.org/10.1371/journal.pone.0164712

Faust, J. J., Doudrick, K., Yang, Y., Westerhoff, P., & Capco, D. G. (2014). Food grade titanium dioxide disrupts intestinal brush border microvilli in vitro independent of sedimentation. *Cell Biology and Toxicology*, *30*(3), 169–188. https://doi.org/10.1007/s10565-014-9278-1

Federal Register. (1966). *Color additives. Washington (DC), USA: Federal Register, Title 21. 31:1065*.

Frank, D. N., St Amand, A. L., Feldman, R. A., Boedeker, E. C., Harpaz, N., & Pace, N. R. (2007). Molecular-phylogenetic characterization of microbial community imbalances in human inflammatory bowel diseases. *Proceedings of the National Academy of Sciences of the United States of America*, *104*(34), 13780–5. https://doi.org/10.1073/pnas.0706625104

French, R. a., Jacobson, A. R., Kim, B., Isley, S. L., Penn, R. L. E. E., & Baveye, P. C. (2009). Influence of ionic strength, pH, andcation valence on aggregation kinetics of titanium dioxide nanoparticles. *Environmental Science and Technology*, *43*(5),

1354–1359. https://doi.org/10.1021/es802628n

Fröhlich, E. E., & Fröhlich, E. (2016, January). Cytotoxicity of nanoparticles contained in food on intestinal cells and the gut microbiota. *International Journal of Molecular Sciences*. https://doi.org/10.3390/ijms17040509

Fröhlich, E., & Roblegg, E. (2016). Oral uptake of nanoparticles: human relevance and the role of in vitro systems. *Archives of Toxicology*. Springer Berlin Heidelberg. https://doi.org/10.1007/s00204-016-1765-0

Future Markets Inc. (2013). *The Global Market for Metal Oxide Nanoparticles to 2020*.

Gao, Y., Masuda, Y., & Koumoto, K. (2004). Light-Excited Superhydrophilicity of Amorphous TiO2 Thin Films Deposited in an Aqueous Peroxotitanate Solution. *Langmuir*, *20*(8), 3188–3194. https://doi.org/10.1021/la0303207

Giacomelli, C. E., Avena, M. J., & De Pauli, C. P. (1997). Adsorption of Bovine Serum Albumin onto TiO 2 Particles. *Journal of Colloid and Interface Science*, *188*(188), 387–395. https://doi.org/10.1006/jcis.1996.4750

Gitrowski, C., Al-Jubory, A. R., & Handy, R. D. (2014). Uptake of different crystal structures of TiO_2 nanoparticles by Caco-2 intestinal cells. *Toxicology Letters*, *226*(3), 264–76. https://doi.org/10.1016/j.toxlet.2014.02.014

Gnoth, M. J., Kunz, C., Kinne-Saffran, E., & Rudloff, S. (2000). Human milk oligosaccharides are minimally digested in vitro. *The Journal of Nutrition*, *130*(12), 3014–20.

Gong, W. (2001). A real time in situ ATR-FTIR spectroscopic study of linear phosphate adsorption on titania surfaces. *International Journal of Mineral Processing*, *63*(3), 147–165. https://doi.org/10.1016/S0301-7516(01)00045-X

Guduru, D., Niepel, M., Vogel, J., & Groth, T. (2011). Nanostructured material surfaces-preparation, effect on cellular behavior, and potential biomedical applications: A review. *International Journal of Artificial Organs*, *34*(10), 963–985. https://doi.org/10.5301/ijao.5000012

Guhmann, M., Thommes, M., Gerber, F., Pöllinger, N., Klein, S., Breitkreutz, J., & Weitschies, W. (2013). Design of biorelevant test setups for the prediction of diclofenac in vivo features after oral administration. *Pharmaceutical Research*, *30*(6), 1483–1501. https://doi.org/10.1007/s11095-013-0974-y

Gui, S., Sang, X., Zheng, L., Ze, Y., Zhao, X., Sheng, L., … Tang, M. (2013). Intragastric exposure to titanium dioxide nanoparticles induced nephrotoxicity in mice, assessed by physiological and gene expression modifications. *Part Fibre Toxicol*, *10*(1), 4. https://doi.org/10.1186/1743-8977-10-4

Guiot, C., & Spalla, O. (2013). Stabilization of TiO2 nanoparticles in complex medium through a pH adjustment protocol. *Environmental Science and Technology*, *47*(2), 1057–1064. https://doi.org/10.1021/es3040736

Gupta, S. M., & Tripathi, M. (2012). A review on the synthesis of TiO2 nanoparticles by solution route. *Central European Journal of Chemistry*, *10*(2), 279–294. https://doi.org/10.2478/s11532-011-0155-y

Hagens, W. I., Oomen, A. G., de Jong, W. H., Cassee, F. R., & Sips, A. J. a M. (2007). What do we (need to) know about the kinetic properties of nanoparticles in the body? *Regulatory Toxicology and Pharmacology : RTP*, *49*(3), 217–29. https://doi.org/10.1016/j.yrtph.2007.07.006

Hannig, M., & Hannig, C. (2010). Nanomaterials in preventive dentistry. *Nature Nanotechnology*, *5*(8), 565–569. https://doi.org/10.1038/nnano.2010.83

Haruta, M. (1997). Size- and support-dependency in the catalysis of gold. *Catalysis Today*, *36*(1), 153–166. https://doi.org/10.1016/S0920-5861(96)00208-8

He, B. B., Preckwinkel, U., & Smith, K. L. (1999). Fundamentals of Two-Dimensional X-ray Diffraction (XRD2). *Advances in X-Ray Analysis*, *43*(c), 273–280. https://doi.org/http://dx.doi.org/10.1154/1.1577355

Higashisaka, K., Yoshioka, Y., & Tsutsumi, Y. (2015). Applications and Safety of Nanomaterials Used in the Food Industry. *Food Safety*, *3*(2), 39–47. https://doi.org/10.14252/foodsafetyfscj.2015005

Hu, R., Gong, X., Duan, Y., Li, N., Che, Y., Cui, Y., … Hong, F. (2010). Neurotoxicological effects and the impairment of spatial recognition memory in mice caused by exposure to TiO2 nanoparticles. *Biomaterials*, *31*(31), 8043–8050. https://doi.org/10.1016/j.biomaterials.2010.07.011

Humbert, B., Carteret, C., Burneau, A., & Gallas, J. P. (2006). Fourier Transform Infrared and Raman Spectroscopic Study of Silica Surfaces. In *Colloidal Silica* (pp. 295–310). CRC Press. https://doi.org/doi:10.1201/9781420028706.ch26

Iler, R. K. (1979). The Chemistry of Silica. *Wiley and Sons, New York*.

Jamei, M., Turner, D., Yang, J., Neuhoff, S., Polak, S., Rostami-Hodjegan, A., & Tucker, G. (2009). Population-based mechanistic prediction of oral drug absorption. *The AAPS Journal*, *11*(2), 225–237. https://doi.org/10.1208/s12248-009-9099-y

Janer, G., Mas del Molino, E., Fernández-Rosas, E., Fernández, a, & Vázquez-Campos, S. (2014). Cell uptake and oral absorption of titanium dioxide nanoparticles. *Toxicology Letters*, *228*(2), 103–10. https://doi.org/10.1016/j.toxlet.2014.04.014

Jani, P., Halbert, G. W., Langridge, J., & Florence, A. T. (1989). The Uptake and Translocation of Latex Nanospheres and Microspheres after Oral Administration to Rats. *Journal of Pharmacy and Pharmacology*, *41*(12), 809–812. https://doi.org/10.1111/j.2042-7158.1989.tb06377.x

Jellison, G. E., Boatner, L. a., Budai, J. D., Jeong, B.-S., & Norton, D. P. (2003). Spectroscopic ellipsometry of thin film and bulk anatase (TiO[sub 2]). *Journal of Applied Physics*, *93*(12), 9537–9541. https://doi.org/10.1063/1.1573737

Ji, Z., Jin, X., George, S., Xia, T., Meng, H., Wang, X., … Zink, J. I. (2010). Dispersion and stability optimization of TiO2 nanoparticles in cell culture media. *Environmental Science & Technology*, *44*(19), 7309–14. https://doi.org/10.1021/es100417s

Joint FAO/ WHO Expert Committee on Food Additives. (2010). Compendium of Food Additive Specifications - 73rd Meeting 2010. *FAO JECFA Monographs*, (10). https://doi.org/http://www.fao.org/docrep/013/i1782e/i1782e.pdf

Jones, K., Morton, J., Smith, I., Jurkschat, K., Harding, A.-H., & Evans, G. (2015). Human in vivo and in vitro studies on gastrointestinal absorption of titanium dioxide

nanoparticles. *Toxicology Letters*, *233*(2), 95–101. https://doi.org/10.1016/j.toxlet.2014.12.005

Jovanović, B. (2015). Critical review of public health regulations of titanium dioxide, a human food additive. *Integrated Environmental Assessment and Management*, *11*(1), 10–20. https://doi.org/10.1002/ieam.1571

Júnior, J. A. A., & Baldo, J. B. (2014). The Behavior of Zeta Potential of Silica Suspensions. *New Journal of Glass and Ceramics*, *4*, 29–37. https://doi.org/http://dx.doi.org/10.4236/njgc.2014.42004

Kathiravan, A., Jhonsi, M., & Renganathan, R. (2011). Photoinduced interaction of colloidal TiO2 nanoparticles with lysozyme: Evidences from spectroscopic studies. *Journal of Luminescence*, *131*(9), 1975–1981. https://doi.org/10.1016/j.jlumin.2011.04.004

Kathiravan, A., & Renganathan, R. (2008). Interaction of colloidal TiO2 with bovine serum albumin : A fluorescence quenching study. *Colloids and Surfaces A : Physicochemical and Engineering Aspects*, *324*, 176–180. https://doi.org/10.1016/j.colsurfa.2008.04.017

Kim, H. J., Huh, D., Hamilton, G., & Ingber, D. E. (2012). Human gut-on-a-chip inhabited by microbial flora that experiences intestinal peristalsis-like motions and flow. *Lab on a Chip*, *12*(12), 2165–74. https://doi.org/10.1039/c2lc40074j

Kim, J. S., Mitchell, S., Kijek, P., Tsume, Y., Hilfinger, J., & Amidon, G. L. (2006). The suitability of an in situ perfusion model for permeability determinations: Utility for BCS class I biowaiver requests. *Molecular Pharmaceutics*, *3*(6), 686–694. https://doi.org/10.1021/mp060042f

Koelsch, M., Cassaignon, S., Ta Thanh Minh, C., Guillemoles, J. F., & Jolivet, J. P. (2004). Electrochemical comparative study of titania (anatase, brookite and rutile) nanoparticles synthesized in aqueous medium. In *Thin Solid Films* (Vol. 451–452, pp. 86–92). https://doi.org/10.1016/j.tsf.2003.11.150

Koeneman, B. a, Zhang, Y., Westerhoff, P., Chen, Y., Crittenden, J. C., & Capco, D. G. (2010). Toxicity and cellular responses of intestinal cells exposed to titanium dioxide. *Cell Biology and Toxicology*, *26*(3), 225–38. https://doi.org/10.1007/s10565-009-9132-z

Kosmulski, M. (2009). Compilation of PZC and IEP of sparingly soluble metal oxides and hydroxides from literature. *Advances in Colloid and Interface Science*, *152*(1–2), 14–25. https://doi.org/10.1016/j.cis.2009.08.003

Kumar, N., Palmer, G. R., Shah, V., & Walker, V. K. (2014). The effect of silver nanoparticles on seasonal change in arctic tundra bacterial and fungal assemblages. *PLoS ONE*, *9*(6), e99953. https://doi.org/10.1371/journal.pone.0099953

Kunitsky, C. (2006). Identification of microorganisms using fatty acid methyl ester (FAME) analysis and the MIDI Sherlock Microbial Identification System. *Encyclopedia of Rapid Microbiological Methods*, 1–18.

Le, Q.-C. (2014). *Caractérisation des interactions entre le dioxyde de titane et des phospholipides en milieu aqueux*. *École Doctorale 3MPL Matière, Molécules, Matériaux en Pays de Loire*. University of Nantes (France).

Le, Q.-C., Ropers, M.-H., Terrisse, H., & Humbert, B. (2014). Interactions between phospholipids and titanium dioxide particles. *Colloids and Surfaces. B, Biointerfaces*, *123*, 150–7. https://doi.org/10.1016/j.colsurfb.2014.09.010

Lee, H.-Y., Chai, L.-C., Tang, S.-Y., Jinap, S., Ghazali, F. M., Nakaguchi, Y., … Son, R. (2009). Application of MPN-PCR in biosafety of Bacillus cereus s.l. for ready-to-eat cereals. *Food Control*, *20*(11), 1068–1071. https://doi.org/10.1016/j.foodcont.2009.01.009

Lefebvre, D. E., Venema, K., Gombau, L., Valerio, L. G., Raju, J., Bondy, G. S., … Stone, V. (2015). Utility of models of the gastrointestinal tract for assessment of the digestion and absorption of engineered nanomaterials released from food matrices. *Nanotoxicology*, *9*(4), 523–42. https://doi.org/10.3109/17435390.2014.948091

Lennernas, H., Lee, I.-D., Fagerholm, U., & Amidon, G. L. (1997). A Residence-Time Distribution Analysis of the Hydrodynamics within the Intestine in Man during a Regional Single-pass Perfusion with Loc-I-Gut: In-vivo Permeability Estimation. *J. Pharm. Pharmacol.*, *49*, 682–686. https://doi.org/10.1111/j.2042-7158.1997.tb06092.x

Ley, R. E., Peterson, D. a, & Gordon, J. I. (2006). Ecological and evolutionary forces shaping microbial diversity in the human intestine. *Cell*, *124*(4), 837–48. https://doi.org/10.1016/j.cell.2006.02.017

Linnankoski, J., Ranta, V. P., Yliperttula, M., & Urtti, A. (2008). Passive oral drug absorption can be predicted more reliably by experimental than computational models - Fact or myth. *European Journal of Pharmaceutical Sciences*, *34*(2–3), 129–139. https://doi.org/10.1016/j.ejps.2008.03.001

Liu, L. Y., Sun, L., Zhong, Z. T., Zhu, J., & Song, H. Y. (2016). Effects of titanium dioxide nanoparticles on intestinal commensal bacteria. *Nuclear Science and Techniques*, *27*(1), 1–5. https://doi.org/10.1007/s41365-016-0011-z

Liu, W., Sun, W., Borthwick, A. G. L., & Ni, J. (2013). Comparison on aggregation and sedimentation of titanium dioxide, titanate nanotubes and titanate nanotubes-TiO2: Influence of pH, ionic strength and natural organic matter. *Colloids and Surfaces A: Physicochemical and Engineering Aspects*, *434*, 319–328. https://doi.org/10.1016/j.colsurfa.2013.05.010

Logothetis, E., & Kaiser, W. (1983). TiO2 film oxygen sensors made by chemical vapour deposition from organometallics. *Sensors and Actuators*, *4*, 333–340. https://doi.org/10.1016/0250-6874(83)85041-0

Lomer, M. C. E., Thompson, R. P. H., & Powell, J. J. (2002). Fine and ultrafine particles of the diet: influence on the mucosal immune response and association with Crohn's disease. *The Proceedings of the Nutrition Society*, *61*(1), 123–130. https://doi.org/10.1079/PNS2001134

Lomer, M. C. E., Thompson, R. R. P. H., Commisso, J., Keen, C. L., & Powell, J. J. (2000). Determination of titanium dioxide in foods using inductively coupled plasma

optical emission spectrometry. *Analyst*, *125*(12), 2339–2343. https://doi.org/10.1039/b006285p

Lori, J. a, & Nok, a J. (2004). Mechanism of adsorption of mucin to titanium in vitro. *Bio-Medical Materials and Engineering*, *14*(4), 557–563.

MacNicoll, A., Kelly, M., Aksoy, H., Kramer, E., Bouwmeester, H., & Chaudhry, Q. (2015). A study of the uptake and biodistribution of nano-titanium dioxide using in vitro and in vivo models of oral intake. *Journal of Nanoparticle Research*, *17*(2), 66. https://doi.org/10.1007/s11051-015-2862-3

Maitz, M. F., Tsyganov, I., Pham, M.-T., & Wieser, E. (2003). Blood compatibility of titanium oxides with various crystal structure and element doping. *J Biomater Appl*, *17*(4), 303–320. https://doi.org/10.1177/088532803033178

Marano, F., & Guadagnini, R. (2012). Cellular Mechanisms of Nanoparticle's Toxicity. *Encyclopedia of Nanotechnology*, (dc). https://doi.org/10.1007/978-90-481-9751-4

Marchesi, J. R., Adams, D. H., Fava, F., Hermes, G. D. a, Hirschfield, G. M., Hold, G., … Hart, A. (2015). The gut microbiota and host health: a new clinical frontier. *Gut*, *65*, 330_339. https://doi.org/10.1136/gutjnl-2015-309990

Martirosyan, A., Polet, M., Bazes, A., & Sergent, T. (2012). Food Nanoparticles and Intestinal Inflammation : A Real Risk ? *INTECH Open Access Publisher.*, *2*(iv). https://doi.org/http://dx.doi.org/10.5772/52887 3

Martra, G. (2000). Lewis acid and base sites at the surface of microcrystalline TiO2 anatase: relationships between surface morphology and chemical behaviour. *Applied Catalysis a-General*, *200*(1–2), 275–285. https://doi.org/10.1016/s0926-860x(00)00641-4

Mass, E., Gadoth, N., Harell, D., & Wolff, A. (2002). Can salivary composition and high flow rate explain the low caries rate in children with familial dysautonomia? *Pediat Dent*, *24*(6), 581–586.

Maurer-Jones, M. A., Gunsolus, I. L., Murphy, C. J., & Haynes, C. L. (2013). Toxicity of engineered nanoparticles in the environment. *Analytical Chemistry*, *85*(6), 3036–3049. https://doi.org/10.1021/ac303636s

Mazza, T., Barborini, E., Piseri, P., Milani, P., Cattaneo, D., Bassi, A. L., … Ducati, C. (2007). Raman spectroscopy characterization of TiO2 rutile nanocrystals. *Physical Review B*, *75*(45416), 1–5. https://doi.org/10.1103/PhysRevB.75.045416

McAllister, M. (2010). Dynamic dissolution: A step closer to predictive dissolution testing? *Molecular Pharmaceutics*. https://doi.org/10.1021/mp1001203

McCracken, C., Dutta, P. K., & Waldman, W. J. (2016). Critical assessment of toxicological effects of ingested nanoparticles. *Environmental Science: Nano*, *3*(2), 256–282. https://doi.org/10.1039/c5en00242g

McDonald, J. a K., Schroeter, K., Fuentes, S., Heikamp-Dejong, I., Khursigara, C. M., de Vos, W. M., & Allen-Vercoe, E. (2013). Evaluation of microbial community reproducibility, stability and composition in a human distal gut chemostat model.

Journal of Microbiological Methods, *95*(2), 167–74. https://doi.org/10.1016/j.mimet.2013.08.008

Mercier-Bonin, M., Despax, B., Raynaud, P., Houdeau, E., & Thomas, M. (2016). Exposition orale et devenir dans l'intestin des nanoparticules alimentaires: exemple de l'argent et du dioxyde de titane. *Cahiers de Nutrition et de Dietetique*, *51*(4), 195–203. https://doi.org/10.1016/j.cnd.2016.03.001

Minekus, M., Alminger, M., Alvito, P., Ballance, S., Bohn, T., Bourlieu, C., … Brodkorb, a. (2014). A standardised static in vitro digestion method suitable for food - an international consensus. *Food & Function*, *5*(6), 1113–24. https://doi.org/10.1039/c3fo60702j

Minekus, M., Smeets-Peeters, M., Bernalier, A., Marol-Bonnin, S., Havenaar, R., Marteau, P., … Huis in't Veld, J. H. (1999). A computer-controlled system to simulate conditions of the large intestine with peristaltic mixing, water absorption and absorption of fermentation products. *Applied Microbiology and Biotechnology*, *53*(1), 108–114. https://doi.org/10.1007/s002530051622

Moda, T. L., & Andricopulo, A. D. (2012). Consensus hologram QSAR modeling for the prediction of human intestinal absorption. *Bioorg Med Chem Lett*, *22*(8), 2889–2893. https://doi.org/10.1016/j.bmcl.2012.02.061

Moellmann, J., Ehrlich, S., Tonner, R., & Grimme, S. (2012). A DFT-D study of structural and energetic properties of TiO2 modifications. *Journal of Physics. Condensed Matter : An Institute of Physics Journal*, *24*(42), 424206. https://doi.org/10.1088/0953-8984/24/42/424206

Motzkus, C., Macé, T., Vaslin-Reimann, S., Ausset, P., & Maillé, M. (2013). Characterization of manufactured TiO2 nanoparticles. *Journal of Physics: Conference Series*, *429*, 12012. https://doi.org/10.1088/1742-6596/429/1/012012

Moulder, J. F., Stickle, W. F., Sobol, P. E., & Bomben, K. D. (1992). *Handbook of X-ray Photoelectron Spectroscopy*. Eden-Prairie MN: Perkin-Elmer Corp.

Murdock, R. C., Braydich-Stolle, L., Schrand, A. M., Schlager, J. J., & Hussain, S. M. (2008). Characterization of nanomaterial dispersion in solution prior to in vitro exposure using dynamic light scattering technique. *Toxicological Sciences : An Official Journal of the Society of Toxicology*, *101*(2), 239–53. https://doi.org/10.1093/toxsci/kfm240

Myers, R. M., Fischer, S. G., Maniatis, T., & Lerman, L. S. (1985). Modification of the melting properties of duplex DNA by attachment of a GC-rich DNA sequence as determined by denaturing gradient gel electrophoresis. *Nucleic Acids Research*, *13*(9), 3111–3129. https://doi.org/10.1093/nar/13.9.3111

Nater, U. M., Rohleder, N., Gaab, J., Berger, S., Jud, A., Kirschbaum, C., & Ehlert, U. (2005). Human salivary alpha-amylase reactivity in a psychosocial stress paradigm. *International Journal of Psychophysiology : Official Journal of the International Organization of Psychophysiology*, *55*(3), 333–42. https://doi.org/10.1016/j.ijpsycho.2004.09.009

Nel, A. (2007). Toxic Potential of Materials. *Science*, *311*(5726), 622–627. https://doi.org/10.1126/science.1114397

Nel, A., Mädler, L., Velegol, D., Xia, T., Hoek, E. M. V, Somasundaran, P., … Thompson, M. (2009). Understanding biophysicochemical interactions at the nano-bio interface. *Nature Materials*, *8*(7), 543–557. https://doi.org/10.1038/nmat2442

NIST. (2012). Standard Reference Material 1898, Titanium dioxide nanomaterial. *National Institute of Standards & Technology*.

Nogueira, C. M., de Azevedo, W. M., Dagli, M. L. Z., Toma, S. H., Leite, A. Z. D. A., Lordello, M. L., … Sipahi, A. M. (2012). Titanium dioxide induced inflammation in the small intestine. *World Journal of Gastroenterology : WJG*, *18*(34), 4729–35. https://doi.org/10.3748/wjg.v18.i34.4729

Oberdörster, G., Oberdörster, E., & Oberdörster, J. (2005). Nanotoxicology: An Emerging Discipline Evolving from Studies of Ultrafine Particles. *Environmental Health Perspectives*, *113*(7), 823–839. https://doi.org/10.1289/ehp.7339

OECD. (2009). OECD Working Party On Manufactured Nanomaterials. *OECD Working Party On Manufactured NanomaterialsBackground Document*.

OECD. (2010). *Toxicokinetics. OECD Guideline for the testing of chemicals Section 4:417*. *OECD Guidline for the Testing of Chemicals*.

OECD. (2014). Report of the OECD Expert meeting on the Pysical Chemical Properties of Manufactured Nanomaterials and Test Guidelines. *ENV/JM/MONO(2014)15*, (41).

OECD. (2015). *DOSSIER ON TITANIUM DIOXIDE -PART 1 -NM 105 ANNEX 8 Series on the Safety of Manufactured Nanomaterials No. 54*.

Ohno, T., Sarukawa, K., Tokieda, K., & Matsumura, M. (2001). Morphology of a TiO2 Photocatalyst (Degussa, P-25) Consisting of Anatase and Rutile Crystalline Phases. *Journal of Catalysis*, *203*(1), 82–86. https://doi.org/10.1006/jcat.2001.3316

Ohsaka, T., Izumi, F., & Fujiki, Y. (1978). Raman spectrum of anatase, TiO2. *Journal of Raman Spectroscopy*, *7*(6), 321–324.

Ohtani, B., Prieto-Mahaney, O. O., Li, D., & Abe, R. (2010). What is Degussa (Evonic) P25? Crystalline composition analysis, reconstruction from isolated pure particles and photocatalytic activity test. *Journal of Photochemistry and Photobiology A: Chemistry*, *216*(2–3), 179–182. https://doi.org/10.1016/j.jphotochem.2010.07.024

Orts-Gil, G., Natte, K., & Österle, W. (2013). Multi-parametric reference nanomaterials for toxicology: state of the art, future challenges and potential candidates. *RSC Advances*, *3*(40), 18202. https://doi.org/10.1039/c3ra42112k

Othman, S. H., Abdul Rashid, S., Mohd Ghazi, T. I., & Abdullah, N. (2012). Dispersion and stabilization of photocatalytic TiO2 nanoparticles in aqueous suspension for coatings applications. *Journal of Nanomaterials*, *2012*, 1–10. https://doi.org/10.1155/2012/718214

Park, E.-J., Lee, G.-H., Yoon, C., Kang, M.-S., Kim, S. N., Cho, M.-H., … Kim, D.-W. (2014). Time-dependent bioaccumulation of distinct rod-type TiO2 nanoparticles: comparison by crystalline phase. *Journal of Applied Toxicology : JAT*, *34*(11),

1265–70. https://doi.org/10.1002/jat.3006

Passalacqua, K. D., Varadarajan, A., Ondov, B. D., Okou, D. T., Zwick, M. E., & Bergman, N. H. (2009). Structure and complexity of a bacterial transcriptome. *Journal of Bacteriology*, *191*(10), 3203–11. https://doi.org/10.1128/JB.00122-09

Payment, S. a., Liu, B., Offner, G. D., Oppenheim, F. G., & Troxler, R. F. (2000). Immunoquantification of Human Salivary Mucins MG1 and MG2 in Stimulated whole Saliva: Factors Influencing Mucin levels. *Journal of Dental Research*, *79*(10), 1765–1772. https://doi.org/10.1177/00220345000790100601

Pele, L. C., Thoree, V., Bruggraber, S. F. a, Koller, D., Thompson, R. P. H., Lomer, M. C., & Powell, J. J. (2015). Pharmaceutical/food grade titanium dioxide particles are absorbed into the bloodstream of human volunteers. *Particle and Fibre Toxicology*, *12*(1), 1–6. https://doi.org/10.1186/s12989-015-0101-9

Peters, R. J. B., van Bemmel, G., Herrera-Rivera, Z., Helsper, H. P. F. G., Hans, H. J. P., Weigel, S., … Bouwmeester, H. (2014). Characterisation of titanium dioxide nanoparticles in food products : Analytical methods to define nanoparticles. *Journal of Agricultural and Food Chemistry*, *62*, 6285–6293. https://doi.org/10.1021/jf5011885

Peters, R., Kramer, E., Oomen, A. G., Herrera Rivera, Z. E., Oegema, G., Tromp, P. C., … Bouwmeester, H. (2012). Presence of nano-sized silica during in vitro digestion of foods containing silica as a food additive. *ACS Nano*, *6*(3), 2441–2451. https://doi.org/10.1021/nn204728k

Petrof, E. O., Gloor, G. B., Vanner, S. J., Weese, S. J., Carter, D., Daigneault, M. C., … Allen-Vercoe, E. (2013). Stool substitute transplant therapy for the eradication of Clostridium difficile infection: “RePOOPulating” the gut. *Microbiome*, *1*(1), 3. https://doi.org/10.1186/2049-2618-1-3

Piccinno, F., Gottschalk, F., Seeger, S., & Nowack, B. (2012). Industrial production quantities and uses of ten engineered nanomaterials in Europe and the world. *Journal of Nanoparticle Research*, *14*(9), 1109. https://doi.org/10.1007/s11051-012-1109-9

Pietroiusti, A. (2012). Health implications of engineered nanomaterials. *Nanoscale*, *4*(4), 1231–47. https://doi.org/10.1039/c2nr11688j

Pietroiusti, A., Magrini, A., & Campagnolo, L. (2016). New frontiers in nanotoxicology: Gut microbiota/microbiome-mediated effects of engineered nanomaterials. *Toxicology and Applied Pharmacology*, *299*, 90–95. https://doi.org/10.1016/j.taap.2015.12.017

Powell, J. J., Faria, N., Thomas-McKay, E., & Pele, L. C. (2010). Origin and fate of dietary nanoparticles and microparticles in the gastrointestinal tract. *Journal of Autoimmunity*, *34*(3), J226-33. https://doi.org/10.1016/j.jaut.2009.11.006

Prieto, P., Hoffmann, S., Tirelli, V., Tancredi, F., González, I., Bermejo, M., & De Angelis, I. (2010). An exploratory study of two Caco-2 cell models for oral absorption: A report on their within-laboratory and between-laboratory variability, and their predictive capacity. *ATLA Alternatives to Laboratory Animals*, *38*(5), 367–386.

Raman, C. V., & Krishnan, K. S. (1928). A New Type of Secondary Radiation. *Nature*,

121(3048), 501–502. https://doi.org/10.1038/121501c0

Rantonen, P. (2003). *Salivary Flow and Composition in Healthy and Diseased Adults*.

Rasmussen, K., Mast, J., Temmerman, P.-J. De, Verleysen, E., Waegeneers, N., Steen, F. Van, … Mech, A. (2014). *Titanium Dioxide, NM-100, NM-101, NM-102, NM-103, NM-104, NM-105: Characterisation and Physico- Chemical Properties*. https://doi.org/10.2788/79554

Reis, J. M., Sinkó, B., & Serra, C. H. R. (2010). Parallel artificial membrane permeability assay (PAMPA) - Is it better than Caco-2 for human passive permeability prediction? *Mini Reviews in Medicinal Chemistry*, *10*(11), 1071–1076. https://doi.org/10.2174/1389557511009011071

Rezwan, K., Studart, A. R., Voros, J., & Gauckler, L. J. (2005). Change of potential of biocompatible colloidal oxide particles uponadsorption of bovine serum albumin and lysozyme. *Enviromental Science and Technology*, *109*(52), 14469–14474.

RIKILT, & JRC. (2014). Inventory of Nanotechnology applications in the agricultural, feed and food sector. *EFSA Supporting Publication*, *EN-621*, 125. https://doi.org/10.2903/sp.efsa.2014.EN-621

Rincón, A. G., & Pulgarin, C. (2005). Use of coaxial photocatalytic reactor (CAPHORE) in the TiO2 photo-assisted treatment of mixed E. coli and Bacillus sp. and bacterial community present in wastewater. In *Catalysis Today* (Vol. 101, pp. 331–344). https://doi.org/10.1016/j.cattod.2005.03.022

Rinnert, E., Carteret, C., Humbert, B., Fragneto-Cusani, G., Ramsay, J. D. F., Delville, A., … Michot, L. J. (2005). Hydration of a Synthetic Clay with Tetrahedral Charges: A Multidisciplinary Experimental and Numerical Study. *The Journal of Physical Chemistry B*, *109*(49), 23745–23759. https://doi.org/10.1021/jp050957u

Roblegg, E., Fröhlich, E., Meindl, C., Teubl, B., Zaversky, M., & Zimmer, A. (2012). Evaluation of a physiological in vitro system to study the transport of nanoparticles through the buccal mucosa. *Nanotoxicology*, *6*(4), 399–413. https://doi.org/10.3109/17435390.2011.580863

Rozehnal, V., Nakai, D., Hoepner, U., Fischer, T., Kamiyama, E., Takahashi, M., … Mueller, J. (2012). Human small intestinal and colonic tissue mounted in the Ussing chamber as a tool for characterizing the intestinal absorption of drugs. *European Journal of Pharmaceutical Sciences*, *46*(5), 367–373. https://doi.org/10.1016/j.ejps.2012.02.025

Rudney, J. D., & Smith, Q. T. (1985). Relationships between levels of lysozyme, lactoferrin, salivary peroxidase, and secretory immunoglobulin A in stimulated parotid saliva. *Infection and Immunity*, *49*(3), 469–475.

Salis, A., Bostr??m, M., Medda, L., Cugia, F., Barse, B., Parsons, D. F., … Monduzzi, M. (2011). Measurements and theoretical interpretation of points of zero charge/potential of BSA protein. *Langmuir*, *27*(18), 11597–11604. https://doi.org/10.1021/la2024605

Sambuy, Y., De Angelis, I., Ranaldi, G., Scarino, M. L., Stammati, A., & Zucco, F. (2005).

The Caco-2 cell line as a model of the intestinal barrier: Influence of cell and culture-related factors on Caco-2 cell functional characteristics. *Cell Biology and Toxicology*. https://doi.org/10.1007/s10565-005-0085-6

Sang, X., Fei, M., Sheng, L., Zhao, X., Yu, X., Hong, J., … Hong, F. (2014). Immunomodulatory effects in the spleen-injured mice following exposure to titanium dioxide nanoparticles. *Journal of Biomedical Materials Research - Part A*, *102*(10), 3562–3572. https://doi.org/10.1002/jbm.a.35034

Sang, X., Li, B., Ze, Y., Hong, J., Ze, X., Gui, S., … Hong, F. (2013). Toxicological mechanisms of nanosized titanium dioxide-induced spleen injury in mice after repeated peroral application. *Journal of Agricultural and Food Chemistry*, *61*(23), 5590–5599. https://doi.org/10.1021/jf3035989

Sang, X., Zheng, L., Sun, Q., Li, N., Cui, Y., Hu, R., … Hong, F. (2012). The chronic spleen injury of mice following long-term exposure to titanium dioxide nanoparticles. *Journal of Biomedical Materials Research - Part A*, *100 A*(4), 894–902. https://doi.org/10.1002/jbm.a.34024

Sarkar, A., Goh, K. K. T., & Singh, H. (2009). Colloidal stability and interactions of milk-protein-stabilized emulsions in an artificial saliva. *Food Hydrocolloids*, *23*(5), 1270–1278. https://doi.org/10.1016/j.foodhyd.2008.09.008

Sekhon, B. (2010). Food nanotechnology–an overview. *Nanotechnology, Science and Applications*, *3*, 1–15.

Sekirov, I., Russell, S., & Antunes, L. (2010). Gut microbiota in health and disease. *Physiological Reviews*, *90*(3), 859–904. https://doi.org/10.1152/physrev.00045.2009.

Sender, R., Fuchs, S., & Milo, R. (2016). Revised estimate for the number of human and bacterial cells in the body. *BioRvix*, 1–21. https://doi.org/http://dx.doi.org/10.1101/036103

Shang, L., Nienhaus, K., & Nienhaus, G. U. (2014). Engineered nanoparticles interacting with cells: size matters. *Journal of Nanobiotechnology*, *12*(5), 1–11. https://doi.org/10.1186/1477-3155-12-5

Sinhaa, V. K., Snoeysb, J., Van Osselaerc, N., Van Peera, A., Mackied, C., & Healde, D. (2012). From preclinical to human - Prediction of oral absorption and drug-drug interaction potential using physiologically based pharmacokinetic (PBPK) modeling approach in an industrial setting: A workflow by using case example. *Biopharmaceutics and Drug Disposition*, *33*(2), 111–121. https://doi.org/10.1002/bdd.1782

Skocaj, M., Filipic, M., Petkovic, J., & Novak, S. (2011). Titanium dioxide in our everyday life; is it safe? *Radiology and Oncology*, *45*(4), 227–247. https://doi.org/10.2478/v10019-011-0037-0

Smyth, J. R., & Mccormick, T. C. (1995). Crystallographic Data For Minerals.

Song, Z.-M., Chen, N., Liu, J.-H., Tang, H., Deng, X., Xi, W.-S., … Wang, H. (2015). Biological effect of food additive titanium dioxide nanoparticles on intestine: an in vitro study. *Journal of Applied Toxicology : JAT*, *35*(10), 1169–1178. https://doi.org/10.1002/jat.3171

Sonthiphand, P., & Neufeld, J. D. (2013). Evaluating Primers for Profiling Anaerobic Ammonia Oxidizing Bacteria within Freshwater Environments. *PLoS ONE*, *8*(3), e57242. https://doi.org/10.1371/journal.pone.0057242

Suenderhauf, C., Hammann, F., Maunz, A., Helma, C., & Huwyler, J. (2011). Combinatorial QSAR modeling of human intestinal absorption. *Molecular Pharmaceutics*, *8*(1), 213–224. https://doi.org/10.1021/mp100279d

Sugano, K. (2009). Introduction to computational oral absorption simulation. *Expert Opin Drug Metab Toxicol*, *5*(3), 259–293. https://doi.org/10.1517/17425250902835506

Suutari, M., & Laakso, S. (1994). Microbial fatty acids and thermal adaptation. *Critical Reviews in Microbiology*, *20*(4), 285–328. https://doi.org/10.3109/10408419409113560

Takeuchi, M., Martra, G., Coluccia, S., & Anpo, M. (2005). Investigations of the Structure of H2O Clusters Adsorbed on TiO2 Surfaces by Near-Infrared Absorption Spectroscopy. *J. Phys. Chem. C*, *109*, 7387–7391. https://doi.org/10.1021/jp040630d

Tantra, R., Tompkins, J., & Quincey, P. (2010). Characterisation of the de-agglomeration effects of bovine serum albumin on nanoparticles in aqueous suspension. *Colloids and Surfaces B: Biointerfaces*, *75*(1), 275–281. https://doi.org/10.1016/j.colsurfb.2009.08.049

Tanuma, S., Powell, C., & Penn, D. (1994). Calculations of electron inelastic mean free paths. *Surface and Interface …*, *21*(September 1993), 165–176.

Tassinari, R., Cubadda, F., Moracci, G., Aureli, F., D'Amato, M., Valeri, M., … Maranghi, F. (2014). Oral, short-term exposure to titanium dioxide nanoparticles in Sprague-Dawley rat: focus on reproductive and endocrine systems and spleen. *Nanotoxicology*, *8*(6), 654–62. https://doi.org/10.3109/17435390.2013.822114

Taurozzi, J. S., Hackley, V. a, & Wiesner, M. R. (2013). A standardised approach for the dispersion of titanium dioxide nanoparticles in biological media. *Nanotoxicology*, *7*(4), 389–401. https://doi.org/10.3109/17435390.2012.665506

Tavelin, S., Taipalensuu, J., Soderberg, L., Morrison, R., Chong, S., & Artursson, P. (2003). Prediction of the oral absorption of low-permeability drugs using small intestine-like 2/4/A1 cell monolayers. *Pharmaceutical Research*, *20*(3), 397–405. https://doi.org/10.1023/A:1022699920043

Tay, C. Y., Fang, W., Setyawati, M. I., Chia, S. L., Tan, K. S., Hsu, C., … Leong, D. T. (2014). Nano-hydroxyapatite and Nano-titanium Dioxide Exhibit Different Subcellular Distribution and Apoptotic Profile in Human Oral Epithelium. *ACS Appl. Mater. Interfaces*, *6*(9), 6248–6256. https://doi.org/10.1021/am501266a

Taylor, A. a., Marcus, I. M., Guysi, R. L., & Walker, S. L. (2015). Metal Oxide Nanoparticles Induce Minimal Phenotypic Changes in a Model Colon Gut Microbiota. *Environmental Engineering Science*, *32*(7), 602–612. https://doi.org/10.1089/ees.2014.0518

Teubl, B. J., Absenger, M., Fröhlich, E., Leitinger, G., Zimmer, A., & Roblegg, E. (2013). The oral cavity as a biological barrier system: Design of an advanced buccal in vitro permeability model. *European Journal of Pharmaceutics and Biopharmaceutics*, *84*(2), 386–393. https://doi.org/10.1016/j.ejpb.2012.10.021

Teubl, B. J., Leitinger, G., Schneider, M., Lehr, C.-M., Fröhlich, E., Zimmer, A., & Roblegg, E. (2014). The buccal mucosa as a route for TiO2 nanoparticle uptake. *Nanotoxicology*, *5390*, 1–9. https://doi.org/10.3109/17435390.2014.921343

Teubl, B. J., Schimpel, C., Leitinger, G., Bauer, B., Fröhlich, E., Zimmer, A., & Roblegg, E. (2015). Interactions between nano-TiO2 and the oral cavity: Impact of nanomaterial surface hydrophilicity/hydrophobicity. *Journal of Hazardous Materials*, *286*, 298–305. https://doi.org/10.1016/j.jhazmat.2014.12.064

Thomas, C., & Oates, P. S. (2002). IEC-6 cells are an appropriate model of intestinal iron absorption in rats. *The Journal of Nutrition*, *132*(September 2001), 680–687.

Tok, J., Szabolcs, M., & Silvers, D. (1998). Detection of clonal T-cell receptor γ chain gene rearrangements by polymerase chain reaction and denaturing gradient gel electrophoresis (PCR/DGGE) in archival. *Journal of the American …*, 453–460.

Tsuang, Y.-H., Sun, J.-S., Huang, Y.-C., Lu, C.-H., Chang, W. H.-S., & Wang, C.-C. (2008). Studies of photokilling of bacteria using titanium dioxide nanoparticles. *Artificial Organs*, *32*(2), 167–174. https://doi.org/10.1111/j.1525-1594.2007.00530.x

Tyrer, P., Ruth Foxwell, A., Kyd, J., Harvey, M., Sizer, P., & Cripps, A. (2002). Validation and quantitation of an in vitro M-cell model. *Biochemical and Biophysical Research Communications*, *299*(3), 377–383. https://doi.org/10.1016/S0006-291X(02)02631-1

Vergères, G., Bogicevic, B., Buri, C., Carrara, S., Chollet, M., Corbino-Giunta, L., … Gijs, M. A. (2012). The NutriChip project--translating technology into nutritional knowledge. *The British Journal of Nutrition*, *108*(5), 762–768. https://doi.org/10.1017/S0007114512002693

Veronesi, G., Brun, E., Fayard, B., Cotte, M., & Carrière, M. (2012). Structural properties of rutile TiO 2 nanoparticles accumulated in a model of gastrointestinal epithelium elucidated by micro-beam x-ray absorption fine structure spectroscopy. *Applied Physics Letters*, *100*(21). https://doi.org/10.1063/1.4720172

Versantvoort, C. H. M., Ondrewater, R. C. A., Duizer, E., Van De Sandt, J. J. M., Gilde, A. J., & Groten, J. P. (2002). Monolayers of IEC-18 cells as an in vitro model for screening the passive transcellular and paracellular transport across the intestinal barrier: Comparison of active and passive transport with the human colon carcinoma Caco-2 cell line. *Environmental Toxicology and Pharmacology*, *11*(3–4), 335–344. https://doi.org/10.1016/S1382-6689(01)00122-3

Versantvoort, C. H. M., Oomen, A. G., Van De Kamp, E., Rompelberg, C. J. M., & Sips, A. J. a M. (2005). Applicability of an in vitro digestion model in assessing the bioaccessibility of mycotoxins from food. *Food and Chemical Toxicology*, *43*(1), 31–40. https://doi.org/10.1016/j.fct.2004.08.007

Walter, E., Janich, S., Roessler, B., Hilfinger, J., & Amidon, G. (1996). HT29-MTX / Caco-2 Cocultures as an in Vitro Model for the Intestinal Epithelium : In Vitro − in Vivo

Correlation with Permeability Data from Rats and Humans. *J Pharm Sci*, *85*(10), 1070–1076.

Wang, J., Li, N., Zheng, L., Wang, S., Wang, Y., Zhao, X., … Hong, F. (2011). P38-Nrf-2 signaling pathway of oxidative stress in mice caused by nanoparticulate TiO2. *Biological Trace Element Research*, *140*(2), 186–197. https://doi.org/10.1007/s12011-010-8687-0

Wang, J., Zhou, G., Chen, C., Yu, H., Wang, T., Ma, Y., … Chai, Z. (2007). Acute toxicity and biodistribution of different sized titanium dioxide particles in mice after oral administration. *Toxicology Letters*, *168*(2), 176–185. https://doi.org/10.1016/j.toxlet.2006.12.001

Wang, L. Q., Ferris, K. F., Shultz, A. N., Baer, D. R., & Engelhard, M. H. (1997). Interactions of HCOOH with stoichiometric and defective TiO2(110) surfaces. *Surface Science*, *380*(2–3), 352–364. https://doi.org/http://dx.doi.org/10.1016/S0039-6028(97)00023-X

Wang, Y., Chen, Z., Ba, T., Pu, J., Chen, T., Song, Y., … Jia, G. (2013). Susceptibility of young and adult rats to the oral toxicity of titanium dioxide nanoparticles. *Small*, *9*(9–10), 1742–1752. https://doi.org/10.1002/smll.201201185

Weir, A., Westerhoff, P., Fabricius, L., Hristovski, K., & Von Goetz, N. (2012). Titanium dioxide nanoparticles in food and personal care products. *Environmental Science and Technology*, *46*(4), 2242–2250. https://doi.org/10.1021/es204168d

White, B. (1993). *PCR protocols: current methods and applications* (Vol. 15).

Williams, D. B., & Carter, C. B. (1996). *Transmission Electron Microscopy a Textbook for Materials Science*.

Winkler, D. a, Mombelli, E., Pietroiusti, A., Tran, L., Worth, A., Fadeel, B., & McCall, M. J. (2013). Applying quantitative structure-activity relationship approaches to nanotoxicology: Current status and future potential. *Toxicology*, *313*(1), 15–23. https://doi.org/10.1016/j.tox.2012.11.005

Xie, G., Wang, C., Sun, J., & Zhong, G. (2011). Tissue distribution and excretion of intravenously administered titanium dioxide nanoparticles. *Toxicology Letters*, *205*(1), 55–61. https://doi.org/10.1016/j.toxlet.2011.04.034

Xiu, Z., Zhang, Q., Puppala, H. L., Colvin, V. L., & Alvarez, P. J. J. (2012). Negligible Particle-Speci fi c Antibacterial Activity of Silver Nanoparticles. *Nano Letters*, *12*(8), 4271–4275. https://doi.org/dx.doi.org/10.1021/nl301934w

Xu, J., Yang, F., An, X., & Hu, Q. (2007). Anticarcinogenic activity of selenium-enriched green tea extracts in vivo. *Journal of Agricultural and Food Chemistry*, *55*(13), 5349–5353. https://doi.org/10.1021/jf070568s

Xu, Z., Liu, X. W., Ma, Y. S., & Gao, H. W. (2010). Interaction of nano-TiO2 with lysozyme: Insights into the enzyme toxicity of nanosized particles. *Environmental Science and Pollution Research*, *17*(3), 798–806. https://doi.org/10.1007/s11356-009-0153-1

Yang, Y., Doudrick, K., Bi, X., Hristovski, K., Herckes, P., Westerhoff, P., & Kaegi, R.

(2014). Characterization of food-grade titanium dioxide: The presence of nanosized particles. *Environmental Science and Technology*, *48*(11), 6391–6400. https://doi.org/10.1021/es500436x

Yeh, C., Dodds, M., Zuo, P., & Johnson, D. (1997). A population-based study of salivary lysozyme concentrations and candidal counts. *Archives of Oral Biology*, *42*(1), 25–31.

Yu, J. C., Zhang, L., Zheng, Z., & Zhao, J. (2003). Synthesis and Characterization of Phosphated Mesoporous Titanium Dioxide with High Photocatalytic Activity. *Chemistry of Materials*, *15*(11), 2280–2286. https://doi.org/10.1021/cm0340781

Yu, L. X., & Amidon, G. L. (1999). A compartmental absorption and transit model for estimating oral drug absorption. *International Journal of Pharmaceutics*, *186*(2), 119–125. https://doi.org/10.1016/S0378-5173(99)00147-7

Zhang, F., Zheng, Z., & Chen, Y. (1998). In vivo investigation of blood compatibility of titanium oxide films. *Journal of Biomedical Materials Research*, *42*(1), 128–133.

Zhu, R. R., Wang, W. R., Sun, X. Y., Liu, H., & Wang, S. L. (2010). Enzyme activity inhibition and secondary structure disruption of nano-TiO2 on pepsin. *Toxicology in Vitro*, *24*(6), 1639–1647. https://doi.org/10.1016/j.tiv.2010.06.002

UNIVERSITE BRETAGNE LOIRE

UNIVERSITÉ DE NANTES

Thèse de Doctorat

William DUDEFOI

Le dioxyde de titane en alimentation : caractérisation, devenir dans les fluides digestifs et impact sur le microbiote intestinal humain

Titanium dioxide particles in food: characterization, fate in digestive fluids and impact on human gut microbiota

Résumé

Le dioxyde de titane (TiO_2) est un oxyde métallique utilisé en tant que pigment blanc, par exemple dans les enrobages de confiseries. Sachant que la forme alimentaire (E171/IN171) contient des nanoparticules (NPs), et que ces dernières sont classifiées comme potentiellement dangereuses par inhalation, nos travaux ont eu pour but de déterminer le devenir et l'impact des particules de E171 après ingestion.
Plusieurs lots de poudre E171 ont été caractérisés et comparés à un lot de poudre P25, variété de référence de TiO_2 en toxicologie (100% NPs). Nos résultats ont confirmé que la forme E171 contient des NPs, cependant à en quantité inférieure au seuil définissant l'étiquetage des nanomatériaux (50%). Comme les mêmes particules de E171 sont retrouvées intactes dans les extraits d'enrobage de plusieurs confiseries et que les propriétés physicochimiques des deux formes E171 et P25 sont très différentes, la forme E171 pourrait ainsi être préférée à l'actuel modèle P25 pour les études portant sur l'impact du TiO_2 par ingestion.
Le suivi des particules des variétés E171 et P25 au cours d'une digestion *in vitro* a montré leur forte agglomération, due à l'adsorption d'ions et de protéines composant les fluides digestifs. Cette forte agglomération (jusqu'à 90 µm dans l'intestin) explique le faible taux d'absorption du TiO_2 observé *in vivo*. Au contact d'une flore intestinale humaine reconstituée, aucune des formes E171 ou P25 n'a eu d'effet sur la viabilité et la richesse écologique du microbiote après exposition à une dose singulière de TiO_2 équivalente à l'ingestion d'une confiserie. Ces résultats doivent être à l'avenir confirmés dans le cadre d'une consommation régulière.

Mots clés
TiO_2, E171, Caractérisation, Nanomatériaux, Digestion, Microbiote

Abstract

Titanium dioxide (TiO_2) is a white metal oxide commonly used as a coloring agent in food products, constituting for example the coating of confectionary. Considering that food-grade TiO_2 (E171/INS171) contains nanoparticles (NPs) and that TiO_2 NPs are classified as potentially harmful for humans by inhalation, we aimed to determine the fate and impact of TiO_2 particles via ingestion.
The physicochemical characterization of E171 samples confirmed that E171 contains NPs, however below the threshold defining the labelling of nanomaterial (50%). Moreover, they resemble TiO_2 extracted from the coating of several confectioneries, indicating that they can be used directly as models of ingested particles. Furthermore, the physicochemical properties of E171 were proved to be very different from those of P25, a kind of TiO_2 used as a reference in toxicology (100% NPs). Food grade E171 TiO_2 may be thus preferred to the currently used model P25 for further studies on the impact of TiO_2 via ingestion.
Monitoring food grade TiO_2 at each step of an *in vitro* digestion showed that, due to interactions with both ions and proteins composing the digestive fluids, TiO_2 particles agglomerated all along the digestion and formed large agglomerates (up to 90µm in the intestinal phase), explaining the low absorption rate of TiO_2 after ingestion observed *in vivo*.
Finally, the impact of TiO_2 on the human gut microbiota was assessed. No impact on the human gut microbiota viability and ecological richness was observed after a single dose of TiO_2 equivalent to the ingestion of one piece of candy. These results are still to be confirmed for a chronic ingestion.

Key Words
TiO_2, E171, Characterization, Nanomaterial, Digestion, Microbiota